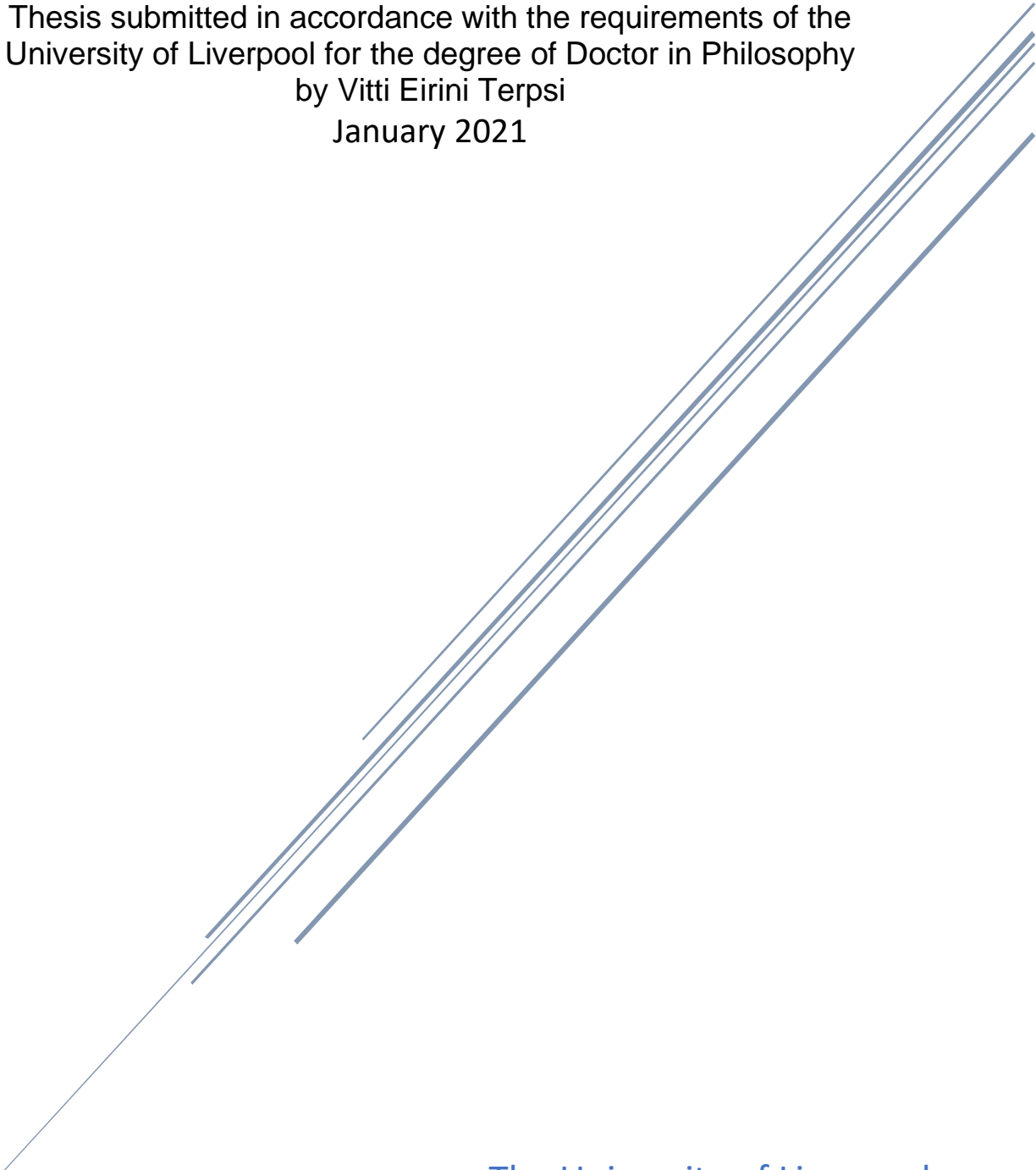


Targeting DNA double-strand break repair sensitises HNSCC cells to x-rays and proton radiation.

Thesis submitted in accordance with the requirements of the
University of Liverpool for the degree of Doctor in Philosophy
by Vitti Eirini Terpsi
January 2021



The University of Liverpool
ISMIB

Abstract

Ionizing radiation (IR) induces various DNA lesions, with the double strand breaks (DSB) be the most threatening to the cell survival. The two main mechanisms that detect and repair DSBs are the non-homologous end joining (NHEJ) and the homologous recombination (HR), that are driven by the DNA repair protein kinases Ataxia telangiectasia mutated (ATM), ATM and Rad3 related (ATR), and the catalytic subunit of DNA-dependent protein kinase (DNA-PKcs). Specific inhibitors suppressing these proteins, restricting the DNA repair process are studied for numerous cancer types. The aim of the work described in this thesis was to investigate and understand the effect of inhibition of ATM, ATR and DNA-PKcs protein kinases on head and neck squamous cell carcinoma (HNSCC) cell lines in combination with either X – rays or Proton beams (PB). A large proportion of HNSCC is driven by human papilloma virus (HPV). Interestingly, clinical data suggest that HPV-positive patients have a better prognosis compared to HPV-negative ones. This was reflected in *in vitro* studies, where HPV-positive HNSCC cell lines were more sensitive to IR compared to the HPV-negative ones. Three inhibitors were used, KU-55933, VE-821 and NU7441, inhibiting ATM, ATR and DNA-PKcs respectively, to investigate the impact of inhibition alone or in combination with IR, in HPV-positive and HPV-negative HNSCC cell lines (UMSCC74A, UMSCC6, UMSCC47, UPCI-SCC090, FaDu, and A253). Cell survival and growth was analysed using 2D clonogenic and 3D spheroid growth assays. Also, the impact of the inhibitors on the respective enzyme target was analysed by immunoblotting, and on DSB signalling by Immunofluorescence (IF) staining and DSB repair foci analysis of histone γ H2AX, 53BP1, and Rad51. My results exhibited reduced phosphorylation levels on the inhibited proteins up to 24 h following exposure to IR, thus demonstrating the effectiveness of the inhibitors at the protein level. Moreover, inhibitor and IR treatment altered all three DSB repair foci formation, where decreased levels but also persistent foci were observed. Finally, inhibition of ATM, ATR, and particularly DNA-PKcs, caused a significant reduction in HNSCC cell proliferation in 2D as well as in 3D, post IR, with less of an impact on the most radiosensitive HPV-positive cell lines. Cumulatively, my results demonstrated that targeting DNA DSB repair via NHEJ or HR can exacerbate the impact

of x – rays and PB in radiosensitising HNSCC cell models, constituting a promising combination treatment for HNSCC.

Acknowledgments

When I was accepted on this research project, I was so excited for the opportunity that was given to me, but also overwhelmed with the responsibility and the work I had ahead of me as a PhD student. Shortly though after started working in the labs, I found myself surrounded by a group of hardworking scientists who motivated me, guided me through every step, and made me feel so welcomed from day 1. Over the years, I have learnt a great deal and grew as a scientist. For all that, I would like to give a huge thank you to Dr Jason Parsons for entrusting me with this PhD project, but also for always being there to support and advise me both in the lab and during writing my thesis. I wish to also thank Dr Katie Nickson, Dr Rachel Carter, Dr Jonathan Hughes, Eleanor Madders, Chumin Zhou, Rachel Clifford and all the other past and present members of the research group for providing me with their help and friendship, making it such an enjoyable experience. Moreover, I would like to express my gratitude Dr Andrzej Kacperek, Brian Marsland and Ian Taylor at the Clatterbridge Cancer Centre for technical assistance with proton irradiation of cells, and Prof Carlos Rubbi for his most valuable assistance with processing IF data. Finally, I also must thank North West Cancer Research for funding this PhD project and giving me the opportunity to study within an international research group and excel in my career.

This PhD journey might not have been implemented without the support of my husband Nikos Kallistis, who has always believed in me, encouraging me to apply for this position, in the first place, and who was there motivating me to become the best I could. This applies to my parents and siblings, Eftichia, Yiorgos and Nick, too, and I wish to thank my Mum and Dad for educating me, being there for me, and inspiring me to achieve more, and all my family for being so enthusiastic about my studies and progress, constantly motivating me and keeping me sane throughout this PhD.

My time in the University of Liverpool was so memorable and I hold it dear in my heart.

Table of Contents

| | |
|-----------------------------------------------------------------------|-----------|
| Abstract | 1 |
| Acknowledgments | 2 |
| List of Figures | 7 |
| List of Tables | 9 |
| List of Abbreviations | 12 |
| Chapter 1: Introduction | 19 |
| 1.1 Ionising Radiation and Radiotherapy | 19 |
| 1.1.1 Electromagnetic Radiation | 19 |
| 1.1.2. Particle Radiation | 22 |
| 1.1.3 Clinically used Radiation types | 26 |
| 1.2 DNA damage and repair | 35 |
| 1.2.1 The DNA..... | 35 |
| 1.2.2 Cell cycle | 39 |
| 1.2.3 Induction of DNA lesions | 41 |
| 1.2.4 DNA damages affected by LET and RBE | 44 |
| 1.2.5 DNA repair | 46 |
| 1.2.6 DNA repair in response to IR-induced DNA damage..... | 54 |
| 1.3 DNA repair regulators | 57 |
| 1.3.1 The role of ATM in DDR..... | 57 |
| 1.3.2 The role of ATR in DDR | 59 |
| 1.3.3 The role of DNA-PKcs in DDR..... | 62 |
| 1.4 Head and Neck Squamous Cell Carcinoma | 64 |
| 1.4.1 Development of HNSCC: Alcohol and tobacco overconsumption. | 64 |

| | |
|--------------------------------------------------------------------------|-----------|
| 1.4.2 Development of HNSCC: HPV infection..... | 65 |
| 1.4.3 HNSCC cell lines for in vitro studies..... | 66 |
| 1.4.4 Targeting DDR in HNSCC cells..... | 67 |
| Chapter 2: Aims | 72 |
| Chapter 3: Methodology..... | 73 |
| 3.1 Materials | 73 |
| 3.2 Cell culture | 73 |
| 3.2.1 Cell line Culture | 73 |
| 3.2.2 Thawing cells | 76 |
| 3.2.3 Passaging Cells..... | 77 |
| 3.2.4 Freezing Cells..... | 77 |
| 3.3 Ionising radiation..... | 78 |
| 3.4 Cell Harvesting following drug and radiation treatment..... | 79 |
| 3.5 Whole cell extracts | 79 |
| 3.6 Bradford Assay | 80 |
| 3.7 SDS-PAGE and Western Blot | 81 |
| 3.8 Immunofluorescent staining and DNA repair foci analysis | 83 |
| 3.9 Colony Formation Assays..... | 86 |
| 3.10 3D Spheroid growth assay..... | 88 |
| Chapter 4: Results I..... | 91 |
| 4.1 Introduction | 91 |
| 4.2 Confirmation of HPV status..... | 92 |
| 4.3 Inhibitor dose titration | 93 |

| | |
|------------------------------------------------------------------------------------------|------------|
| 4.4 Impact of DNA repair inhibitors in combination with x – ray irradiation | 96 |
| 4.4.1 The impact of ATMi on ATM phosphorylation..... | 96 |
| 4.4.2 The impact of ATRi on ATR phosphorylation | 97 |
| 4.4.3 The Impact of DNA-PKcsi on DNA-PKcs phosphorylation | 100 |
| 4.5 Impact of DNA repair inhibitors in combination with proton irradiation. | 105 |
| 4.5.1 The impact of ATMi on ATM phosphorylation..... | 105 |
| 4.5.2 The impact of ATRi on ATR phosphorylation | 107 |
| 4.5.3 The Impact of DNA-PKcsi on DNA-PKcs phosphorylation | 109 |
| 4.6 Conclusions..... | 113 |
| Chapter 5: Results II..... | 115 |
| 5.1 Introduction | 115 |
| 5.2 Immunofluorescence staining and foci analysis in response to x – rays. | 116 |
| 5.2.1 Impact of ATMi | 117 |
| 5.2.2 Impact of ATRi | 121 |
| 5.2.3 Impact of DNA-PKcsi..... | 124 |
| 5.3 Immunofluorescence staining and foci analysis in response to protons. | 128 |
| 5.3.1 Impact of ATMi | 128 |
| 5.3.2 Impact of ATRi | 131 |
| 5.3.3 Impact of DNA-PKcsi..... | 135 |
| 5.4 Conclusions..... | 139 |
| Chapter 6: Results III..... | 143 |

| | |
|------------------------------------------------------------------------------------------------------------------------|------------|
| 6.1 Introduction | 143 |
| 6.2 Impact of the DNA repair inhibitors as a monotherapy in 2D .. | 144 |
| 6.3 Impact of IR on cell survival in 2D | 145 |
| 6.3.1 Comparative radiosensitivity in response to x – rays..... | 145 |
| 6.3.2 Comparative radiosensitivity in response to protons. | 146 |
| 6.4 Impact of DNA repair inhibitors on 2D cell survival in combination with IR..... | 148 |
| 6.4.1 X- rays | 148 |
| 6.4.2 Protons | 151 |
| 6.5 3D spheroid growth in HNSCC cell lines | 155 |
| 6.6 Impact of DNA repair inhibition on non irradiated 3D spheroid growth in HNSCC. | 161 |
| 6.7 Impact of DNA repair inhibition in combination with x – rays on 3D spheroid growth in HNSCC..... | 164 |
| 6.7.1 ATMi | 165 |
| 6.7.2 ATRi..... | 168 |
| 6.7.3 DNA-PKcsi | 172 |
| 6.8 Impact of DNA repair inhibition in combination with proton irradiation on 3D spheroid growth in HNSCC. | 176 |
| 6.8.1 ATMi | 176 |
| 6.8.2 ATRi..... | 179 |
| 6.8.3 DNA-PKcsi | 183 |
| 6.9 Conclusions..... | 188 |
| Chapter 7: Discussion | 193 |
| 7.1 Overview | 193 |

| | |
|-----------------------------------------------------------------------|-----------------|
| 7.2 DNA repair inhibitors delay or downregulate DDR activation | .195 |
| 7.3 DNA repair inhibitors delay or downregulate DDR signalling | ..200 |
| 7.4 DNA repair inhibitors reduce cell survival |204 |
| 7.5 Future perspectives |208 |
| 7.6 Conclusions |211 |
| References |213 |
| Appendix |231 |

List of Figures

Chapter 1

| | |
|---------------------------------------------------------------------------|---------|
| Figure 1. 1 Electromagnetic radiation interaction with matter |21 |
| Figure 1. 2 Schematic representation of charged particles tracks in water |25 |
| Figure 1. 3 Bremsstrahlung – Deceleration effect |28 |
| Figure 1. 4 Schematic representation of an x – ray tube |30 |
| Figure 1. 5 Relative radiation dose in depth |32 |
| Figure 1. 6 Schematic representation of a cyclotron |34 |
| Figure 1. 7 DNA Components |37 |
| Figure 1. 8 DNA structure and base formation |38 |
| Figure 1. 9 Induction of DNA damage |44 |
| Figure 1. 10 Schematic representation of Base excision repair (BER) |47 |
| Figure 1. 11 Schematic representation of Nucleotide excision repair (NER) |48 |
| Figure 1. 12 Schematic representation of NHEJ repair pathway |51 |
| Figure 1. 13 Schematic representation of HR repair pathway |53 |
| Figure 1. 14 The role of ATM, ATR and DNA-PKcs in the DNA damage response |61 |

Chapter 3

| | |
|-----------------------------------------------------|---------|
| Figure 3. 1 Threshold discrimination in IF analysis |85 |
|-----------------------------------------------------|---------|

Chapter 4

| | |
|-------------------------------------------------------------------------|-----|
| Figure 4. 1 p16 expression as a marker of HPV positivity in HNSCC | 93 |
| Figure 4. 2 Inhibitor dose titration | 95 |
| Figure 4. 3 Impact of ATMi on pATM S1981..... | 97 |
| Figure 4. 4 Impact of ATRi on pATR S428 in extended time course..... | 98 |
| Figure 4. 5 Impact of ATRi on pATR T1989 | 100 |
| Figure 4. 6 Impact of DNA-PKcsi on pDNA-PKcs T2609 | 102 |
| Figure 4. 7 Impact of DNA-PKcsi on pDNA-PKcs S2056 | 105 |
| Figure 4. 8 Impact of ATMi on pATM S1981..... | 107 |
| Figure 4. 9 Impact of ATRi on pATR T1989 | 109 |
| Figure 4. 10 Impact of DNA-PKcsi on pDNA-PKcs S2056..... | 112 |

Chapter 5

| | |
|-------------------------------------------------------------------|-----|
| Figure 5. 1 DNA repair focus formation in response to IR. | 116 |
| Figure 5. 2 Impact of ATMi on DSB marker γ H2AX. | 118 |
| Figure 5. 3 Impact of ATMi on DSB repair marker 53BP1 | 119 |
| Figure 5. 4 Impact of ATMi on DSB repair marker Rad51. | 120 |
| Figure 5. 5 Impact of ATRi on DSB marker γ H2AX..... | 122 |
| Figure 5. 6 Impact of ATRi on DSB repair marker 53BP1..... | 123 |
| Figure 5. 7 Impact of ATRi on DSB repair marker Rad51..... | 124 |
| Figure 5. 8 Impact of DNA-PKcsi on DSB marker γ H2AX | 125 |
| Figure 5. 9 Impact of DNA-PKcsi on DSB repair marker 53BP1 | 126 |
| Figure 5. 10 Impact of DNA-PKcsi on DSB repair marker Rad51 | 127 |
| Figure 5. 11 Impact of ATMi on DSB marker γ H2AX | 129 |
| Figure 5. 12 Impact of ATMi on DSB repair marker 53BP1 | 130 |
| Figure 5. 13 Impact of ATMi on DSB repair marker Rad51 | 131 |
| Figure 5. 14 Impact of ATRi on DSB marker γ H2AX..... | 132 |
| Figure 5. 15 Impact of ATRi on DSB repair marker 53BP1 | 133 |
| Figure 5. 16 Impact of ATRi on DSB repair marker Rad51..... | 134 |

| | |
|--------------------------------------------------------------------|-----|
| Figure 5. 17 Impact of DNA-PKcsi on DSB marker γ H2AX | 136 |
| Figure 5. 18 Impact of DNA-PKcsi on DSB repair marker 53BP1..... | 137 |
| Figure 5. 19 Impact of DNA-PKcsi on DSB repair marker Rad51 | 138 |

Chapter 6

| | |
|-----------------------------------------------------------------------------------------|-----|
| Figure 6. 1 Impact of DNA repair inhibitors on cell survival as a monotherapy | 145 |
| Figure 6. 2 Impact of x – ray irradiation on cell survival | 146 |
| Figure 6. 3 Impact of proton irradiation on cell survival..... | 147 |
| Figure 6. 4 Impact of DSB inhibitors in combination with x – rays on cell survival..... | 150 |
| Figure 6. 5 Impact of DSB inhibitors in combination with protons on cell survival | 153 |
| Figure 6. 6 3D spheroid formation and growth in HNSCC cell lines..... | 157 |
| Figure 6. 7 3D spheroid growth following x – ray irradiation in HNSCC cell lines..... | 158 |
| Figure 6. 8 3D spheroid growth following proton irradiation in HNSCC cell lines. | 159 |
| Figure 6. 9 3D spheroid formation and growth in HNSCC cell lines..... | 160 |
| Figure 6. 10 3D spheroid growth following x - rays or protons in HNSCC cells..... | 161 |
| Figure 6. 11 3D spheroid growth following DSB repair inhibition in HNSCC cells..... | 163 |
| Figure 6. 12 Impact of ATMi on 3D spheroid growth following x - rays..... | 167 |
| Figure 6. 13 Impact of ATRi on 3D spheroid growth following x - rays..... | 170 |
| Figure 6. 14 Impact of DNA-PKcsi on 3D spheroid growth following x - rays | 174 |
| Figure 6. 15 3D spheroid formation and growth in HNSCC cell lines..... | 175 |
| Figure 6. 16 Impact of ATMi on 3D spheroid growth post proton irradiation..... | 178 |
| Figure 6. 17 Impact of ATRi on 3D spheroid growth post proton irradiation | 182 |
| Figure 6. 18 Impact of DNA-PKcsi on 3D spheroid growth post proton irradiation..... | 185 |
| Figure 6. 19 3D spheroid formation and growth in HNSCC cell lines..... | 187 |

List of Tables

Chapter 1

| | |
|---------------------------------------------------------------------------------------|----|
| Table 1. 1 Comparisons of DSBs induced by PBT versus photon RT | 42 |
| Table 1. 2 DSB repair pathway choice following proton versus photon irradiation | 56 |

Chapter 3

| | |
|---------------------------------------------------------------------------|----|
| Table 3. 1 List of the primary antibodies..... | 74 |
| Table 3. 2 List of the fluorescently tagged secondary antibodies..... | 75 |
| Table 3. 3 List of HNSCC cell lines..... | 76 |
| Table 3. 4 Passaging of HNSCC cell lines | 78 |
| Table 3. 5 Seeding densities for colony formation assays | 87 |
| Table 3. 6 Cell concentration seeding for 3D spheroid growth assays | 89 |

Chapter 5

| | |
|--------------------------------------------------------------------------------------------------------------------------------|-----|
| Table 5. 1 ATMi on γ H2AX, 53BP1, and Rad51 foci formation alone, or in combination with x – rays or protons..... | 140 |
| Table 5. 2 ATRi on γ H2AX, 53BP1, and Rad51 foci formation alone, or in combination with x – rays or protons..... | 141 |
| Table 5. 3 DNA-PKcsi on γ H2AX, 53BP1, and Rad51 foci formation alone, or in combination with x – rays or protons. | 142 |

Chapter 6

| | |
|------------------------------------------------------------------------------------------------------------|-----|
| Table 6. 1 ATMi, ATRi or DNA-PKcsi, and x – rays decrease HNSCC cell survival..... | 150 |
| Table 6. 2 DER of ATMi, ATRi or DNA-PKcsi versus DMSO controls in HNSCC cells in response to x- rays | 151 |
| Table 6. 3 ATMi, ATRi or DNA-PKcsi and protons decrease HNSCC cell survival | 154 |
| Table 6. 4 DER of ATMi, ATRi or DNA-PKcsi versus DMSO controls in HNSCC cells in response to protons | 155 |
| Table 6. 5 Impact of ATMi, ATRi or DNA-PKcsi as a monotherapy on HNSCC spheroid growth. | 164 |
| Table 6. 6 GSR following ATMi, ATRi, or DNA-PKcsi as a monotherapy..... | 164 |
| Table 6. 7 HNSCC spheroid growth in response to ATMi and x – rays..... | 168 |
| Table 6. 8 GSR following ATM inhibition in combination with x – rays | 168 |

| | |
|--------------------------------------------------------------------------------------------------------------------|-----|
| Table 6. 9 HNSCC spheroid growth in response to ATRi and x – rays | 171 |
| Table 6. 10 GSR following ATR inhibition in combination with x – rays..... | 171 |
| Table 6. 11 HNSCC spheroid growth in response to DNA-PKcsi and x – rays | 174 |
| Table 6. 12 GSR following DNA-PKcsi inhibition in combination with x – rays | 175 |
| Table 6. 13 HNSCC spheroid growth in response to ATMi and protons | 179 |
| Table 6. 14 GSR following ATM inhibition alone or in combination with protons | 179 |
| Table 6. 15 HNSCC spheroid growth in response to ATRi and protons..... | 182 |
| Table 6. 16 GSR following ATR inhibition in combination with protons..... | 183 |
| Table 6. 17 HNSCC spheroid growth in response to DNA-PKcsi and protons..... | 186 |
| Table 6. 18 GSR following DNA-PKcsi inhibition in combination with protons..... | 186 |
| Table 6. 19 Impact of DSB repair inhibitors as a monotherapy on cell survival in 2D and 3D..... | 189 |
| Table 6. 20 Impact of ATMi in combination with x – rays or low LET protons on cell survival in 2D and 3D | 190 |
| Table 6. 21 Impact of ATRi in combination with x – rays or low LET protons on cell survival in 2D and 3D. | 190 |
| Table 6. 22 Impact of DNA-PKcsi in combination with x – rays or low LET protons on cell survival in 2D and 3D..... | 191 |

List of Abbreviations

| | |
|------------------|-----------------------------------------------------------------|
| 53BP1 | p53-binding protein 1 |
| 2D | 2 dimensional |
| 3D | 3 dimensional |
| A | Adenine |
| aDMEM/F12 | Advanced Dulbecco's Modified Eagle Medium/Nutrient mixture F-12 |
| AP site | Apurinic/apyrimidinic site |
| APE1 | AP endonuclease 1 |
| APE2 | AP endonuclease 2 |
| APLF | Aprataxin-and-PNK-like factor |
| APS | ammonium persulphate |
| ATM | Ataxia telangiectasia mutated |
| ATMi | ATM inhibitor KU-55933 |
| ATR | ATM and Rad3-related |
| ATRi | ATR inhibitor VE-821 |
| BER | Base excision repair |
| BIR | break-induced replication |
| BLM | Bloom Syndrome |
| BNCT | Boron – Neutron Capture Therapy |
| BRCA1 | Breast cancer associated protein 1 |
| BRCA2 | Breast cancer associated protein 2 |
| BSA | Bovine serum albumin |
| C | Cytosine |
| Cdc2 | Cyclin-dependent kinase 1 |
| Cdc25A | M-phase inducer phosphatase 1 |
| Cdc25C | M-phase inducer phosphatase 3 |
| CDD | Complex DNA damage |

| | |
|-------------------------|------------------------------------------------|
| CdkN2A | Cyclin dependant kinase inhibitor 2A |
| Cdk4 | Cyclin-dependent kinase 4 |
| Chk1 | Checkpoint kinase 1 |
| Chk2 | Checkpoint kinase 2 |
| CO₂ | Carbon dioxide |
| CPP32 | Caspase 3-like protease |
| ¹³⁷Cs | Radioactive caesium source |
| CT | Computed Tomography |
| CtIP | C-terminal binding protein interacting protein |
| DDB1 | DNA damage binding protein 1 |
| DDB2 | DNA damage binding protein 2 |
| DDR | DNA damage response |
| DER | Dose enhancement ratio |
| DF | Differential trypsinisation |
| DMEM | Dulbecco's modified eagle medium |
| DNA | Deoxyribonucleic acid |
| DNA lig 4 | DNA ligase 4 |
| DNA-PKcs | DNA-dependent protein kinase catalytic subunit |
| DNA-PKcsi | DNA-PKcs inhibitor NU7441 (KU-57788) |
| DSB | Double strand break |
| E6, E7 | E6, E7 oncoproteins/oncogenes |
| EC | Electron Capture |
| EDTA | Ethylenediaminetetraacetic acid |
| EGF | Epidermal growth factor |
| ERCC1 | Excision repair cross complementing protein 1 |
| EXO1 | Exonuclease 1 |
| FBS | Fetal bovine serum |

| | |
|---------------------------------|-----------------------------------------------|
| FGF | fibroblast growth factors |
| G | Guanine |
| GG-NER | Global Genome Nuclear excision repair |
| γ-H2AX | Gamma H2Ax |
| GSR | Growth suppression ratios |
| Gy | Gray |
| H2AX | Histone H2AX |
| HCT116 | Human colorectal carcinoma epithelial cells |
| HEPES | Hydroxyethyl piperazineethanesulfonic acid |
| His | Histidine |
| HNSCC | Head and neck squamous cell carcinoma |
| HPV | Human papilloma virus |
| HR | Homologous Recombination |
| ICL | interstrand crosslinks |
| IF | Immunofluorescence staining and foci analysis |
| IGPT | Image guided proton therapy |
| IMRT | Intensity modulated radiotherapy |
| IR | Ionising Radiation |
| JNK | Jun Kinase |
| kDa | Kilodalton |
| LET | Linear energy transfer |
| Lig | DNA ligase |
| Lig IIIa | DNA ligase IIIa |
| LINAC | Linear accelerator |
| MDM2 | Mouse double mutant 2 homolog |
| MEM | Minimum Essential Medium |
| MLH | Mute L homologs |

| | |
|--------------------|---------------------------------------------------------|
| MMR | Mismatch repair |
| MRI | Magnetic Resonance Imaging |
| MRN complex | Mre11-Rad50-Nbs1 |
| MSH | Mute S homologs |
| MW | Molecular weight |
| NBS1 | Nibrin |
| NER | Nuclear excision repair |
| NHEJ | Non-homologous End-joining repair |
| NI | Non-irradiated |
| NTH1 | Endonuclease III-like protein 1 |
| OARs | Organs at risk |
| OGG1 | 8-oxoguanine DNA glycosylase |
| p53 | Cellular tumour antigen p53 |
| P73 | Cellular tumour antigen p73 |
| PARP1 | Poly (ADP-ribose) polymerase 1 |
| PBS | Phosphate buffered saline |
| PBT | Proton beam therapy |
| PCNA | Proliferating cell nuclear antigen |
| PCV | Packed cell volume |
| PDO | Patient derived organoids |
| PDX | Patient derived xenografts |
| PE | Plating efficiency |
| PET | Positron Emission Tomography |
| PIKK | phosphatidylinositol-3 (PI-3) kinase-like kinase family |
| PMSF | Phenylmethylsulfonyl fluoride |
| PNKP | polynucleotide kinase-phosphatase |
| Pol b | DNA polymerase beta |

| | |
|--------------------------------------------|------------------------------------------------------------|
| Pol δ | DNA polymerase delta |
| Pol η, ζ, ι | DNA polymerase eta, zeta, iota |
| Pol II IV | DNA polymerase 2, 4 |
| Pol μ, λ | DNA polymerase mi, lambda |
| pRb | Retinoblastoma protein |
| PVDF | polyvinylidene difluoride membrane |
| RAD23B | RAD23 homolog B |
| RAD50 | DNA repair protein RAD50 |
| RAD51 | DNA repair protein RAD51 |
| RAD52 | DNA repair protein RAD52 |
| RAD53 | DNA repair protein RAD53 |
| RAD54 | DNA repair protein RAD54 |
| RAD57 | DNA repair protein RAD57 |
| RBE | Relative biological effectiveness |
| RF | Radio Frequencies |
| RNA | Ribonucleic acid |
| ROS | Reactive oxygen species |
| RPA | replication protein A |
| RT | Radiotherapy |
| S1981 | Serine 1981 |
| S2056 | Serine 2056 |
| S428 | Serine 428 |
| SCC | squamous cell carcinoma |
| SDSA | namely synthesis-dependent strand annealing |
| SDS-PAGE | Sodium dodecyl sulphate-polyacrylamide gel electrophoresis |
| SF | Survival fraction |
| SOBP | Spread-out Bragg Peak |

| | |
|--------------------|-----------------------------------------------------------------------|
| SSB | Single strand break |
| ssDNA | Single stranded DNA |
| T | Thymine |
| T1989 | threonine 1989 |
| T2609 | threonine 2609 |
| TC-NER | Transcriptional coupled Nuclear excision repair |
| TEMED | tetramethylethylenediamine |
| TFIIH | Transcription initiation factor IIH |
| TLS | Translesion synthesis |
| TMZ | Temozolomide |
| TopBP1 | DNA Topoisomerase II Binding Protein 1 |
| TOPIIIa | Topoisomerase III A |
| UMSCC47 | University of Michigan squamous cell carcinoma-47 |
| UMSCC6 | University of Michigan squamous cell carcinoma-6 |
| UMSCC74A | University of Michigan squamous cell carcinoma-74A |
| UPCI-SCC090 | University of Pittsburgh cancer institute squamous cell carcinoma-090 |
| UPCI-SCC154 | University of Pittsburgh cancer institute squamous cell carcinoma-154 |
| UV | Ultraviolet radiation |
| WB | western blot |
| WHO | World health organisation |
| WRN | Werner's syndrome helicase |
| WT | Wild type |
| XLF | XRRC4-like factor |
| XP | Xeroderma pigmentosum |
| XPA | Xeroderma pigmentosum complementation group A |
| XPB | Xeroderma pigmentosum complementation group B |
| XPC | Xeroderma pigmentosum complementation group C |

| | |
|--------------|-----------------------------------------------|
| XPD | Xeroderma pigmentosum complementation group D |
| XRCC1 | X-ray repair cross complementing protein 1 |
| XRCC2 | X-ray repair cross complementing protein 2 |
| XRCC3 | X-ray repair cross complementing protein 3 |
| XRCC4 | X-ray repair cross complementing protein 4 |
| NEAA | Non-essential amino acids |

Chapter 1: Introduction

1.1 Ionising Radiation and Radiotherapy

The physics of Radiobiology constitutes the basis for the understanding and development of modern medical applications in the widely expanding areas of diagnostic radiology, radiotherapy and nuclear medicine. It involves using radiation for numerous techniques, from imaging to therapy, and studies the radiation effects on biological tissue.

Radiation in physics describes the distinct units of energy, waves or particles, that transmit or emit through space and matter. There are several types of radiation, including electromagnetic, such as visual light, infrared and ultraviolet, acoustic radiation, such as the sound and the seismic waves, and particle radiation, such as alpha and beta radiation.

1.1.1 Electromagnetic Radiation

In electromagnetic radiation, the energy has the properties of both waves and particles, these small particles (quantum of energy) are called photons, and they have no mass and no electric charge. The energy of photons can vary widely resulting in a range of physical characteristics. High energy photons have a high frequency and a very small wavelength, as frequency and wavelength are inversely proportional according to the Planck–Einstein relation (equation 1.1). In contrast, lower energy photons, have a smaller frequency and a bigger wavelength.

$$E = h \cdot \nu \quad (1.1) \quad \nu = \frac{c}{\lambda} \quad (1.2)$$

$$E = \frac{h \cdot c}{\lambda} \quad (1.3)$$

E , is the photon energy and is measured in electron volt (eV) where 1 eV describes the energy gained by an electron as it is accelerated through a potential difference of 1 volt; $h = 6.63 \cdot 10^{-34}$ J s, is the Planck's constant; ν , is the frequency quantified in Hertz (Hz); c , is the speed of light counted in meters per second (m/s); and λ , is the wavelength measured in meters (m) (1).

As photons transmit through matter, they interact with atoms along their track losing energy and eventually stop, therefore the bigger energy and smaller wavelength allows photons to penetrate deeper into matter.

The amount of energy carried by photons is defined by the frequency of the radiation. The wide range of the electromagnetic frequencies is called electromagnetic spectrum. On the one side of the spectrum are the lower frequencies, such as radio waves ($10^7 - 10^9$ Hz) and microwaves ($10^9 - 10^{11}$ Hz), and on the other side are higher frequency radiations including x-rays ($10^{17} - 10^{18}$ Hz) and gamma rays ($10^{18} - 10^{19}$ Hz). Within that range also lies the visible spectrum ($\sim 10^{13}$ Hz), from red at a wavelength of 700 nm to violet at 400 nm. There is no distinct line between the different areas of the spectrum, on the contrary the frequency windows rather overlap with each other. The quantum nature of radiation is more important in the smaller wavelengths and higher frequencies, it is dominant in the high energy x – rays and γ – rays, but not as significant in the lower energies in radio waves and microwaves (2).

Radiation that carries enough energy, higher than that of the electrons binding energy, can temporarily or permanently remove orbital electrons from the atoms it interacts with, when travelling through matter. These atoms get excited, their electrical status changes, and they are then called ions. There are positive ions, known as cations, and negative ions, known as anions. This type of radiation is called Ionising Radiation (IR), as it can ionise the matter. Photons at very high frequencies of x-rays and γ – rays have enough energy to ionise atoms and molecules along their track into matter. As shown in Figure 1.1, in electromagnetic radiation an ionisation occurs when fast-moving photons with sufficient energy excite electrons mostly via the photoelectric, Compton and pair production effects (3).

The photoelectric effect is the most important in the lower ionising energies, between 50 and 100 keV, where the photon energy is equivalent to the binding energy of the planetary electrons in the atoms of the matter (absorber). Specifically, in that interaction, an electron in the inner orbit absorbs all of an incoming photon's energy and gets ejected, leaving a vacancy. This is filled by another electron from the outer orbit that while it drops, releases the excess energy (characteristic energy), in the form of photons. Electrons ejected from K-shell, release characteristic K x – rays and so on, and

these are characteristic of the absorber's material. Production of characteristic x – rays dominate for high atomic number materials, however for low atomic number materials such as water or tissue, auger electrons are typically emitted instead of characteristic x-rays. Either way, the atom then becomes a positively charged ion, as it has lost an electron. The photoelectric effect is used in diagnostic radiology, to produce low energy x – rays (4).

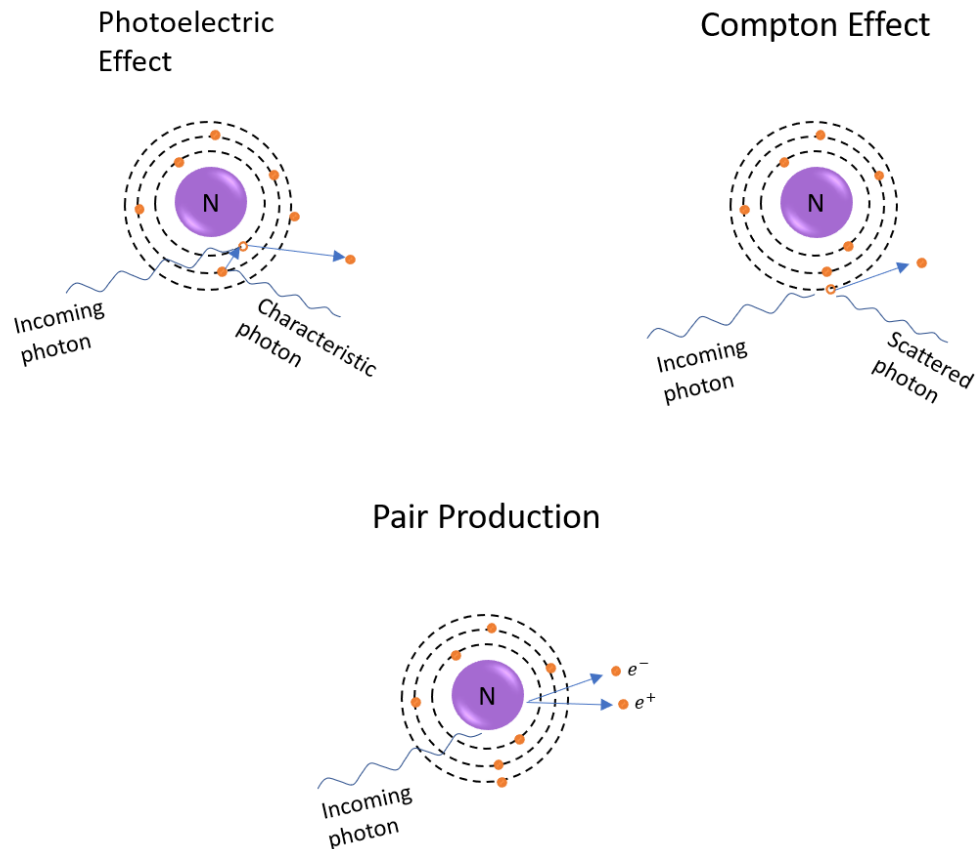


Figure 1. 1. Electromagnetic radiation interaction with matter. Electromagnetic radiation is ionising matter through 3 main mechanisms. The photoelectric effect which occurs in the lower energies, the Compton effect which is the most important effect in the median energies and the pair production which is only relevant at higher energies and above a threshold.

The Compton effect is the most important interaction in biological tissue in the middle ionising energies, between 100 keV and 10 MeV, where the photons have plenty of energy to excite an outer orbit electron, and thus ionise the atom. In this phenomenon, photons lose only part of their energy to the ejected electron, they get scattered and continue their transmission and further interactions through the absorber (5).

Finally, pair production occurs at higher energies and above a threshold of 1.02 MeV, that equals the sum of the mass (energies) of the produced particles. The higher the photons energy the most possible is an event of pair production. During this process, a fast moving photon in close proximity to a nucleus is absorbed by nucleus directly and provides all its energy to the production of a pair of an electron and positron, any remaining energy is distributed between the pair as kinetic energy. The presence of the nucleus satisfies the conservation of momentum. Spontaneous ejection of neutrons may occur simultaneously. This effect arises in radiotherapy units, where x – rays of at least 10 MV are used, raising the shielding requirements to protect not only from the high penetrate x – rays but also from the produced neutrons (3).

1.1.2. Particle Radiation

In particle radiation, the energy is transmitted and emitted in particles. In this radiation type, particles are the equivalent of photons of the electromagnetic radiation. There are numerous types of particle radiations, named usually after the main particle carrying the energy. The particles can be positively or negatively charged, such as protons and electron respectively, as well as electrically uncharged, including neutrons. Moreover, particle radiation can consist of heavier particles, atoms or ions, an example being the carbon ion radiation. Here are discussed some well-studied particle radiations.

Similarly to photons, as particles transmit through matter they interact with atoms along their track in many small steps, losing energy. Thus, generally the higher the particle's energy, the further it can penetrate into matter. Particles with energy greater than the binding energy of the planetary electrons (ionising energy) can produce multiple ionisations along their track. Following a few interactions and possible change of direction, the particles eventually stop. The depth that they can penetrate into matter is called the particle range, that is defined by the Bethe – Bloch formula as the mean energy loss per distance travelled and is dependent on the atomic number and density of the absorber, as well as the mass and the energy of the particles (6, 7).

Charged particles interact directly with the absorber's atoms, mainly with Coulomb forces. These interactions occur between the electric field of the charged particle and the electric field of the absorber's electrons or nuclei. There are three categories of

particle interactions; the hard collisions where there is close encounter, equivalent to the atomic radius, between the charged particle and the orbital electron; the soft collisions, where there is distant encounter, greater than the atomic radius, between the charged particle and the orbital electron; and the radiative collisions, where there is a very close encounter between the charged particle and the nucleus.

In all three collision types, the momentum conservation law dictates that the particles velocity and therefore its energy, is inversely proportional to the energy transfer, as indicated in equation 1.8. In other words, high energy particles transfer only a small amount of energy to the atomic electrons, as they have a large velocity and only stay in the proximity of the electrons a short amount of time. Moreover, the energy transfer is inversely proportional to the encounter distance, hence the closer the proximity between the interacting parts, the larger the energy transfer. This is particularly important in high density materials, where the atoms are closely packed, and the interaction probability increases for particles of a given velocity. Therefore, the incoming particles lose energy quicker and cannot penetrate deep into high density materials. Such high-density materials are used as shielding in radiology and radiotherapy units, due to their ability to block radiation penetrance.

$$E = mv^2 \quad (1.4) \quad \vec{p} = m\vec{v} \quad (1.5)$$

$$\Delta E = \frac{(\Delta p)^2}{2m_o} \quad (1.6)$$

$$\Delta p = \int F dt = \frac{a}{b v} \quad (1.7)$$

$$\Delta E = \frac{a^2}{2m_o b^2 v^2} = \frac{a^2}{2m_o b} \frac{m}{E} \quad (1.8)$$

E, is the particle's energy; m, the particle's mass; and v, is velocity; p, is the particle's momentum (1.5). ΔE and Δp refer to the alteration in the energy and the momentum of the particle during the collision and describe the occurring energy transfer; and m_o, is the rest mass of the particle (1.6). F, is the force applied in the particle by the electric field of the nucleus and electrons; dt, is the time alteration and refers to how much time the interaction lasted; α, is a variable defined by a number of factors including, the radius of the atom, the electric charge and the rest mass of the particle; b, is a variable describing the distance between the particle and the nucleus during the interaction (1.7, 1.8) (8).

Finally, the particles mass is proportional to the energy transfer, so heavier particles are more likely to have less interactions with bigger energy losses as they travel through matter (8, 9).

In hard collision, the ejected electron absorbs a large amount of energy and is transmitted through the absorber, having its own interactions and ionisations along its track, the amount of hard collisions however is small. In soft collisions, the ejected electron absorbs a part of energy that is inversely proportional to the original energy, and proportional to the mass of the incident particle, and thus is most important in heavier particles of lower energies. Finally, in the radiative collision, a fast-moving charged particle approaching the nucleus, gets trapped in the electrostatic field. The particle then accelerates and diverts from its path as it momentarily orbits around the nucleus, before it is released with simultaneous emission of electromagnetic radiation (x – rays). The particle then gets decelerated and follows the diverted track. The emitted x – rays interact with the absorber, ionizing atoms along their track via the electromagnetic radiation effects. The energy loss in this effect is inversely proportional to the mass of the particle, therefore is most important in lighter particles. In fact, the energy from the deceleration of electrons is around 4 million times higher than that of equivalent kinetic energy protons. The x – ray production through this deceleration effect is known as bremsstrahlung, which means *braking radiation* in German. Bremsstrahlung will be further discussed below.

It is worth noting that hard collisions between free electrons (incoming particle radiation) and atomic electrons may also result in large energy loss and diverted trajectories, not observed in the rest of the charged particles radiations. This is partly because the two interacting parts have the same mass, but also due to the small mass of the electrons, which makes the relativistic effects important even from low energies, and large energy loss and change in the direction is more often (8, 9).

In general, as illustrated in a schematic representation in Figure 1.2, charged particles lose energy gradually in multiple collisions with mostly small energy transfers. As the mass and energy of the particles increases, there are less interactions, but they carry bigger energy depositions and there is less diversion from the original track. Whereas

light particles of lower energies (electrons and positrons) lose energy in multiple ionisations, get scattered and decelerate, soon after they enter matter.

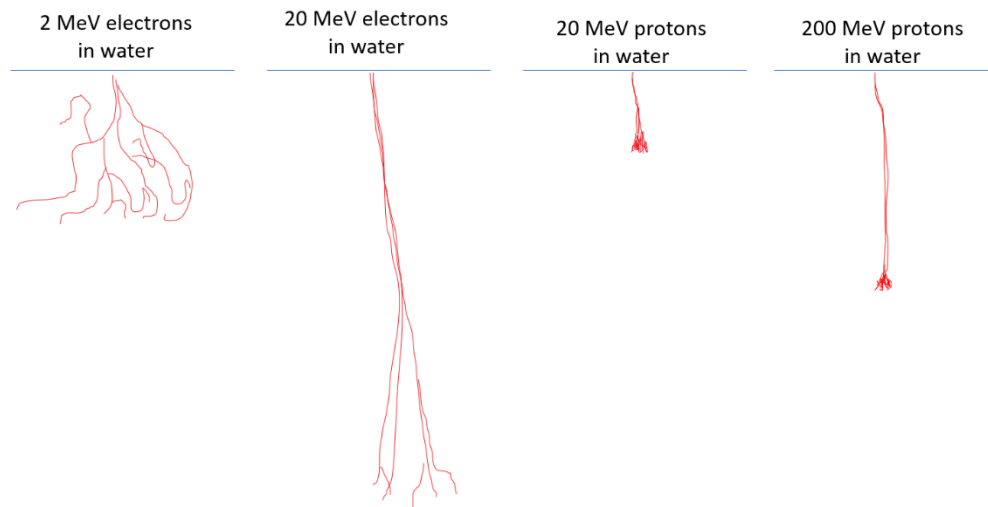


Figure 1. 2. Schematic representation of charged particles tracks in water. The energy transfer is inversely proportional to the particles energy and proportional to the particles mass. Lighter particles, such as electrons, of low energies are more likely to have plenty of interactions with small energy transfers and they are not expected to penetrate deep into matter. As their energy increases, so does their velocity, and the number of interactions decreases since they only stay in the proximity of the atomic electrons a short amount of time; they get less scattered and penetrate deeper into matter. For similar energy, heavier particles like protons, produce a few interactions yet with big energy losses and the particles stop before they travel deep in to matter. As the heavy particles energy increase, they can reach further into matter without interacting before they give all their energy in very few collisions and eventually stop.

Uncharged particles (neutrons), interact with matter in a different way compared to the charged particles, as they have mass but no electric charge. The energy loss is defined by the neutrons energy and the density of the absorber, and occurs in multiple steps through the elastic scattering, inelastic scattering, radioactive integration and nuclear reactions. Elastic scatter is the most important mechanism of energy transfer in biological tissues. Approximately 85% of the energy loss of neutrons occurs following the elastic scattering of the fast neutrons by the hydrogen atoms (H_2) of the tissue. In inelastic scattering, electromagnetic energy (γ – ray) is released and is more important in heavier absorbers (with higher atomic and mass number). In radioactive integration, a fast neutron is captured by a nucleus, the produced nucleus is then unstable and decays with the ejection of electrons and γ – rays. Finally, during nuclear reactions, a

mother nucleus captures the fast neutron to produce a daughter nucleus and other particles, like protons, neutrons or other smaller nuclei (10).

1.1.3 Clinically used Radiation types

Radiation has multiple uses in medicine, both in diagnosis and in treatment. In this section, the most used radiation types are discussed in more detail.

1.1.3.1. Alpha particle radiation

The α particle radiation, is produced through the α disintegration. In this nuclear process α particles, which are in fact Helium atoms (${}^4_2\text{He}$) consisting of 2 protons and 2 neutrons, are emitted when an unstable heavy nucleus decays spontaneously into an α particle and another heavy nucleus, in order to become more physically stable. The α particles absorb a part of the released nuclear energy as their own kinetic energy. They have a positive charge and produce intense ionisations by stripping the electrons from the atoms along their track. They usually have a high energy, but very small range, and are stopped within μm of biological tissue (11, 12). α particle emitters are often used in brachytherapy, a type of radiation therapy where a radioactive source is inserted into or next to the area of interest. This is achieved either as an open source treatment, where the high energy and small range of α particles is ensuring significant targeted tumour damage; or as sealed sources, where the tumour damage is achieved by secondary γ -rays or other emissions associated with the decay of α particles (13).

1.1.3.2 Beta particle radiation

β particle radiation occurs through the β decay via three different types. The β^- radiation, is produced when an unstable heavy nucleus spontaneously decays by emitting β^- particles, which in fact are electrons, and energy. Similarly, the β^+ -radiation is released when an unstable heavy nucleus spontaneously decays by emitting β^+ -particles, also known as positrons (positive electrons), and energy. Finally, the Electron Capture (EC) process occurs when an unstable heavy nucleus absorbs an atomic electron, usually from the K-shell, realising energy. The K-shell vacancy is then filled by an electron of the outer orbit with the simultaneous release of x-rays. This process is antagonistic to the β^+ decay. In all cases, the nucleus decays to produce a more stable daughter nucleus, and

the nuclear energy released is distributed between the products of the decay (11, 14). β particles carry enough energy to produce multiple ionisations, but also offer a relatively narrow range between μm to mm , depending on the isotope producing them, and are profoundly used in brachytherapy (13).

1.1.3.3 Gamma radiation (γ – rays)

γ radiation is electromagnetic radiation, travelling through space and matter in the form of waves and photons. The γ rays are emitted following nuclear reactions and are usually the by-product of an α or β decay, as in most cases the daughter nucleus is created in an already excited state. These short living nuclei are de-excited mainly through γ decay, releasing γ – rays with a discrete spectra characteristic of the parent-daughter nuclei. The γ – rays are highly penetrating as they often carry a large proportion of the nuclear excitation energy (15). γ – rays were used in radiotherapy (i.e. cobalt units), but these have now been replaced by modern x – ray units, and are currently used in Gamma Knife for stereotactic radiosurgery (16). They are currently used in Positron emission tomography (PET) scan for diagnostic purposes, where annihilation of the a positron with an electron emit two back-to-back 0.511MeV γ – ray photons, as a result of mass being converted to energy, imaging the metabolic activity of tumours (17).

1.1.3.4 X – rays

As electromagnetic radiation, x – rays consist of photons. They have a similar spectrum range to γ – rays, the only difference being the origin of the radiation, γ – rays are the product of radio nuclear reaction, whereas x – rays are produced through the photoelectric effect, where there is distinct characteristic spectrum, and through the deceleration effect, known as bremsstrahlung. As demonstrated in Figure 1.3, bremsstrahlung occurs when a fast charged particle (e.g. electron) travelling in close proximity to a nucleus, is temporarily trapped in the electrostatic field and accelerates while it orbits around the nucleus, then decelerates producing x – rays before it breaks free to continue travelling in a diverted track. The energy of the newly produced x – rays depends on the energy lost, hence of the acceleration – deceleration process of the electron while it deflects trapped in the nucleus field. The longer it stays in orbit, the

more it accelerates and the more energy is released when it decelerates, resulting in higher energy x – rays (Figure 1.3) (15, 18).

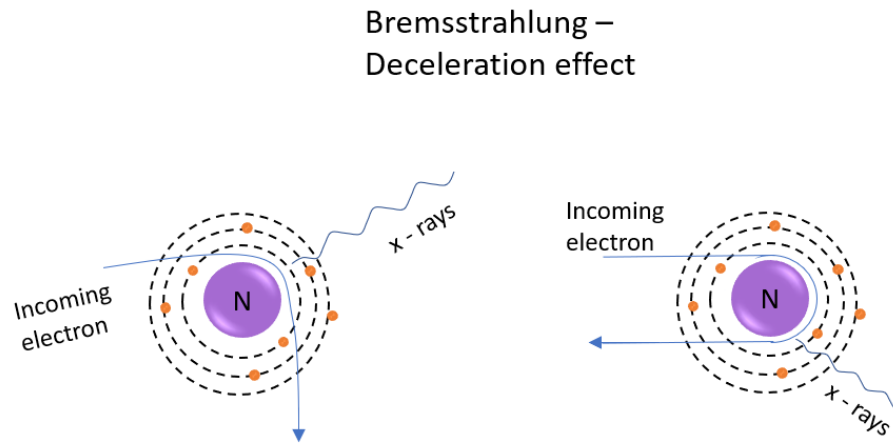


Figure 1. 3. Bremsstrahlung – Deceleration effect. Bremsstrahlung occurs when a charged particle and the nucleus are in close proximity. The particle gets trapped in the electrostatic field and accelerates while orbits around the nucleus, then decelerates producing x – rays before it breaks free to continue travelling in a diverted track. The longer it stays in orbit, the more it accelerates, and the more energy is released when it decelerates, resulting in higher energy x – rays, of higher frequency and smaller wavelength. This phenomenon is much more important in electrons than in any other charged particle, due to its small mass.

X – rays transmitting through biological tissue, lead to several ionisations due to the photon interaction with atoms, but moreover due to the subsequent production of quite a few electrons. When each of these electrons slows down, they too interact with the tissue producing further ionisations. Therefore, the biological effect of x – rays depends not only on the initial radiation, but also on the secondary electrons produced.

X – rays are widely used in medicine, lower energies for imaging in radiology and dentistry and higher energies for therapy, particularly in cancer patients. The most commonly used x – ray generators are the x – ray tubes, which consist of an evacuated glass cylinder that contains a tungsten filament cathode and an anode, usually made also of tungsten, illustrate in Figure 1.4. When the filament is heated there is a significant

number of electrons that escape its surface, the electrons travel then through the vacuum to the positively charged anode forming a current, and they get accelerated. Once the electrons reach the anode, they hit the high-density material and slow down, producing x – rays. The x – rays produced are emitted to all directions, and only a small amount of them, that head to the exit window, will be used, while the rest are absorbed by the anode. The tube current depends on the voltage applied, the target material and the filament excitation but also on other tube characteristics such as the distance between the cathode – anode and the filament temperature (8).

Diagnostic and therapeutic tubes produce quite a different x – ray spectrum. Lower voltage (≤ 100 kV) applied in diagnostic tubes result in only about 1% production of x – rays through bremsstrahlung and about 30% production of characteristic x – rays, since most of the electrons will be either absorbed by the anode producing heat or produce secondary ionisation through soft collisions. Whereas, the higher voltage (\sim few MV) applied in therapeutic tubes leads to almost 95% bremsstrahlung x – rays and only 1-2% characteristic x – rays, as the majority of electrons will interact with radiative collision (8, 18). The x – ray units used in cancer radiotherapy are mostly linear accelerators (LINAC) that use high voltage electric field and accelerate electrons through a long tube to produce high energy photon beams. LINACS usually offer two modes, the photon and the electron mode. The former is the produced photon beam, the latter is an electron beam, consisting of the accelerated electrons that exit the tube without hitting the target (19).

Once the beam exits the LINACS tube, it is processed through a series of components, used in both modes. The photon or electron beam is shaped through a series of high-density collimators, to produce the required field of radiation and gets flattened to become evenly distributed across the field. Low energy electrons that can contaminate the beam, and increase the skin (surface) radiation dose, without contributing into image quality or radiotherapeutic result, are removed using appropriate filters. The radiation dose is monitored through a pair of ion chambers and finally a light localizer is used to confirm right positioning of the patient before any radiation is applied. The head of the LINAC, called a gantry, is designed to turn 360° around its axis, allowing to irradiate without any change in patient position. Accuracy and reproducibility of the

positioning and proper delivery of radiation is highly important, to achieve tumour control while protecting the surrounding healthy tissue, particularly the organs at risk (OARs). Many modern LINACs are now combined with imaging guidance units such as MRI (Magnetic Resonance Imaging) or cone beam CT (computed tomography) to optimise the therapeutic potential while ensuring safe and accurate treatment delivery (20-23).

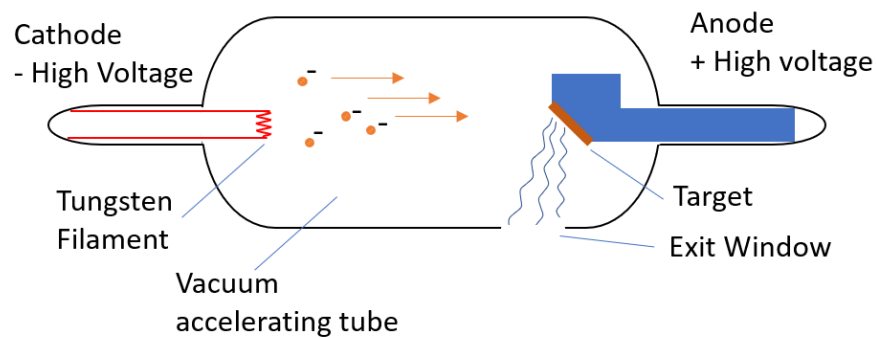


Figure 1. 4. X – ray tube. Schematic representation of an x – ray tube. The x – rays are generated in a vacuum cylinder that contains a negatively charged cathode and a positively charged anode. The cathode’s tungsten filament is heated, and a number of electrons escape its surface, and travel through the vacuum getting accelerated. The fast electrons hit the high-density material and slow down, producing x -rays. The x – ray energy depends on the tube characteristics like the voltage applied, the target’s material and any subsequent filtration.

1.1.3.5 Proton radiation

Proton radiation is positively charged particle radiation. High energy protons can travel through matter with minimal interactions, releasing small energy units, before they eventually stop depositing all their remaining energy in a small and finite region. This is due to only few ionisations occurring along their track and multiple hard collisions in depth of the biological tissue. As shown in Figure 1.5, these physical characteristics, present protons with a great advantage over conventional x – ray radiotherapy, as they produce a low entrance dose that peaks in depth at a narrow and well-defined range, called the Bragg peak, sparing the surrounding tissue and OARs in close proximity to the tumour – target, which is particularly important for children and younger patients.

A combination of beams with different initial energies can produce a wider peak, the so-called spread-out Bragg peak (SOBP), allowing to irradiate larger target volumes (24).

Proton beams are typically accelerated in circular accelerators called cyclotrons. A cyclotron consists of two poles of a large circular magnet over two D-shaped conductors, (electrodes) with a narrow gap in between, connected to an oscillator of high frequency (radio waves) and high alternating voltage (~ 20 keV) (Figure 1.6). The magnet produces a strong magnetic field while the oscillator produces a high frequency electric field. The two hollow conductors have opposite polarity, and they switch potential constantly oscillating between positive and negative charge. The electromagnetic field can be variable to achieve the desired particle accelerations by shifting the frequency of the applied electric field. The cyclotron frequency is not dependent on the particle's energy and radius, but rather on their charge to mass ratio (e/m). The cyclotron unit is placed within a vacuum cylinder. Modern cyclotrons now include superconducting magnets that are particle and energy variable and can reach relativistic energies for most ions.

In proton cyclotrons, protons are released between the two electrodes, when hydrogen atoms are bombarded by electrons escaping a tungsten filament, similar to the one used in x – ray tubes (Figure 1.4). The electric forces push the positive protons on to the negative electrode. Once there, the magnetic forces shove protons to move along the electrode in circular or spiral trajectories gaining speed and energy. When the polarity changes, protons move towards the new negative conductor, due to the electric forces and as soon as they reach it, they again move in the arc of the electrode, gaining speed and energy. As they move faster, they orbit in a larger circle. That process continues and the particles get accelerated until they reach the required energy before they exit the cyclotron. Cyclotrons produce very high and very stable energy particle beams, but they have high requirements for power consumption and its relatively difficult to achieve different beam energies (25-27).

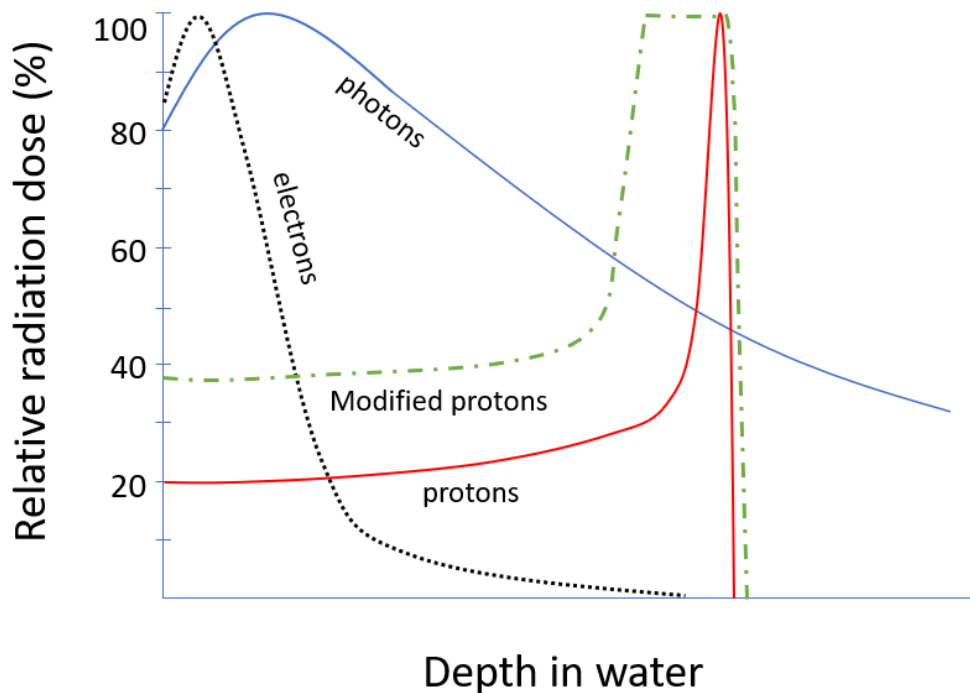


Figure 1. 5. Relative radiation dose in depth. Qualitative representation of energy deposition in water (biological tissue equivalent). Photons deposit their maximum energy after a short build-up region, and they continue to interact with mater releasing energy along their track. Electrons energy deposition peaks very close to the surface but quickly lose all their energy and eventually stop. Monoenergetic protons travel through matter with minimal interactions, before they completely stop depositing all their energy in a small and finite region, the Bragg Peak. Similarly, modified energy protons have a low entrance dose and give multiple neighbouring peaks that produce a wider peak, the so-called spread-out Bragg peak.

Extraction of the proton beam is achieved by placing an electrostatic deflector at the extraction radius of the cyclotron. The deflector consists of a complex of two electrodes, one with ground potential and one with high negative voltage, that greatly attracts the positively charged particles. The strong electric field guides the thin monoenergetic proton beam outside of the cyclotron's magnetic field. A series of bending magnets, that can both deflect and focus the beam (dipole magnets and quadruple magnets respectively), drive the beam through the vacuum to the patient either as a fixed beam line or through a gantry. A proton gantry, similar to an electron or x – ray gantry, can turn 360° around its isocentre, to access the tumour from any angle (28-30). The energy can be modulated, through a range shifter, and it can break into multiple energy beams

that will deposit their peak energy over multiple depths, covering a bigger volume of the tumour. In order to broaden the radiation field laterally, a set of scatter foils is used, equivalent to a photon flattening filter. The first one, is a uniform foil that creates a Gaussian distribution of protons, while the second one is a non-uniform foil through which the central protons of the beam are scattered to a greater degree compared to the outer protons, resulting in a uniform radiation field. The beam is then shaped, through a series of high-density collimators, and the radiation dose is monitored, using a pair of ionisation chambers. This is called a passive scattered system. A newer system, called a spot scanning system, uses magnets to shift the proton beam across the tumour, allowing for better shaping of the distal and proximal ends of the proton beam. Moreover, it provides the advantage of precise 3D dose distribution, also called dose painting (31, 32).

Cyclotrons are also used for the acceleration of heavier particles in medicine, including carbon ions, but they are not suitable for the acceleration of uncharged particles, since the electric field is not able to set them into movement. Equally, the cyclotron is not suitable for the acceleration of electrons, because the relativistic effects are important, and their mass will significantly increase with velocity even in low energies (8). The relativistic effects in protons are important for energies higher than some tens of MeV. To overcome this limitation and achieve higher energy proton beams, two alternate cyclotrons are available. The first is a synchrocyclotron, where a stable magnetic field is applied along with an accelerating radio frequency (RF) field, following the mass acceleration, to provide particle synchronism. The second is an isochronous-cyclotron, where a stable RF field and a variable magnetic field is applied causing particles to maintain a constant orbital period (25, 26, 28, 33).

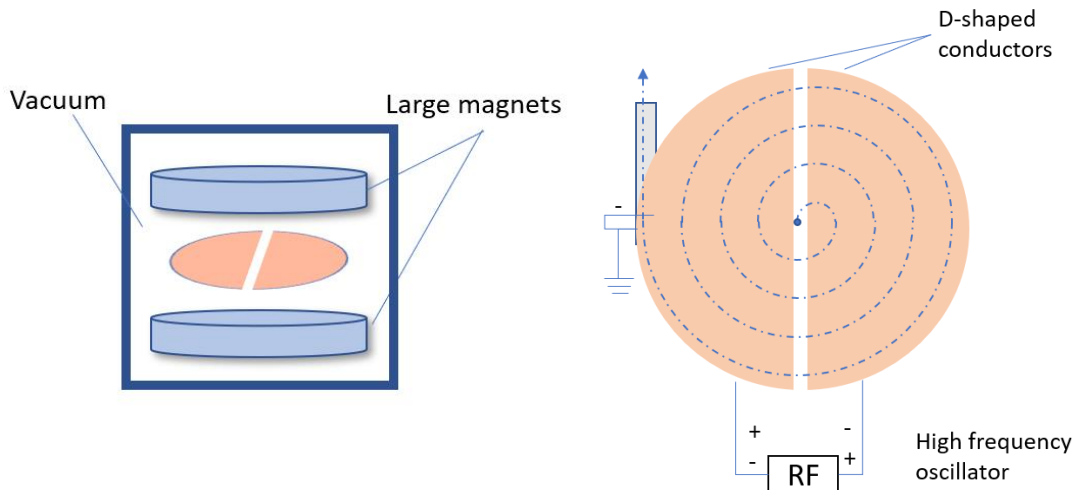


Figure 1. 6. Schematic representation of a cyclotron. A cyclotron consists of the two poles of a large circular magnet over two D – shaped conductors, with a narrow gap in between, placed within a vacuum cylinder. The magnet produces a strong magnetic field while the conductors are connected to an oscillator, that produces a high frequency (RF) alternating electric field. The two hollow conductors have opposite polarity, and they switch potential constantly. The electric forces push the positive protons on to the negative electrode, once there, the magnetic forces force the protons to move along the electrode gaining speed and energy. A deflector extracts the beam with a strong negatively charged electric field.

Proton beams accelerated in medical cyclotrons have many more applications in medicine apart from directly been used in cancer radiotherapy. For example they are used in Boron Neutron capture therapy (BNCT), where the accelerated protons produce neutron beams, that are directed on to the Boron injected tumour. The Boron – Neutron interaction releases high energy α particles, that due to their small range (few mm), selectively and severely damage the tumour (34). Another use of proton beams outside proton radiotherapy is for the production of radioisotopes for positron emission tomography (PET) imaging (35).

1.2 DNA damage and repair

Induction of DNA damage occurs naturally and spontaneously during the lifespan of mammalian cells. It has been estimated that each cell suffers tens of thousands DNA lesions per day that may be through endogenous sources, including via metabolism and errors during DNA replication, or externally induced by stressing factors, such as heat fluctuation, ultraviolet and ionising radiation (IR), environmental chemicals and more (36). As discussed previously, IR produces multiple ionisations in the atoms, inducing DNA damage which could potentially kill the cells. This property of IR is used therapeutically in radiation oncology, where tumour are exposed to high doses of IR, eventually promoting tumour cell death. External photon beam radiotherapy, a well – established treatment used worldwide includes different techniques, such as conventional radiotherapy (RT), 3D RT, intensity modulated RT (IMRT), and image guided RT (IGRT), where this utilises high voltage x – ray irradiation (photons) (37, 38). Proton beam therapy (PBT), uses protons instead of photons, it is a fairly new and promising radiation treatment, including a variety of delivery methods, such as image guided proton therapy (IGPT) and dose painting PBT, that is gaining ground in radiation oncology thanks to its radiobiological and physical advantages over photon radiotherapy (39-41). Both radiation modalities have a common target, to introduce severe physical damage, that lead to chemical and biological damage within the DNA of the cells, threatening the genome stability and proliferation of the tumour cells.

1.2.1 The DNA

Damage into the cellular DNA can affect the integrity of the molecule, which is required for cell survival. DNA, deoxyribonucleic acid, is a macromolecule that carries all the genetic information required for cell proliferation, stored in the cell's nucleus. In eukaryotes small amounts of DNA is also stored in mitochondria. The structure of the DNA was discovered in 1953 to be a double helix, similar to a twirling ladder, using x – ray diffraction analysis (42). The two long polymer strands are composed by 4 types of nucleotides. The chemical structure of the nucleotides is that of a five – carbon sugar, in the case of DNA the sugar is deoxyribose, a phosphate group (PO_4H_3), and a nitrogen – containing base, which can be either adenine (A), thymine (T), guanine (G) or cytosine

(C) (Figure 1.7). Phosphodiester bonds between sugar – phosphate backbone, strongly connects the nucleotides producing the basis of the two chains, while hydrogen bonds between the bases hold the two chains together. The bases face inside the double helix and are complementary to each other, two-ring bases, called purines, pair with single-ring bases, called pyrimidines. In fact, A always pairs with T, and G with C, to hold an equal distance between the two chains and secure the most stable structure (Figure 1.8).

After every ten base pairs the helix completes a full turn, to maximize its stability. The chain structure provides a chemical polarity, as along the chain there are several nucleotides with the same orientation, but at the end of the chain can be either a phosphate group at the 5' end, or a sugar (containing a terminal hydroxyl group) at the 3' end. The double helix is formed by antiparallel chains with opposite polarities, this means that in the one end of the double helix there is a 5' end on strand A and a 3' end on strand B, on the other end of the helix there is a 3' end on strand A and a 5' end on strand B (Figure 1.8).

The DNA sequence is encoded using the 4 nucleotides. Human cells contain DNA that consists of approximately 3.2×10^9 nucleotides and is about 2 m long if stretched in a straight line, yet is securely packed to fit within the 6 μm in diameter nucleus of the cell. To achieve that, the genetic information is stored in compact structures called chromosomes. Each chromosome consists of a very long but tightly and orderly packed DNA molecule, along with proteins, histones and non-histone chromosomal proteins. The complex of DNA and proteins is also known as chromatin.

The long DNA molecule is folded, around histone octamers, a combination of eight histone proteins, two of each of H2A, H2B, H3, and H4, forming core particles called nucleosomes. The DNA helix is wrapped in two tight turns around each octamer. Nucleosomes contain 146 nucleotide pairs and are connected with linker DNA of up to 80 nucleotide pairs, but the spacing between the nucleosomes varies. Human cells have approximately 30 million nucleosomes stored in 23 pairs of chromosomes.

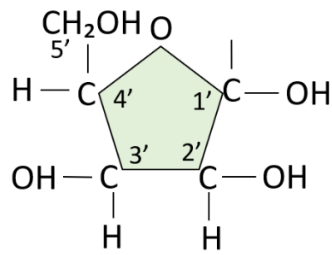
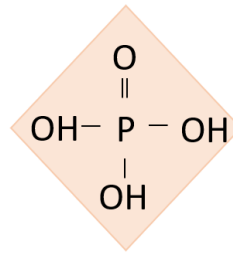
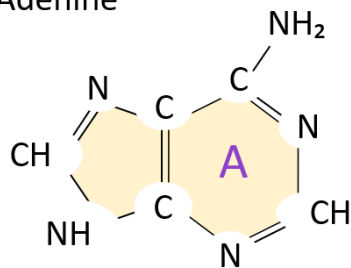
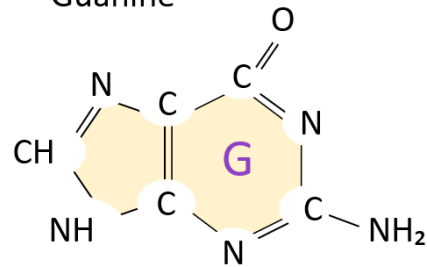
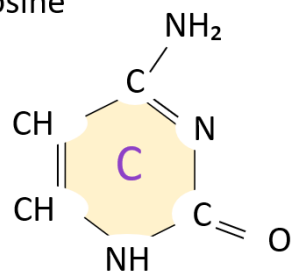
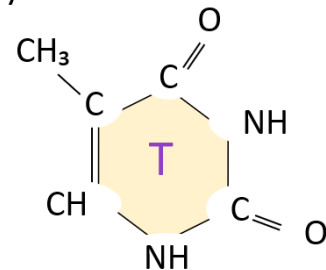
A Pentose Deoxyribose**B Phosphate****C Purines****Adenine****Guanine****D Pyrimidines****Cytosine****Thymine**

Figure 1. 7. DNA Components. A nucleotide consists of a five-carbon sugar, a phosphate group and a nitrogen containing base. A) Pentose Deoxyribose is the five-carbon sugar found in the DNA nucleotides. B) Phosphate group, PO_4H_3 , and pentose are linked with phosphodiester bonds in the 3' and 5' carbon of the sugar to form the core of the DNA strand. C) Purines, are the two ring Nitrogen containing bases, Adenine and Guanine. D) Pyrimidines, are the single ring Nitrogen containing bases, Cytosine and Thymine.

Cellular genome is composed of genes, DNA segments encoding the sequence to produce a specific protein or a set of related proteins, and RNA molecules, responsible for the structural and catalytic function of the cells. There are about 30,000 genes included in the human DNA, the average size of a human gene is 27,000 nucleotide pairs, yet only about 1,300 nucleotide pairs are required to encode an average size protein (approximately 430 amino acids). The remaining parts are either sequences that regulate proper gene expression, or large noncoding DNA sequences, called introns, in between the coding parts of the sequence, called exons. Interestingly, there are plenty of noncoding DNA segments, also called junk DNA, that contain non-essential information, and that its role and importance has not yet been identified.

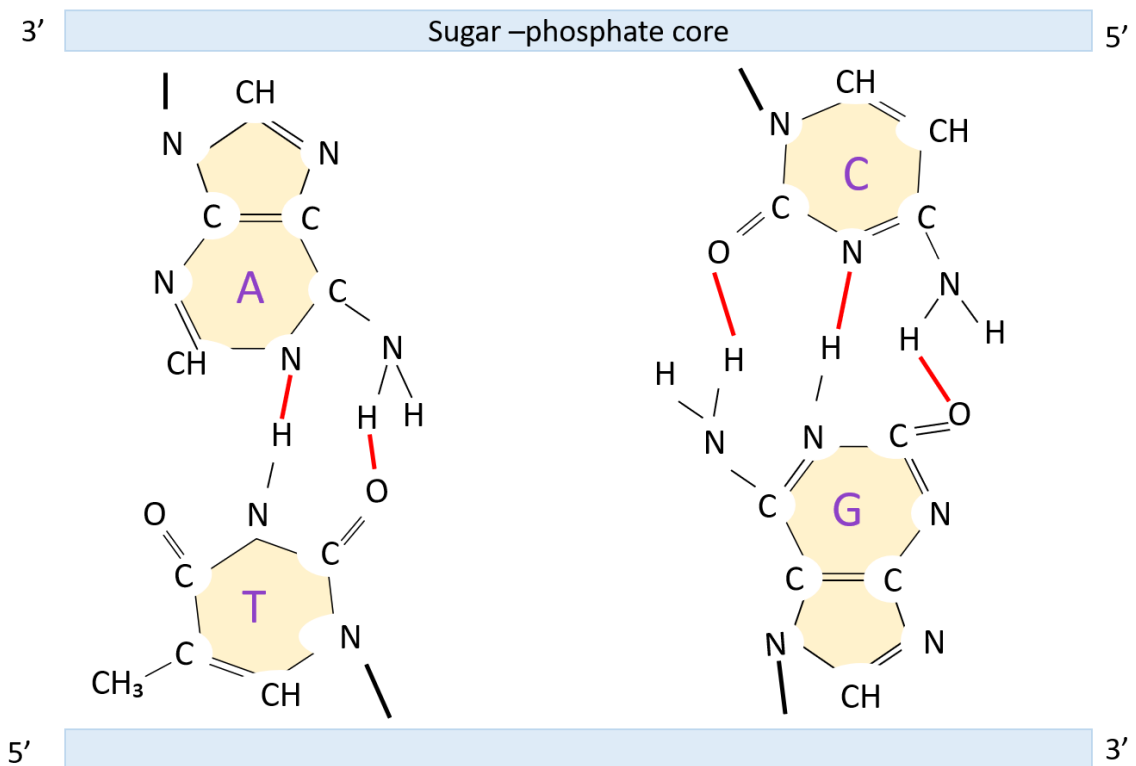


Figure 1. 8. DNA structure and base formation. The DNA helix is composed of a series of nucleotides, with the sugar-phosphate backbone forming the strong core of the two antiparallel strands, and the inside facing bases holding the two strands together, forming base pairs. A is always paired with T, G is always paired with C, to hold an equal distance between the two chains and secure the most stable structure. The bases are connected with Hydrogen bonds shown in red lines.

Generally, the more complex species tend to have more genes, nevertheless due to the large amounts of excess DNA there is no direct connection between species complexity and chromosomal number or genome size, and there are big differences observed even in closely related species (43).

1.2.2 Cell cycle

The genetic information, encoded in the DNA of the cell is passing from a parent cell to its daughter cells, through repetitive cell divisions. A cell is essentially created by a parental cell, that grows and duplicates its contents before it divides into two new genetically identical daughter cells. Cell life, known as cell cycle, is divided in four phases and is controlled and coordinated by a complex network of regulatory proteins, that promote progression from one phase to the next one or can temporarily hold it and even lead cell to programmed cell death (apoptosis) if necessary.

1.2.2.1 Cell cycle phases

The two major cell cycle phases are synthesis (S) and mitosis (M), separated by two interfering phases the gap 1 (G1) and the gap 2 (G2) phases. In addition to these, there is an extra phase, the gap 0 (G0), which includes cells at a resting stage that can last from days to years before cells resume proliferation or be led to apoptosis.

The cell cycle begins at G1, allowing time for cell growth but also ensuring extracellular environmental conditions are suitable before progressing into the next phases. Next is S, a long-lasting phase (10 – 12 hours for mammalian cells) during which the DNA is carefully replicated. The chromosomes get untangled, and the two DNA strands are separated, each to be used as a template for the creation of a complementary strand to produce two full DNA double helices. G2 follows, allowing time for further cell growth as well as replication of other cell components such as proteins and organelles. Finally, when all the components are ready the cell is divided in M phase, a process that is completed within 1 h. During M phase, the duplicated DNA is concentrated into chromosomes, which are aligned on the assembled mitotic spindle in the central region of the cell. The sister chromatids are separated and head in opposite directions of the dividing cell, forming two intact nuclei while the cytoplasm is torn into two (43, 44).

1.2.2.2 Cell cycle control

The cell cycle control system is driven by a family of cyclin-dependent protein kinases (Cdks). Their activation is regulated by cyclins, cyclically activated subunits, and results in phosphorylation of intracellular proteins that initiate cell cycle progression to the next phase and prevents any of the completed phases to be repeated. The main cyclin complexes in eukaryotic cells are G1-Cdk, where extracellular signals initiate the cell cycle, G1/S-Cdk, which drive the cell to enter S phase, S-Cdk, which lead to cell replication, and M-Cdk that trigger mitosis.

In addition the Cdk protein complexes can arrest the cell cycle at specific checkpoints. A negative signal can block progression into the next phase until the one undergoing is fully completed. This is particularly important in case of DNA damage, where the checkpoints allow for DNA repair. For example DNA damage in cells in G1 phase results in phosphorylation of p53, a regulatory protein that stimulates transcription of several genes including p21, a protein that binds in G1-Cdk and G1/S-Cdk complexes, prohibiting their activation and progression in S phase. DNA damage in cells in G2 initiates a series of protein kinases that block activation of M-Cdk complexes and thus progression to M phase (43, 44).

1.2.2.3 Programmed cell death – apoptosis

To secure genomic integrity, cells that are no longer needed or with irreparable DNA damage can undergo programmed cell death, also known as apoptosis. Apoptosis is a neat process, during which the cell collapses from within, the biological components get recycled, and there is no damage caused to the neighboring cells. The process is driven by the proteolytic enzymes caspases that can cleave specific proteins initiating cell death. Multiple caspases exist within the cells in the inactive form of procaspases and can be activated by either extracellular or intracellular signals. Once activated caspase cleaves and activates more procaspases, within the cell, leading to an irreversible caspase cascade and cell death (45).

1.2.3 Induction of DNA lesions

DNA damage, as well as being continuously formed endogenously, is also exogenously induced by several damaging agents, with IR being one of the most critical ones. IR interacts with matter on multiple levels, there are numerous events triggered instantly post-exposure and effects that can be seen from weeks to even years later. The events can be broadly divided in three main phases, according to the main effects produced, the physical ($\leq 10^{-14}$ s), the chemical ($10^{-12} - 10^{-3}$ s) and the biological (10 s \sim days). Late stage effects fall into physiological and epidemiological processes. There are no distinct lines to discriminate the different phases, rather they overlap. The physical and chemical phases overlap in the physiochemical phase ($10^{-14} - 10^{-12}$ s), while the chemical and biological phases overlap at $10^{-3} - 10$ s post-irradiation (46). There are a variety of mechanisms involved in the radiobiological processes that are discussed below.

1.2.3.1 Physical damage

Immediately after exposure to IR, the physical phase begins where distribution of ionisation events and energy deposition in the cellular components occurs. The energy deposition depends on the radiation dose, the initial beam energy as well as the type of the radiation. At this stage, there are two types of effects initiated; direct ionisation in the atoms of the DNA molecule and thus direct damage, such as strand breaks and base losses (abasic sites); and ionisations and energy deposition in the atoms of other cellular components, particularly the water that constitutes about 70 % of the cell mass (47). The physical damage at the cellular level is considered a stochastic effect, meaning that there is a proportional (linear) dependence on radiation dose. In other words, the higher the radiation dose the more the ionisations and DNA breaks (42). However, for a given radiation type, higher initial beam energy results in increased penetration, and a peak of energy deposition deeper into biological tissue, something that alters the ionisation track, particularly for particle beams. Therefore, in each region the amount of physical damage depends on the beam's energy.

Furthermore, different radiation types have different interactions and effective ranges, as discussed in Chapter 1.1.3. X – rays travel through biological tissue losing energy in many small steps, resulting in plenty of ionisations in the cellular atoms along their track, and fewer direct breaks including single and double strand breaks (SSB and DSB) within

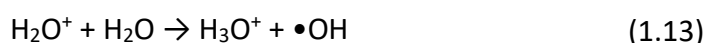
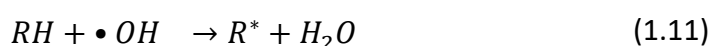
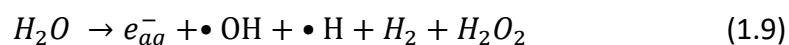
the DNA molecule. In contrast, protons have minimal interactions upon entering biological tissue, yet at and around their peak, they undergo through few big energy transfers in a very small range. This way, protons produce less sparse ionisation along their track but denser ionisation as well as an increased number of SSB, DSB and complex DNA damage (CDD; containing multiple DSBs in close proximity, within a short DNA region of up to 15–20 bp (48)) in depth. In fact, it has been estimated that 1 Gy (radiation dose unit) of x-rays and high energy (entrance dose) protons produces ~70,000 ionisations in the cell nucleus and ~2000 ionisations directly on the DNA molecule that yields ~1000 SSB and ~40 DSB (49, 50). However, it has been reported that PBT induces more DSBs (which may also vary in complexity) compared to photon RT, particularly at the Bragg peak and distal edge, which I have summarised in a recent review (Table 1.1) (51). Nevertheless, it is suggested that PBT is biologically more effective than x – rays (52-55).

Table 1. 1 Comparisons of DSBs induced by PBT versus photon RT (taken from (51)).

| Cell line | Method(s) | Proton energy | Photon energy | Findings |
|------------------------------------------------------------------------------|------------------------------------------------------------|----------------------------------------------------|--------------------------------------------|------------------------------------------------------------------------------------------------|
| ONS76 medulloblastoma; MOLT4 leukemia cells | Immunofluorescence γ H2AX foci analysis | 200 MeV | 10 MV x-rays | 1.2-1.5-fold increase in size and amount of foci following PBT, 30 min to 6 h post-irradiation |
| HeLa; SQ20B HNSCC | Pulse-field gel electrophoresis | 76 MeV, 201 MeV | 0.662 MeV ¹³⁷ Cs γ -rays | 1.2-fold increase in DSB. No differences between PBT energies nor along the SOBP. |
| IN528 and T4213 Glioblastoma stem-like cells | Alkaline and neutral comet assay | - | 320 kV x-rays | ~1.2–1.6-fold higher numbers of DSBs at 20–48 h post-irradiation |
| TrC1 prostate cancer cells; murine embryonic fibroblasts | Histone γ H2AX and 53BP1 foci by Immunofluorescence | 187 MeV bragg-peak and plateau protons | 320 kV x-rays | Similar numbers of foci. Delayed, bigger and irregular in size for bragg peak protons. |
| AG01522 skin fibroblasts | 53BP1 foci by Immunofluorescence | 60 MeV entrance dose | 225 kV x-rays | Similar numbers of DSBs at 0.5–24 h post-irradiation |
| Wild type, HR-deficient, and NHEJ-deficient Chinese hamster ovary cell lines | Histone γ H2AX foci by Immunofluorescence | 138 MeV | 200 kV x-rays | Similar initial induction of DSBs, yet reduced survival. |
| HeLa; UMSCC74A and UMSCC6 HNSCC cells | Neutral comet assay | 58 MeV entrance dose 11 MeV distal edge of SOBP | 100 kV x-rays | No significant difference in the DSB repair kinetics. Reduced survival in the 11 MeV. |

1.2.3.2 Chemical damage

On top of the direct breaks that threaten the cell survival, all the peripheral ionisations can lead to chemical changes within the cellular components, during the physiochemical phase, that contribute to further damage on the DNA molecule. Since water constitutes ~70 % of the cell mass, it is the most affected cellular component. IR-induced water radiolysis (equation 1.9) generates reactive oxygen species (ROS), which are unstable and highly reactive free radicals with a range of ~10 nm, such as the hydroxyl radical ($\bullet\text{OH}$), ionized and radical water (H_2O^+ , H_2O^*), hydrogen radical ($\bullet\text{H}$) and hydrated electrons (e_{aq}^-). ROS have rapid chemical reactivity and generate additional damaging agents and secondary products, including superoxide (O_2^*) and hydrogen peroxide (H_2O_2) that react with the organic and inorganic cellular components, and induce various secondary lesions (56). ROS can trigger indirect DNA damage, enzyme and protein synthesis inactivation, and damage to cellular constituents, nutrients and other building blocks of macromolecules (57). They are considered a major factor contributing to DNA damage and there is evidence of elevated levels of ROS particularly following PBT, promoting its cell-killing efficacy (58, 59).



Shown are some typical reactions of ROS following water radiolysis (1.9), includes secondary reactions of the reactive water radiolysis products with water molecules (1.10), and with organic molecules (RH) (1.11), as well as secondary products of reaction of radical organic molecules (46).

1.2.3.3 Biological damage

Following physical and chemical phases, a variety of DNA lesions are induced along the radiation track (direct DNA damage) and ROS have been generated (Figure 1.9). During the biological damage phase, chemical interactions trigger further (indirect) DNA damage, including base oxidation, methylation and alkylation, sites of base loss (abasic

sites), and DNA SSBs that are most abundantly generated. Moreover, the formation of DNA DSBs, clustered DNA damage containing two or more DNA lesions in close proximity (within 1–2 helical turns of the DNA) and CDD containing multiple DSBs within a short DNA region of up to 15–20 bp, are less frequent, although these are considered the most lethal (36, 48, 60). At this stage, any DNA damage requires immediate processing and repair or else it can lead to chromosomal aberrations or collapse, resulting in loss of genetic information, gene mutations and cell inactivation, which can ultimately lead to human disease development, including cancers. As soon as the damage is recognised, there are numerous proteins and enzymes activated to initiate DNA repair. If the repair of the DNA damage is not successful or if the damage is beyond repair, in a single or group of cells, specific proteins promote cell death to protect the survival of the organism (43).

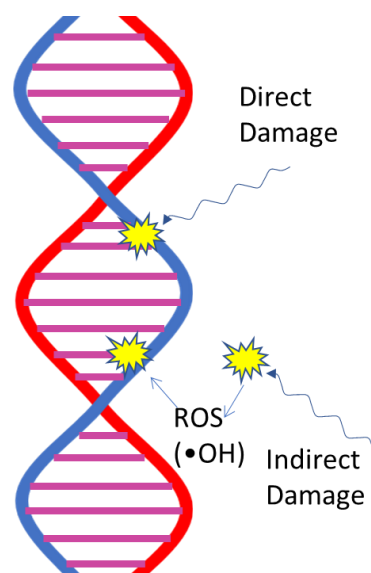


Figure 1. 9. Induction of DNA damage. Direct damage is induced when photons, electrons protons or heavy ions directly break the DNA molecule by interrupting the DNA strand core, or by removing a DNA base. Indirect damage occurs when the radiation interacts with other cellular molecules, particularly the water surrounding the DNA, which generates ROS, that in turn chemically damage the DNA molecule.

1.2.4 DNA damages affected by LET and RBE

A physical unit describing the energy loss and, therefore dose deposition along the path of the beam is the linear energy transfer (LET) and is a measure of ionisation density. High LET results in denser ionisations, which cause more extensive damage induction

compared to low LET. Photons present a low LET along their track, whereas protons and heavier particles present a variable LET. In the entrance of the beam, the LET is relatively low and similar to those of photons for high energy entrance dose, yet the LET increases as their energy drop further along their track, particularly at and around the Bragg peak (61, 62). The median energy transfer is the absorbed dose and is counted in grays (Gy), where 1 Gy = 1 Joule/Kg and describes how much energy is absorbed by 1 kg of matter.

LET is inextricably linked with another physical unit, the relative biological effectiveness (RBE), that is used to correlate the biological response of a given radiation, usually photons, with the biological response of other types of radiation. For example, RBE is the ratio of the reference radiation (x – rays) dose divided by proton radiation dose required to cause the same biological effect.

$$RBE = \frac{D_{10} \text{ x-rays}}{D_{10} \text{ protons}} \quad (1.13)$$

D_{10} refers to the dose required to achieve 10% survival post irradiation.

RBE is a complicated quantity, it has been reported that its value depends on both physical factors, including the radiation dose, the proton beam energy, the dose fractionation, and dose rate, as well as biological factors, such as the type of the tissue, the cell cycle phase, the oxygenation level, but also the position along the SOBP. The RBE will typically increase with decreasing dose (and biological effect), due the linear quadratic shape of the reference radiation (63, 64). LET is one of the parameters mostly determining RBE, which is 1 for low LET radiation. For clinical protons RBE will also vary on initial energy and size of SOBP and gradually increases as the LET increases across the track and reaches its maximum at the peak and distal edge of the curve, before dropping down due to the overkilling effect. For high energy protons, a constant value of 1.1 is currently used in clinical practice. Nevertheless, in vitro experimental data suggest that RBE increases from 1.35 in the centre of the SOBP, to 1.6 in the distal edge and 1.7 at the distal fall off of the SOBP (65-67), and there is an ongoing debate about whether the use of a constant RBE of 1.1 is the optimal solution or variable RBE values would be more appropriate in radiotherapy treatment (61, 62, 68).

1.2.5 DNA repair

Preservation of the genetic information stored in the DNA, considering the vast variety of DNA damage possible, requires not only a high accuracy DNA replication system but also advanced and rapid DNA damage response and repair mechanisms. Indeed, there are multiple DNA repair pathways activated in response to different kinds of DNA lesion, with usually more than one pathway covering a certain type of lesions. The very structure of the DNA offers a huge advantage for its own repair, as the information is stored in duplicate, once in each of the strands of the double helix. In addition, the chemical structure of the bases enables the distinction between damaged and undamaged bases. Most of the repair pathways use the complementary strands as a template, however certain mechanisms must repair DNA damage occurring on both copies of the DNA strand, these types of damage are rare but most critical. There are six major DNA repair pathways in human cells, that are discussed in this section.

1.2.5.1 Base excision repair (BER)

One of the most important DNA repair pathways, base excision repair BER, is triggered in response to, damaged or altered bases, including deaminated cytosines and adenines, alkylated and oxidised bases, opened ring bases, and degraded carbon – carbon single bond bases. This is a constitutively active process given the large amount of such DNA damage generated per cell per day. As shown in Figure 1.10, DNA glycosylases are a family of enzymes (11 present in human cells in total), each of whom recognise a different type of DNA base damage, that proofread each base pair largely using a base-flipping mechanism, recognise and hydrolytically remove any damaged base. Then, AP endonuclease enzymes, particularly APE1, detects the abasic nucleotide, called apurinic/aprimidinic site (AP) for a purine or a pyrimidine loss respectively, and breaks the sugar-phosphate phosphodiester bonds on the DNA chain, resulting in a single nucleotide gap in the sequence. Next, DNA polymerase enzymes, particularly DNA polymerase β (Pol β), catalyse DNA synthesis and fills the gap using the complementary strand as a template. There are two routes at this stage, the short-patch pathway mediated by Pol β , and the long-patch pathway co-ordinated by DNA polymerases δ/ϵ (pol δ/ϵ) along with Proliferating Cell Nuclear Antigen (PCNA), in the same manner that natural DNA replication is processed. Finally, DNA ligase enzymes, DNA ligase I (for long-

patch repair) or DNA ligase III α -XRCC1 complex (for short-patch repair), seal the nicks in the DNA strand. Furthermore, BER is triggered in response to the very frequent SSB and DNA damage caused by depurination, a chemical reaction that releases purines (A and G) from the DNA helix. BER is also co-ordinated by the SSB binding protein poly (ADP-ribose) polymerase 1 (PARP1) in response to DNA damage, and multiple PARP1 inhibitors have been clinically approved for the treatment of specific tumours, including breast and ovarian cancers, through BER inhibition (69-74).

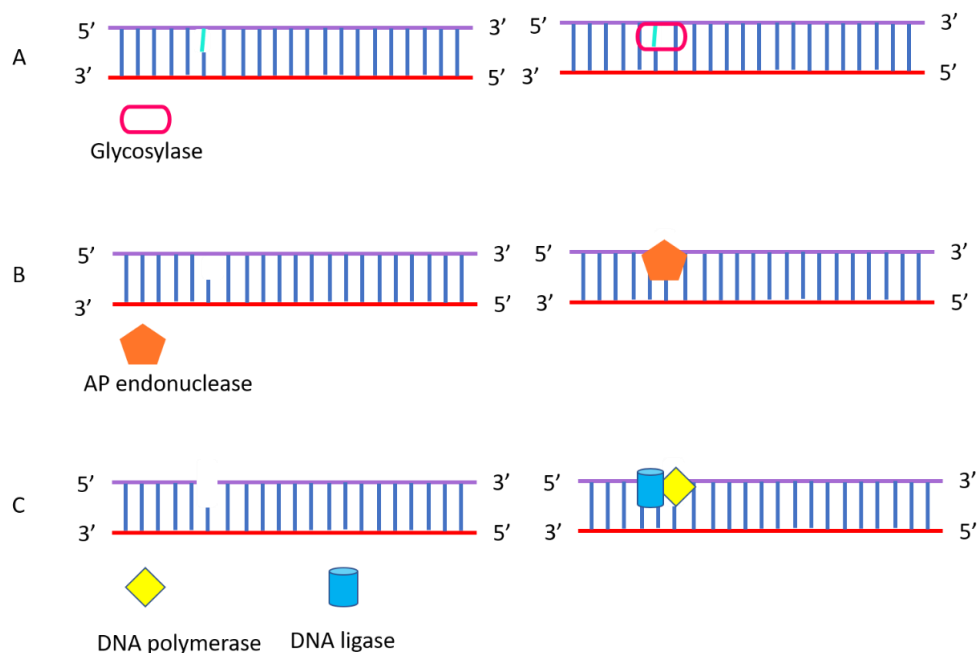


Figure 1. 10. Schematic representation of Base excision repair (BER). A) DNA glycosylase enzymes scan the DNA sequence and remove misplaced or damaged bases. B) APE1 and APE2 locate the abasic sites, break the phosphodiester bond between the nucleotides, and create a gap. C) the nucleotide gap is then synthesised and filled by DNA polymerase (Pol β and pol λ / pol δ , pol ϵ and PCNA) and is reconnected to restore the DNA strand by DNA ligase (DNA ligase I, DNA ligase III α -, XRCC1).

1.2.5.2 Nucleotide excision repair (NER)

For the repair of larger changes in the DNA sequence, the nucleotide excision repair (NER) pathway is activated. NER is the chosen pathway for the repair of bulky DNA lesions and adducts, particularly those induced by ultraviolet radiation. There are two types of NER in eukaryotic cells; the global genome repair (GG-NER) which slowly inspects the entire genome, in a transcription independent manner; and the transcription coupled repair (TC-NER). The two sub-pathways differ only in the initial

step, as shown in Figure 1.11. In GG-NER, a multienzyme DNA-binding complex consisting of DNA-damage binding 1 and 2 (DDB1 and DDB2) along with Xeroderma pigmentosum complementation group C (XPC)-Rad23B complex, scan the DNA sequence, recognise and bind on distortions.

In TC-NER, RNA polymerase detects and stalls on the lesion signalling for NER factors to process the repair. The damaged bases are then excised by the excision repair complex TFIIH, by breaking the nucleotide phosphodiester bonds of the DNA strands on both sides of the lesion. Immediately, the DNA helicase enzymes (XPD and XPB) separates the two strands and removes the oligonucleotide fragment. DNA polymerases then resynthesise the DNA fragment by using the complementary strand as a template, and DNA ligase complete the repair by sealing the nick in the DNA strand. In human cells, the removed fragments can be more than 24 nucleotides long. This is a major mechanism that can repair almost any kind of large DNA damage (75-78).

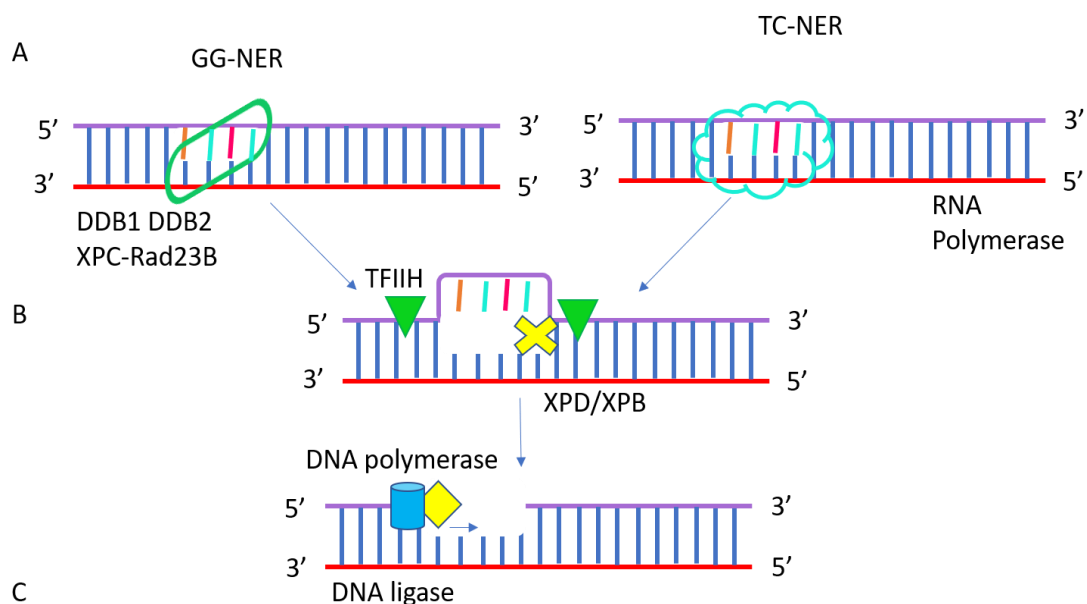


Figure 1. 11. Schematic representation of Nucleotide excision repair (NER). A) There are two types of NER in eukaryotic cells, GG-NER, catalysed by the DDB1, DDB2 and XPC-Rad23B complexes, and TC-NER, initiated by RNA polymerase damage recognition. B) TFIIH complex excises the damaged site, and DNA helicases XPD/XPB separate the two strands and remove the fragment. C) DNA polymerase enzymes synthesise the new fragment and DNA ligase enzymes seal the nick in the DNA strand.

1.2.5.3 Mismatch repair (MMR)

Mistakes occurring during DNA replication and go undetected by DNA polymerases, are resolved by mismatch repair (MMR). This pathway can identify mispaired bases but also insertion or deletion of mispairs, where there are up to 10 unpaired nucleotides in one of the DNA strands. The heterodimer MutS Homologs (MSH) complex, consisting of MSH2-MSH6 and MSH2-MSH3, proofread the DNA strands and bind on the DNA lesion. The heterodimeric MutL homologs (MLH) complexes, consisting of MLH1-PMS2 and MLH1-MLH3, then identify and cleave the oligonucleotide fragment containing the lesion, recruiting DNA helicase II to separate the two strands. Finally, Pol δ and PCNA replicate the DNA strand, replacing the appropriate DNA bases, and DNA ligase I completes the repair process. MMR is also a key pathway for the detection and repair of DNA adducts, caused by chemotherapeutic agents. Deficiency in MMR introduces high rate mutations and has been associated with numerous human cancers (79-82).

1.2.5.4 Translesion synthesis (TLS) repair

Translesion synthesis repair (TLS) occurs during the S phase of the cell cycle, where there is ongoing DNA replication. This process enables DNA synthesis to be carried out past certain DNA lesions, ensuring genome replication and cell survival. In fact, TLS initiates DNA lesion bypass, preventing DNA damage to cause delays in the DNA synthesis, and thus preventing blockage or collapse of the replication forks. This pathway is mediated by the post-translational modification of PCNA that upon recognition of a blocked replication fork, gets ubiquitinated, and recruits low stringency TLS polymerases. PCNA then regulates a switch between the regular synthesis Pol δ/ϵ , which lead the synthesis of the two strands with specific TLS polymerases. There are several TLS polymerases in mammalian cells, including pol η , pol ι , pol ζ , pol II, IV and V, that due to their different substrate specificities, deal with many different types of DNA damage by surpassing the blocked region resuming DNA replication, allowing for later repair of the DNA damage. PCNA progressively switches between the required polymerase until the process is completed. TLS is a low fidelity repair process and is often error prone leading to further DNA damage and/or mutagenesis, therefore other repair mechanisms are required to complete the repair process. However, it is important in preventing degradation of

simpler DNA damage that could generate chromosomal aberrations or induce cell death, early in the cell cycle and therefore allowing time for further DNA repair (83-86).

1.2.5.5 Non-homologous end joining (NHEJ)

Simultaneous damage on both sides of the double helix lead to DSBs, highly toxic DNA lesions that if not repaired can cause mutations, chromosomal disruption and severe loss of genetic information. One of the major mechanisms for DSB repair and chromosome restoration, is the non-homologous end joining (NHEJ) repair pathway. It is the predominant mechanism throughout the cell cycle in mammalian cells, particularly for direct DSBs, in a template independent manner (87). This pathway, shown in Figure 1.12, is mediated by a complex of the Ku70/80 heterodimer, composed of the Ku70 and Ku80 subunits, and the large catalytic subunit of DNA-dependant protein kinase (DNA-PKcs), that rapidly detect the broken DNA ends. The Ku heterodimer produces a ring-shaped structure, that binds onto the sugar-phosphate backbone of the DNA strand, yet do not bind onto the bases, making it DNA sequence independent, and this then recruits DNA-PKcs to form the repair platform. This binding protects the DNA ends from nonspecific processing, that could lead to chromosomal aberrations and genomic instability, but also attracts other NHEJ factors to promote repair. X-ray cross complementing protein 4 (XRCC4), DNA Ligase IV, XRCC4-like factor (XLF) and Aprataxin-and-PNK-like factor (APLF), are NHEJ repair factors that are recruited to the DSB site. There is no particular order in the recruitment process, neither is one factor necessary for the recruitment of the other factors, on the contrary this rather depends on the complexity of the DNA damage.

Simple DSBs, after DNA-PK binding may require only XRCC4, Ligase IV, and XLF for their repair. In contrast, for repair of more complex DSBs, the process relies on DNA-PKcs possibly recruiting ataxia-telangiectasia mutated (ATM) which is a member of phosphatidylinositol-3 (PI-3) kinase-like kinase family (PIKK). Either way, the DNA-PK complex produce a stable core at the DSB site (88). Subsequently, the DNA gaps are filled and the DNA ends get compatible for ligation, by specific DNA end processing enzymes and proteins, recruited by either XRCC4 and DNA-PKcs, including Artemis, aprataxin, ligase IV, polynucleotide kinase-phosphatase (PNKP), DNA Polymerases μ and λ , Werner protein (WRN), and APLF (88-91). Finally, DNA ligase IV, mediated by XRCC4, XLF, and

likely APLF, connects the loose ends without checking for their homology, and despite any remaining gaps. The NHEJ complex is then dissolved and the repair is completed. NHEJ repair is an error-prone pathway that could join broken DNA ends with little or no homology, however there is evidence that it may be acting synergistically with HR to maintain genomic integrity (92, 93). Also considering the majority of the DNA sequence is non-coding, NHEJ is a good enough mechanism, that can rapidly repair damaged chromosomes, crucial for maintenance of the genomic information and cell survival (92).

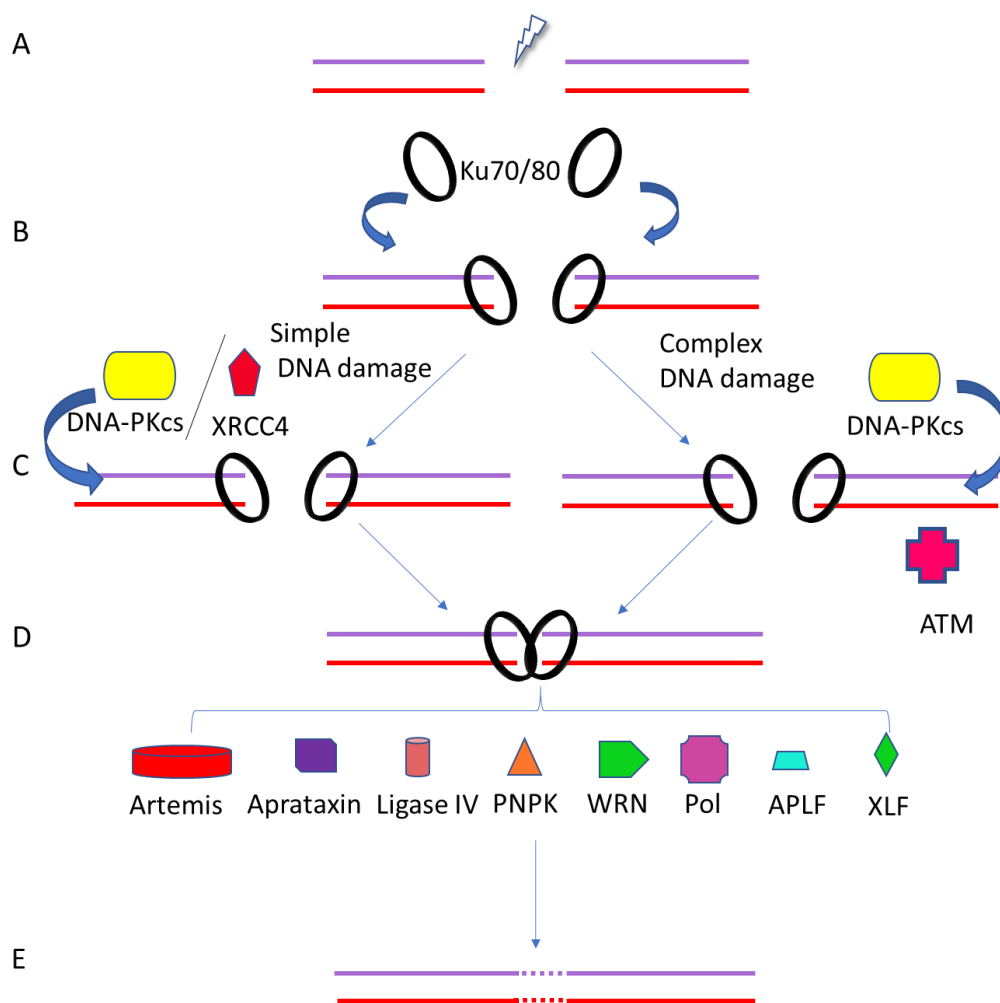


Figure 1. 12. Schematic representation of non-homologous end joining repair pathway (NHEJ). A) DNA damage induction; B) The Ku-70/80 heterodimer recognises and binds onto the broken ends of the DNA strands, and recruits DNA-PKcs to form the DNA-PK complex; C) Simple DNA damage is getting processed by DNA-PKcs or XRCC4, while Complex DNA damage is assisted by ATM, recruited by DNA-PKcs. (D) Artemis, aprataxin, ligase IV, PNPK, DNA Polymerases μ and λ , Werner protein (WRN), APLF and XLF, are independently recruited by DNA-PK, interact with each other and form a stable DNA repair complex to process the broken DNA ends. E) Processing of the DNA ends marks the end of the repair process, and the DNA repair complexes are dissolved.

1.2.5.6 Homologous recombination (HR)

The second key mechanism for DSB repair is the homologous recombination (HR) pathway. In addition to DSB repair, HR is the main mechanism for the repair of blocked or collapsed replication forks, but also for resolving of DNA gaps and DNA interstrand crosslinks (ICL) (94). HR repair is a high-fidelity error free mechanism that is active only during late S and G2 phases of the cell cycle, when the sister chromosome is present, and used as a template for the repair of the broken DNA helices. In fact, HR prefers using the sister chromosome rather than the homolog chromosome as a template to reduce the risk of loss of heterozygosity. It is a prominent mechanism for genome preservation, in addition to NHEJ for the repair of DSBs and to TLS for DNA damage surpass and tolerance (95).

Particularly for the DSB repair, HR pathway can be separated into three phases as shown in Figure 1.13; the pre-synapses, the synapses, and the post-synapses. During the pre-synapses phase, the broken DNA ends are recognised and are resected in a 5' to 3' direction. One of the broken strands is processed to a 3'-OH ending single-stranded DNA (ssDNA) tail, that along with Rad51 the central protein to HR, forms the Rad51-ssDNA presynaptic helical filament. Since this is antagonistic to the ssDNA-binding protein replication protein A (RPA), promoter proteins enable Rad51 to surpass the inhibition by RPA, and subsequently to replace RPA in the filament.

In the second phase, synapses, Rad51 firstly catalyses an homology search in the DNA strands where recombination proteins locate the matching DNA sequences between the sister chromatids, and secondly promotes DNA strand invasion, where the Rad51-ssDNA filament generates a D-loop in the homolog chromosome. There are five human Rad51 paralogs, Rad51B, Rad51C, Rad51D, XRCC2 and XRCC3, and these form complexes catalysing the process that have non-overlapping functions. Multiple core factors and mediator proteins are also involved in the progress of the repair process including, but not limited to, ATM, ATM and Rad3 related (ATR), WRN, Rad52, Rad54, Rad55, Rad57 and breast cancer associated gene 1 and 2 (BRCA1 and BRCA2). Moreover, for the repair of IR-induced DSBs, the Mre11-Rad50-Xrs2 (MRX) complex is specifically required, and it has been shown that defects in this complex lead to significant IR sensitivity (95).

During the post synapses phase, DNA replication proteins copy the missing genetic information to the broken helix, repairing it and restoring the DNA sequence. Following the generation of the D-loop, there are (at least) three alternative pathways to complete the repair, namely synthesis-dependent strand annealing (SDSA), break-induced replication (BIR) and the double-strand break repair (DSBR).

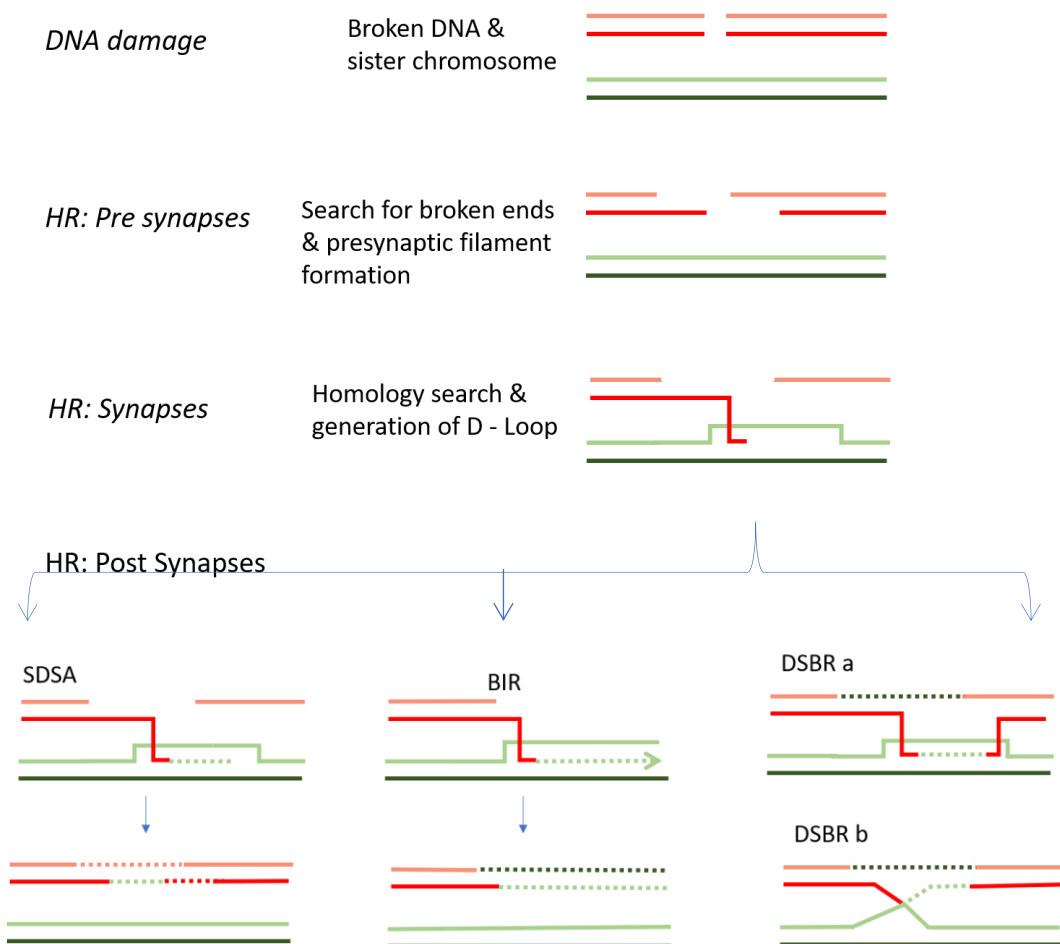


Figure 1. 13. Schematic representation of Homologous recombination repair pathway (HR). HR can be divided into three main phases; The pre-synapses: recognition of DSB and formation of the complex Rad51 - ssDNA tail presynaptic filament. The synapses: homology search between the sister chromosomes and generation of the D – loops. The post-synapses: repair of the broken strand through 1) SDSA (synthesis – dependent strand annealing) often in multiple cycles, 2) BIR (the break – induced replication) where the D-loop is assembled into a full replication fork or 3) DSBR (the double – strand break repair) a) by double independent strand invasion or by second end capture and b) double Holliday junction dissolution/resolution. Rad51 is the core HR protein but several proteins mediate the repair process across the different stages including ATM, ATR, WRN, Rad52, Rad54, Rad55, Rad57 BRCA1, BRCA2

SDSA is the preferred mechanism in mammalian cells. It is performed in successive rounds of DNA strand invasion, short DNA synthesis off the template chromatid, D-loop disruption, disengagement of the newly synthesised end and annealing with the second end of the broken strand. This leads to localized conversion without crossover, and therefore a loss of heterozygosity produced by somatic crossovers is avoided. BIR is a straightforward non-crossover process where the D-loop is assembled into a full replication fork, and the entire distal part of the DNA strand gets synthesised, copying the template chromosome. This process may result in loss of heterozygosity in the chromosome, as the second strand does not engage in the repair and the genetic information of the fragment may be lost. DSBR involves both ends of the DSB being engaged in the repair, either by double-independent strand invasion or by second end capture through DNA annealing. The latter leads to double Holliday junction formation, a four-way branched DNA joint molecule, that is resolved by structure-specific endonucleases, such as Mus81–Mms4, Slx1–Slx4, and Yen1, to yield either crossover or non-crossover products. Moreover, double Holliday junctions can be dissolved by a mechanism involving Bloom Syndrome (BLM) DNA helicase, that migrates the two junctions towards each other, and type 1 TOPOIII α topoisomerase, that topologically links the two duplexes, leading exclusively to non-crossover products. Finally, Resolvase A, whose specific activity is yet to be determined, has been shown to cleave Holliday junctions into crossover and non-crossover products. Once the synthesis and ligation of the broken ends is completed and the DNA strand is restored, it is then used as a template for the repair of the complementary strand and the repair process is therefore finished (95-98).

1.2.6 DNA repair in response to IR-induced DNA damage

PBT and conventional radiotherapy (RT) present fundamental physical differences. As discussed in Chapter 1.1.3, the physical interaction of protons, as particles with mass and positive charge, is fundamentally different than that of photons who have neither mass nor charge (99). Consequently, the biological response following proton and x – ray induced DNA damage differs (100-102). The choice of the appropriate repair mechanism depends on many different factors, with the cell cycle stage to be one of the

first contributors identified, but also the DNA lesion induction process, the radiation type and beam energy, and the DNA repair protein competence all associated with DNA repair pathway choice (103-106).

1.2.6.1 Types of DNA damage

PBT is suggested to induce more DSBs and CDD compared to conventional RT (Table 1.1) (100, 101, 107, 108). DSBs can be quantified indirectly by measuring the phosphorylated histone H2AX (γ H2AX) foci formation that are rapidly generated in response to DSBs, and attract other DSB repair proteins (109). Multiple *in vitro* studies have reported increased amounts of DNA repair γ H2AX foci formation following proton irradiation, that they were also larger in size and persisted for longer, suggesting a more CDD in comparison to photon induced foci (100, 101). This indicated not only a greater number of DSBs and clustered lesions, but also persistent DNA damage that was trickier to be resolved (108). Interestingly, it has also been reported that the initial induction of DSBs was similar, following clinically relevant protons and x – rays *in vitro*. However, PBT induced more lethal DNA lesions than x – rays. These results suggested the quality rather than the amount of DNA damage induced was the reason for the different effectiveness (102). Finally, high LET radiation, derived from low energy protons, α particles, carbon ions and other heavy particles, is considered even more prominent in cell killing than low LET and photon radiation. Both *in vitro* studies and computer simulations reported increased CDD induction, with plenty DSB in close proximity that determine its enhanced biological effectiveness for the same physical radiation dose, compared with low LET and photon radiation (110-114).

1.2.6.2 DNA repair pathway choice

The pathway choice for DSB repair following different radiation modalities, is a field of ongoing research with rather contradicting findings currently available in literature. Between the two major DSB repair mechanisms detailed above, there are a number of *in vitro* experimental evidence suggesting that while HR is important, NHEJ repair is the major repair pathway in response to both photon and low LET proton radiation. Consequently, DNA-PKcs is considered the main protein involved in resolving IR-induced

DSBs (115-117). In these studies, wild type, HR-deficient, as well as NHEJ-deficient Chinese hamster ovary cell lines presented increased sensitivity to both radiation types, with, however, no significant difference in the DNA repair kinetics following either proton or x – ray irradiation. These data are summarised in Table 1.2, taken from our recent review (51). In contrast, it is also reported that whilst NHEJ repair pathway is the major mechanism for DSB repair following x – ray irradiation, there is increased dependence on HR for repair of proton induced DSBs *in vitro* (102, 118, 119). In these studies, PBT was more efficient in killing HR-deficient compared to NHEJ-deficient Chinese hamster cell lines, but was less effective in DNA-PKcs inhibited human A259 lung cancer and glioblastoma cell lines compared to x – rays. In addition, the proportion of cells undergoing HR following PBT versus x – rays was reported to be higher in HeLa cells (119). Therefore, further investigation is required to resolve the conflicting evidence.

Table 1. 2 DNA double strand break (DSB) repair pathway choice following proton beam therapy (PBT) versus photon irradiation (taken from (51)).

| Cell line | Irradiation | Outcome |
|---------------------------------------------------------------------|--------------------------------------------------------------|-------------------------------------------------------------|
| wild type, NHEJ- and HR-deficient Chinese hamster cell lines | 200 MeV protons and ¹³⁷ Cs γ-rays | NHEJ is the major pathway, for photons and low LET protons. |
| wild type and NHEJ-deficient Chinese hamster ovary cell lines | 14.4 MeV plateau protons and 667 kV ¹³⁷ Cs γ-rays | NHEJ is the major pathway, for photons and low LET protons. |
| Wild type, HR-, and NHEJ-deficient Chinese hamster ovary cell lines | 138 MeV protons and 200 kv x-rays | Enhanced dependence on HR following proton. |
| A549 lung cancer; glioblastoma cells | 138 MeV protons and 200 kv x-rays | Enhanced dependence on HR following proton. |
| HeLa | 21 MeV protons | High proportion of cells undergo HR following protons |
| Non-small-cell lung cancer cell lines | 235 MeV protons and 250 kv x-rays | HR only partly required following protons |

1.3 DNA repair regulators

Radiotherapy is one of the three major cancer treatments, particularly for treatment of head and neck cancers, currently used alone or in combination with surgery and/or chemotherapy. As discussed above, this involves using ionizing radiation to induce significant DNA lesions and lead to tumor cell death. Among the vast variety of DNA damage induced, DSBs are the most cytotoxic lesions, and a single unrepaired or mis-repaired DSB can be lethal. However, the sophisticated DNA damage response (DDR) system initiates DNA repair upon recognition of a DNA lesion, to protect the genomic stability of the cell. Three protein kinases ataxia telangiectasia mutated (ATM), ataxia-telangiectasia mutated and Rad3 related (ATR) and the catalytic subunit of DNA-dependent (DNA-Pkcs), are actively involved in the DDR, and play a key role in the detection and repair of DSBs via the NHEJ and HR repair mechanisms (120-122).

1.3.1 The role of ATM in DDR

ATM is central in signaling DNA damage and repair, particularly in response to DNA DSBs and is a key factor for activation of several DNA repair proteins and cell cycle checkpoints. Moreover, ATM deficiency has been associated with severe sensitivity to IR and other DNA damaging agents, as well as acute apoptotic rates (123). ATM is actively involved in the two major DSB repair mechanisms, HR and NHEJ with hundreds of substrates phosphorylated in an ATM-dependent manner, highlighting the complexity of DDR pathways (121). Upon DSB induction, ATM is activated and instantly an intermolecular auto-phosphorylation on Serine 1981 (S1981) is initiated. It is then recruited by the Mre11-Rad50-Nbs1 (MRN) complex, which is rapidly assembled on DSB sites, and acts as a damage sensor that can also form a physical bridge spanning the DSBs (124, 125). Recruitment of ATM has also been associated with Nbs1, that also enhances ATM kinase activity (126). ATM in turn, activates several proteins associated directly with DNA repair, such as histone H2AX, BRCA1, as well as proteins critical for the regulation of the cell cycle, at G1, S and G2/M checkpoints, including p53 and Chk2, indirectly promoting DSB repair.

Phosphorylation of histone H2AX opens up chromatin to allow DNA repair enzymes to access the DSBs. ATM is reported to phosphorylate histone H2AX at serine 139 (called γ H2AX) both *in vitro* and *in vivo*, being one of the earliest kinases to be activated in the cellular response to DSBs (127). Furthermore, BRCA1 expression is considered critical for the appropriate resolution of IR-induced DSBs and colocalizes with the key HR protein Rad51, as well as the Nbs1-Mre11-Rad50 complexes involved in both HR and NHEJ. ATM phosphorylates CtIP (C-terminal binding protein interacting protein), a BRCA1 suppressor protein, subsequently driving dissociation of CtIP from BRCA1 and essentially upregulating BRCA1 expression, promoting DSB repair (128, 129).

The tumor suppressor protein p53 regulates cell cycle progression by controlling the G1/S checkpoint preventing cell proliferation until the DNA damage is resolved, or the cell is led to apoptosis in the case of irreparable damage. ATM promptly phosphorylates p53, at serine 15, and upregulates its expression by phosphorylating the E3 ubiquitin ligase mouse double minute 2 homolog (MDM2). This stabilizes p53, preventing in parallel its rapid degradation (130-132). Similarly, ATM-driven activation of jun kinase (JNK), leads to reduced JNK binding on p53 and thus upregulation and decreased degradation of p53 (133). Another protein also phosphorylated by ATM in response to DNA damage is the checkpoint kinase 2 (Chk2), a kinase that mediates cell cycle progression in both S and M phases. Chk2 subsequently phosphorylates the mitosis-inducing phosphatase, M-phase inducer phosphatase 3 (Cdc25C) on an inhibitory site, causing G2/M arrest, preventing entry into mitosis and giving extra time for DNA repair. Moreover, Chk2 rapidly phosphorylates p53 on serine 20 and stabilises the protein by inhibiting MDM2 binding resulting in G1 arrest (134, 135). Activation of Chk2, also mediates and promotes degradation of the S-phase promoter phosphatase, M-phase inducer phosphatase 1 (Cdc25A), delaying DNA synthesis (136).

Finally, ATM has been shown to mediate apoptosis by promoting activation of p73, a regulator of DNA damage induced apoptosis. During IR-induced apoptosis, a cascade of caspases (cysteine aspartic acid proteases) cleave cellular proteins. ATM is cleaved by the caspase-3-like apoptotic protease, generating a truncated protein with limited kinase activity, only enough to retain its DNA binding ability, to prevent DNA repair and

DNA damage signaling, suggesting a counterproductive DNA repair upon commitment to apoptosis (123). The contribution of ATM to the DDR is summarised in Figure 1.14

1.3.2 The role of ATR in DDR

ATR is a key factor in the HR repair pathway of DSB repair, and promoter of genome stability. As indicated by its name (ATM and Rad53 related), ATR is closely linked to ATM. Both ATM and ATR are activated in response to IR-induced DNA damage, yet ATR is also activated in response to ultraviolet radiation (UV)-induced damage. Interestingly, ATM and ATR are in general activated by different types of DNA damage. ATM is associated with direct DSB, while ATR is correlated with the repair of single stranded DNA (ssDNA) structures that arise from various types of DNA damage, such as stalled DNA replication forks and resected DNA DSBs, and it is therefore essential for cell survival even in the absence of exogenous genotoxic agents (121).

Following generation of ssDNA, RPA binds to form an RPA-ssDNA complex. In parallel, ATR is activated via an intramolecular auto-phosphorylation on threonine 1989 (T1989). This phosphorylation is critical for ATR function and is promptly recognised by DNA Topoisomerase II Binding Protein 1 (TopBP1), which in turn attracts the complex ATR-ATR interacting protein (ATRIP) that directly interact with the RPA-ssDNA complex, promoting ATR-driven cell cycle regulation and DNA repair. Moreover, formation of the RPA-ssDNA complex recruits the Rad17-RFC complex at ssDNA- dsDNA junctions, which engages the Rad9-Hus1-Rad1 heterodimer to bind on to the DNA ends, attracting TopBP1 and further promoting ATR phosphorylation and ATR-driven cell cycle regulation and DNA repair (121, 137, 138). Phosphorylation of BRCA1 by ATR occurs in distinct sites that overlap with ATM phosphorylated sites in response to IR induced DNA damage (123).

The contribution of ATR in the DDR is particularly critical in providing cell cycle control. Likewise to ATM, ATR directly activates p53 at serine 15 but also at serine 37, in a way that is both overlapping and non-redundant in regulating p53 expression, and thus ATR indirectly mediates the G1/S cell cycle checkpoint (139). In addition, ATR phosphorylates Checkpoint kinase 1 (Chk1), a serine/threonine-specific protein kinase principal

regulator of the cell cycle that impacts progression in three different phases of the cell cycle, the S phase, G2/M transition and M phase. Chk1 activation regulates cell cycle control on multiple phases, firstly on G1/S phase as it phosphorylates p53 on serine 20, upregulating and stabilizing p53 expression, thus delaying entry into the S phase (140). Secondly, during the S phase, as it mediates degradation of the S-phase promoter phosphatase Cdc25A, prohibiting DNA synthesis (141, 142). Thirdly, Chk1 acts on the G2/M cell cycle checkpoint, by the degradation of Cdc25A along with the phosphorylation of Cdc25C on serine 216, that reduces its ability to activate nuclear Cyclin-dependent kinase 1 (Cdc2), and in turn prevent entry into mitosis allowing further time for DNA repair (143-145). Figure 1.14 summarises the role of ATR in regulation of the DDR.

Overall, ATM and ATR mediate distinct repair pathways, although these partially overlap. Together, they regulate over 700 identified possible targets in response to DNA damage, many of which are common, such as p53 and BRCA1. Although ATM is mainly associated with G1/S phase cell cycle control, and ATR with intra S phase and G2/M phase cell cycle regulation, they often switch depending on the DNA damage and the cellular context. The two kinases cooperate in mediating damage response, promoting genome stability, and they are both required for effective DNA repair. In fact, it is suggested that the two pathways may be complimentary to each other and that defects in one pathway are substituted by the respective other pathway (121).

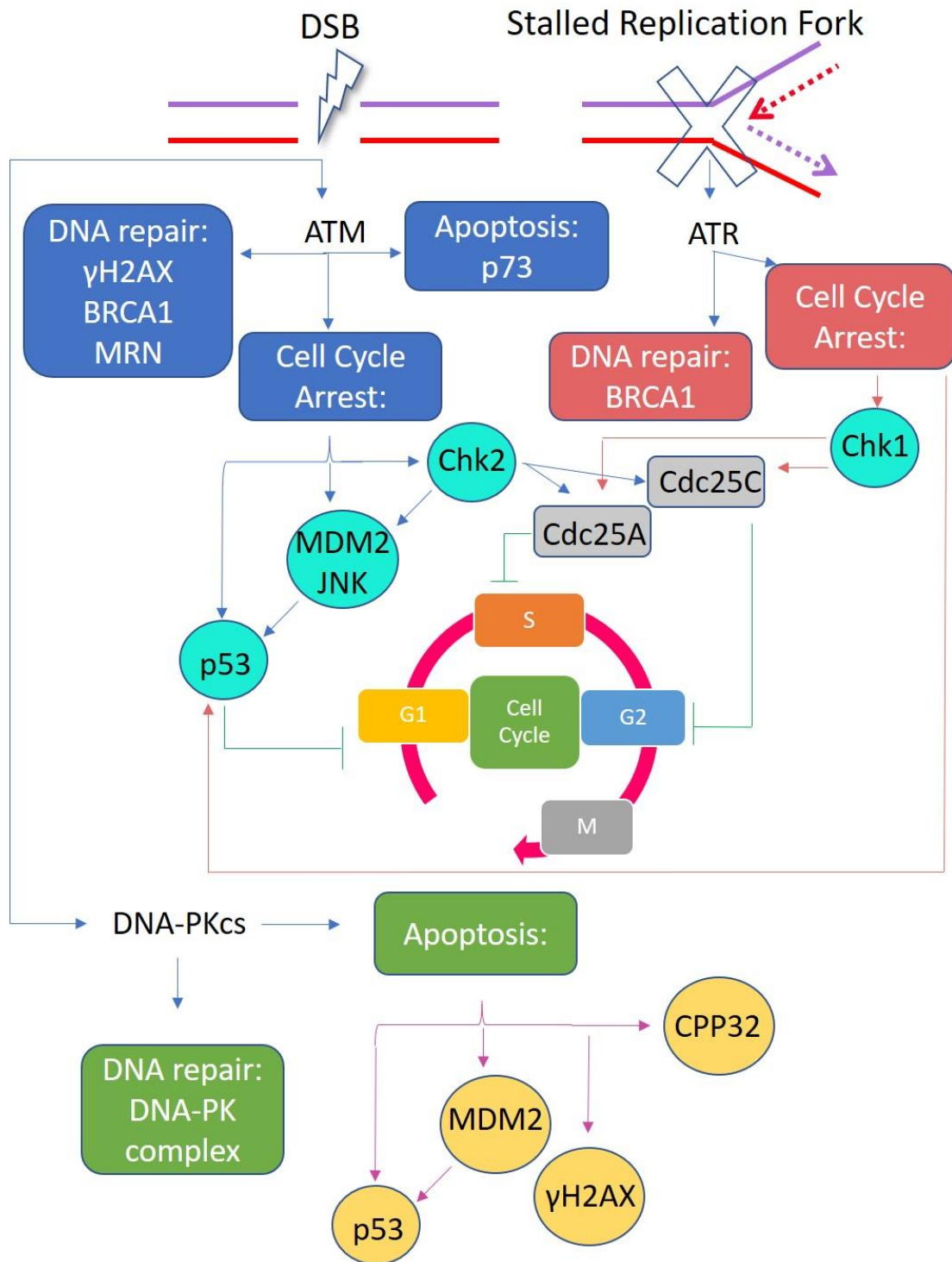


Figure 1. 14. The role of ATM, ATR and DNA-PKcs in the DNA damage response. Protein kinases central to DDR, are activated and have multiple interactions to promote DNA repair. ATM and ATR are signalling kinases that regulate several factors involved in DNA damage repair, as well as cell cycle control. DNA-PKcs, is directly involved in DSB repair via the NHEJ pathway. ATR is activated in response to stalled replication forks, while ATM and DNA-PKcs are triggered in response to DSBs and are key in mediating cellular apoptosis.

1.3.3 The role of DNA-PKcs in DDR

Another member of the PIKK family actively involved in the DDR is DNA-PK, a complex of Ku70/80 heterodimer and DNA-PKcs. DNA-PKcs is a major regulator of and directly involved in NHEJ repair. Deficiencies in DNA-PKcs has been associated with enhanced sensitivity to IR and other DNA damaging agents, while increased resistance to IR has been linked to DNA-PKcs overexpression (146-148). Similarly to ATM, DNA-PKcs is triggered in response to DSBs, yet the two proteins have separate and distinct functions in DSB repair (Figure 1.14). As discussed in Section 1.3.1, ATM acts as a signalling kinase, initiating several factors to promote DNA repair, in contrast with DNA-PKcs which mediates and contributes directly in the repair of the DSBs (146). Phosphorylation of DNA-PKcs promotes the opening of the DNA – DNA-PKcs complex to let other NHEJ factors access, process, and ligate the DNA ends. DNA-PK is phosphorylated on at least 40 amino acid sites but mutation on two of them, the Serine 2056 (S2056) and the Threonine 2609 (T2609), have been linked with inability to release the tight DNA – DNA-PKcs complex, suggesting they mediate the complex opening and thus progression of the repair. S2056 is primarily auto-phosphorylated, whilst T2609 is suggested to be partly phosphorylated by ATM (146, 147, 149, 150). The two sites have distinct roles in DSB repair, S2056 is reported to promote DSB ligation and T2609 to initiate the end processing (151, 152). Interestingly, DNA-PK activation and phosphorylation are not necessary for initial recruitment to DNA damage sites yet are required for efficient repair of DSBs (146).

The reasoning on how cells choose the appropriate repair pathway is yet to be determined. Interestingly, DNA-PKcs is proposed to be critical in the DSB repair pathway choice, between NHEJ and HR. While NHEJ is the predominant mechanism throughout the cell cycle, it is suggested that modulation of DNA-PKcs phosphorylation sites can promote either NHEJ or HR, by phosphorylating sites with a negative impact on NHEJ, in certain types of DNA damage where accurate repair is required. This illustrates that the two pathways are not just antagonistic, but also complementary (153, 154).

On another note, in addition to contribution to DNA repair, DNA-PKcs play a major role in promoting signalling of apoptotic pathways, in case of excessive and irreparable DNA damage. DNA-PKcs is suggested to mediate p53 expression in response to DNA damage.

Actually, it phosphorylates p53 at serines 15 and 37 leading to apoptosis, but also phosphorylates MDM2 preventing its inhibitory action on p53, contributing to further promotion of apoptosis. Moreover, DNA-PKcs deficiencies have been linked with suppressed p53-dependent apoptosis but remarkably not cell cycle arrest (155-157). Furthermore, phosphorylation of histone H2AX (γ H2AX) that occurs in apoptotic cells, in parallel with DNA fragmentation, was shown to be DNA-PKcs initiated and driven. In fact, inhibition of DNA-PKcs phosphorylation activity resulted in retention of DSBs, which was highlighted by γ H2AX persistency. ATM is also linked to H2AX phosphorylation however this occurs early in response to DSBs and is degraded well before cell commitment to apoptosis (146, 158). During the final steps of apoptosis, DNA-PKcs is targeted by caspase 3-like protease (CPP32), cleaved into fragments of 240-, 150-, and 120-kDa and therefore inactivated further demonstrating that DNA repair is counterproductive once apoptosis is activated (159, 160).

1.4 Head and Neck Squamous Cell Carcinoma

Head and neck squamous cell carcinoma (HNSCC) is a disease comprised of a heterogeneous group of cancers originating in the wider area of the head and neck, which includes the lip and oral cavity, the paranasal sinuses and nasal cavity, the oropharyngeal (pharynx and larynx), laryngeal, nasopharyngeal, and hypopharyngeal cavities. About 90 % of head and neck cancers are squamous cell carcinomas (161), also called epidermoid carcinomas. They arise from squamous cells, which are flat and thin cells, that reside in the epidermis, the outer layer of the skin, and in the mucous membranes, the lining of the hollow organs of the body, but also in the lining of the respiratory and digestive tracts (162). HNSCCs as a group ranks seventh in the list of the most frequent cancer types worldwide, and ninth in the most fatal cancer types according to the World Health Organization (WHO) (163). It accounts for approximately 600,000 new cases diagnosed per year worldwide (164, 165), with the majority being locally advanced, often treated locally with surgery and radiotherapy, followed by chemotherapy (166). Squamous cell carcinoma (SCC) is considered to display a high metastatic rate, especially in cases where the carcinomas are large, deep, or poorly differentiated, where they are located on the lip, ear, temple and cheek, or where there is perineural invasion.

Even though it is regarded as a group, the fact that HNSCC originates in multiple regions of the head and the neck, with potentially varying molecular mechanisms regulating DNA repair, makes it extremely divergent between cases. Thus, it is of great importance to understand the origin of the differences in the DNA repair process within the individual HNSCC sub-types, and to exploit new treatment pathways that can selectively enhance the therapeutic result (167).

1.4.1 Development of HNSCC: Alcohol and tobacco overconsumption.

Development of HNSCC has been associated with extensive consumption of alcohol and tobacco products, with high frequencies of carcinogenesis particularly in the most exposed areas of the upper aero-digestive track in smokers and drinkers (168). In fact, a combination of alcohol and the known carcinogens contained in tobacco products have

been linked to enhanced genetic disruptions, responsible for HNSCC development. Multiple studies have provided evidence for genetic changes including oncogene overexpression, muted tumor suppressor genes, chromosomal alterations and aberrations, that lead to excess cell proliferation, tumor growth and metastatic invasion. It has been suggested that 60 % of HNSCC cell lines displayed deletions in chromosomes (3p) coding for multiple tumor suppressor genes, resulting in dysfunctional proteins encoded by these genes (169-171). Moreover, up to 50 % of HNSCC cases has been reported to display chromosomal amplifications in 11q13, resulting in overexpression of Cyclin D1 and cortactin, that may promote tumor progression and are related to poor clinical prognosis and increased metastasis (172-176). Finally, HNSCC has also been strongly associated with mutation and loss of function of the tumor suppressor protein p53 (177).

1.4.2 Development of HNSCC: HPV infection

Another major risk factor in HNSCC development is infection with Human papilloma virus (HPV). The proportion of HNSCC containing HPV DNA is relatively high and is estimated to be around 40 – 70 % (178) and approximately 80 % of HPV-positive HNSCCs are high-risk type 16 HPV (179). Interestingly, HPV-positive HNSCCs are clinically and molecularly distinct from HPV-negative HNSCCs and have a better prognosis irrespective of the treatment (180-185). Multiple studies have reported that survival rates in patients with HPV-positive are higher than that of HPV-negative HNSCC (186, 187). Although it is not fully understood how the HPV-associated cellular alterations respond to known therapies, recent studies have demonstrated that HPV-positive HNSCC cell line cells are more sensitive to IR compared to the HPV-negative ones *in vitro* (188-191).

HPV is a family of viruses, that consists of at least 200 subtypes, and can be broadly divided in two categories; the cutaneous HPV types that infect the basal epithelial cells of the hands and feet and the mucosal types that infect the inner lining of tissues, like the respiratory tract, the oropharyngeal region, or the anogenital epithelium. HPVs contain cyclical, double stranded DNA, coding approximately 8 genes, including the E1, E2, E4, E5, E6 and E7 genes. Although all viral genes are necessary for the replication and proliferation of the virus, the E6 and E7 are consistently expressed in HPV-positive

carcinomas. These oncogenes transcript the respective oncoproteins, E6 and E7, which are multifunctional proteins known to regulate cell cycle progression and proliferation, and transmembrane signaling. Also due to their transformation properties, E6 and E7 oncoproteins are known to regulate the transformation of established cell lines, immortalization of primary cell lines and chromosomal stability.

E7 is a small protein consisting of approximately 100 amino acids, that binds on to the 'pocket domains' and consequently downregulates the expression of the retinoblastoma protein (pRB), a tumor suppressor protein that represses the activation of multiple replication enzymes. E7 forces indirectly, the infected cells into S-phase and thus promotes replication. E6, a 158 long amino acid protein, consequently stimulates degradation and downregulation of the tumor suppressor protein p53, to prevent apoptosis following unscheduled cell cycle progression. This way E6 promotes cell cycle progression and tumor growth (179, 192-194). A third less studied oncogene, E5, has been recently associated with upregulation of DNA synthesis and cell cycle progression in keratinocytes, however it has been suggested that its function is most crucial in the initial steps of the viral infection as its expression is often lost following HPV integration (179, 195).

1.4.3 HNSCC cell lines for in vitro studies

Patient-derived cell lines are a tool offering a tumor specific model for scientific research. They are commonly used in translational research to investigate basic molecular and biochemical mechanisms, as well as genetic and immunological properties in various types of mammalian cancers. In addition, they are utilised to assess potential treatment responses. These offer significant advantages, such as low cost, high sample homogeneity, and most importantly avoidance of legal and ethical issues associated with animal experiments (177). The most common technique for HNSCC cell line generation is the *explant cultured method*, during which, fresh tumor tissue is surgically removed. The tumor fragments (epithelial cells) grow in culture medium supplemented with amino acids and serum, and fibroblasts are removed frequently using a cell scraper or differential trypsinization (DF). Next, the cells are cultured and maintained under standard conditions of oxygen, CO₂, and temperature resembling that

of the human body. After a short *lag* phase where cell growth is minimal, cells pass in the *log* phase and are growing exponentially. During log phases the cells go through several passages, which has been reported to affect their resemblance of the original tumor, nevertheless *in vitro* studies in genetic and molecular cytogenetic of HNSCC cells suggested that they do closely resemble the primary tumors (177, 196-198).

It is reported that more than 300 HNSCC immortalized cell lines have been established and are commercially available for *in vitro* studies, with plenty of HPV-negative cell lines, particularly from the oral cavity and the larynx, but limited HPV-positive cell lines. It is worth noting that generation of HPV-positive HNSCCs primary cell lines has been profoundly difficult (177). Indeed, there are only six immortalized HPV-positive HNSCC cell lines available. However, only recently a new HPV-positive oropharyngeal SCC cell line was established, yet it has been reported to be extremely slow to initiate, with a doubling time 3 times slower than those in other HNSCC cell lines, and a success rate for establishment of <5% that also required the use of xenografts in nude mice (199). Unfortunately, there are major disparities between HPV-negative and the available HPV-positive cell lines, as the latter largely originate from both the oral and oropharyngeal cavities and are derived from heavy smokers and alcohol drinking patients. On top of that, both HPV-positive and HPV-negative HNSCC cell lines have proven challenging for *in vitro* culture, with slow doubling times and increased risk of contamination, although the reason behind this is yet to be determined. In spite of these drawbacks, these cell lines have been fully characterised, have a confirmed HPV status and constitute a reasonably reliable model. Also, the fact that these cell lines have gone through carcinogenesis *in vivo*, as they have been derived directly from tumor tissue, offers an improved viral model of HPV-positive cancer, in comparison with experimental transfection of E6 and E7 into normal squamous cell lines (200).

1.4.4 Targeting DDR in HNSCC cells

Despite the continuous technological developments, and the ongoing improvement of current and novel treatments as well as the advanced delivery techniques, the mortality rates of HNSCC have not shown significant improvement over the last few decades. The mortality rate for HNSCC patients in the United States have been estimated to be as high

as 60 %, with a five - year survival of only 40 % under standard treatment (177). In the United Kingdom, according to cancer research UK, there are 12,200 new cases per year, 2/3 of which are male patients, making HNSCC the 8th most common cancer type. Mortality is estimated to be around 33 % and over the last decade, have increased by almost 16 % (201). This is due to the great risk of invasive spread and regional metastasis. In fact, head and neck cancers are associated with cervical lymph nodes metastasis followed by spread to distant sites, mainly the lung and liver. However, HPV-positive HNSCCs and particularly oropharyngeal SCCs, display a much lower risk of regional recurrences and higher chances of tumor control and increased overall survival (202). In addition to the dependence on HPV status and environmental factors such as consumption of alcohol and tobacco products, the peculiarity of the region must be considered. Head and neck cancers are accounted as a group, yet they consist of biologically distinct units that possibly exhibit vast variations in their molecular mechanisms underlying development and progression of HNSCC and thus likely result in variable therapeutic outcomes (200).

The improved outcome and survival rates demonstrated in patients with HPV-positive HNSCC in comparison to patients with HPV-negative disease, is largely due to increased responsiveness of HPV-positive tumours to radiotherapy and chemotherapy (186, 187, 203, 204). Several studies have reported differences in radiotherapy response between HPV-positive and HPV-negative HNSCC in cultured cells derived from patients. It has been indicated that the delayed DSB repair observed via comet assay and DNA repair foci analysis, is caused by defects in the signalling and repair of DSBs in HPV-positive HNSCC cells (168, 178, 205, 206). However, there are some discrepancies in relation to the specific DSB repair defect, as reduced expression of proteins involved in both NHEJ (53BP1 and DNA-Pk) and HR (BRCA2 and RAD51) have been observed. In addition, upregulated levels of enzymes involved in the base excision repair (BER) pathway, including XRCC1 and PARP-1 in HPV-positive HNSCC cells, have been demonstrated (207).

The fact that the improved outcome in HPV-positive HNSCC patients has been associated with altered capacity for DNA repair in HNSCC cells *in vitro*, revealed that targeting the DDR, particularly in relatively radioresistant HPV-negative HNSCC, that

display proficient DNA repair mechanisms, may be an effective strategy for the radiosensitisation of the tumour (208). Specifically, the major protein kinases that coordinate the repair of DNA DSBs through NHEJ and HR, ATM, ATR and DNA-PKcs, are increasingly being investigated as targets for inhibitors to increase cellular sensitisation to IR, in particular x – ray irradiation. Targeting ATM in HNSCC cells was only examined in one study. The ATM inhibitor GSK635416A (2 μ M) was demonstrated to increase radiosensitivity in five HPV-negative HNSCC cell lines, the UTSCC2, UTSCC8, UTSCC24A, UTSCC36 and UTSCC40, as suggested by the accumulation and persistence of DNA DSBs observed by gel electrophoresis (209).

A number of studies have also focused on targeting ATR in HNSCC cells. Utilising siRNA treatment to knockdown ATR activity significantly increased the radiosensitivity in three HPV-negative HNSCC cells, the UPCI-SCC029B, UPCI-SCC040 and UPCI-SCC131. These relatively radioresistant cell lines contained loss of chromosome 11q, associated with increased radioresistance and poor patient prognosis (210). In addition, treatment with ATR inhibitors VE821 (1 μ M) and AZD6738 (0.25 μ M) have demonstrated increased radiosensitivity in one HPV-negative HNSCC cell line, SQ20B (211), and four HPV-negative HNSCC cells in two separate studies, the Cal27 and FaDu (212); HN4 and HN5 (213) respectively, revealing abrogated HR via γ H2AX and Rad51 foci and cell cycle progression, with subsequent increased apoptosis. The majority of these studies have focused on utilising clonogenic assays as an end point. In addition, targeting ATR in combination with radiation was shown to enhance radiosensitivity in HNSCC 3D spheroids. Specifically, ATR inhibitor AZD6738 (1 μ M) was shown to impede growth of HPV-negative FaDu spheroids, which are more representative of the original tumour *in vivo* (214).

Finally, other studies examined DNA-PKcs as a target for radiosensitisation in HNSCC cells included siRNA as well as inhibitor treatments. Specifically, depleting DNA-PK using siRNA was demonstrated to significantly radiosensitise two HPV-negative HNSCC cell lines, the UTSCC15 and UTSCC45, as shown by the persistent DSBs revealed by the increased γ H2AX and 53BP1 foci 24 h post irradiation (215). Moreover, the specific DNA-PKcs inhibitor KU0060648 (0.25 μ M) have been shown to enhance radiosensitivity in two HPV-negative HNSCC cell lines, the HN4 and HN5 (213). Similarly, the DNA-PKcs

inhibitor IC87361 (3.3 μM) enhanced the radiosensitivity in three HPV-negative HNSCC cell lines, the UTSCC54C, UTSCC74B and UTSCC76B, as demonstrated by the reduced survival observed via clonogenic assays (216). Lastly, the DNA-PKcs inhibitor NU7441 (1 and 2.5 μM), effectively radiosensitised HPV-negative, SQD9, SC263 and Cal27, but also HPV-positive UMSCC47, UPCISCC104 and UPCI-SCC154 HNSCC cell lines. Following DNA-PKcs inhibition, persistence of γH2AX foci, and therefore of DSBs, was observed 24 post IR in two HNSCC cell lines, the SQD9 and UPCI-SCC154. In addition, *in vivo* models were utilised in the same study, demonstrating that treatment with NU7441 in combination with IR led to delayed tumour growth in SQD9 and UPCISCC154 HNSCC xenografts, but also HPV-negative HNSCC patient-derived xenografts HNC019 and HNC021 (217).

Cumulatively, these data demonstrated to enhance the radiosensitivity of HNSCC cells *in vitro* with some evidence also being generated in xenograft models *in vivo*, although a variability in response was observed that was associated with the specific cell line or model utilised. Furthermore, it was unclear whether these discrepancies depended on the HPV status and were selective for HPV-positive and/or HPV-negative HNSCC cells. Such a dependency could be due to the inherently altered proficiency of DSB repair mechanisms of these cells which therefore resulted in their differential radiosensitivity. However, the accumulating evidence of targeting strategies in combination with radiotherapy suggested that targeting the DSB repair pathway can be an effective approach for increasing the radiosensitivity of HNSCC cells in response to x – rays.

In addition to x – ray radiotherapy, PBT is increasingly being utilised for HNSCC treatment (218). This is due to the precise delivery of the radiation dose to the tumour via this radiotherapy technique, resulting in sparing of the normal tissues and OARs. However, there is still uncertainty about the biological impact of protons versus photons, and the use of targeted drugs to optimise tumour cell radiosensitivity, which is important in defining potential combinational strategies (51). As discussed in Section 1.2.6, there is contrasting literature regarding proton induced DSB repair, with a number of studies suggesting that HR is the major pathway for the repair of DNA DSBs, which would indicate that targeting ATR would be a successful radiosensitisation strategy (102, 118, 119). While other studies largely reflect that NHEJ, co-ordinated by ATM and DNA-PKcs, is the major DSB repair pathway employed following proton irradiation (105, 115-117).

It is most likely that there are tumour specific dependences on the DNA DSB repair pathway majorly employed in response to protons, which could also be dependent on cell confluency and therefore cell cycle stage at which the cells are irradiated. Nevertheless, studies specifically comparing the response of HPV-positive and HPV-negative HNSCC cells to both photons and protons and the impact of DNA DSB repair inhibition have not previously been reported.

Chapter 2: Aims

DSBs are mainly resolved via NHEJ and HR repair, which are driven by ATM, ATR and DNA-PKcs protein kinases. These repair mechanisms although important for cell proliferation, also contribute to tumor resistance in IR, complicating radiotherapy. This includes x – rays (conventional radiotherapy) and proton beam therapy, which is increasingly being utilised due to precise delivery of the radiation dose to the tumor, although the biological impact of protons versus photons is largely unknown. Interestingly, defects in the signaling and repair of DSBs found in HPV infected HNSCC patients has been associated with improved survival rates compared to HPV-negative associated disease. Indeed, recent studies have shown that HPV-positive HNSCC cells are more sensitive to IR. This has revealed that targeting the DNA damage response, may be an effective strategy for radiosensitising of the tumour.

DNA repair inhibitors are widely used in research, as a monotherapy or in combination with DNA damaging agents with several studies demonstrating that inhibition of ATM, ATR or DNA-PKcs can significantly sensitise tumor cells to x – rays including breast, pancreatic, and prostate cancer cells. Few studies have shown radiosensitisation of HNSCC cell lines in response to x – rays, although the impact of these inhibitors on HPV-positive versus HPV-negative HNSCC cells is yet to be determined. Moreover, there are currently no published studies investigating the impact DSB repair inhibition in combination with PBT in HNSCC.

With a long-term goal to improve current treatments for HNSCC patients, I aimed to explore potent inhibitors for ATM, ATR, or DNA-PKcs in the radiosensitisation of HNSCC cells in response to both x – rays and protons. The specific aims of this study were to:

1. Investigate the impact of DSB repair pathway inhibition, in HNSCC cells *in vitro*, alone or in combination with IR (x – rays and protons).
2. Exploit potential differences in the DNA damage response, between HPV-negative and HPV-positive HNSCC cells.
3. Decrypt differences in cellular responses following exposure to x – ray and proton irradiation, and how these regulate the DNA repair pathway choice.

Chapter 3: Methodology

3.1 Materials

The protein kinase inhibitors KU-55933 (ATM Inhibitor; ATMi), NU7441 (also called KU-57788, DNA-PKcs Inhibitor; DNA-PKcsi) and VE-821 (ATR Inhibitor; ATRi) were purchased by Selleckchem (Munich, Germany) and dissolved in dimethyl sulfoxide (DMSO).

Cell culture reagents were obtained from Sigma-Aldrich (St Louis, USA), and general laboratory reagents were obtained from Sigma-Aldrich (St Louis, USA), Bio-Rad (Hemel, Hempstead, UK), or Fisher Scientific (Loughborough, UK).

Primary and secondary antibodies were purchased by Cell Signaling Technology, (Leiden, The Netherlands), Sigma-Aldrich (Gillingham, UK), Abcam (Cambridge, UK), Thermo Fisher Scientific (Massachusetts, USA), Li-Cor Bioscience (Nebraska, USA), Bethyl Laboratories (Montgomery, USA) and BD Bioscience (California, USA) were used to probe for specific proteins of interest during immunoblot analysis, and specific foci formation during Immunofluorescent staining and DNA repair foci analysis. The antibodies used are listed in Tables 3.1 and 3.2, summarising their individual characteristic.

3.2 Cell culture

3.2.1 Cell line Culture

Tissue culture work was carried out in aseptic conditions. It was performed in class II hood cabinets with laminar flow that was cleaned with 70% ethanol both before and after use, and was sterilised with 20 min UV light exposure between two uses. Cells were maintained and grown in standard conditions equivalent to the human body at 37°C and 5 % CO₂ in a humidified cell culture incubator and were cultured using tissue culture grade plastics. All cell culture reagents (obtained from Sigma Aldrich, St Louis, USA) were pre-warmed in a water bath at 37°C before use and are listed below.

- Dulbecco's Modified Eagle's Medium (DMEM) – 25 mM HEPES and sodium bicarbonate, 4500 mg/L glucose, sterile filtered.

- Minimal Essential Medium (MEM) – 25 mM HEPES, without L- glutamine sterile filtered.
- Dulbecco’s Modified Eagle’s Medium/Nutrient Mixture F-12 Ham (adMEM/F12) - With 15 mM HEPES and sodium bicarbonate, without L-glutamine, liquid, sterile-filtered, Medium for Spheroid assays, supplemented with 1 % B27, 1 % L-Glut, 1 % P/S, 0.5 % N2 and 0.1 % Heparin, as well as 2:10000 EGF and 1:10000 FGF just before use.
- 0.25% Trypsin-EDTA solution –sterile filtered, 2.5 g porcine trypsin, 0.2 g EDTA, 4Na/L Hanks’ Balanced Salt Solution with phenol red.
- Dulbecco’s Phosphate Buffered Saline (PBS)

Table 3. 1. Primary antibodies. List of the primary antibodies used throughout this research project. Host organism, clonality, dilution and source are displayed.

| <i>Antibody</i> | <i>Host organism</i> | <i>Clonality</i> | <i>Dilution</i> | <i>Source</i> |
|-------------------------------------------|----------------------|------------------|-----------------|-----------------|
| <i>Anti-phosphoATM S1981</i> | Rabbit | monoclonal | 1:1000 | Cell Signalling |
| <i>Anti-phosphoATR S428</i> | Rabbit | polyclonal | 1:1000 | Cell Signalling |
| <i>Anti-phosphoATR T1989</i> | Rabbit | polyclonal | 1:1000 | Cell Signalling |
| <i>Anti-phosphoDNA-PKcs T2609</i> | Mouse | monoclonal | 1:1000 | Abcam |
| <i>Anti-phosphoDNA-PKcs S2056</i> | Rabbit | monoclonal | 1:5000 | Abcam |
| <i>Anti-Actin γH2AX</i> | Mouse | monoclonal | 1:20000 | Sigma-Aldrich |
| <i>53BP1</i> | Mouse | monoclonal | 1:5000 | Sigma-Aldrich |
| <i>Rad51</i> | Rabbit | polyclonal | 1:4000 | Bethyl Labs |
| <i>p16</i> | Rabbit | monoclonal | 1:5000 | Abcam |
| | Mouse | monoclonal | 1:500 | BD bioscience |

Table 3. 2. Secondary Antibodies. List of the fluorescently tagged secondary antibodies used throughout this research project to target the primary antibodies. Host organism, target immunoglobulin isotype, dilution and source are displayed.

| <i>Antibody</i> | <i>Host organism</i> | <i>Dilution</i> | <i>Source</i> | <i>Exp</i> |
|----------------------------------------|----------------------|-----------------|---------------|------------|
| <i>Alexa Fluor 680 Anti-Mouse IgG</i> | Goat | 1:10000 | Invitrogen | WB |
| <i>Alexa Fluor 680 Anti-Rabbit IgG</i> | Goat | 1:10000 | Invitrogen | WB |
| <i>IR Dye 800 Anti-Rabbit IgG</i> | Goat | 1:10000 | Li-Cor | WB |
| <i>IR Dye 800 Anti-Mouse IgG</i> | Goat | 1:10000 | Li-Cor | WB |
| <i>Alexa Fluor 555 Anti-Mouse</i> | Goat | 1:500 | Invitrogen | IF |
| <i>Alexa Fluor 488 Anti-Rabbit</i> | Goat | 1:500 | Invitrogen | IF |

Human cancer cell lines used in this research study were the HPV-positive UMSCC47 and two HPV-negative UMSCC6 and UMSCC74A oropharyngeal squamous cell carcinoma cell lines, kindly gifted by Prof T. Carrey, University of Michigan, USA. The HPV-negative A253 HNSCC cells originated from the submaxillary gland were supplied from ATCC (Teddington, UK). All of them were cultured in Dulbecco's Modified Eagle Medium (DMEM) supplemented with 10 % fetal bovine serum (FBS), 2mM L-glutamine, 1 % penicillin – streptomycin and 1 % non-essential amino acids (NEAA). Moreover, the HPV-positive oropharyngeal squamous cell carcinoma cells UPCI-SCC090 were kindly provided by Dr S. Gollin from the University of Pittsburgh; the HPV-negative cells from the hypopharynx, FaDu HNSCC, originated from ATCC (Teddington, UK), and the HPV-positive cells from the oral cavity UPCI-SCC154 HNSCC were cultured in Minimal Essential Medium (MEM) supplemented with 10 % fetal bovine serum (FBS), 2mM L-glutamine, 1 % penicillin – streptomycin and 1 % non-essential amino acids (NEAA). The individual characteristics of these cell lines are summarised in Table 3.3. All cells were incubated under standard conditions in 5 % CO₂ at 37°C and were authenticated in our laboratory by STR profiling.

Table 3. 3. HNSCC cell lines. List of HNSCC cell lines used in this research project, summarising their individual characteristics, region of origin, HPV status, p53 status, age & sex of the patient, TNM (Tumour, Node, Metastasis) stage. wt: wild type, mut: mutant y.o.: year old, M: male, F: Female, NS: not specified (177, 219, 220). *Derived from metastatic site: tongue

| Cell line | Region | HPV | p53 | Age / Sex | TNM stage |
|-------------|-----------------------------------|-----|-----|-----------|-----------|
| UMSCC6 | Oropharynx (base of the tongue) | - | wt | 32y.o./ M | T2N0M0 |
| UMSCC47 | Oral cavity (lateral tongue) | + | wt | 53y.o./ M | T3N1M0 |
| UMSCC74A | Oral cavity (base of the tongue) | - | wt | 51y.o./ M | T3N0M0 |
| UPCI-SCC090 | Oropharynx (base of the tongue) * | + | wt | 46y.o./ M | T2N0 |
| UPCI-SCC154 | Oral cavity (tongue) | + | wt | 54y.o./ M | T4N2 |
| A253 | Oral cavity (salivary gland) | - | mut | 54y.o./ M | NS |
| FaDu | Hypopharynx | - | mut | 56y.o./ M | NS |

3.2.2 Thawing cells

Cells, long termed stored in liquid nitrogen (N₂), were kept in cryovials containing 90 % FBS and 10 % DMSO. They were defrosted in a water bath at 37°C for 30 sec. As high concentration of DMSO can be toxic, 1 ml fresh medium was added dropwise to the cells, before complete defrost, and gently mixed via pipetting. The cell suspension was then transferred into a sterile 15 ml tube and 8 ml of warm medium was gently added, before centrifugation at 1500 rpm for 5 min at room temperature. The DMSO-containing supernatant was removed, and the cell pellet was resuspended in 1 ml fresh medium and transferred to a T75 culture flask containing 11 ml medium. The flask was then incubated in a humidified cell culture incubator under standard conditions at 37°C and 5 % CO₂.

3.2.3 Passaging Cells

Cells growing exponentially in tissue culture flasks reach confluency and need to be split (passaged) into new flask, in order to have room to grow and nutrients to be fed. When cells were 70 – 90 % confluent, the old medium was removed by aspiration, and 7 ml warm PBS were added to wash the monolayer of cells and then removed. Then, 1 ml of 0.25% trypsin-ETDA was added and the cells were incubated for 2 - 10 min in the humidified cell culture incubator under standard conditions at 37° C and 5 % CO₂, allowing time for enzyme activation and cell detachment from the plastic. Following that, 9 ml of warm medium were added in order to neutralise the trypsin and cells were mixed via pipetting to create a single-celled suspension. Cells were then either used for in vitro experimental work, and/or a certain portion of the cells were transferred into a new culture flask, and this was topped up with fresh medium to have 12 ml in total. Fast growing cells were split in 1:10 ratio twice a week, and slower growing cells were split in 1:2 once a week, with the HPV-positive cells were specifically slow growing. In fact, during their culture period, splitting ratios varied slightly when cells were undergoing more rapid or slower growth than usual. Table 3.4 summarises the individual growing characteristics for the cell lines used in this research study. Cells were then stored in the humidified cell culture incubator under standard conditions. Cells were cultured for up to 20 passages and then were replaced by freshly thawed cells to secure behavioural consistency.

3.2.4 Freezing Cells.

Cells need replacement after approximately 20 passages, and a stock of early passage number cells must be stored and replaced in the liquid N₂. Therefore, newly thawed cells were split into multiple flasks and let to grow. Once the flasks were 70 – 90 % confluent, medium was removed, and the cell were washed with PBS as described above. 0.25 % Trypsin-EDTA was added for 2 – 10 min, and once the cells detached from the plastic surface were mixed with 9 ml of medium. The cell suspension was then transferred to a 15 ml tube and was centrifugated at 1500 rpm for 5 min in room temperature. The medium was removed, and the cell pellet was resuspended in 1 – 2 ml freezing medium (90 % FBS with 10% DMSO) and transferred to 1 or 2 cryovials depending on the size of

the pellet. Finally, the cryovials were placed in a cell freezing container, (CoolCell Freezing Container, Corning, Sigma Aldrich, St Louis, USA) and placed into a -80° C freezer for 24 h, for a slow and contained drop in their temperature, before being transferred to long-term storage in liquid N₂.

Table 3. 4. Passaging of cells. HNSCC cell lines used in this research project along with their splitting ratio and frequency as well as the size of the flask used for maintenance and culture are displayed.

| <i>Cell line</i> | <i>Splitting ratio</i> | <i>Frequency</i> | <i>Flask</i> | <i>Medium</i> |
|--------------------|------------------------|------------------|--------------|---------------|
| <i>UMSCC6</i> | 1:3 | Twice a week | T75 | DMEM |
| <i>UMSCC47</i> | 1:5 | Twice a week | T75 | DMEM |
| <i>UMSCC74A</i> | 1:10 | Twice a week | Y75 | DMEM |
| <i>UPCI-SCC090</i> | 1:2 | Once a week | T25/T75 | MEM |
| <i>UPCI-SCC154</i> | 1:2 | Once a week | T25 | MEM |
| <i>A253</i> | 1:10 | Twice a week | T75 | DMEM |
| <i>FaDu</i> | 1:5 | Every 5 days | T25/T75 | MEM |

3.3 Ionising radiation

X – ray *in vitro* irradiations were performed in the lab using the CellRad x – ray irradiator (Faxitron Bioptics, Tucson, USA). The radiation dose (1 – 4 Gy) was delivered in a time-controlled manner with a standard rate of 3 Gy/min, 3 mA and 100 kV with no additional filtration on the x – ray beam. 6-well plates and petri dishes (35, 60, or 100 mm) were placed in the centre of the irradiation field.

Proton *in vitro* irradiations were performed using a horizontal, passive - scattered beam line of 60 MeV maximal energy from the Douglas Cyclotron at Clatterbridge Cancer centre (221). Cells in 35 mm petri dishes were positioned at the isocentre 70 mm from a brass collimator (43 mm diameter) and were irradiated directly by an approximately 1 keV/μm pristine beam of 58 MeV effective energy (dose rate of approximately 5 Gy/min).

3.4 Cell Harvesting following drug and radiation treatment.

Cells were pre-seeded in petri dishes, usually 60 or 35 mm, and incubated overnight. When 80-90 % confluent, the cells were pre-treated for 1 h with the inhibitors dissolved in medium, or DMSO dissolved in medium as a control. The concentrations used were 10 μ M of KU-55933 (ATMi), 1 μ M of NU7441 (DNA-PKcsi), 1 μ M of VE-821 (ATRi) or 10 μ M of DMSO. Then the dishes were irradiated with 4 Gy x-rays or protons and the medium was changed, with fresh medium containing the inhibitor or DMSO at the same concentration. Cells were then incubated in a humidified cell culture incubator under standard conditions of 5 % CO₂ at 37°C for up to 24 h and were removed to be harvested at different time points (0, 1 h, 2 h, 4 h, 8 h, 24 h) post irradiation. To harvest the cells, the medium was removed and surface of the dishes were washed with ice cold PBS, fresh PBS was added and then the cells were carefully scrapped off the plastic and transferred into a pre-cooled 15 ml tube, the scraping in fresh PBS was performed twice. Then the pellet was collected by centrifugation at 1500 rpm for 5 min at 4°C, the supernatant was removed, and the pellet was resuspended in 1 ml of cold PBS and was transferred to a pre-cooled 1.5 ml tube, which was then centrifuged at 1500 rpm for 5 min at 4°C. Supernatant was removed and the pellet was stored at -80°C.

3.5 Whole cell extracts

Whole cell extract was produced from a frozen cell pellet. Pellets were left in -80°C for at least 1 h, then pellet volume was estimated and resuspended in an equivalent of in one volume of Tanaka Buffer 1 [10 mM Tris-HCl (pH 7.8), 200 mM KCl, and 1 μ g/ml of each protease inhibitor: pepstatin, aprotinin, chymostatin and leupeptin, 1 mM PMSF and 1 mM DTT, as well as 10 mg/ml of the phosphatase inhibitor cocktail 3] and two volumes of Tanaka Buffer 2 [10 mM Tris-HCl (pH 7.8), 600 mM KCl, 40 % glycerol, 0.1 mM EDTA, 0.2 % Nonidet P-40, 1 μ g/ml of each protease inhibitor: pepstatin, aprotinin, chymostatin and leupeptin, 1 mM PMSF and 1 mM DTT, and 10 mg/ml of the phosphatase inhibitor cocktail 3, (P0044 , Sigma-Aldrich, St Louis, USA)]. The cell suspension was thoroughly mixed for 30 min by rotation at 4° C. Cell debris was pelleted

by centrifugation at 40,000 rpm for 20 min at 4°C. The supernatant, containing the whole cell protein extracts, was collected and transferred to a pre-cooled 1.5 ml Eppendorf tube and kept for long term storage in -80°C, while the solid residues remaining in the tube were discarded.

3.6 Bradford Assay

Protein concentrations in the whole cell extracts were determined via the Bradford assay spectroscopic analysis. During this, three different types of solutions were prepared in individual 3 ml plastic cuvettes, one blank, one containing a protein standard as control, and one for each sample to be measured. The blank was made up with 960 µl of Bradford reagent (Bio-Rad Laboratories, California, USA), and 40 µl of dH₂O, the control was composed of 960 µl of Bradford reagent and 40 µl of 0.2 mg/ml BSA (Bovine serum albumin; Thermo Fisher Scientific, Massachusetts, USA). Finally, for each sample a separate solution was prepared with 960 µl of Bradford reagent, and 40 µl of dH₂O containing protein extract. The volume of protein extract added varied between 1-4 µl, thus the amount of dH₂O was changing accordingly between 36-39 µl, in order to have 40 µl in total, with higher volumes of protein extract required when concentration was low (e.g. when protein extract derived from a small cell pellet), and vice versa. The solutions were mixed and left to react with Bradford reagent for 5 min at room temperature. Using a UV spectrophotometer (Cecil Instruments Limited, Cambridge, UK) following zeroing with the blank sample and calibration with the control sample, optical density was measured by the absorbance at 595 nm, for each protein extract sample. Then, the sample concentrations were calculated using the equation 3.1.

$$C \left(\frac{mg}{ml} \right) = \frac{0.2}{BSA} * a * x \quad (3.1)$$

C: protein extract concentration; BSA: value of the BSA control sample; α: can be 40, 20, or 10 when 1 µl, 2 µl or 4 µl of protein extract were added to the solution; x: value of the sample in question.

3.7 SDS-PAGE and Western Blot

The whole cell extracts contain multiple proteins that were then separated according to their molecular weight utilising the Sodium dodecyl sulphate-polyacrylamide gel electrophoresis (SDS-PAGE) technique. For higher molecular weight proteins, pre-cast 10-well gradient gels of 4-12 % Tris-glycine were used (Invitrogen, Thermo Fisher Scientific, Loughborough, UK). For lower molecular weight proteins, 10-well 16% Tris-glycine gels were prepared in the laboratory. To produce these, a separating and a stacking gel were prepared and poured into empty 1.5 mm gel cassette (Novex, Thermo Fisher Scientific, Loughborough, UK). The separating part of the gel was made up of 377 mM Tris-HCl pH 8.8, 0.1 % SDS, 2 mM EDTA, 16 % acrylamide/bis solution (30:0.8; Bio-Rad, Hemel, Hempstead, UK), 0.1 % ammonium persulphate (APS), and 0.1 % tetramethylethylenediamine (TEMED) and it was poured up to the $\frac{3}{4}$ of the cassette. The gel solution was then left to set for at least 30 min and topped up with 1 ml of 100% ethanol to prevent and remove any bubbles. Once the gel had set, the ethanol was removed, and the cassette was washed with dH₂O and dried with clean filter paper. The stacking part of the gel was a 5 % stacking gel solution consisting of 125 mM Tris-HCl pH 6.8, 0.1 % SDS, 2 mM EDTA, 5 % acrylamide/bis solution (30:0.8; Bio-Rad, Hemel, Hempstead, UK), 0.1 % ammonium persulphate (APS), and 0.1 % tetramethylethylenediamine (TEMED) that was poured on the remaining $\frac{1}{4}$ of the cassette, on top of the separating gel. Finally, a 10-well comb was inserted into the gel solution within the cassette and the gel was left to set for at least 30 min. The gel was then wrapped in wet cloth and kept in 4° C to be used within 2 weeks.

In each gel well, protein extracts were loaded in the form of SDS-PAGE sample buffer, this consisted of 1/3 of 3xSDS dye (25 mM Tris-HCl pH 6.8, 2.5 % mercaptoethanol, 1 % SDS, 10 % glycerol, 0.05 mg/ml bromophenol blue, and 1 mM EDTA) and 2/3 protein extract (25 – 40 µg) and dH₂O. Due to differences in the initial concentration of the whole cell extracts, varying volumes were added in the solution of each sample and dH₂O was added to top this up to reach the 2/3 of the volume required. Moreover, the amount of protein (µg) added could differ between gels yet was the same within an individual gel. Once all the components were added, the samples were vortexed, and then heated for 5 min in 95° C. Following, the samples were loaded on the gel and

electrophoresed in 1x Tris-glycine SDS (TGS) running buffer (25 mM Tris-HCl pH 8.3, 192 glycine, and 0.1 % SDS; Fisher Scientific, Loughborough, UK) at 125 V for 2 h, in SDS-PAGE Mini Gel Tanks (Fisher Scientific, Loughborough, UK). Typically, in the first well of the gel, 1µl of the Precision Plus Protein All Blue Prestained Protein Standards (10 kDa – 250 kDa; Bio-Rad Laboratories, California, USA) were loaded as standard protein marker.

During electrophoresis, proteins were separated according to their molecular weight and after this, proteins were then transferred onto an Immobilon FL polyvinylidene difluoride membrane (PVDF) (Millipore, Watford, UK), in order to probe for and visualise specific proteins of interest. The transfer was performed utilising a Mini Blot Module (Fisher Scientific, Loughborough, UK) that was loaded into the Mini Gel Tank, used in the electrophoresis step after this was rinsed off with clear water. The gel cassette was opened and the acrylamide gel was removed and placed directly over the PVDF membrane that was activated in 100 % methanol for 15 sec, washed in dH₂O for 1 min and washed in cold transfer buffer [1x Tris-glycine (TG; 25 mM Tris-HCl pH 8.3, 192 mM glycine; Fisher Scientific, Loughborough, UK), 20 % methanol] for at least 1 min. The duo was then enclosed within a set of filter papers and a set of sponges, fully covered in cold transfer buffer. The so-called sandwich of membrane-gel was then placed inside the Mini Blot Module, that was filled with more cold transfer buffer. Finally, the Mini Gel Tank was filled with cold water to keep a low temperature during the transfer, which was conducted at 25 V for 1 h.

Next, the membranes were removed from the Mini blot Module, washed in PBS for 5 min, and were blocked for non-specific binding using Odyssey blocking buffer (Li-cor Biosciences, Cambridge, UK) diluted 1:1 in PBS, for 1 h at room temperature with rocking at 27 rpm. The membrane was then incubated with the primary antibody, made up in 1:1 solution of Odyssey blocking buffer and 1x PBS, containing 0.1 % Tween 20, overnight at 4°C rocking at 27 rpm. The next day, membranes were washed three times with PBS containing 0.1 % Tween 20 for 5 min with gentle rocking, and were incubated with secondary antibodies, made up in 1:1 solution of Odyssey blocking buffer and 1x PBS containing 0.1% Tween 20, for 1 h at room temperature with 27 rpm rocking. After that, they were treated with three 5 min washes with PBS containing 0.1 % Tween 20 and 1 time with PBS, at room temperature and gentle rocking. Lastly, the membranes were

scanned using the Odyssey image analysis system (Li-cor Biosciences, Cambridge, UK) in order to image and quantify the proteins.

Following the same steps, the primary antibody for Actin (acting as a loading control) was added for 1 h in room temperature, washed 3 times, before being incubated with secondary antibodies for 1 h at room temperature and further washed three times. It was then scanned for the second time using the Odyssey image analysis system in order to visualize and quantify actin, to normalise this relative to the protein of interest.

3.8 Immunofluorescent staining and DNA repair foci analysis

Visualisation and analysis of DNA repair progression was achieved by studying the formation, persistence or resolving of DNA repair focus formation, at the sites of DSB. For this technique, following the first steps of passaging cells described in Section 3.2.3, cells were trypsinised from a 70 – 90 % confluent flask. From a thoroughly mixed cell suspension, a sample of 15 μ l were taken onto a haemocytometer, and cells were counted under a light microscope, in order to estimate the cell concentration of the suspension and calculate the volume to obtain the required number of cells. Three cell lines were used, two HPV-negative and one HPV-positive, and the number of cells seeded per ml for this technique were UMSCC74A $1.5 \cdot 10^4$ cells/ml, UMSCC47 $2 \cdot 10^4$ cells/ml, and UMSCC6 $4 \cdot 10^4$ cells/ml. The cells were seeded on round glass coverslips, 13 mm in diameter (Nunc Thermanox, Fisher Scientific, Loughborough, UK), that were pre-sterilised in 100 % ethanol. For x – ray experiments, single coverslips were placed in 24-well plates (Greiner CELLSTAR® multiwell culture plates, Sigma-Aldrich, St Louis, USA) and 0.5 ml of the premade cell suspension was added in each well. There were two coverslips per condition. For proton irradiation, 4 coverslips were placed within a 35 mm dish, two for each condition, and 2 ml of the premade cell suspension were added, while extra care was paid to avoid overlap of the coverslips. After seeding, cells were incubated for 48 h in a humidified cell culture incubator under standard conditions at 37° C and 5 % CO₂, to allow cell growth. On the treatment day, the old medium was removed from the plates by aspiration and fresh medium containing either of the inhibitors or DMSO, as control, was added, 0.5 ml in the individual wells of the 24-well

plates, or 1.5 ml in the 35 mm dishes. The concentrations of the drug were 10 μ M of KU-55933 (ATMi), 1 μ M of NU7441 (DNA-PKcsi), 1 μ M of VE-821 (ATRI) or 10 μ M of DMSO and cells were further incubated with the drug under standard conditions for 1 h prior to irradiation. Following that, the cells received 4 Gy of IR, either x – rays or protons, and immediately after irradiation the medium was changed with fresh one, containing the same concentration of the inhibitors or DMSO. Cells were then incubated for up to 24 h under in 5 % CO₂ at 37° C in a humidified cell culture incubator, to allow time for DNA repair progression and the foci formation. Then at specific time points the cells were fixed, which stopped any biological processes at the stage they were left. Three foci markers were investigated, γ H2AX, 53BP1, and Rad51, the time points for the first two markers were 1 h, 4 h, and 8 h post irradiation, while the time points for Rad51 were 8 h, 16 h, and 24 h.

At the appropriate time, plates were taken out of the incubator, medium was removed by aspiration and cells were washed with PBS twice (0.5 ml per coverslip), before been fixed using 4 % paraformaldehyde (PFA; Sigma-Aldrich, St Louis, USA) for 10 min at room temperature (0.1 ml per coverslip). Coverslips were then washed with PBS, and cells were permeabilised with 0.2 % Triton X-100 in PBS (Cell Signalling Technology, Leiden, The Netherlands) for 10 min (0.2 ml per coverslip), and then washed three times with 0.1 % Tween-20 (Sigma-Aldrich, St Louis, USA) at room temperature. Coverslips were blocked to avoid non-specific staining via incubation with 2 % BSA (bovine serum albumin powder, Sigma-Aldrich, St Louis, USA) in PBS for 30 min at room temperature, rocking at 27 rpm (0.2 ml per coverslip) and then were further incubated with either γ H2AX, 53BP1 or RAD51 antibodies (Table 3.1), made in fresh 2 % BSA (1:50 in PBS), overnight at 4°C rocking at 27 rpm.

The following day, the antibodies were removed and following three 5 min washes with PBS with gentle rocking at room temperature, coverslips were incubated with either of the appropriate fluorescent secondary antibodies (Table 3.2), made in 2% BSA, for 1 h at room temperature, rocking at 27 rpm, covered in foil to protect them from exposure to light. Finally, the fixed cells were washed with PBS in triplicate for 10 min on a rocking platform, in the dark, and were mounted on microscope slides using Fluoroshield

containing DAPI (Sigma-Aldrich, St. Louis, USA). The slides and mounting media were left to set and were then stored in 4°C, protected from the light.

Cells were examined using an Olympus BX61 upright fluorescent microscope with a 40x Plan Super Apo 0.9NA objective, and a Photometrics CoolSNAP HQ2 CCD camera. MicroManager 1.4 software was used to capture images, 5 representative images were captured from each coverslip, and there were two coverslips for each condition. The images were then analysed using CellProfiler v.2.2.0 running a purpose-written analysis pipeline kindly provided by Prof Carlos Rubbi (University of Liverpool). This provided us with data that constructed spot frequency curves and ROC curves (Receiver operating characteristic) per cell line and treatment, that illustrated the true positive rates (TPR) against the false positive rates (FPR) and allowed to discriminate the appropriate threshold, Figure 3.1. The number of foci per nucleus were counted and averaged. The average number of foci per coverslip of the two replicate coverslips were then averaged and that was used as the respective number of foci per cell line per condition from each biologically independent experiment.

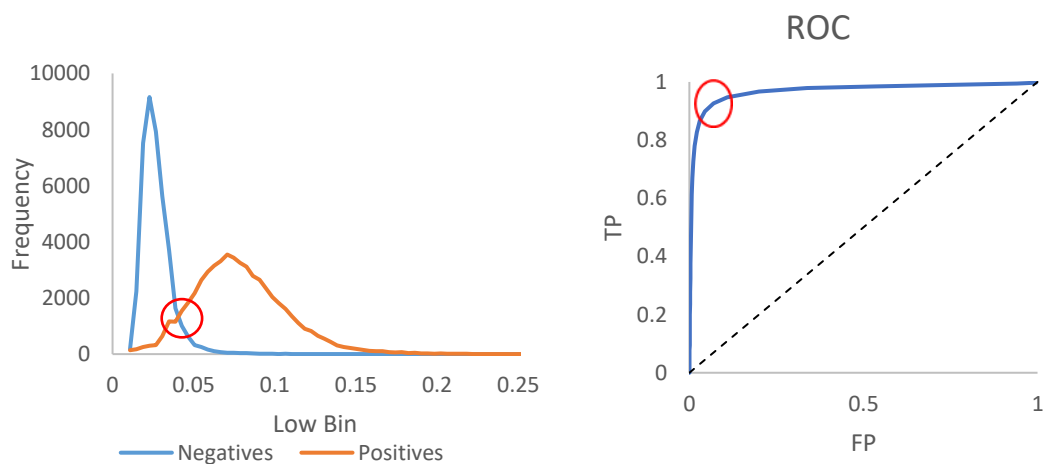


Figure 3. 1. Threshold discrimination in IF analysis. γ H2AX, 53BP1 and Rad51 foci formation was counted in HNSCC cell lines in response to inhibitor treatment and exposure to IR. Here 53BP1 foci formation in UMSCC47 was calculated above the threshold, marked with the red circle, to avoid counting of false positive spots. A) Spot frequency versus intensity curve, Negatives: spots in untreated cells, Positives: spots in treated cells (inhibitor, IR, or both); B) ROC curve, TP: true positive, FP: false positive; in blue line is the ratio TP/FP.

3.9 Colony Formation Assays

To assess cell survival and proliferation following treatment with a drug and/or exposure to IR, the colony formation (clonogenic) assay was utilised. For this technique, cells from a confluent flask were trypsinised and counted as described above (Section 3.2.3 and 3.8 respectively), and a defined number of single cells were pre-seeded in 6-well plates (Greiner CELLSTAR® multiwell culture plates, Sigma-Aldrich, St Louis, USA) for experiments involving x – ray irradiation, or 35 mm petri dishes (Falcon, Coning, New York, USA) for experiments involving proton irradiations. The plates were left overnight in a humidified cell culture incubator, allowing time for the cells to attach. 24 h later, the medium was removed by aspiration and 1.5 ml of fresh medium containing either of the inhibitors or DMSO, as control, was added 1 h prior to irradiation in each well. The concentrations used were, 10 μ M KU-55933 (ATMi), 1 μ M NU7441 (DNA-PKcsi), 1 μ M VE-821 (ATRi) and 10 μ M DMSO. After 1 h of incubation with the inhibitor or DMSO under standard conditions, cells were irradiated with increasing radiation doses, for x – rays 1 – 3 Gy, and for protons 2 – 6 Gy. Immediately after irradiation, the medium was replaced by fresh one, containing the same concentration of either of the inhibitors or DMSO, and cells were further incubated for 24 h. The next day, the medium was replaced again, with fresh medium without any inhibitors or DMSO, and the plates were further incubated for 6-10 days in a humidified cell culture incubator allowing time to the damaged single cells seeded to be repaired, proliferate, and creating colonies of cells.

Four cell lines were utilised, two HPV-positive and two HPV-negative, the UMSCC6, UMSCC47, UMSCC74A and UPCI-SCC090. The seeding densities varied between the cell lines and were determined according to their individual characteristics such as doubling time, colony morphology and size, as well as their plating efficiency, which is the ratio of colonies produced by untreated cells over the total amount of cells seeded in the well (equation 3.1). Increasing number of cells were seeded for increasing doses of IR, to secure that enough cells would survive the treatment and grow into colonies. For x – ray irradiations, the cells were seeded in two densities per condition in each 6-well plate, three replicates of the starting density in the upper row and three replicates of twice the starting density in the lower row of the plate. For proton irradiation, the cells were

seeded in separate 35 mm dishes and there were 3 dishes per condition. In table 3.5 are presented the seeding densities, along with the plating efficiencies for each cell line in x – rays (A) and protons (B).

Table 3. 5. Seeding densities for colony formation assays. The number of cells seeded for colony formation assays for each cell line and radiation dose are displayed, along with their respective plating efficiencies (PE), in unirradiated conditions. A. Cells seeded in 6-well plates and expose to x – rays in two densities per condition. B. Cells seeded in 35 mm dishes and exposed to proton.

| A | Cell line | 0 Gy | 1 Gy | 2 Gy | 3 Gy | PE |
|---|-------------|-------|-------|-------|-------|------|
| | UMSCC6 | 1000 | 2000 | 4000 | 6000 | 10 % |
| | | 2000 | 4000 | 8000 | 12000 | |
| | UMSCC47 | 500 | 1000 | 2000 | 4000 | 10 % |
| | | 1000 | 2000 | 4000 | 8000 | |
| | UMSCC74A | 500 | 1000 | 2000 | 4000 | 14 % |
| | | 1000 | 2000 | 4000 | 8000 | |
| | UPCI-SCC090 | 8000 | 12000 | 16000 | 24000 | 3 % |
| | | 16000 | 24000 | 32000 | 48000 | |

| B | Cell line | 0 Gy | 1 Gy | 2 Gy | 3 Gy | PE |
|---|-------------|-------|-------|-------|-------|------|
| | UMSCC6 | 1000 | 2000 | 4000 | 8000 | 8% |
| | UMSCC47 | 1000 | 2000 | 4000 | 8000 | 7 % |
| | UMSCC74A | 500 | 1000 | 2000 | 4000 | 10 % |
| | UPCI-SCC090 | 12000 | 18000 | 24000 | 30000 | 1 % |

$$PE = \frac{\text{number of colonies}}{\text{number of cells seeded}} \quad (3.1)$$

PE was calculated upon non treated and non irradiated cells

After the required incubation period, where distinct colonies of at least 50 cells per colony had been formed, the plates were removed from the incubator, the medium was aspirated out, and the wells were washed with PBS, before fixing and staining the cells

with Crystal Violet (6 % glutaraldehyde and 0.5 % crystal violet) for at least 30 min. The plates were then washed with clean water, left to air dry, and the colonies were counted using the GelCount colony analyser (Oxford Optronics, Oxford, UK). The colonies detected on the edges of the wells were excluded from counting, as they were underdosed due to shielding effect. The relative surviving fraction (SF), also called Colony Formation (CF), were determined from number of colonies over the number of cells seeded at individual IR doses (equation 3.2). SF were then compared between inhibitor treated versus DMSO treated cells (control) to demonstrate the impact of the inhibitor alone or in combination with IR. The 6 wells of the plates (for x – rays) or the 35 mm dishes (for protons) were averaged for each condition and were normalised to the 0 Gy of each treatment, to constitute one biologically independent experiment.

Moreover, to correlate a given radiation dose (eg D50) with the respective SF, data were fitted to the exponential equation 3.3. Then, Dose enhancement ratio (DER), were calculated by the ratio of the dose required to achieve 50 % survival in the control cells (DMSO treated) divided by the dose required to achieve 50 % survival in the drug treated cells (ATMi, ATRi, DNA-PKcsi), equation 3.4 and 3.5.

$$SF = \frac{\text{number of colonies per condition}}{\text{number of cells seeded}} \quad (3.2)$$

$$SF = e^{-\alpha D} \Rightarrow \ln(SF) = -\alpha D \quad (3.3)$$

α is the equations' constant and D is the radiation dose.

$$D50 = -\frac{\ln(0.5)}{\alpha} \quad (3.4)$$

$$DER = \frac{D50_{DMSO}}{D50_{drug}} \quad (3.5)$$

3.10 3D Spheroid growth assay

Another technique used to investigate the impact of DNA repair inhibitors treatment alone or in combination with IR, on cell survival and proliferation in HNSCC cells *in vitro* is the 3D spheroid growth assay, that better represents tumour growth. In this technique cells were growing in microscopic spheres (3D) in suspension rather than the previously

described techniques where cells were growing as monolayer attached to the culture plastic. On Day 1, cells were trypsinised off a 70 – 90 % confluent flask as described in Section 3.2.3, the suspension was then transferred in a 15 ml tube and was centrifuged for 5 min at 1500 rpm in room temperature. The excess medium was removed, and the cell pellet was resuspended in 2 – 5 ml (volume depended on the pellet size) of spheroid medium (adMEM/F12, Sigma-Aldrich St Louis, USA), supplemented with 0.02 % EGF and 0.01% FGF before use. Concentration of the new cell suspension was estimated by counting a sample with a haemocytometer, as described in Section 3.8. A seeding stock was prepared, but different concentrations were used for each cell line according to the physical characteristics of the cells, including their ability to form a spheroid and the doubling time of the spheroid. The number of cells seeded per cell lines are summarised in Table 3.6. 100 µl/well of the seeding stock was then added on ultra-low attachment surface 96-well plates, with rounded well bottom (Costar, Sigma-Aldrich, St Louis, USA), in triplicate per condition, using a precise repeater pipette (Gilson Pipettes, France) to increase accuracy. Usually not all the 96 wells were filled with cell stock and the remaining empty wells were filled with 100 µl/well PBS to boost humidity within the plate and prevent medium from drying, over the incubation period. The plates were incubated for 48 h in humidified cell culture incubator under standard conditions of 5 % CO₂ and 37°C. During this time the cells merged, forming microscopic spheroids, approximately 200 µm in diameter.

Table 3. 6. Cell concentration seeding for 3D spheroid growth assays. The number of cells seeded for 3D spheroid growth assays for each cell line are displayed. Cells were seeded on Day 1 and left to form a sphere before any treatment.

| <i>Cell concentration (cells/ml)</i> | <i>5000</i> | <i>10000</i> | <i>20000</i> |
|--------------------------------------|-------------|--------------|--------------|
| | FaDu | UMSCC6 | UPCI-SCC090 |
| | A253 | UMSCC47 | UPCI-SCC154 |
| | | UMSCC74A | |

On Day 3, when spheroids were fully developed, they were individually imaged using a light microscope (AMG EVOS, Thermo Fisher Scientific, Massachusetts, USA), with 4x magnification. 50 µl out of 100 µl of medium was removed from each well and replaced

by 50 µl of spheroid medium containing either of the inhibitors or DMSO as control. Since the added medium was half of the total volume, the concentrations of the inhibitors and DMSO were doubled, to achieve a final 1x time concentration. Thus, the concentrations used were, 20 µM KU-55933 (ATMi), 2 µM NU7441 (DNA-PKcsi), 2µM VE-821 (ATRi) and 20 µM DMSO, to have a final concentration of 10 µM, 1 µM, 1µM and 10 µM respectively. Following 1 h incubation with the drugs in a cell culture incubator, the plates were irradiated with 1 Gy, 2 Gy, and 3 Gy of x – rays, or 2 Gy, 4 Gy, and 6 Gy of protons. Immediately after exposure, 50 µl of medium was removed from each well, and replaced by 50 µl of fresh spheroid medium containing the respective inhibitors at 1x time concentration (10 µM ATMi, 1 µM DNA-PKcsi, 1µM ATRi and 10 µM DMSO), and were further incubated with the drugs for 24 h in a cell culture incubator. On Day 4, 60 µl of medium was removed from each well and was replaced by 100 µl spheroid medium without inhibitors or DMSO, to minimise concentration of the drugs as possible, and the plates were incubated for up to 15 days to monitor spheroid growth. On Day 5 and every two days, the individual spheroids were imaged using a light microscope and the images were then analysed using Image-J software, where the diameter of the growing spheroids was measured. The diameter was then converted into radius (r) and using the equation 3.5 the volume (V) was calculated.

$$V = \frac{4}{3}\pi r^3 \quad (3.5)$$

The three replicates of each condition were averaged, the volumes were then normalised against the volume on Day 3 (IR day) for each condition which was set to 1, and that constituted one independent biological experiment. Growth suppression ratios (GSR) were calculated via the ratio of the volume of DMSO treated versus drug treated spheroid on a given day and treatment and then was averaged across Day 5 to Day 15, equation 3.6.

$$GSR = \frac{V_{DMSO}}{V_{drug}} \quad (3.6)$$

Chapter 4: Results I

4.1 Introduction

Three protein kinases directly involved in DNA damage response, ATM, ATR and DNA-PKcs, are reported to play key role in the repair of DSB via NHEJ and HR pathways. Although important for cell proliferation, activity of these proteins contribute to tumour resistance in chemotherapy and radiotherapy, thus these proteins are increasingly being investigated as targets for inhibitors to increase cellular sensitisation to IR and other DNA damaging agents. The impact of three potent and well established inhibitors was examined in HNSCC cell lines, as a monotherapy as well as a combination therapy with x – ray or proton irradiation. Different end points were evaluated in order to obtain an understanding of how these drugs affected the DNA repair process. The inhibitor KU-55933 targeted ATM (ATMi), VE-821 targeted ATR (ATRi) and NU7441 targeted DNA-PKcs (DNA-PKcsi).

First the impact of the drugs on protein level was investigated via immunoblotting. ATM is reported to be one of the first proteins initiated in response to DSB induction. It is activated through an intermolecular auto-phosphorylation on a single site, Serine 1981, and regulates a number of DNA repair proteins, such as H2AX, BRCA1, as well as proteins involved in cell cycle control, including p53 and Chk2, therefore indirectly promoting DSB repair (124, 125). ATR is reported to be triggered in response to ssDNA and to be activated via an autophosphorylation at Serine 428, Serine 435 and Threonine 1898 (137). S428 is suggested to be associated with UV – induced DNA damage and is considered an ATR initiator (222). Similarly, T1989 autophosphorylation is shown to be critical for ATR activation, in response to endogenous, UV induced, and IR induced DSBs. Following its activation, ATR in turn regulates numerous factors involved in both DNA repair and cell cycle control. Finally, DNA-PKcs association with DNA repair progress has been linked with phosphorylation on two sites, T2609 and S2056, that are reported to regulate the DNA-PK complex dissociation from the site of DSB allowing other NHEJ repair factors to access the site and progress repair.

In this chapter, activation of the proteins via phosphorylation, in response to treatment with the respective inhibitors and x – ray or proton irradiation was examined at various

time points. It is worth noting, that direct comparison between the two radiation types was not a major goal. This is due to the fundamental differences of x – ray and proton irradiation, but more importantly due to the difference in the delivery technique. For x – ray irradiations, cells were treated in a laboratory x – ray unit, operating at 100 kV. For proton irradiations, cells were exposed to a passive scattered horizontal proton beam line of 60 MeV maximal energy and cells were positioned at the entrance dose of a pristine (unmodulated) beam (~ 1 keV/ μm). The necessary dosimetry tests were regularly performed to confirm the radiation dose delivered via both techniques. That been said, the impact of the DNA repair inhibitors alone or in combination with IR is investigated, as well as the differences in the inhibitor impact with x – rays versus protons.

4.2 Confirmation of HPV status

The expression of the tumour suppressor protein p16, also known as CDKN2A (cyclin-dependent kinase inhibitor 2A), a small protein with a molecular weight of 16 kDa, is associated with HPV-positive HNSCC. Naturally, p16 is involved in cell cycle control, regulating progression from G1 to the S phase. Mutations or deletions in the p16 gene are often found in many types of human cancers, however in HNSCC p16 overexpression is observed in HPV-positive tumours. In fact, it was suggested that the E7 HPV oncoprotein inactivates pRb, which induces upregulation of p16 (223). The expression of p16, as a marker of HPV positivity, was evaluated in 4 oropharyngeal HNSCC cells, the HPV-negative UMSCC6 and UMSCC74A cells, as well as the HPV-positive UMSCC47 and UPCI-SCC090 cells (Figure 4.1). Exponentially growing cells, without any prior treatment, were harvested and protein level were examined for p16 as a confirmation of the HPV status. Indeed, there was no expression of p16 in the two HPV-negative UMSCC6 and UMSCC74A cells. However, an overexpression of p16 was observed in the two HPV-positive cell lines, UMSCC47 and UPCI-SCC090, as expected.

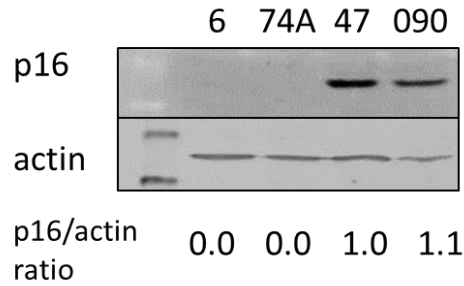


Figure 4. 1. p16 expression as a marker of HPV positivity in HNSCC. Exponentially growing cells were harvested without any treatment, and protein levels of p16 (16 kDa) were imaged via Western blot. 6: UMSCC6, 74A: UMSCC74A, 47: UMSCC47 and 090: UPCI-SCC090. The p16/actin quantification ratio were normalised against the HPV-positive UMSCC47 which was set to 1.

4.3 Inhibitor dose titration

In order to decide the optimum dose of each drug for our experiments a dose titration was performed in two HPV-negative UMSCC74A and UMSCC6 and two HPV-positive UMSCC47 and UPCI-SCC090 HNSCC cell lines (Figure 4.2). Dose recommendations were available by several studies utilising the ATMi, ATRi and DNA-PKcsi for multiple types of human cancers including prostate, pancreatic and colon cancers (120, 121, 224-226). However, there were limited data available regarding the impact of these inhibitors in HNSCC cancer cells, with only one study utilising DNA-PKcsi and another utilising ATRi, yet no published studies examined ATMi (227). Therefore, several concentrations were examined, the most commonly used in the literature, which were 10 μ M ATMi, 1 μ M ATRi, and 1 μ M DNA-PKcsi, as well as 3 and 10 times higher, and protein levels were analysed for ATM phosphorylated (pATM on S1981, 370 kDa), ATR phosphorylated (pATR on S428, 300 kDa), and DNA-PKcs phosphorylated (pDNA-PKcs on T2609, 470 kDa). The cells were treated with the respective drug or DMSO as control for 1 h before exposure to 4 Gy x – ray irradiation and for 1 h after, before been harvested.

In all cell lines ATM phosphorylation on S1981 was maximum in the DMSO treated irradiated cells and minimum in the DMSO treated non irradiated cells. Upon treatment with the inhibitor at 10 μ M and IR, the level of pATM S1981 did not increase demonstrating that ATMi suppressed phosphorylation of its target. Treatment with increasing concentration of the drug did not majorly affect the degree of suppression of

ATM phosphorylation, but have the potential to lead to off target effects. Interestingly, the impact of ATMi in suppressing S1981 pATM was equal in HPV-positive and HPV-negative cell lines, indicating that the drug can be effective in both tumour cell types.

In contrast to ATMi, the ATRi did not suppress phosphorylation of ATR on S428. The protein showed a baseline expression in DMSO treated non irradiated cells, that did not increase following exposure to IR. Moreover, the pATR expression did not change after a combination treatment with IR and 1x, 3x, and 10x times concentration of ATRi (1 μ M) and the level of pATR S428 remained fairly the same. These observations suggested that neither IR alone nor a combination of IR and ATRi could affect phosphorylation of ATR in this site within the time frame of this experiment. Although, this could also be associated with low efficiency and/or specificity of the antibody used. That was the case in all 4 HNSCC cell lines utilised, irrespective of the HPV status. Considering that ATR is involved in HR which occurs later in the cell cycle, the impact of ATRi was then investigated in extended time course as well as in different phosphorylation site (Sections 4.4.2, Figures 4.4 and 4.5).

Finally, phosphorylation of DNA-PKcs following inhibitor treatment and IR exposure was the most variable between the different cell lines. The level of pDNA-PKcs T2609 in non-irradiated cells was minimal and increased after exposure to IR. Following combination treatment of drug and IR, expression level of DNA-PKcs T2609 was suppressed in one cell line, UPCI-SCC090 (HPV-positive), and the decrease was proportional with the concentration of the inhibitor, as increasing drug dose resulted in decreasing pDNA-PKcs expression. Nevertheless, no major impact was observed in one HPV-negative cell line, UMSCC6, where there was only a minimal decrease in phosphorylation at the higher drug concentration. In contrast, in two cell lines UMSCC74A and UMSCC47 HPV-negative and positive respectively, the phosphorylation increased at the higher concentrations. These contradicting findings suggested a cell line dependence regarding the impact of DNA-PKcsi in the phosphorylation of T2609 and required further investigation of different phosphorylation sites as well as extended time course (Section 4.4.3, Figures 4.6 and 4.7). In order to decide on the appropriate dose while minimise potential off-target effects, preliminary 2D cell proliferation studies (clonogenic assays) were performed (data not shown) and the lowest efficient concentration was decided to be

used, which specifically was 10 μ M ATMi, 1 μ M ATRi, and 1 μ M DNA-PKcsi, although different phosphorylation sites and other time points were also investigated.

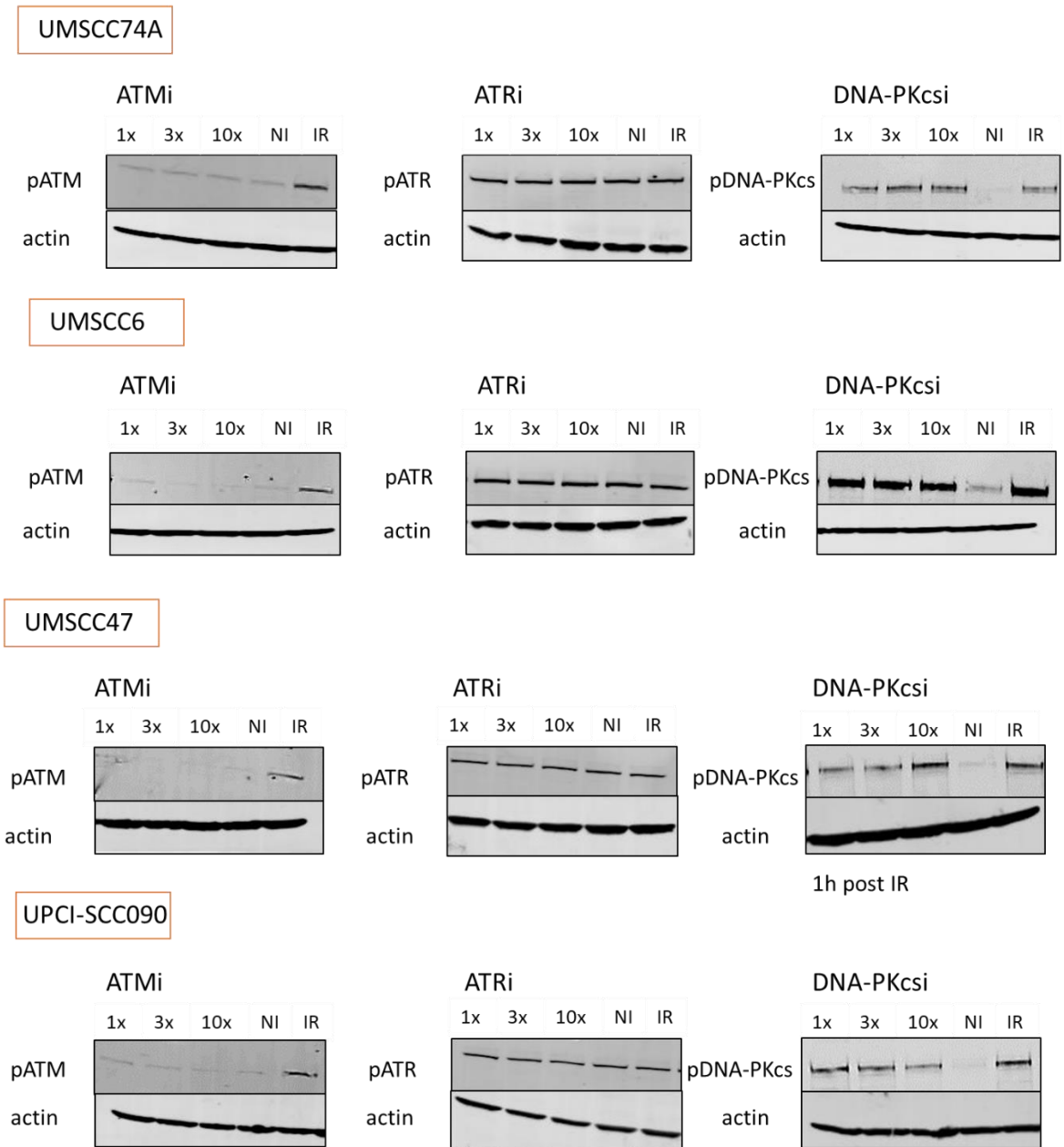


Figure 4. 2. Inhibitor dose titration. 4 HNSCC cell lines were treated for 1 h with the respective inhibitor at 1x the recommended concentration (10 μ M ATMi, 1 μ M ATRi, and 1 μ M DNA-PKcsi), 3x and 10x. Cells were then exposed to 4 Gy x-ray irradiation and were further incubated with the inhibitor for 1 h before been harvested. pATM: phosphorylated ATM (on S1981), pATR: phosphorylated ATR (on S428) pDNA-PKcs: phosphorylated DNA-PKcs (on T2609); NI: Non irradiated DMSO treated cells, IR: irradiated DMSO treated cells.

4.4 Impact of DNA repair inhibitors in combination with x – ray irradiation

The dose titrations (discussed in Section 4.3) were performed utilising increasing concentrations of each drug and harvesting the cells at a single time point, 1 h post exposure to IR. In order to evaluate the impact of the DNA repair inhibitors on phosphorylation of their target proteins over a longer period, later time points post irradiation were examined. From the previous results, ATMi resulted in a clear suppression of pATM in S1981 1 h after exposing cells to 4 Gy x – rays, however data were insufficient regarding the effect of ATRi and DNA-PKcsi in phosphorylation of their target proteins. This was addressed with further investigation on protein level following the same set up, of 1 h pre-treatment with the respective drug, followed by 4 Gy x – ray irradiation and by further incubation with the drug until harvesting of the cells. This allowed cells time to process the IR induced DNA damage via the required repair mechanisms and therefore time for activation and involvement of the targeted proteins in the repair process.

4.4.1 The impact of ATMi on ATM phosphorylation.

4.4.1.1 pATM S1981 expression up to 4h post x – ray irradiation.

ATM is reported to be one of the first proteins to be activated in response to DNA damage. Therefore, phosphorylation of ATM at S1981 was evaluated at 1 h, 2 h, and 4 h post x – ray irradiation. Four HNSCC cell lines, UMSCC6, UMSCC74A, UMSCC47 and UPCI-SCC090 were utilised to evaluate phosphorylation of ATM on S1981. The base line expression of pATM was negligible in the non-irradiated cells whether they were inhibitor treated or DMSO treated, and it was upregulated (3- to 6.2- fold) within 1 h after exposure to IR in the DMSO treated cells. As previously seen in the dose titration experiments (Figure 4.2), pATM was again effectively inhibited in the presence of ATMi in all four HNSCC cell lines post irradiation, irrespective of their HPV status (Figure 4.3). Post irradiation, UMSCC74A DMSO treated cells displayed high levels of pATM S1981, increased between 3- to 5- fold above baseline, that was almost completely inhibited in ATMi treated cells. In UMSCC6 DMSO treated cells, pATM expression peaked 1 h post irradiation by 4.2- fold above baseline, and gradually dropped in the later time points,

yet in ATMi treated cells expression of pATM was remarkably reduced throughout the time course with the biggest difference observed 1 h post IR where there was an 8- fold reduction. Similarly, in the HPV-positive UMSCC47 and UPCI-SCC090, ATM was phosphorylated in DMSO treated cells throughout the time course up to 12- and 6.5- fold respectively, but this phosphorylation was severely downregulated by 6- and 7- fold respectively in the presence of ATMi, compared to DMSO treatment.

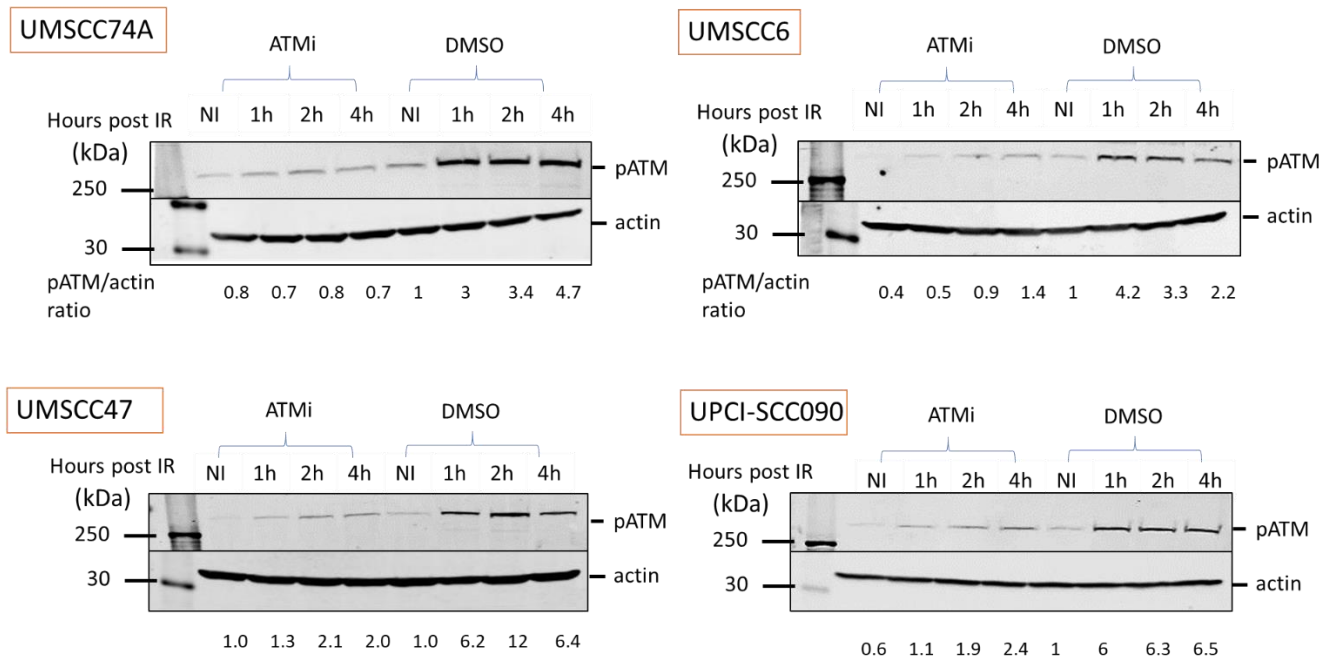


Figure 4. 3. Impact of ATMi on pATM S1981. Expression of pATM S1981 (370 kDa) was investigated in 4 HNSCC cell lines, two HPV-positive and two HPV-negative. Cells were treated with 10 μ M of ATMi or 10 μ M DMSO as control, for 1 h before exposure to 4 Gy x – ray irradiation, and were harvested 1 h, 2 h and 4 h later. Actin (42 kDa) was probed as control. NI: non-irradiated cells. NI: non irradiated cells. The pATM/actin quantification ratios were normalised against the NI DMSO, which was set to 1.

4.4.2 The impact of ATRi on ATR phosphorylation

4.4.2.1 pATR S428 expression up to 24h post x-ray irradiation.

Next, ATR phosphorylation on S428 was examined 1 h, 2 h, and 4 h after treatment with a single dose of ATRi (1 μ M), or DMSO (1 μ M) as control, and 4 Gy x – rays. 4 HNSCC cell lines, UMSCC74A, UMSCC6, UMSCC47 and UPCI-SCC090 were utilised, all of which exhibited comparable results, irrespective of the HPV status. Interestingly, neither of exposure to IR alone, treatment with ATRi alone or combination of ATRi and IR had an impact on pATR S428 expression in none of the cell lines.

Considering ATR is actively involved in HR that occurs later in the cell cycle, expression of pATR S428 was then assessed in the same 4 HNSCC cells, but at later time points, 8 h and 24 h post ATRi and IR treatment. These time points were chosen to cover the peak period of ATR phosphorylation however, the impact of irradiation and/or ATRi treatment was again insignificant in all four cell lines examined and irrespective of the HPV status (Figure 4.4). Exposure to IR alone and/or treatment with ATRi did not alter ATR phosphorylation at S428 up to 24 h post irradiation. These findings demonstrated that IR did not induce ATR phosphorylation at S428 in HNSCC cells, so we could not examine the effectiveness of ATRi on this phosphorylation site. Therefore, different phosphorylation sites needed to be examined, to investigate how ATRi impact on DSB repair.

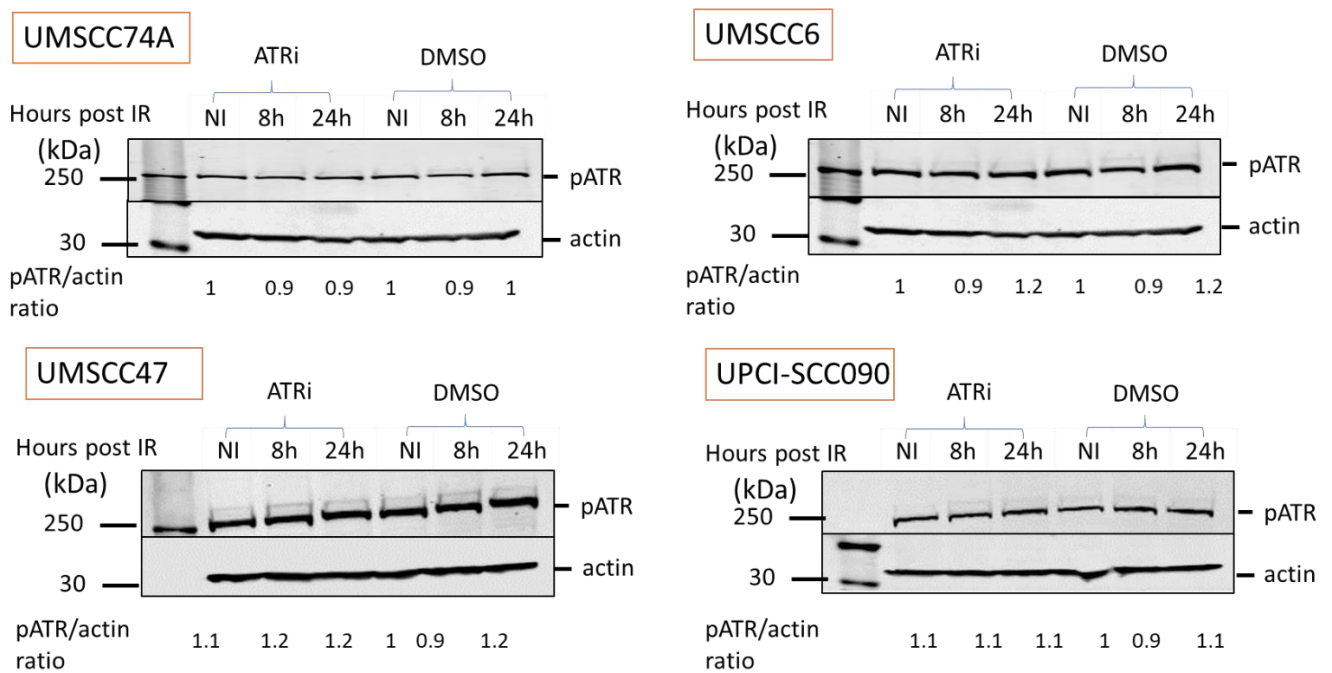


Figure 4. 4. Impact of ATRi on pATR S428 in extended time course. pATR S428 (300 kDa) activation was investigated in 4 HNSCC cell lines, two HPV-positive and two HPV-negative. Cells were treated with 1 μ M ATRi or 1 μ M of DMSO for 1 h prior to 4 Gy x- ray irradiation and were harvested 8 h and 24 h after. Actin (42 kDa) was probed as control. NI: non irradiated cells. The pATR/actin quantification ratios were normalised against the NI DMSO, which was set to 1.

4.4.2.2 pATR T1989 expression up to 24 h post x – ray irradiation.

The phosphorylation site ATR T1989, which is reported to be directly involved in activation of ATR in response to single stranded DNA (ssDNA) structures was then

investigated. This phosphorylation is critical for ATR function and is promptly recognised by TopBP1, promoting ATR driven cell cycle regulation and DNA repair. The same 4 HNSCC cells were harvested 8 h and 24 h post exposure to IR and following treatment with a single dose of ATRi (1 μ M) or DMSO (1 μ M) as control. These time points were chosen to cover the peak period of ATR phosphorylation.

In all cell lines, expression of pATR T1989 was similar and relatively low in DMSO treated cells and ATRi treated cells in the absence of IR, however after exposure to IR, pATR T1989 was activated in DMSO treated cells. In contrast, ATRi treatment suppressed phosphorylation on T1989 following exposure to IR, although to a different extent in each of the HNSCC cell lines examined (Figure 4.5). In UMSCC74A pATR expression had a 5- fold peak at 8 h and then dropped at 24 h post irradiation in DMSO treated cells, yet remained at baseline expression following combination treatment of ATRi and IR. Expression of pATR T1989 in UMSCC6 cells peaked at 24 h post irradiation in DMSO treated cells, with a 3.6- fold increase above baseline, but in the ATRi treated cells was considerably downregulated, by 1.8- and 3.3- fold at 8 h and 24 h respectively. The same trend in pATR T1989 suppression was exhibited in the two HPV-positive HNSCC cell lines, UMSCC47 and UPCI-SCC090. Phosphorylation of ATR on T1989 peaked 24 h post irradiation in the DMSO treated cells (3.2- to 4- fold increase above baseline), yet in ATRi treated cells was downregulated by approximately 2.5- fold 24 h post irradiation. Cumulatively, these results highlighted the ATRi potency to delay ATR phosphorylation on T1989 and thus contribute to regulation of x – ray induced DSB repair.

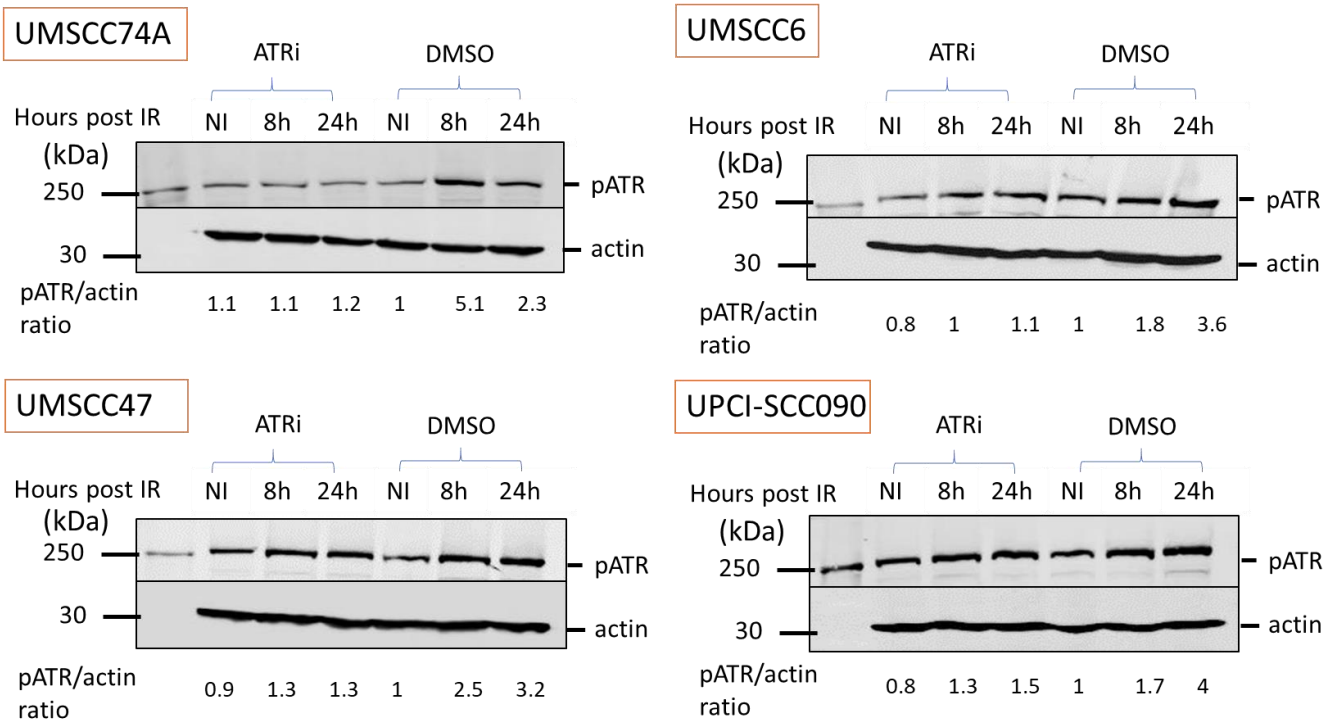


Figure 4. 5. Impact of ATRi on pATR T1989. Expression of pATR T1989 (300 kDa) was investigated in 4 HNSCC cell lines, two HPV-positive and two HPV-negative. Cells were treated with 1 μ M of ATRi or 1 μ M DMSO as control, for 1 h before exposure to 4 Gy x – ray irradiation and were harvested 8 h and 24 h later. Actin (42 kDa) was probed as control. NI: non irradiated cells. The pATR/actin quantification ratios were normalised against the NI DMSO, which was set to 1.

4.4.3 The Impact of DNA-PKcsi on DNA-PKcs phosphorylation

4.4.3.1 pDNA-PKcs T2609 expression up to 4 h post x – ray irradiation.

The third inhibitor, DNA-PKcsi, and its impact on phosphorylation of DNA-PKcs on T2609 was then investigated. UMSCC6, UMSCC74A, UMSCC47, UPCI-SCC090 cells were pre-treated for 1 h with a single dose of DNA-PKcsi (1 μ M) or DMSO (1 μ M) as control, and then were exposed to 4 Gy x – ray irradiation. Cells were further incubated with the inhibitor or DMSO and were harvested 1 h, 2 h, and 4 h post irradiation (Figure 4.6). Expression of pDNA-PKcs T2609 in the non-irradiated cells, either treated with DMSO or with DNA-PKcsi, was baseline and roughly the same between the four cell lines, irrespective of the HPV status. However, the response to treatment with the inhibitor in combination with x – ray irradiation was quite variable between the cell lines (Figure 4.6).

Phosphorylation of DNA-PKcs on T2609 peaked 1 h post x – ray irradiation (8.5- fold above baseline) and gradually dropped in the later time points in the HPV-negative UMSCC74A DMSO treated cells, but it was delayed and peaked 4 h post irradiation in DNA-PKcsi treated cells. In the HPV-negative UMSCC6 cells, phosphorylation of DNA-PKcs T2609 peaked at 1 h post irradiation, with a 10- fold increase in DMSO treated cells. Interestingly, in DNA-PKcsi treated cells, pDNA-PKcs T2609 peaked too at 1 h post x - rays with a higher increase of 12- fold above baseline. Over the time course the activation gradually dropped in DMSO treated UMSCC6 cells, but appeared to persist in DNA-PKcsi treated cells.

In the HPV-positive UMSCC47 cells, phosphorylation of DNA-PKcs T2609 peaked at 2 h (4- fold above baseline) and decreased by 4 h post irradiation in the DMSO treated cells, yet in the DNA-PKcsi treated cells, the peak was delayed, to 4 h post IR, and upregulated 6.4- fold above baseline. Remarkably, severe DNA-PKcs protein cleavage was observed at ~250 kDa, 1 h and 2 h post exposure to IR in the inhibitor treated cells, indicating increased apoptosis occurring shortly after DNA damage induction in this radiosensitive cell line. Finally in the HPV-positive UPCI-SCC090 cells, pDNA-PKcs expression peaked 4 h post x- rays in both DMSO treated and inhibitor treated cells, although it was slightly upregulated in the inhibitor treated cells throughout the time course, by 6.2- and 7.2- fold above baseline respectively. These finding suggested that phosphorylation of T2609 is cell line dependent but is not dramatically affected by HPV status. Interestingly, these findings demonstrated that, even though DNA-PKcsi delayed phosphorylation on T2609 in two cell lines, it also moderately enhanced DNA-PKcs activation in all cell lines examined, which could be an indication that the drug caused increased persistency of DSB in the later time points. Further phosphorylation sites were then examined.

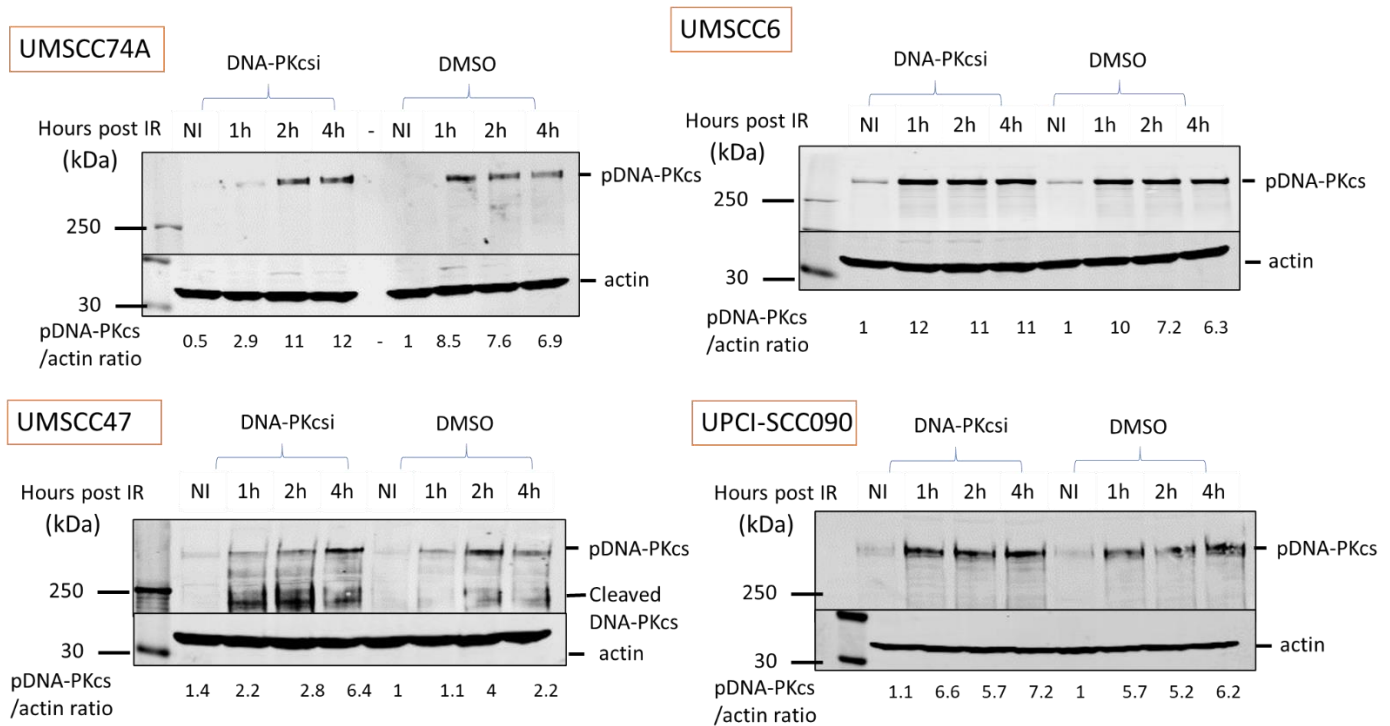


Figure 4. 6. Impact of DNA-PKcsi on pDNA-PKcs T2609. Expression of DNA-PKcs T2609 (470 kDa) was investigated in 4 HNSCC cell lines, two HPV-positive and two HPV-negative. Cells were treated with 1 μ M of DNA-PKcsi or 1 μ M DMSO as control, for 1 h before exposure to 4 Gy x – ray irradiation, and were harvested 1 h, 2 h and 4 h later. Actin (42 kDa) was probed as control. NI: non irradiated cells. The pDNA-PKcs/actin quantification ratios were normalised against the NI DMSO, which was set to 1.

4.4.3.2 Impact of DNA-PKcsi on pDNA-PKcs S2056 up to 8 h post irradiation.

In order to obtain a better understanding of the DNA-PKcsi impact on phosphorylation of its target protein, the second phosphorylation site associated with DNA repair progression, S2056, was then examined. Auto-phosphorylation of DNA-PKcs on S2056 is reported to promote dissolution of the DNA-PK complex from the DNA ends, allowing other DNA repair factors to access the damage site and process the repair. In a preliminary experiment, two HNSCC cell lines were utilised, UMSCC74A, and UMSCC47 to investigate the phosphorylation of DNA-PKcs on S2056 in response to 1 h pre-treatment with a single dose of DNA-PKcsi (1 μ M) or DMSO (1 μ M) as control, 1h, 2h, and 4h post 4 Gy x – ray irradiation. Expression of pDNA-PKcs S2056 was low in non irradiated cells and increased only after 4 h post exposure to x – ray irradiation in DMSO treated cells. However, it was suppressed in the presence of DNA-PKcsi.

These findings demonstrated that the phosphorylation site S2056 was impacted by DNA-PKcsi in response to IR, and subsequently an extended time course up to 8 h post irradiation as well as multiple HNSCC cell lines were then examined. Auto-phosphorylation of DNA-PKcs on S2056 was investigated in four HNSCC cell lines, UMSCC6, UMSCC74A, UMSCC47 and UPCI-SCC090, following 1 h pre-treatment with DNA-PKcsi (1 μ M) or DMSO (1 μ M), and 4 Gy x – ray irradiation (Figure 4.7).

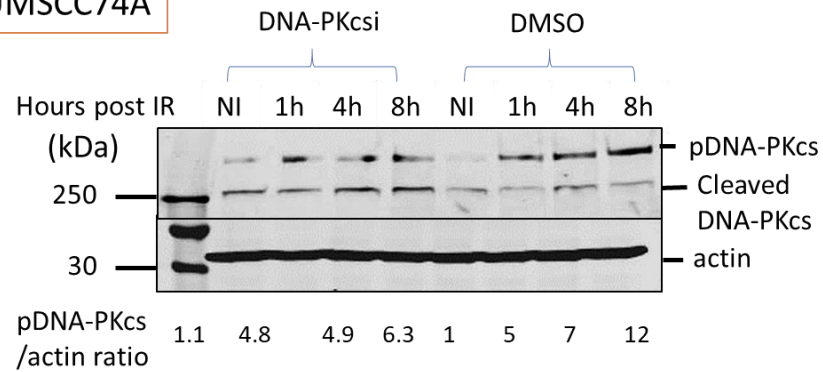
Treatment with the inhibitor alone did not impact phosphorylation of DNA-PKcs on S2056 in the absence of IR, which remained low and was approximately the same to the protein expressed in DMSO treated cells. Exposure to IR triggered activation on DNA-PKcs S2056 in both DMSO and DNA-PKcsi treated cells, however, DNA-PKcsi treatment resulted in nearly 2- fold downregulations in phosphorylation of DNA-PKcs on S2056 in all cell lines. Specifically, in the HPV-negative UMSCC74A cells, phosphorylation on S2056 peaked (12- fold above baseline) 8 h post IR in DMSO treated cells yet the increase was limited to 6.3- fold in inhibitor treated cells. Likewise, in UMSCC6 cells, S2065 phosphorylation exhibited a 19- fold increase 8 h post IR, following DMSO treatment but only an 8- fold increase above baseline was observed in DNA-PKcsi treated cells 8 h post exposure to x – ray irradiation. In the HPV-positive UMSCC47 cells, DNA-PKcs phosphorylation on S2056 was delayed compared to the other 3 cell lines, this occurred at 4 h post IR, and peaked 4 h later exhibiting a 27- fold increase above baseline in DMSO treated cells. However, the activation was less than half in DNA-PKcsi treated cells, where an 11- fold increase was observed. Finally, the S2056 phosphorylation in HPV-positive UPCI-SCC090 cells presented a 10- fold increase above baseline following DMSO treatment 8 h post x – rays which was limited to a 6.5- fold increase following DNA-PKcsi treatment in the same time point.

Moreover, DNA-PKcs cleavage was exhibited 4 h and 8 h post irradiation in UMSCC74A and UPCI-SCC090 inhibitor treated cells as well as at 8 h post irradiation in UMSCC47 inhibitor treated cells, while this remained low in the DMSO treated cells. However, cleavage of DNA-PKcs, as a potential marker of apoptosis, was not observed in UMSCC6 cells up to 8 h post exposure to x – rays.

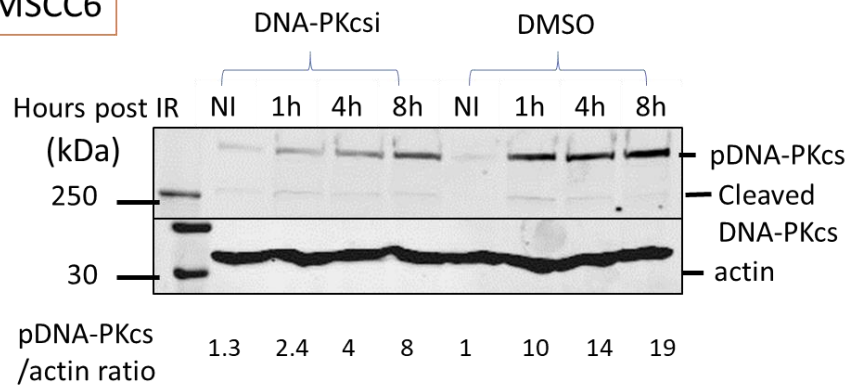
These findings further demonstrated DNA-PKcsi blocked S2056 auto-phosphorylation, which in turn prevented DNA-PK complex dissociation from the DSB sites and therefore

suppressed DNA repair. Something that was also highlighted was the increased DNA-PKcs cleavage, indicating increased apoptosis of cells possibly due to unrepaired DNA DSBs. This added to the reports that during the final steps of apoptosis, DNA-PKcs is targeted by caspase 3-like protease (CPP32), is cleaved into fragments and therefore gets inactivated (159, 160).

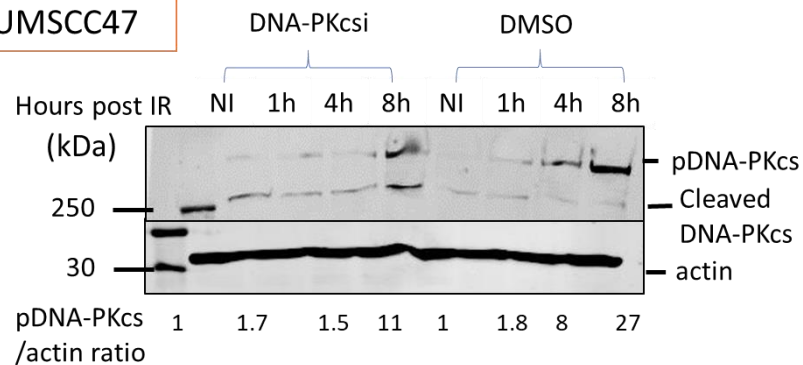
UMSCC74A



UMSCC6



UMSCC47



phosphorylation of S1981 was negligible in the non-irradiated inhibitor treated or DMSO treated cells, in all 4 cell lines. pATM was upregulated only after exposure to IR in the DMSO treated cells. However, it was suppressed in the presence of the inhibitor in all four HNSCC cell lines post irradiation, irrespective of their HPV status (Figure 4.8).

In UMSCC74A, phosphorylation of ATM in S1981 in DMSO treated cells increased across the time course and peaked 4 h post irradiation (5- fold above baseline), yet in the ATMi treated cells, the increase was delayed and reduced (2.2- fold). In UMSCC6, pATM expression peaked 2 h post proton irradiation in DMSO treated cells (4.2- fold above baseline) but was downregulated to 1.4- fold above baseline in the ATMi treated cells post proton irradiation. The HPV-positive UMSCC47 DMSO treated cells exhibited high and sustained pATM expression post irradiation, that was majorly inhibited, by almost 10- fold, after treatment with ATMi. Similarly, in UPCI-SCC090 HPV-positive cells, phosphorylation of ATM on S1981 remained almost baseline in the presence of ATMi and proton irradiation, in contrast to the increased and persistent phosphorylation shown in DMSO treated cells post PBT (2.7- to 5.5- fold above baseline).

Concluding, the impact of ATMi on phosphorylation of S1981 in combination with proton irradiation was irrespective of the HPV status and exhibited an equivalent trend in downregulation of pATM S1981 in the four cell lines examined.

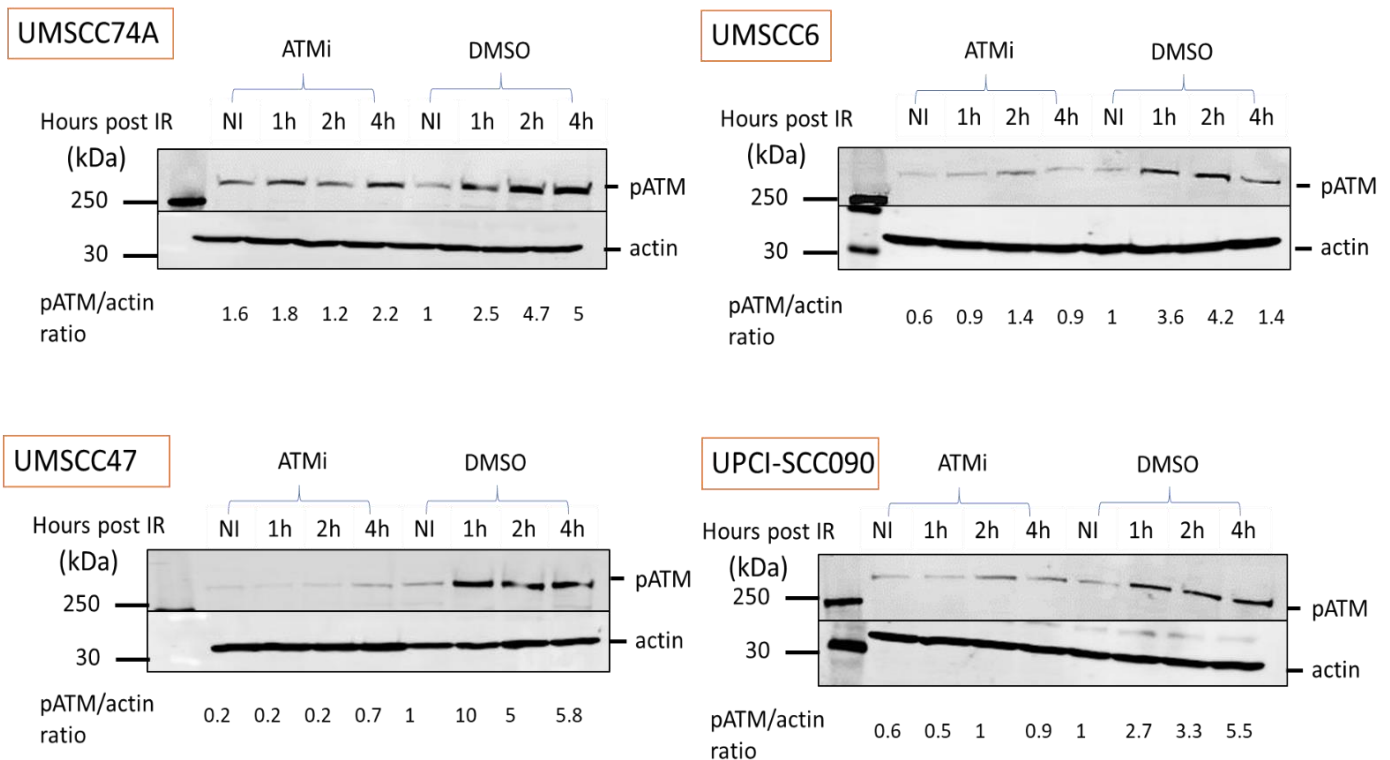


Figure 4. 8. Impact of ATMi on pATM S1981. Expression of pATM S1981 (370 kDa) was investigated in 4 HNSCC cell lines, two HPV-positive and two HPV-negative. Cells were treated with 10 μ M of ATMi or 10 μ M DMSO as control, for 1 h before exposure to 4 Gy proton irradiation, and were harvested 1 h, 2 h and 4 h later. Actin (42 kDa) was probed as control. NI: non irradiated cells. The pATM/actin quantification ratios were normalised against the NI DMSO, which was set to 1.

4.5.2 The impact of ATRi on ATR phosphorylation

4.5.2.1 pATR S428 expression up to 4h post proton irradiation.

Two targets of ATRi, S428 and T1989, previously investigated in response to x – rays with only one been impacted by the drug (Section 4.4.2) were further investigated in response to protons. ATR phosphorylation in S428 was examined 1 h, 2 h, and 4 h after treatment with a single dose of ATRi (1 μ M) or DMSO (1 μ M) as control and 4 Gy protons in UMSCC74A, UMSCC6, UMSCC47 and UPCI-SCC090 HNSCC cell lines. Similarly with x – rays, there was baseline expression of pATR S428 across the time course in all cell lines examined. Neither exposure to protons alone, nor in combination with ATRi affected ATR phosphorylation at S428 and therefore was not further examined.

4.5.2.2 pATR T1989 expression up to 24 h post proton irradiation.

ATR phosphorylation on T1989, which is directly involved in ATR driven repair, was then assessed in the same 4 HNSCC cells, 8 h and 24 h post exposure to proton irradiation and following treatment with ATRi (1 μ M) or DMSO (1 μ M) as a control. In all cell lines, baseline expression of pATR T1989 did not majorly vary between the non-irradiated DMSO and ATRi treated cells, however in the presence of proton irradiation, ATR T1989 was phosphorylated in the DMSO treated cells. Nevertheless, ATRi downregulated this phosphorylation on T1989 when compared with DMSO, yet to a different extent in each HNSCC cell lines examined (Figure 4.9).

In agreement with the x – ray findings, pATR expression peaked 8 h (1.6- fold above baseline) and then dropped 24 h post protons in UMSCC74A DMSO treated cells, whereas phosphorylation peaked at 24 h post proton irradiation in DMSO treated cells of the other three cell lines. In UMSCC74A ATRi treated cells, pATR was reduced by 2-fold compared to DMSO treated cells 8 h post protons. In UMSCC6 and UMSCC47 ATRi treated cells, pATR T1989 remained at or below baseline expression across the time course, and \sim 1.8 - 2- fold lower compared to irradiated DMSO treated cells. Finally, in UPCI-SCC090 ATRi treated cells, ATR phosphorylation on T1989 was only downregulated 24 h post proton irradiation by a factor of \sim 1.8.

Summing up, these findings demonstrated the ATRi potency to delay and even inhibit DNA repair process, by blocking ATR phosphorylation in T1989 in combination with proton irradiation, despite that no impact was observed on S428.

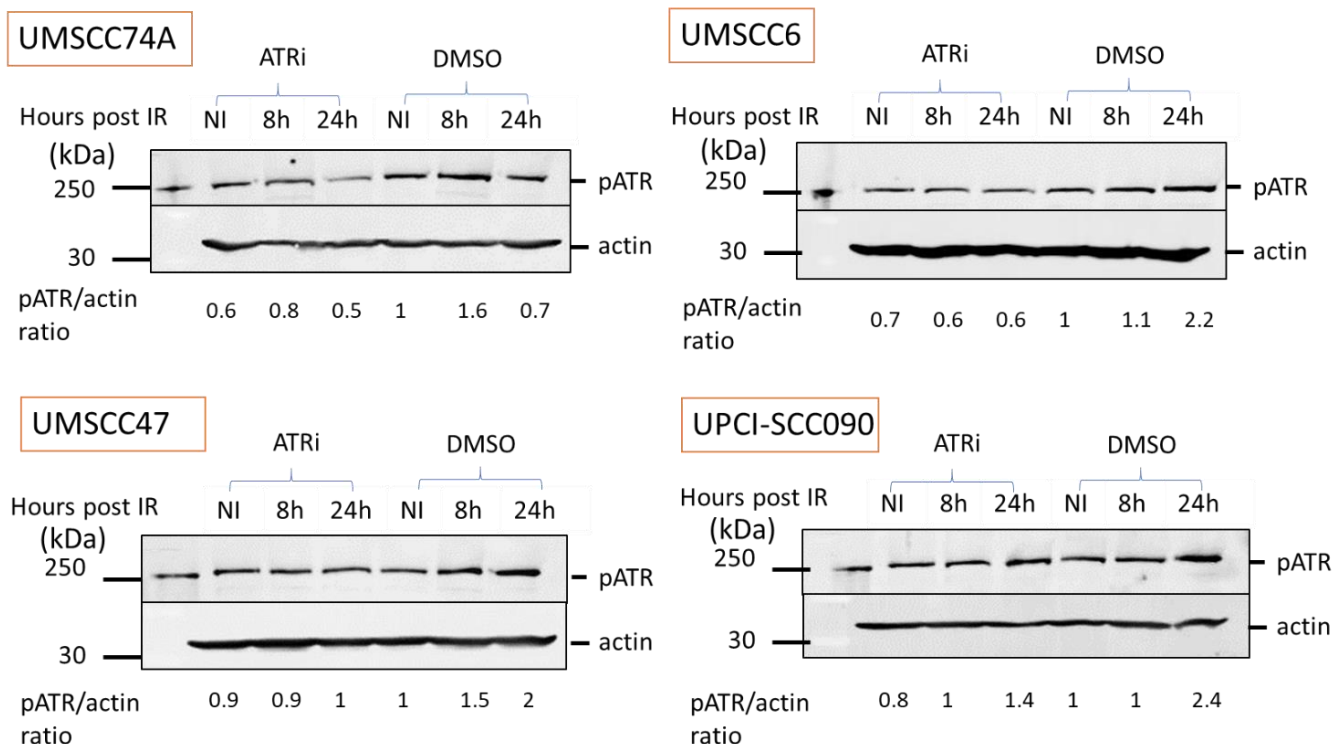


Figure 4. 9. Impact of ATRi on pATR T1989. Expression of pATR T1989 (300 kDa) was investigated in 4 HNSCC cell lines, two HPV-positive and two HPV-negative. Cells were treated with 1 μ M of ATRi or 1 μ M DMSO as control, for 1 h before exposure to 4 Gy proton irradiation, and were harvested 8 h and 24 h later. Actin (42 kDa) was probed as control. NI: non irradiated cells. The pATR/actin quantification ratios were normalised against the NI DMSO, which was set to 1.

4.5.3 The Impact of DNA-PKcsi on DNA-PKcs phosphorylation

4.5.3.1 pDNA-PKcs T2609 expression up to 4 h post proton irradiation.

The impact of DNA-PKcsi on phosphorylation of T2609 and S2056 varied in response to x – rays (Section 4.4.3) and was further investigated following proton irradiation. For investigation of T2609 phosphorylation, two HNSCC cell lines, UMSCC74A and UMSCC47, were treated with DNA-PKcsi (1 μ M) or DMSO (1 μ M) as control, and irradiated with 4 Gy protons. Cells were then harvested 1 h, 2 h, and 4 h post irradiation. No difference was observed in expression of pDNA-PKcs T2609 in DMSO and DNA-PKcsi treated non irradiated cells. In UMSCC74A cells, phosphorylation on T2609 was induced in DMSO treated cells post protons, yet the DNA-PKcsi treatment suppressed this phosphorylation but also upregulated DNA-PKcs protein cleavage suggesting increased apoptosis at earlier time points. In contrast, UMSCC47 phosphorylation of DNA-PKcs

remained low and was not affected by proton irradiation and/or inhibitor treatment. Since the results were inconclusive, this site was not examined further.

4.5.3.2 pDNA-PKcs S2056 expression up to 8 h post proton irradiation.

DNA-PKcs S2056 phosphorylation was then assessed in response to DNA-PKcsi and proton irradiation in four HNSCC cells, UMSCC6, UMSCC74A, UMSCC47 and UPCI-SCC090. Cells were pre-treated with DNA-PKcsi (1 μ M) or DMSO (1 μ M) as control for 1 h, before exposure to 4 Gy protons. Cells were further incubated with the inhibitor or DMSO and were harvested 1 h, 4 h, and 8 h post irradiation (Figure 4.10), given that these time points covered the peak period of S2056 phosphorylation following x – ray irradiation. Phosphorylation of DNA-PKcs in S2056 was relatively minimal in non irradiated cells, either inhibitor or DMSO treated, and was only triggered after exposure to IR. In agreement with the x – ray findings, phosphorylation of DNA-PKcs S2056 was downregulated in all 4 HNSCC cell lines following proton irradiation in presence of the inhibitor compared to DMSO, although to a different extent for each cell line.

DNA-PKcs phosphorylation on S2056 in UMSCC74A DMSO treated irradiated cells, was initiated within 1 h and peaked at 8 h post exposure to protons, by 5.2- fold above baseline, while it was severely downregulated in DNA-PKcsi treated cells, where it generally remained at baseline expression across the time course. Moreover, severe DNA-PKcs protein cleavage was observed 8 h post inhibitor treatment and proton irradiation, that was much stronger compared to a combination of inhibitor and x – ray treatment (Section 4.4.3, Figure 4.7). This indicated increased apoptotic rates in response to protons and DNA-PKcsi treatment.

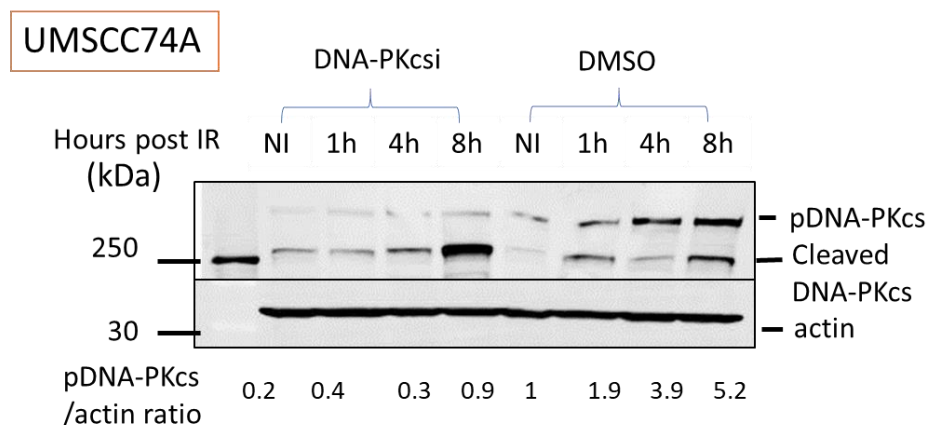
In UMSCC6 cells, phosphorylation was triggered within 1 h and peaked at 8 h post proton irradiation in DMSO treated cells (7.8- fold above baseline). The same trend was exhibited in inhibitor treated cells, yet pDNA-PKcs expression was reduced overall by a factor of \sim 1.4 to \sim 2.4. Combination of DNA-PKcsi and protons resulted in some DNA-PKcs protein cleavage 1 h and 4 h post irradiation, indicating increased apoptosis following protons irradiation in this radioresistant cell line.

In HPV-positive UMSCC47 DMSO treated cells, DNA-PKcs phosphorylation on S2056 peaked 8 h post exposure to protons with a 9.9- fold increase above baseline, but

remained low in DNA-PKcsi treated cells, across the time course. In addition, DNA-PKcs protein cleavage was observed in DMSO treated cells induced by proton irradiation alone, which was enhanced by the inhibitor 4h and 8 h post proton irradiation. This cleavage was much stronger compared to a combination of inhibitor and x – ray treatment (Section 4.4.3, Figure 4.7) and indicated increased apoptotic rates in response to protons and DNA-PKcsi treatment.

Finally, in UPCI-SCC090 cells, expression of pDNA-PKcs S2056 post irradiation was high across the time course in the DMSO treated cells (2.6- to 4.2- fold above baseline) yet was noticeably reduced by a factor of ~1.8 – 2.6 in the inhibitor treated cells. Again, cleaved DNA-PKcs was introduced due to proton irradiation in DMSO treated cells, but this was enhanced in inhibitor treated cells and peaked 8 h post proton irradiation.

These findings demonstrated delayed or deficient S2056 phosphorylation, due to treatment with DNA-PKcsi and protons, that was directly linked to increased DNA-PKcs cleavage, indicating increased apoptosis of cells containing unrepaired DNA damage. Altogether, it appeared that DNA-PKcsi was effective in suppressing phosphorylation of DNA-PKcs in S2056, in combination with protons, with no major differences respective to the HPV status.



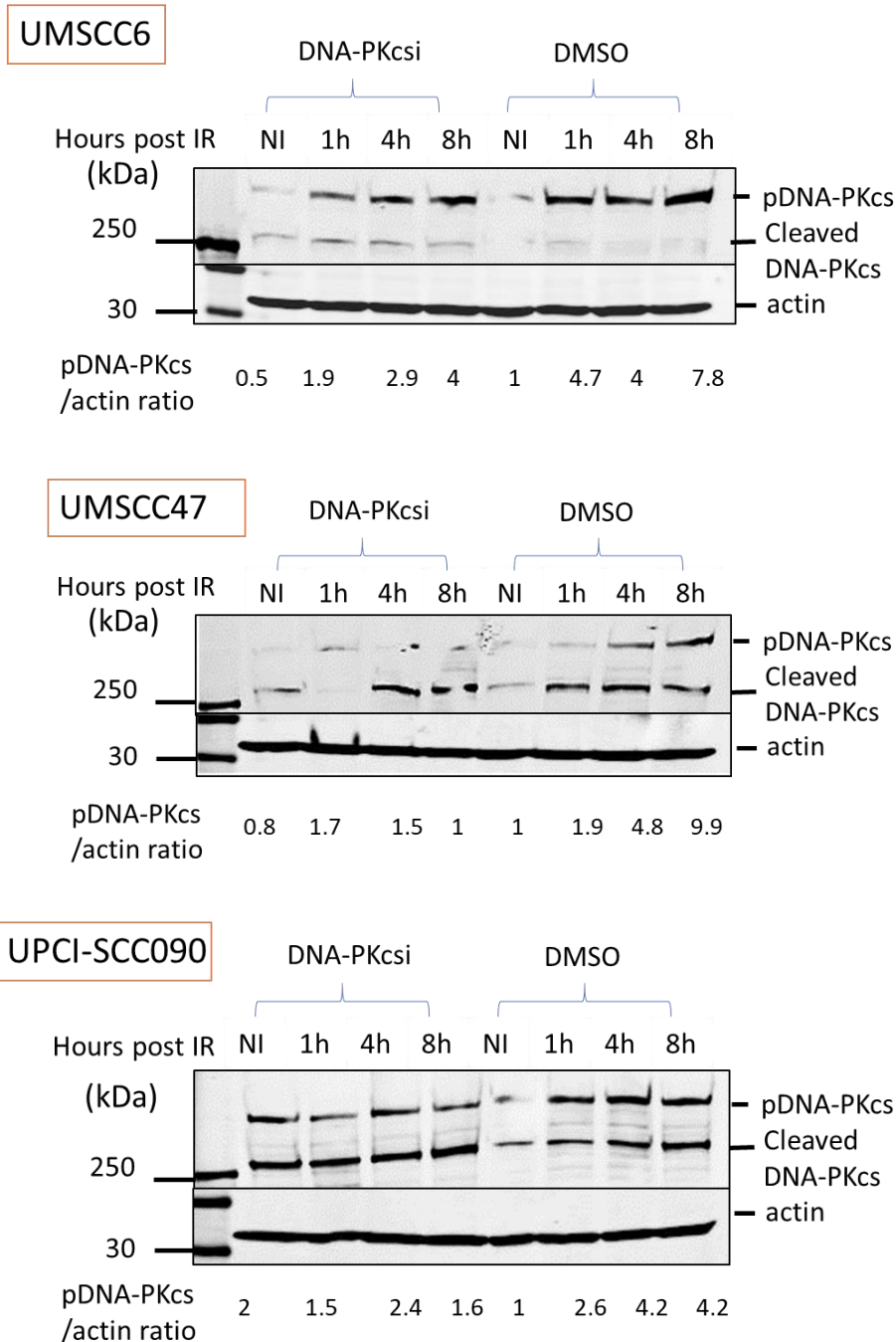


Figure 4. 10. Impact of DNA-PKcsi on pDNA-PKcs S2056. Expression of DNA-PKcs S2056 (470 kDa) was investigated in 4 HNSCC cell lines, two HPV-positive and two HPV-negative. Cells were treated with 1 μ M of DNA-PKcsi or 1 μ M DMSO as control, for 1 h before exposure to 4 Gy x – ray irradiation, and were harvested 1 h, 4 h and 8 h later. Actin (42 kDa) was probed as control. NI: non-irradiated cells. The pDNA-PKcs/actin quantification ratios were normalised against the NI DMSO, which was set to 1.

4.6 Conclusions

As a starting point of this research, the HPV status of the cell lines involved was confirmed through investigation of p16 expression, as a marker of HPV infection. Next, technique optimisation included inhibitor dose titration, to decide the correct drug concentrations, as well as time titration, to investigate the inhibitor's impact on extended time courses. Treatment with either of the inhibitor, in the absence of IR did not majorly impact on phosphorylation levels on any of the sites investigated within ATM, ATR, and DNA-PKcs, and for all HNSCC cell lines examined, irrespective of the HPV status. This was an indication that, at least at protein level, the drug alone did not affect normal DDR behaviour by inducing or reducing phosphorylation of the critical DSB repair protein sites.

ATMi was found to effectively suppress ATM phosphorylation on S1981, immediately and up to 4 h post irradiation, in combination with IR. The impact of ATMi was similar in both HPV-positive and HPV-negative cell lines, indicating that the drug can be effective in both tumour cell types. In addition, the impact on pATM S1981 was equivalent following x – rays or protons, in the four cell lines examined, demonstrating that the drug can be effective in response to either radiation modalities, but also that it was the same phosphorylation site that got activated irrespective of the DNA damage inducer.

ATRi was found to have no impact on ATR S428 phosphorylation, either alone or in combination with x – rays and protons. In fact, ATR S428 exhibited a standard expression across the 4 HNSCC cell lines, which was not affected by exposure to either x – rays or proton irradiation, irrespective of the HPV status and up to 24 h post any treatment. This made it impossible to study any potential impact induced by ATRi on the phosphorylation on S428. In contrast, ATRi in combination with IR was found to delay and decrease ATR T1989 phosphorylation, in all 4 HNSCC cell lines. T1989 phosphorylation, was impacted by the drug in response to x – rays as well as protons, with no major differences between the two radiation modalities. These findings highlighted the ATRi potency to inhibit ATR activation, irrespective of the HPV status and the radiation type.

DNA-PKcsi, was shown to delay yet upregulate phosphorylation on DNA-PKcs T2609 in combination with x – rays, and irrespective of the HPV status up to 4 h post irradiation. However, T2609 was downregulated following inhibitor and proton treatment with simultaneous upregulation of DNA-PKcs cleavage, demonstrating increased apoptosis in one cell line, while had almost no effect in the other. On the other hand, DNA-PKcsi downregulated phosphorylation of DNA-PKcs S2056 in all 4 HNSCC cell lines in response to x – ray as well as proton irradiation. Interestingly, DNA-PKcs protein cleavage was more readily observed following proton irradiation in DMSO treated cells irrespective of the HPV status, suggesting that protons were more effective than x – rays in inducing apoptosis. This cleavage was amplified in the presence of DNA-PKcsi indicating that the drug suppressed DSB repair, possibly leading to increased cell death.

Cumulatively, these findings confirm that ATMi, ATRi, and DNA-PKcsi targeted phosphorylation of at least one site of the respective proteins, and therefore dysregulated the DNA damage response, however more in depth analysis was required. In the next chapter, the impact of the three protein kinase inhibitors in the DDR signalling and DNA repair process was investigated in response to either x – ray or proton irradiation.

Chapter 5: Results II

Impact of DNA repair inhibitors on the DDR signalling

5.1 Introduction

Exposure to IR is known to induce significant amount of DNA damage, and importantly DSBs, that immediately initiate the DDR. In Chapter 4, I demonstrated that inhibition of the protein kinases ATM, ATR and DNA-PKcs suppressed their phosphorylation on critical sites that could lead to delayed or insufficient DNA repair (207). Naturally, and upon DSB induction, histone H2AX is phosphorylated on Serine 139 through NHEJ pathway and it has been reported that both ATM and DNA-PKcs phosphorylate H2AX in response to DSBs in a redundant, overlapping manner, but phosphorylation of H2AX was independent of ATR (228). However, other studies reported that ATM is the major kinase responsible for H2AX phosphorylation and that DNA-PKcs is unable to phosphorylate H2AX in the absence of ATM (120, 225). Phosphorylated H2AX, also called γ H2AX, are rapidly generated surrounding DSBs to form foci, marking the sites to attract the appropriate repair proteins and as the repair process progresses, they disappear. DSBs can be quantified indirectly by visualization and counting of the γ H2AX foci formation, as they appear in a manner of one focus per one DSB (225), as illustrated in example images in Figure 5.1.

Simultaneously, the tumour suppressor p53 binding protein 1 (53BP1) is phosphorylated, and forms foci that colocalise with γ H2AX. The initial recruitment and phosphorylation of 53BP1 depends on the activation of the protein kinases ATM and DNA-PKcs (228, 229). Interestingly, γ H2AX foci are not involved in the initial recruitment of 53BP1, yet are required for the stable formation and retention of 53BP1 foci. 53BP1 foci are considered markers of DSB repair processing through NHEJ and are diminishing accordingly during the repair process (207).

Subsequently, HR takes over and the protein Rad51 is recruited. ATM and ATR interact with and phosphorylate Rad51, but DNA-PKcs is not directly involved. The formation of Rad51 foci highlight the sites where HR is active (230). Rad51 foci are reduced as the repair processes progresses, however these foci are delayed compared to γ H2AX and 53BP1 foci as they are only formed once the cells reach the S/G2 phase of their cycle

(231). All these foci can be visualized by microscopy and give us an insight of the repair process and the role of the three basic protein kinases in the regulation of NHEJ and HR repair post irradiation. The impact of ATM, ATR, and DNA-PKcs inhibition in γ H2AX, 53BP1 and Rad51 foci formation and persistence was investigated alone or in combination with x – rays and proton irradiation.

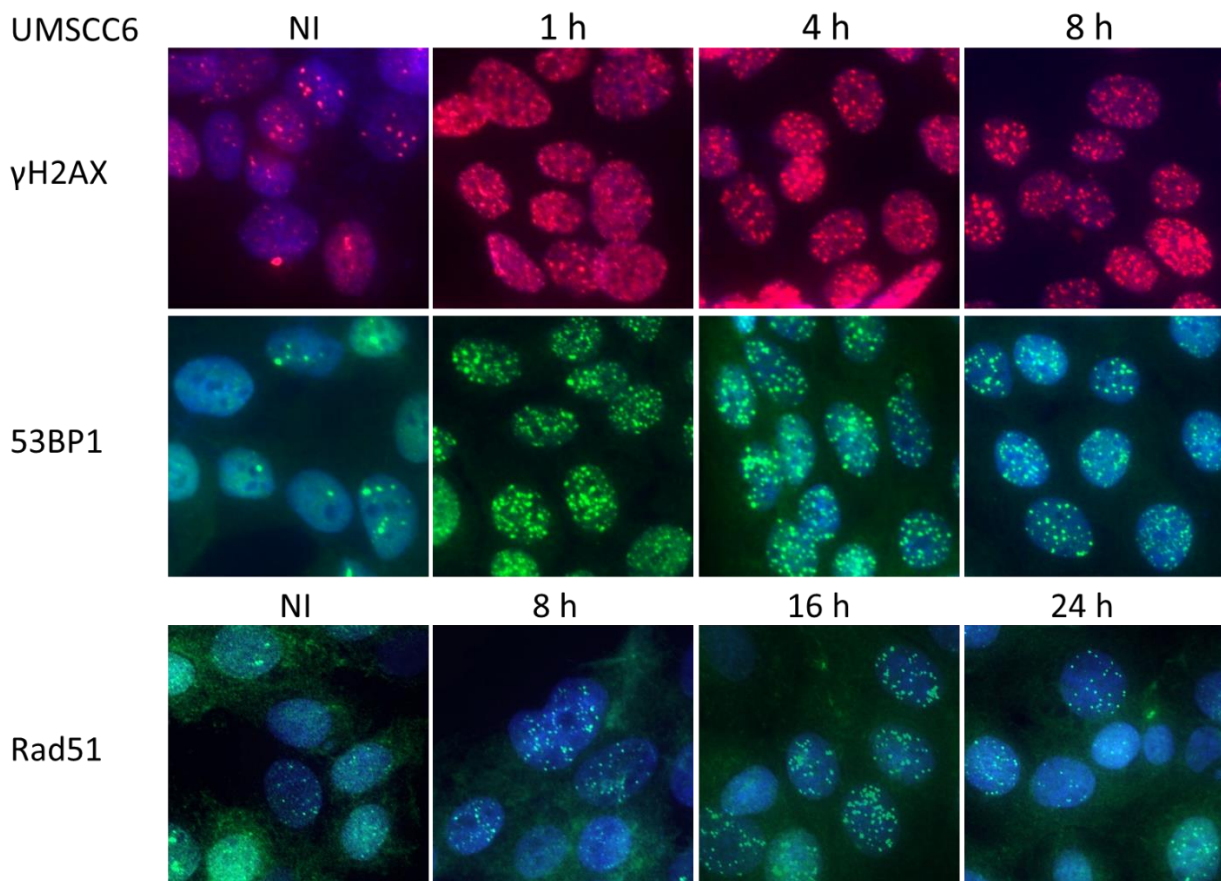


Figure 5. 1. DNA repair focus formation in response to IR. Representative images of γ H2AX (red), 53BP1 (green) and Rad51 (green) foci in UMSCC6 HNSCC cells non irradiated (NI) or 1 h, 4 h, 8 h, 16 h and 24 h post exposure to 4 Gy x – rays, and nuclei were stained with DAPI (blue). A small number of foci was present in non irradiated cells, marking the endogenous DNA damage and repair. Exposure to IR generated high number of each foci that peaked and dropped over the incubation period.

5.2 Immunofluorescent staining and foci analysis in response to x – rays.

In this chapter, the result of DSB repair inhibition was investigated at the molecular level. Specifically, the markers of DSB sites and DSB repair, namely γ H2AX, 53BP1 and Rad51, were examined in response to monotherapy of the DNA repair inhibitors ATMi, ATRi and DNA-PKcsi as well as a combination therapy of the inhibitors and IR, in HNSCC cell lines.

Two HPV-negative, UMSCC6 and UMSCC74A, and one HPV-negative, UMSCC47, HNSCC cell lines were utilised. Due to the morphological characteristics of the HPV-positive UPCI-SCC090, where cells grow on top of each other in culture, the use of confocal microscopy was investigated, however foci determination in individual z-stacks was still extremely difficult. Either high resolution microscopy or possibly sectioning of cells following cell embedding would be necessary, in order to distinct and count the individual foci and thus it was decided to exclude this cell line for the purpose of this experiment. In DMSO treated cells the number foci per nucleus varied in the 3 different cell lines between 80-100 of γ H2AX foci and 60-85 of 53BP1 foci 1 h post 4 Gy x – rays and 30-50 of Rad51 foci 8 h post 4 Gy x – rays.

5.2.1 Impact of ATMi

First, the impact of ATMi was assessed on the three foci markers alone, or in combination with x – rays. Cells were pre-treated with 10 μ M ATMi or 10 μ M DMSO as control for 1 h and then were exposed to 4 Gy x – rays. The cells were then further incubated with the inhibitor up to 24 h to allow for DNA repair progression. Finally, cells were fixed and incubated with antibodies for γ H2AX, 53BP1 or Rad51, then were imaged and analysed.

5.2.1.1 Impact of ATMi on γ H2AX

Formation of γ H2AX designates the sites of DSB and recruits other DNA repair factors to process the DNA damage. Foci formation is reported to occur immediately upon DSB induction and to persist until the damage is resolved (232, 233). Therefore, γ H2AX foci were assessed 1 h, 4 h and 8 h post IR exposure. γ H2AX foci were present even in the DMSO treated and non irradiated cells, highlighting that DSBs can naturally occur (Figure 5.1). As shown in Figure 5.2, treatment with ATMi alone, under non irradiated conditions, did not have a significant impact on foci formation in any of the three cell lines examined. Exposure to IR, severely increased γ H2AX foci (by 4- to 7- fold) in the DMSO treated cells 1 h after irradiation, but the increase was suppressed in ATMi treated cells in all cell lines. In ATMi treated cells, the number of foci was reduced 1 h post IR by a factor of \sim 1.4 - 1.5. This suggested that ATMi inhibited DSB recognition and designation by γ H2AX in response to x – rays in both HPV-negative and positive cell lines.

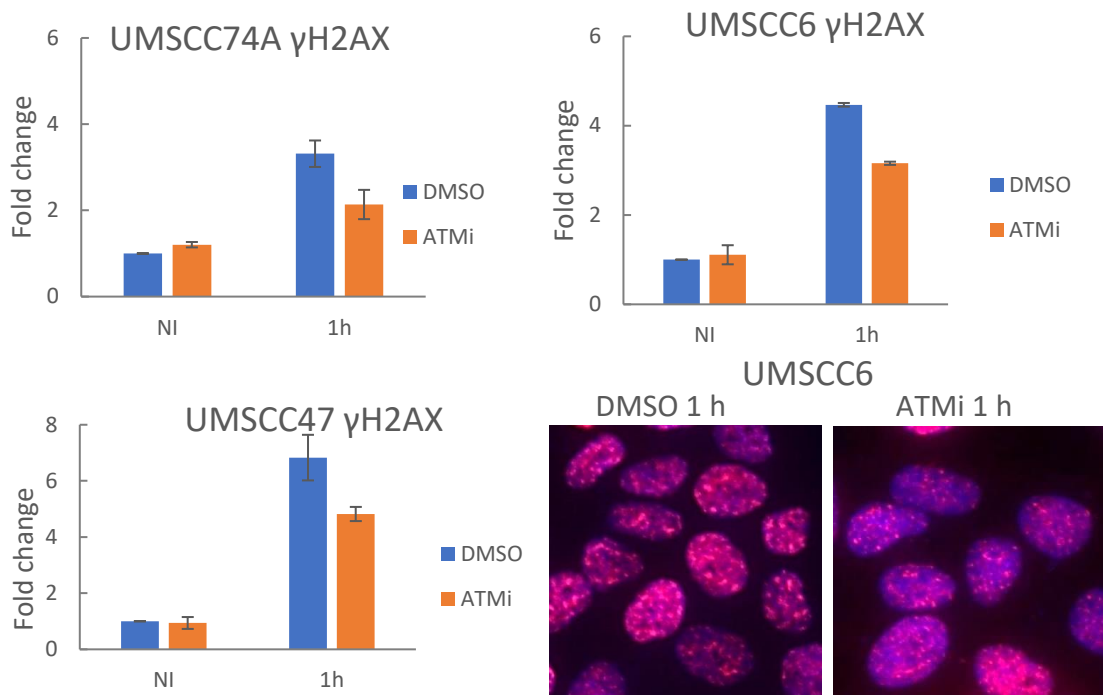


Figure 5.2. Impact of ATMi on DSB marker γ H2AX. γ H2AX foci formation was investigated in 3 HNSCC cell lines. Cells were treated for 1 h with 10 μ M ATMi or 10 μ M DMSO, exposed to 4 Gy x-rays and fixed and stained for γ H2AX 1 h post irradiation. NI: non irradiated. 5 representative images were captured, containing at least 20 cells per coverslip. Values were the means of 2 biologically independent experiments, were normalised against the non irradiated DMSO treated cells, which was set to 1, and are presented with their standard error.

5.2.1.2 Impact of ATMi on 53BP1

Formation of 53BP1 foci that colocalise with γ H2AX, mark the areas of DSB repair via NHEJ. Foci formation is reported to occur almost simultaneously with γ H2AX immediately upon DSB induction and to persist until the damage is resolved (234). Therefore, 53BP1 foci were assessed at the same time points, 1 h, 4 h and 8 h post IR exposure. 53BP1 foci are too present in the DMSO treated and non irradiated cells, highlighting the naturally occurring and repaired DSBs (Figure 5.1). Treatment with ATMi alone, in the absence of IR, did not have a major impact on 53BP1 foci formation (Figure 5.3) in any of the three cell lines. Upon exposure to IR, formation of 53BP1 foci was induced in DMSO treated cells with a 2.5- to 4- fold increase. However, this was only marginally inhibited in ATMi treated cells where the number of 53BP1 foci was reduced by 1.2- to 1.5- fold 1 h post irradiation compared to the number of foci observed in

DMSO treated cells, yet this difference was diminished by 8 h. Surprisingly, 53BP1 foci persisted up to 8 h post x – rays even in DMSO treated cells, suggesting very little repair in all cell lines, which could be related to these specific cell lines or due to overlapping of foci masking any progress of the repair. Overall, these findings demonstrated that DSB repair as shown by 53BP1 recruitment was slightly delayed by ATMi only at 1 h following x – ray irradiation in all cell lines, irrespective of the HPV status.

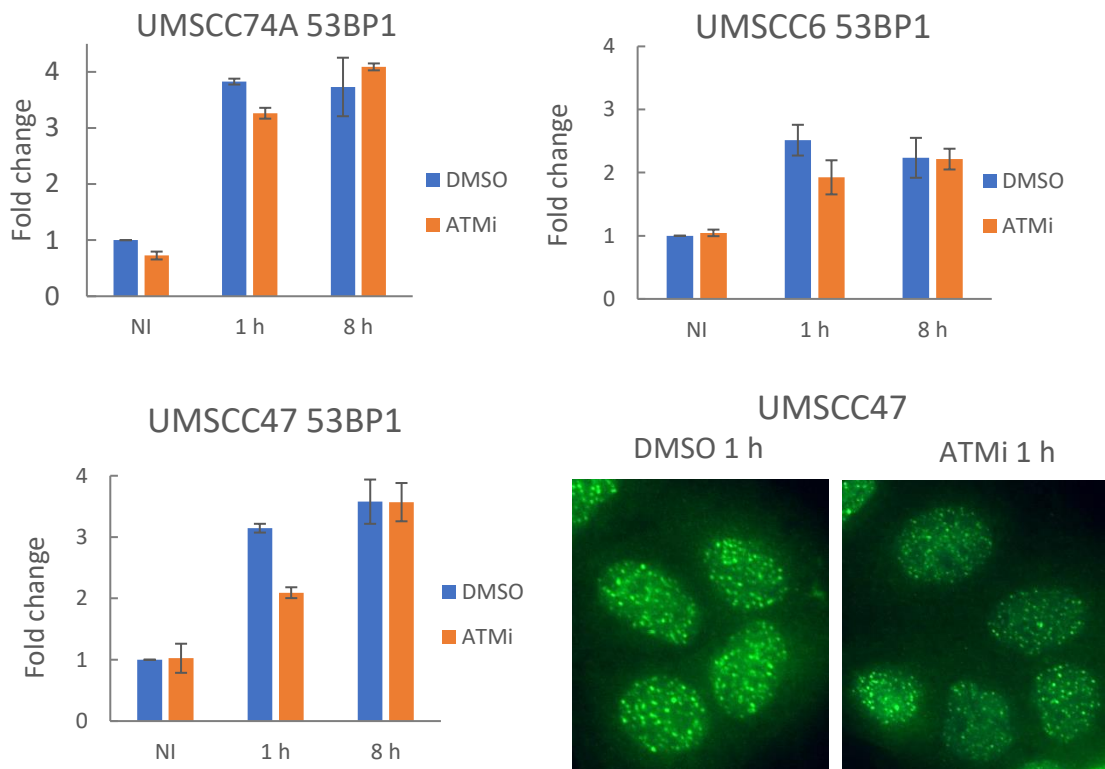


Figure 5.3. Impact of ATMi on DSB repair marker 53BP1. 53BP1 foci formation was investigated in 3 HNSCC cell lines. Cells were treated for 1 h with 10 μ M ATMi or 10 μ M DMSO, exposed to 4 Gy x – rays and fixed and stained for 53BP1 1 h and 8 h post irradiation. NI: non irradiated. 5 representative images were captured, containing at least 20 cells per coverslip. Values were the means of 2 biologically independent experiments, were normalised against the non-irradiated DMSO treated cells, which was set to 1, and are presented with their standard error.

5.2.1.3 Impact of ATMi on Rad51

The third foci formation assessed, Rad51 as a marker of DSB repair via HR, occurs later in the cell cycle and thus cells were investigated 8 h, 16 h and 24 h post 4 Gy x – ray irradiation. Similarly with the two markers previously addressed, formation of Rad51 foci occurred in the DMSO treated non irradiated cells, highlighting the naturally induced

and repaired DSBs (Figure 5.1). In the absence of IR, comparable Rad51 foci formation was observed in DMSO and ATMi treated cells in two cell lines, but the inhibitor moderately upregulated foci formation in UMSCC6 cells, signifying increased HR activity, possibly due to increased endogenous DSBs, induced by the drug alone (Figure 5.4).

Following exposure to x – rays, Rad51 foci formation in DMSO treated cells peaked at 16 h post irradiation, where it exhibited a 2- to 3- times higher number of foci when compared to the DMSO treated non irradiated cells. However, in ATMi treated cells Rad51 foci formation was suppressed in all cell lines. The downregulation was ~1.5- fold in UMSCC6 and UMSCC47 ATMi treated cells, and ~1.3- fold in UMSCC74A ATMi treated cells, compared to the DMSO irradiated cells. These results indicated downregulated Rad51 involvement in DSB repair and thus reduced HR activity in all cell lines in response to inhibitor treatment and to x – rays, that was not associated with the HPV status.

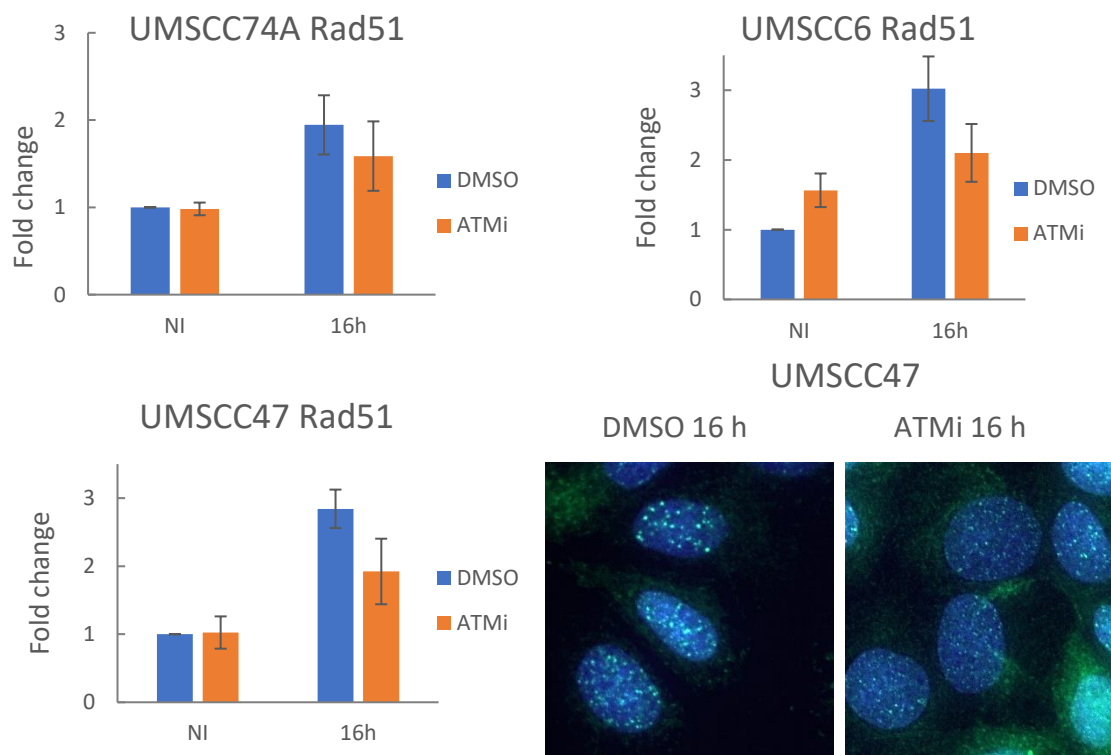


Figure 5. 4. Impact of ATMi on DSB repair marker Rad51. Rad51 foci formation was investigated in 3 HNSCC cell lines. Cells were treated for 1 h with 10 μ M ATMi or 10 μ M DMSO, exposed to 4 Gy x – rays and fixed and stained for Rad51 16 h post irradiation. NI: non irradiated. 5 representative images were captured, containing at least 20 cells per coverslip. Values were the means of 2 biologically independent experiments, were normalised against the non irradiated DMSO treated cells, which was set to 1, and are presented with their standard error.

5.2.2 Impact of ATRi

Next, the impact of ATRi on the DNA repair process was investigated in HNSCC cells. The foci formation and persistency were assessed in cells treated with the inhibitor alone, or in combination with IR. Cells were pre-treated with 1 μ M ATRi or 10 μ M DMSO as control for 1 h and then were exposed to 4 Gy x – rays. The cells were then further incubated with the inhibitor up to 24 h to allow for DNA repair progression. Finally, cells were fixed and incubated with antibodies for γ H2AX, 53BP1 or Rad51, then were imaged and analysed.

5.2.2.1 Impact of ATRi on γ H2AX

In the absence of IR, there was no impact by ATRi on γ H2AX foci in two cell lines, as seen in Figure 5.5. However, in UMSCC6 there was an upregulation (1.6- fold above baseline) in γ H2AX foci formation in non irradiated ATRi treated cells, suggesting increased number of endogenous DSBs. In DMSO treated cells γ H2AX foci formation peaked within 1 h post irradiation (by 4- to 7- fold) and the foci were gradually resolved at the later time points in all three cell lines. The impact of ATRi on γ H2AX foci formation in response to x – rays was insignificant in UMSCC74A cells, confirming that ATR does not greatly involved in γ H2AX foci development. However, formation of γ H2AX foci was downregulated in ATRi treated UMSCC6 and UMSCC47 cells by a factor of \sim 1.2 and \sim 1.4 respectively following irradiation highlighting a possible ATR involvement in DSB recognition.

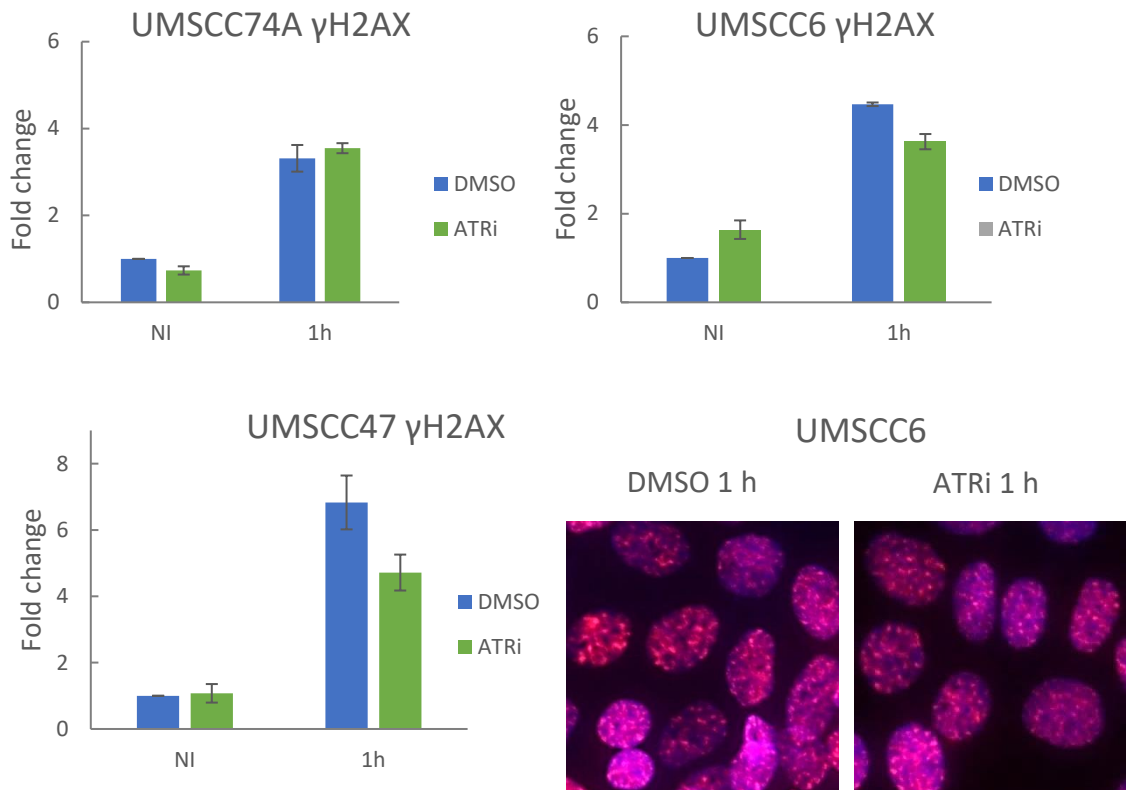


Figure 5.5. Impact of ATRi on DSB marker γ H2AX. γ H2AX foci formation was investigated in 3 HNSCC cell lines. Cells were treated for 1 h with 1 μ M ATRi or 10 μ M DMSO, exposed to 4 Gy x-rays and fixed and stained for γ H2AX 1 h post irradiation. NI: non irradiated. 5 representative images were captured, containing at least 20 cells per coverslip. Values were the means of 2 biologically independent experiments, were normalised against the non-irradiated DMSO treated cells, which was set to 1, and are presented with their standard error.

5.2.2.2 Impact of ATRi on 53BP1

Treatment with ATRi alone had no significant effect on endogenous NHEJ repair as suggested by the minor impact on 53BP1 foci formation in the absence of IR. Formation of 53BP1 foci 1 h post exposure to IR was very similar between DMSO and ATRi treated HPV-negative cells, UMSCC6 and UMSCC74A (Figure 5.6). Considering that ATR is not directly involved in 53BP1 recruitment, these findings were not surprising. A downregulation of 53BP1 foci formation (by 1.2- fold) was observed in the HPV-positive UMSCC47 cell line, which however was within the standard error and therefore insignificant.

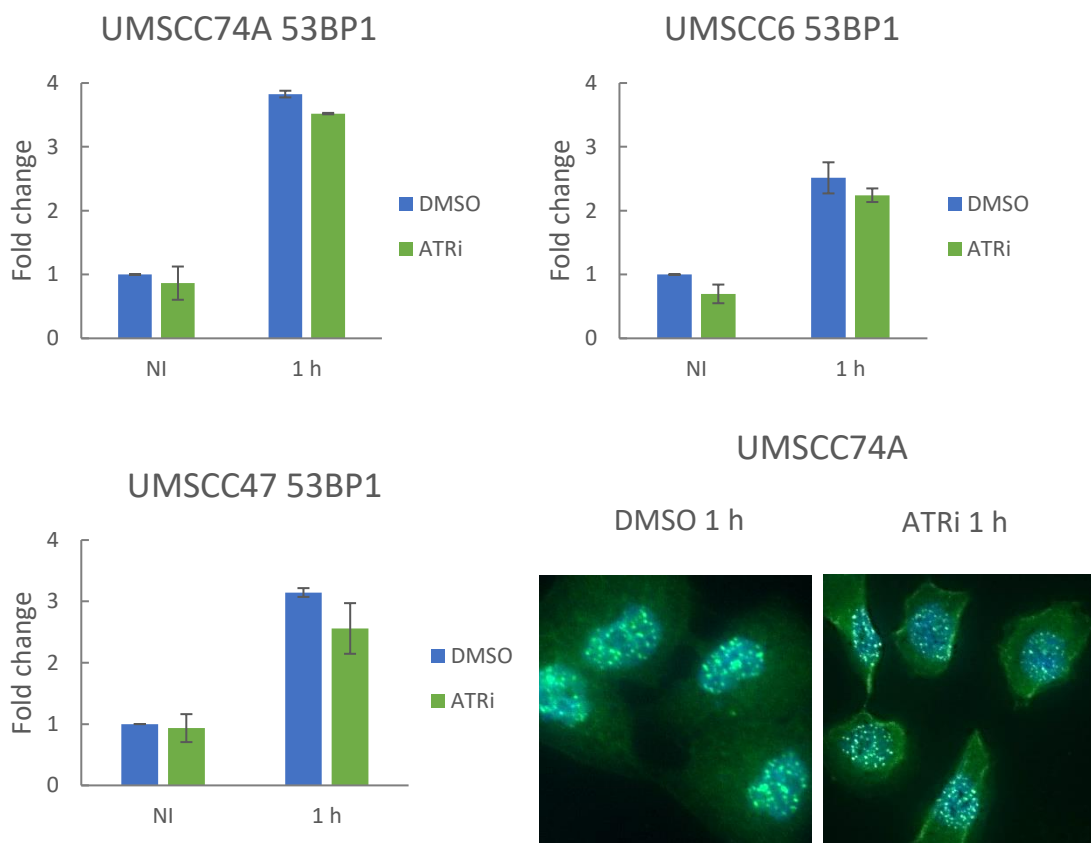


Figure 5.6. Impact of ATRi on DSB repair marker 53BP1. 53BP1 foci formation was investigated in 3 HNSCC cell lines. Cells were treated for 1 h with 1 μ M ATRi or 10 μ M DMSO, exposed to 4 Gy x – rays and fixed and stained for 53BP1 1 h post irradiation. NI: non irradiated. 5 representative images were captured, containing at least 20 cells per coverslip. Values were the means of 2 biologically independent experiments, were normalised against the non irradiated DMSO treated cells, which was set to 1, and are presented with their standard error.

5.2.2.3 Impact of ATRi on Rad51

Rad51 foci formation was investigated in response to ATRi alone and in combination with IR. A fluctuation in numbers of Rad51 foci was observed between the DMSO treated and ATRi treated non irradiated cells, in the different cell lines, suggesting a possible cell line dependant HR regulation by ATRi. Rad51 foci peaked at 16 h post irradiation in DMSO treated cells, with a 2- to 3- fold increase. But importantly, in ATRi treated cells formation of Rad51 foci was severely downregulated in all cell lines and the amount of foci remained almost at baseline. Altogether, these results highlighted the key role of ATR in HR repair, as inhibition of this protein kinase had a major impact on Rad51 foci formation.

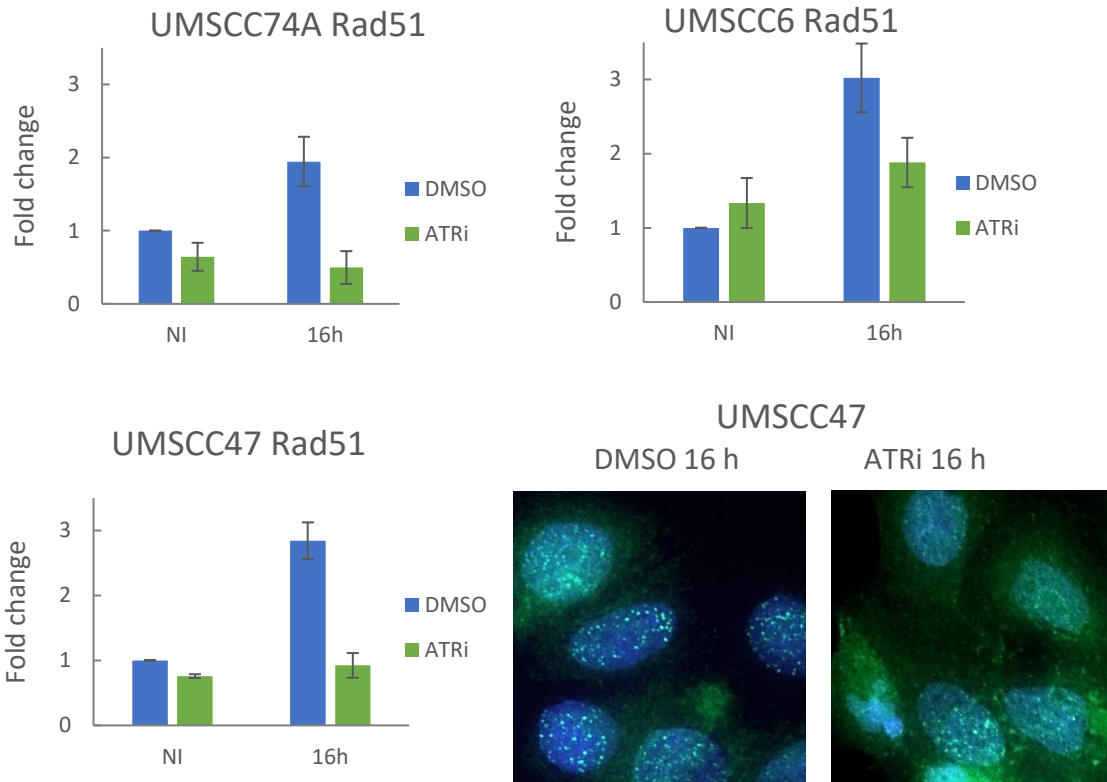


Figure 5. 7. Impact of ATRi on DSB repair marker Rad51. Rad51 foci formation was investigated in 3 HNSCC cell lines. Cells were treated for 1 h with 1 μ M ATRi or 10 μ M DMSO, exposed to 4 Gy x – rays and fixed and stained for Rad51 16 h post irradiation. NI: non irradiated. 5 representative images were captured, containing at least 20 cells per coverslip. Values were the means of 2 biologically independent experiments, were normalised against the non irradiated DMSO treated cells, which was set to 1, and are presented with their standard error.

5.2.3 Impact of DNA-PKcsi

The impact of the third inhibitor, DNA-PKcsi, alone or in combination with IR was then examined on the three DSB repair markers. The same three HNSCC cell lines were utilised, and cells were pre-treated with 1 μ M DNA-PKcsi or 10 μ M DMSO as control for 1 h and then were exposed to 4 Gy x – rays. The cells were then further incubated with the inhibitor up to 24 h to allow for DNA repair progression. Finally, cells were fixed, and incubated with antibodies for γ H2AX, 53BP1 or Rad51, then were imaged and analysed.

5.2.3.1 Impact of DNA-PKcsi on γ H2AX

No increase was exhibited in the number of γ H2AX foci formed in the presence of the inhibitor alone, and thus in the amount of endogenous DSB induction and recognition in DNA-PKcsi treated cells in the absence of IR (Figures 5.8). In DMSO treated cells γ H2AX

foci formation reached a 3- to 6- fold increase above baseline at 4 h post irradiation, and the foci were gradually resolved in UMSCC6, but persisted in UMSCC74A (HPV-negative) and UMSCC47 (HPV-positive) cell lines, suggesting a possible cell line deficiency for the resolvent of these foci. However, upregulation and increased persistency in γ H2AX foci was observed in the presence of DNA-PKcsi 4 h and 8 h post irradiation, with \sim 1.5- fold higher amount of γ H2AX foci in inhibitor compared to DMSO treated cells. This demonstrated persistent and unrepaired DSB up to 8 h post irradiation that suggested insufficient DSB repair due to DNA-PKcsi in combination with x – rays.

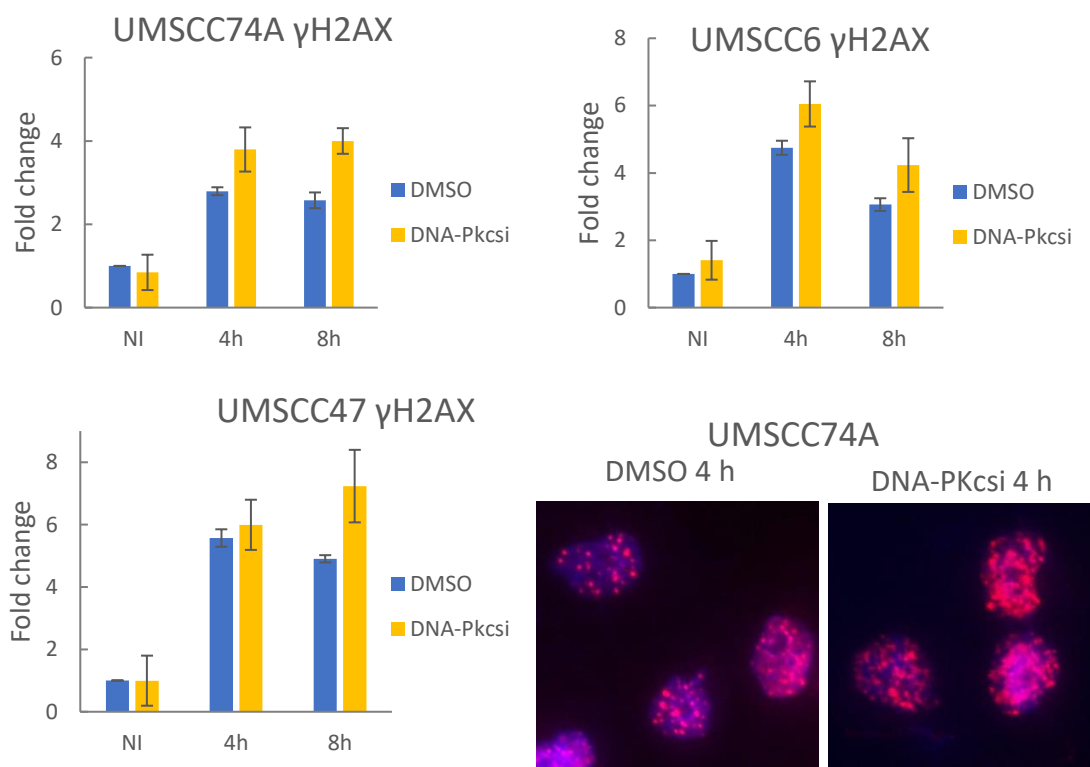


Figure 5.8. Impact of DNA-PKcsi on DSB marker γ H2AX. γ H2AX foci formation was investigated in 3 HNSCC cell lines. Cells were treated for 1 h with 1 μ M DNA-PKcsi or 10 μ M DMSO, exposed to 4 Gy x – rays and fixed and stained for γ H2AX 4 h and 8 h post irradiation. NI: non irradiated. 5 representative images were captured, containing at least 20 cells per coverslip. Values were the means of 2 biologically independent experiments, were normalised against the non irradiated DMSO treated cells, which was set to 1, and are presented with their standard error.

5.2.3.2 Impact of DNA-PKcsi on 53BP1

Formation and persistence of 53BP1 foci was investigated as a marker of NHEJ repair. A minor decrease was observed in the number of 53BP1 foci in UMSCC6 and UMSCC47

DNA-PKcsi treated cells in the absence of IR, by a factor of ~ 1.5 and ~ 1.3 respectively, compared to the DMSO treated cells, as seen in Figure 5.9. This suggested that the inhibitor alone moderately reduced 53BP1 recruitment and thus involvement in DSB repair via NHEJ. 53BP1 was recruited post exposure to IR, displaying a 3- to 5- fold increase in the DMSO treated cells at 4 h which was reduced by 8 h in the HPV-negative cell lines, but persisted in the HPV-positive UMSCC47 cells, highlighting their increased radiosensitivity. But in accordance with the γ H2AX foci, 53BP1 foci exhibited increased persistency 4 h and 8 h post irradiation in DNA-PKcsi treated cells, by a factor of ~ 1.2 in the HPV-positive UMSCC47, and ~ 1.4 in the HPV-negative UMSCC6 and UMSCC74A cells. These findings showed that combination treatment with DNA-PKcsi and x – rays, impacted 53BP1 recruitment leading to persistent unrepaired DSB. Also, this suggested that NHEJ is dysregulated through inability of 53BP1 to dissociate from the DSB.

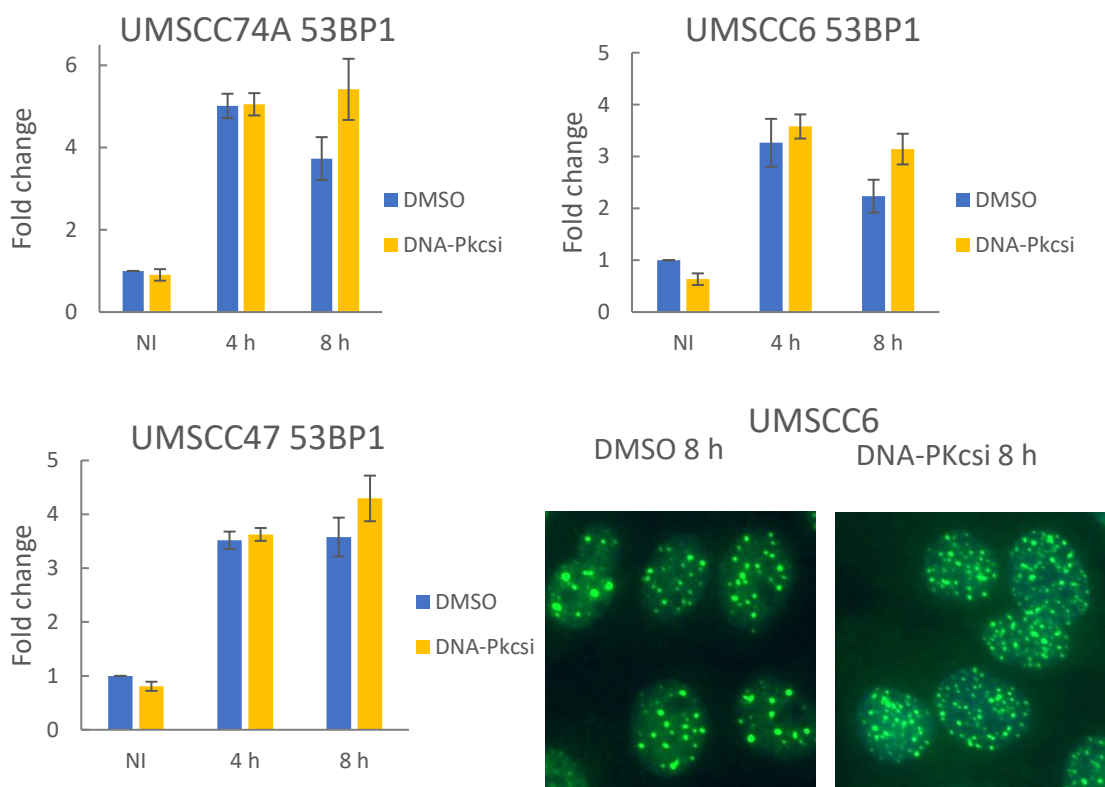


Figure 5. 9. Impact of DNA-PKcsi on DSB repair marker 53BP1. 53BP1 foci formation was investigated in 3 HNSCC cell lines. Cells were treated for 1 h with 1 μ M DNA-PKcsi or 10 μ M DMSO, exposed to 4 Gy x – rays and fixed and stained for 53BP1 4 h and 8 h post irradiation. NI: non irradiated. 5 representative images were captured, containing at least 20 cells per coverslip. Values were the means of 2 biologically independent experiments, were normalised against the non irradiated DMSO treated cells, which was set to 1, and are presented with their standard error.

5.2.3.3 Impact of DNA-PKcsi on Rad51

The third marker, Rad51, was investigated in response to DNA-PKcsi alone and in combination with x – rays, even though DNA-PKcs is not directly involved in HR. No major difference was observed between the number of Rad51 foci in DMSO treated cells and DNA-PKcsi treated cells, in the absence of IR, as seen in Figure 5.10. In DMSO treated cells, Rad51 peaked at 16 h (1.9- to 3- fold above baseline) and dropped by 24 h post IR. Yet foci levels were higher in UMSCC6 and UMSCC74A DNA-PKcsi treated cells by ~1.4 at 16 h and ~2.3- fold at 24 h post IR. In UMSCC47 cells, Rad51 foci persisted only at 24 h post IR where they were 1.6- fold higher. This demonstrated increased Rad51 recruitment that could mean increased DSB repair via HR following DNA-PKcsi treatment, possibly because of HR employment as a substitute following an insufficient NHEJ repair of DSBs.

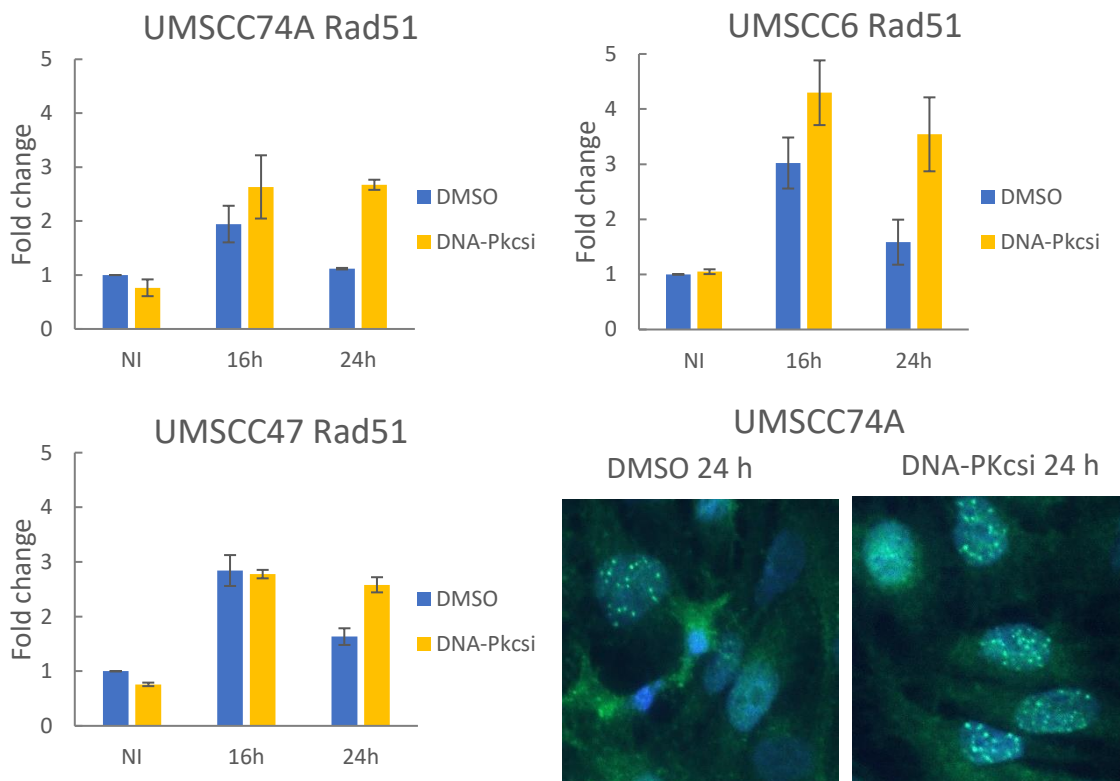


Figure 5. 10. Impact of DNA-PKcsi on DSB repair marker Rad51. Rad51 foci formation was investigated in 3 HNSCC cell lines. Cells were treated for 1 h with 1 μ M DNA-PKcsi or 10 μ M DMSO, exposed to 4 Gy x – rays and fixed and stained for Rad51 16 h and 24 h post irradiation. NI: non irradiated. 5 representative images were captured, containing at least 20 cells per coverslip. Values were the means of 2 biologically independent experiments, were normalised against the non irradiated DMSO treated cells, which was set to 1, and are presented with their standard error.

5.3 Immunofluorescent staining and foci analysis in response to protons.

Investigation of the impact of DNA repair inhibition on γ H2AX, 53BP1 and Rad51 foci formation in combination with x – rays, demonstrated that all three drugs directly or indirectly affected DSB repair via NHEJ and HR repair. The outcome of this inhibition in combination with proton irradiation was then investigated. As previously described, the markers of DSB sites and DSB repair were examined in response to monotherapy of the DNA repair inhibitors ATMi, ATRi and DNA-PKcsi as well as in combination with IR, in UMSCC6, UMSCC74A and UMSCC47 HNSCC cell lines. In DMSO treated cells the number foci per nucleus varied in the 3 different cell lines between 100-150 of γ H2AX foci and 90-110 of 53BP1 foci 1 h post 4 Gy protons and 35-55 of Rad51 foci 8 h post 4 Gy protons.

5.3.1 Impact of ATMi

First, the impact of ATMi alone, or in combination with proton irradiation was assessed in the three markers. Cells were pre-treated with 10 μ M ATMi or 10 μ M DMSO as control for 1 h and then were exposed to 4 Gy protons. The cells were then further incubated with the inhibitor for up to 24 h to allow for DNA repair progression. Finally, cells were fixed and incubated with antibodies for γ H2AX, 53BP1 or Rad51, then were imaged and analysed.

5.3.1.1 Impact of ATMi on γ H2AX

Formation of γ H2AX, as a marker of DSB sites, was assessed 1 h, 4 h and 8 h post proton irradiation. No major difference was observed in γ H2AX focus formation between DMSO treated and ATMi treated cells in the absence of protons (Figures 5.2 and 5.11). Following treatment with proton irradiation the amount of foci rapidly increased by 5- to 7- fold 1 h post irradiation, in DMSO treated cells in all cell lines examined. However, formation of γ H2AX foci in ATMi treated cells, was delayed and reduced by 1.45- fold in UMSCC6 and UMSCC74A, and by 2.3- fold in UMSCC47, compared to the DMSO treated cells, 1 h post proton irradiation. These results suggested that ATMi in combination with protons, delayed the DSB recognition through generation of γ H2AX foci and therefore delayed DNA repair initiation and progression.

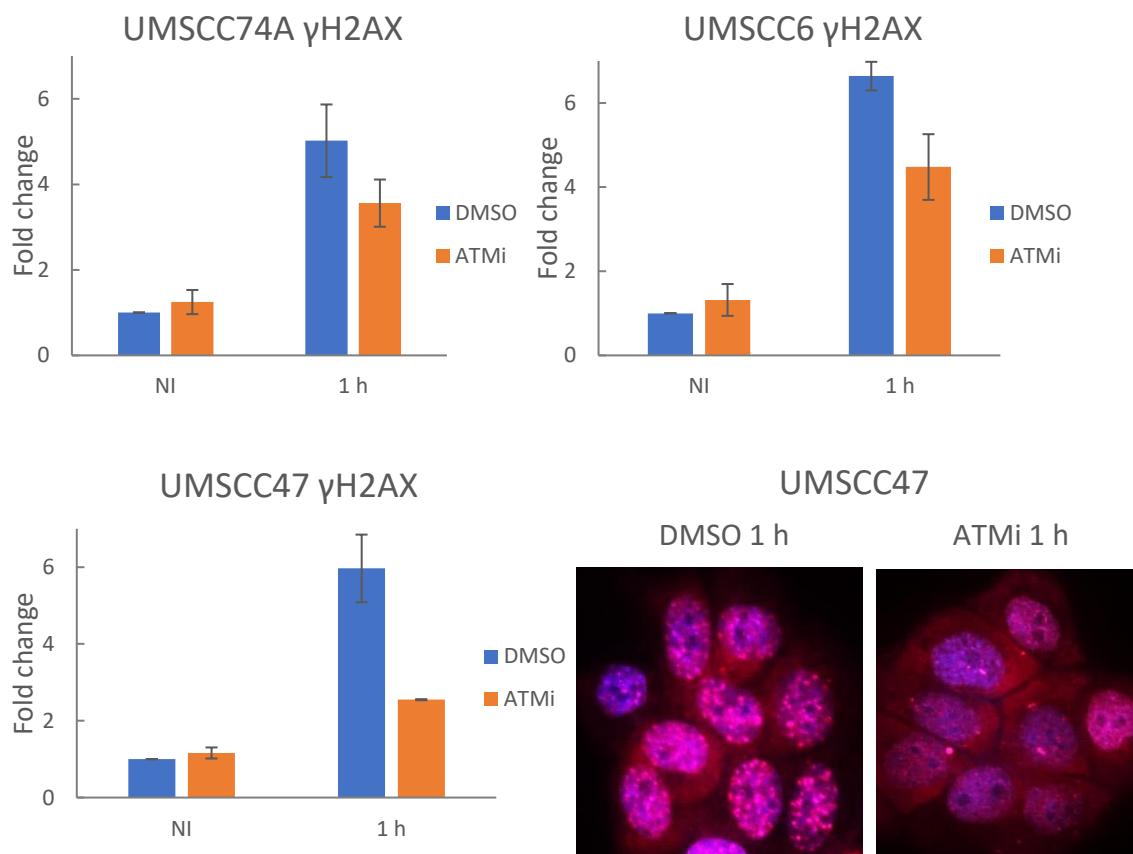


Figure 5. 11. Impact of ATMi on DSB marker γ H2AX. γ H2AX foci formation was investigated in 3 HNSCC cell lines. Cells were treated for 1 h with 10 μ M ATMi or 10 μ M DMSO, exposed to 4 Gy proton irradiation and fixed and stained for γ H2AX 1 h post irradiation. NI: non irradiated. 5 representative images were captured, containing at least 20 cells per coverslip. Values were the means of 2 biologically independent experiments, were normalised against the non irradiated DMSO treated cells, which was set to 1, and are presented with their standard error.

5.3.1.2 Impact of ATMi on 53BP1

As shown in Figure 5.12 (and Figure 5.3), formation of 53BP1 was not affected by treatment with ATMi alone, in the absence of proton irradiation. In the DMSO treated cells, the number of 53BP1 foci increased by 2.3- to 3.4- fold above baseline at 4 h post exposure to protons, and was moderately at 8 h post IR in UMSCC6 cells. However, similarly to x – rays, 53BP1 foci persisted up to 8 h post protons in UMSCC74A and UMSCC47, which could be related to these specific cell lines or due to overlapping of foci masking any progress of the repair. In proton irradiated ATMi treated cells, 53BP1 foci formation was not delayed 1 h post protons, however it persisted at 8 h indicating persistent DSBs. This increased persistency of DSBs and NHEJ repair activity in the later

time points, could suggest that protons possibly induce more complex DNA damage that are more difficult to be repaired.

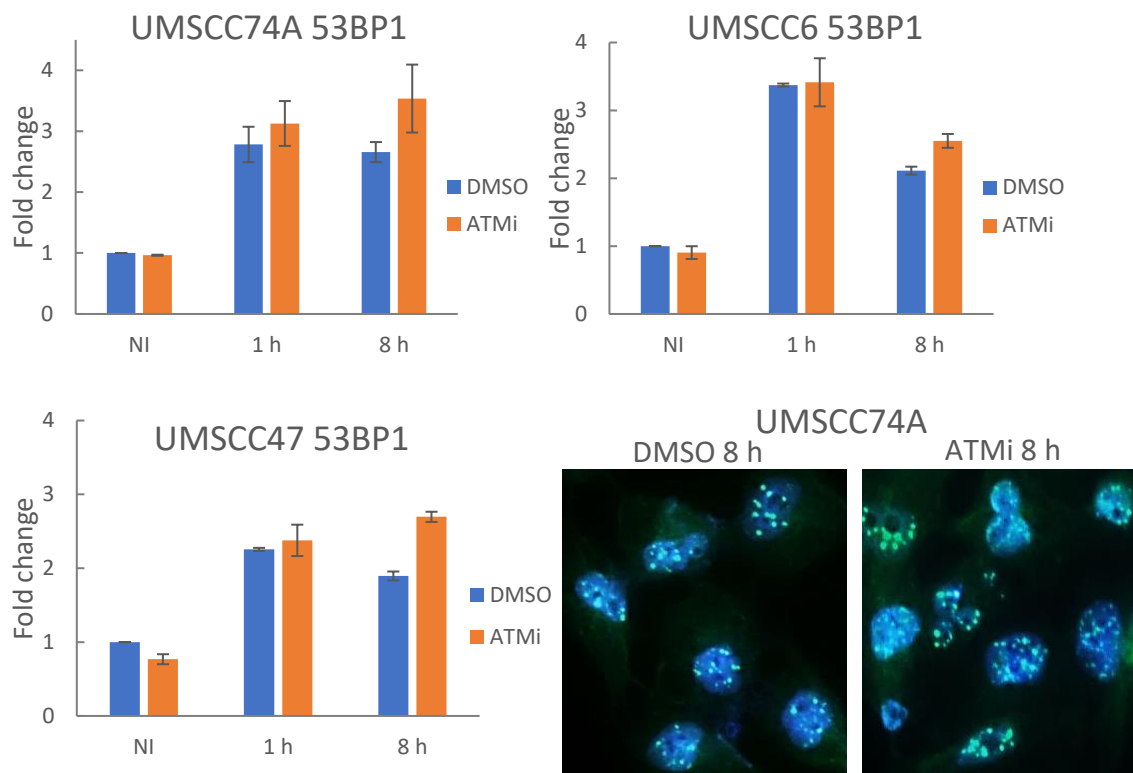


Figure 5. 12. Impact of ATMi on DSB repair marker 53BP1. 53BP1 foci formation was investigated in 3 HNSCC cell lines. Cells were treated for 1 h with 10 μ M ATMi or 10 μ M DMSO, exposed to 4 Gy proton irradiation and fixed and stained for 53BP1 1 h and 8 h post irradiation. NI: non irradiated. 5 representative images were captured, containing at least 20 cells per coverslip. Values were normalised to the non-irradiated DMSO treated cells, which was set to 1, and are presented with their standard error.

5.3.1.3 Impact of ATMi on Rad51

Formation of Rad51 foci was investigated and no impact on Rad51 was observed by ATMi alone in two cell lines (Figure 5.13 and Figure 5.4) in the absence of proton irradiation, yet the numbers were elevated in UMSCC6, suggesting increased dependence on ATM driven DSB repair in this cell line. In DMSO treated irradiated cells, Rad51 foci peaked at 16 h post irradiation in all cell lines by 3- to 4.3- fold above baseline. ATMi treatment reduced Rad51 foci at 16 h post proton irradiation in all cell lines but to a different extent. The HPV-negatives UMSCC74A and UMSCC6 cells exhibited a \sim 1.2- and \sim 1.4- fold decrease in Rad51 foci respectively compared to DMSO treated cells. The HPV-positive UMSCC47 cells exhibited the most substantial reduction in the number

Rad51 foci, ~2.4 fold lower in inhibitor treated cells compared to DMSO treated cells. These findings suggested that ATMi suppressed HR repair following proton irradiation.

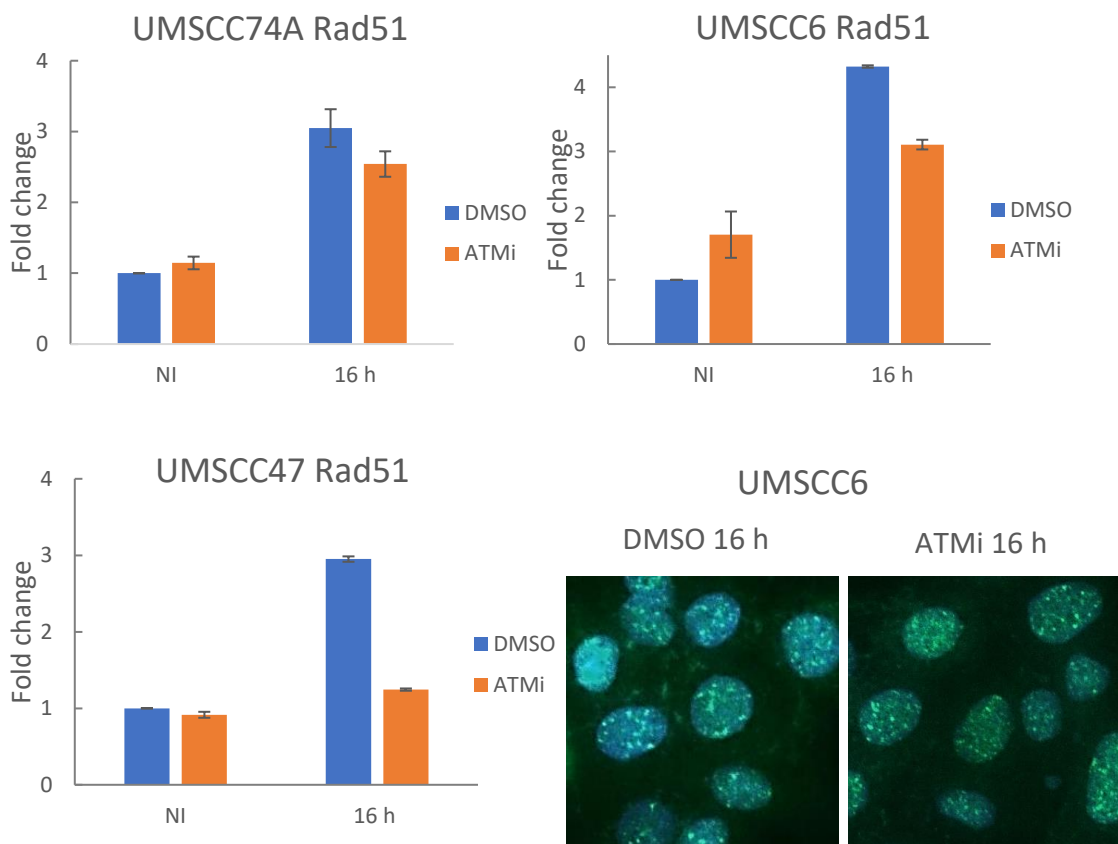


Figure 5. 13. Impact of ATMi on DSB repair marker Rad51. Rad51 foci formation was investigated in 3 HNSCC cell lines. Cells were treated for 1 h with 10 μ M ATMi or 10 μ M DMSO, exposed to 4 Gy proton irradiation and fixed and stained for Rad51 16 h post irradiation. NI: non irradiated. 5 representative images were captured, containing at least 20 cells per coverslip. Values were the means of 2 biologically independent experiments, were normalised against the non irradiated DMSO treated cells, which was set to 1, and are presented with their standard error.

5.3.2 Impact of ATRi

Next, the impact of ATRi alone or in combination with proton irradiation was investigated on the DSB repair markers γ H2AX, 53BP1 and Rad51. Cells were pre-treated with 1 μ M ATRi or 10 μ M DMSO as a control for 1 h and then were exposed to 4 Gy protons. The cells were then further incubated with the inhibitor up to 24 h to allow for DNA repair progression. Finally, cells were fixed and incubated with antibodies for γ H2AX, 53BP1 or Rad51, then were imaged and analysed.

5.3.2.1 Impact of ATRi on γ H2AX

γ H2AX foci formation was not affected by ATRi alone in UMSCC47 yet was increased (1.6- fold above baseline) in UMSCC6 and UMSCC74A (Figure 5.14), suggesting a possible increase in baseline DSB levels. Upon exposure to protons, γ H2AX foci formation in DMSO treated cells peaked within 1 h post irradiation (5- to 7- fold) in all three cell lines. In ATRi treated and proton irradiated cells, 1 h post protons there was an almost negligible fluctuation within the standard error, in the number of γ H2AX foci in all cell lines, whilst foci numbers were slightly down in UMSCC6 and UMSCC47 cells. Altogether, the impact of ATRi in γ H2AX foci post protons was largely insignificant, confirming that ATR is not directly associated with γ H2AX foci regulation. Arguably, there is a potential involvement for ATR in response to protons, also observed in response to x – rays (Figure 5.5) in DSB designation by γ H2AX in the HPV-positive UMSCC47 cells and HPV-negative UMSCC6 cells to a lesser extent.

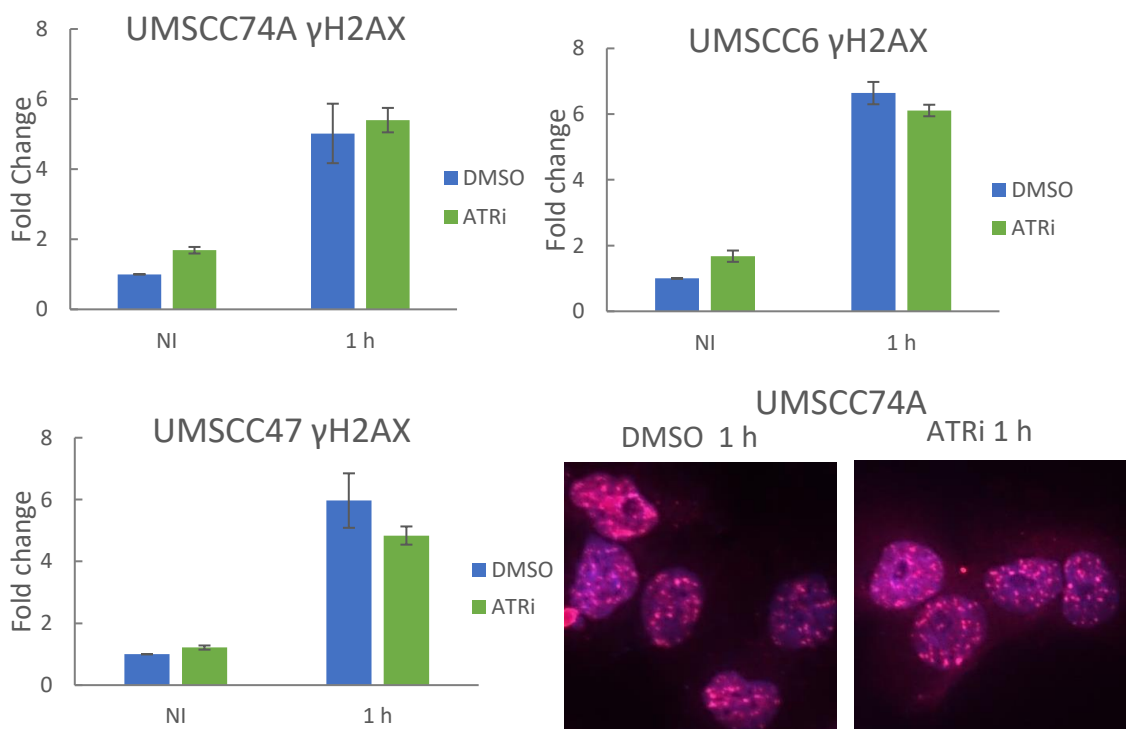


Figure 5. 14. Impact of ATRi on DSB marker γ H2AX. γ H2AX foci formation was investigated in 3 HNSCC cell lines. Cells were treated for 1 h with 1 μ M ATRi or 10 μ M DMSO, exposed to 4 Gy proton irradiation and fixed and stained for γ H2AX 1 h post irradiation. NI: non irradiated. 5 representative images were captured, containing at least 20 cells per coverslip. Values were the means of 2 biologically independent experiments, were normalised against the non irradiated DMSO treated cells, which was set to 1, and are presented with their standard error.

5.3.2.2 Impact ATRi on 53BP1

Formation of 53BP1 foci in the presence of ATRi alone was minorly downregulated in the three cell lines, suggesting the ATRi alone did not have a significant impact on generation of 53BP1 foci and thus on the endogenous NHEJ repair (Figure 5.15), similar to Figure 5.6. Following proton irradiation in DMSO treated cells, the foci were formed within 1 h post irradiation in all cell lines peaking between 2.3- and 3.4- fold above baseline. Following a combination of ATRi treatment and proton irradiation, a minor fluctuation within the standard error in the number of 53BP1 foci was exhibited 1 h post irradiation in UMSCC6 and UMSCC74A cells. However, in UMSCC47 cells, 53BP1 foci formation were upregulated, by a factor of ~1.4, in inhibitor treated cells 1 h post protons, demonstrating increased NHEJ repair in this HPV-positive cell line, which was not observed following x – rays. This further demonstrated a potentially increased role of ATR in DSB designation and therefore repair in UMSCC47 HPV-positive cells, also shown with γ H2AX (discussed in section 5.3.2.1).

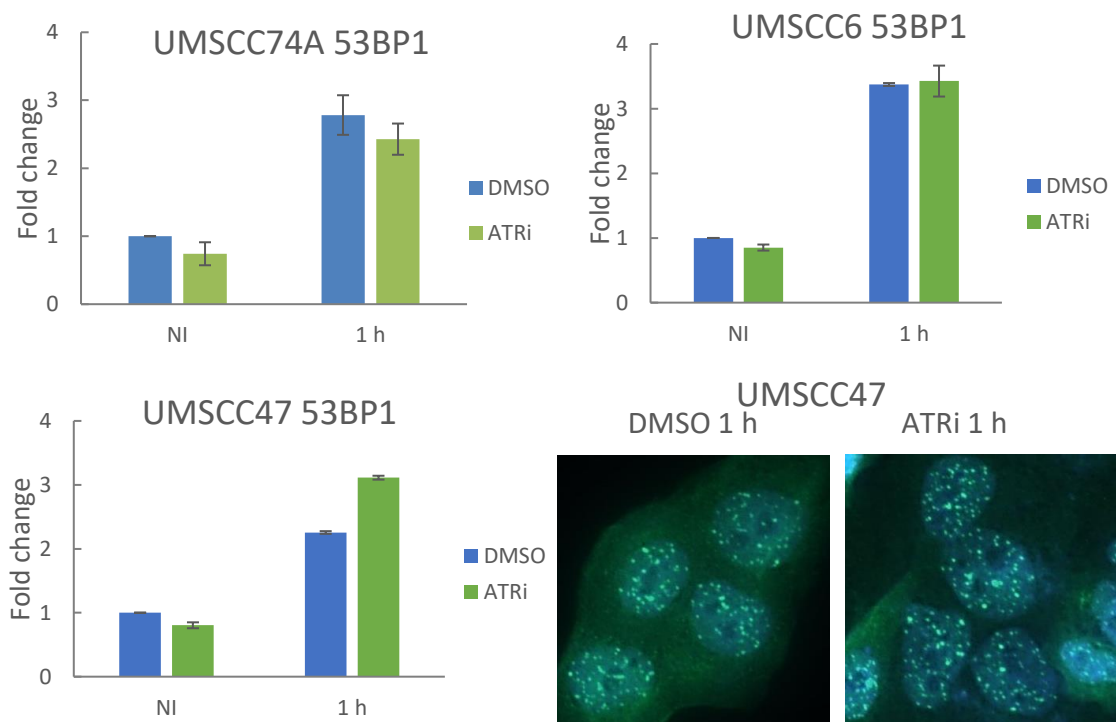


Figure 5. 15. Impact of ATRi on DSB repair marker 53BP1. 53BP1 foci formation was investigated in 3 HNSCC cell lines. Cells were treated for 1 h with 1 μ M ATRi or 10 μ M DMSO, exposed to 4 Gy proton irradiation and fixed and stained for 53BP1 1 h post irradiation. NI: non irradiated. 5 representative images were captured, containing at least 20 cells per coverslip. Values were the means of 2 biologically independent experiments, were normalised against the non irradiated DMSO treated cells, which was set to 1, and are presented with their standard error.

5.3.2.3 Impact of ATRi on Rad51

Rad51 foci formation was shown to be increased in ATRi treated non irradiated cells, compared to DMSO treated non irradiated cells in UMSCC6 and UMSCC74A (Figure 5.16) suggesting increased HR repair possibly due to increased amount of endogenously generated DSBs. Exposing DMSO treated cells to protons resulted in Rad51 foci peak at 16 h, which was 3- to 4.3- fold above baseline, in all cell lines. Following protons and ATRi treatment a considerable reduction in the amount of Rad51 foci was observed at 16 h post irradiation. Specifically, the number of foci was reduced by 1.7-, 4.8-, and 2.1- fold in UMSCC6, UMSCC74A, and UMSCC47 respectively. The dysregulation of Rad51 foci by ATRi in response to protons highlighted the limited DSB repair via HR under these conditions.

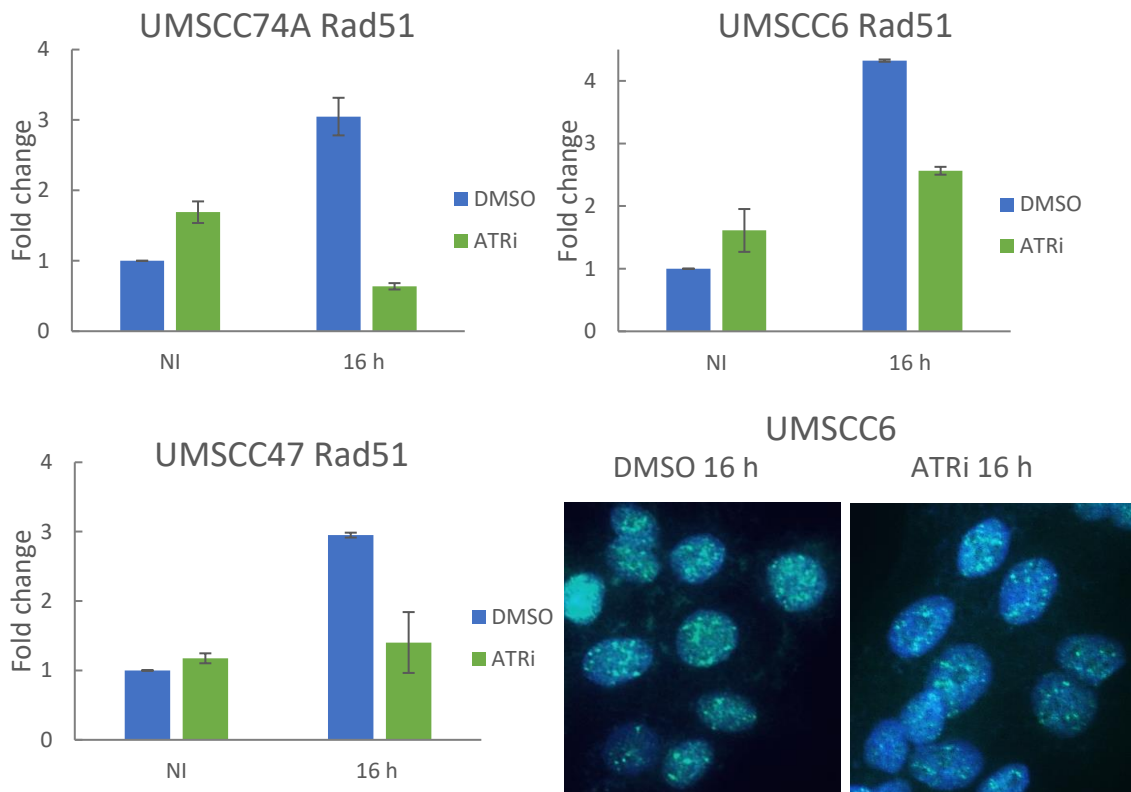


Figure 5. 16. Impact of ATRi on DSB repair marker Rad51. Rad51 foci formation was investigated in 3 HNSCC cell lines. Cells were treated for 1 h with 1 μ M ATRi or 10 μ M DMSO, exposed to 4 Gy proton irradiation and fixed and stained for Rad51 16 h post irradiation. NI: non irradiated. 5 representative images were captured, containing at least 20 cells per coverslip. Values were the means of 2 biologically independent experiments, were normalised against the non irradiated DMSO treated cells, which was set to 1, and are presented with their standard error.

5.3.3 Impact of DNA-PKcsi

The impact of the third inhibitor, DNA-PKcsi, alone or in combination with protons was then examined in the DSB repair markers, in UMSCC6, UMSCC74A and UMSCC47 HNSCC cell lines. Cells were pre-treated with 1 μ M DNA-PKcsi or 10 μ M DMSO as control for 1 h and then were exposed to 4 Gy protons. The cells were then further incubated with the inhibitor up to 24 h to allow for DNA repair progression. Finally, cells were fixed and incubated with antibodies for γ H2AX, 53BP1 or Rad51, then were imaged and analysed.

5.3.3.1 Impact of DNA-PKcsi on γ H2AX

Formation of γ H2AX foci was not impacted by DNA-PKcsi treatment alone in the absence of proton irradiation as shown in Figure 5.17 and Figure 5.8. In DMSO treated cells, γ H2AX foci formation reached \sim 4- fold above baseline at 4 h post proton irradiation, and the foci were gradually reduced in all three cell lines 4 h later. However, DNA-PKcsi treated cells exhibited an upregulation and increased persistency in γ H2AX foci 4 h and 8 h post proton irradiation. Specifically, the numbers of γ H2AX foci were higher by \sim 1.1- to 1.3- fold in UMSCC6 cells, \sim 1.4- to 1.9- fold in UMSCC74A cells, and \sim 1.5- to 1.4- fold in UMSCC47 cells, at 4h and 8h respectively. This demonstrated the persistency of unrepaired DSB up to 8 h post irradiation, indicating insufficient NHEJ repair in response to protons, in all cell lines and irrespective of the HPV status.

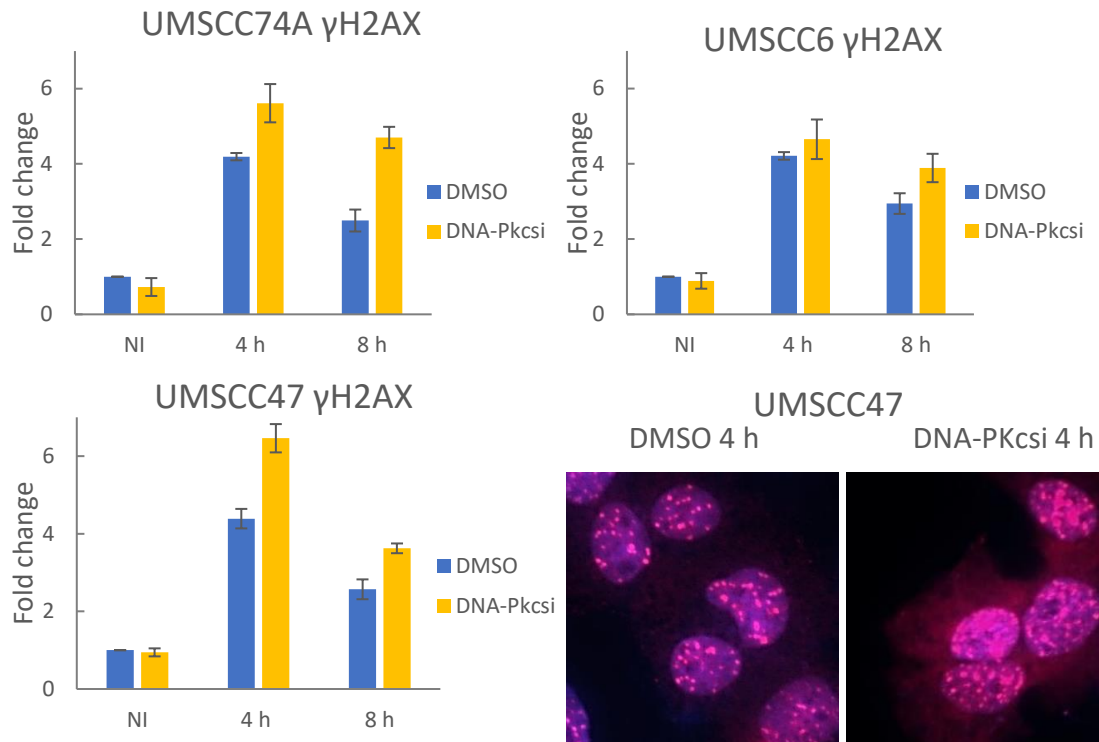


Figure 5. 17. Impact of DNA-PKcsi on DSB marker γ H2AX. γ H2AX foci formation was investigated in 3 HNSCC cell lines. Cells were treated for 1 h with 1 μ M DNA-PKcsi or 10 μ M DMSO, exposed to 4 Gy proton irradiation and fixed and stained for γ H2AX 4 h and 8 h post irradiation. NI: non irradiated. 5 representative images were captured, containing at least 20 cells per coverslip. Values were the means of 2 biologically independent experiments, were normalised against the non irradiated DMSO treated cells, which was set to 1, and are presented with their standard error.

5.3.3.2 Impact of DNA-PKcsi on 53BP1

Formation of 53BP1 foci exhibited a marked decrease in DNA-PKcsi treated cells, in the absence of proton irradiation, particularly in UMSCC6 and UMSCC74A cells (Figure 5.18) which was 1.5- and 1.7- fold below baseline respectively, suggesting that monotherapy reduced the sites of 53BP1 recruitment for the repair of endogenous DSB repair via NHEJ. Following proton irradiation, in DMSO treated cells the number of 53BP1 foci was increased between 2- to 2.7- fold above baseline 4 h and persisted up to 8 h post protons, also observed following x – rays. In DNA-PKcsi treated cells, the number of 53BP1 foci was further increased at 4 h post irradiation, by a factor of \sim 1.5 in UMSCC6 cells, \sim 1.2 in UMSCC74A cells, and \sim 1.4 in UMSCC47 cells. This matched the γ H2AX trend, further demonstrating that DNA-PKcsi and protons increased DSB persistence. The number of 53BP1 foci was reduced by 8 h in the presence of DNA-PKcsi although

remained above baseline in UMSCC6 and UMSCC74A, despite the persistent DSBs highlighted by the increased γ H2AX foci (Figure 5.17). This suggested reduced 53BP1 recruitment at later time points following proton irradiation.

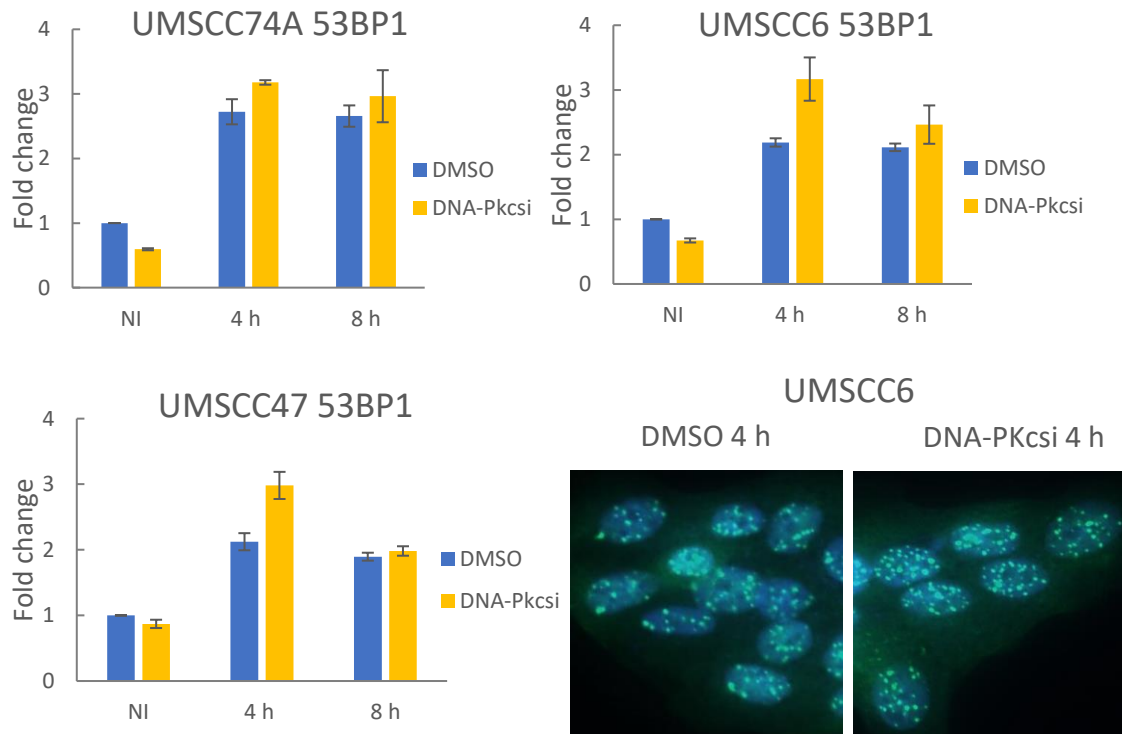


Figure 5. 18. Impact of DNA-PKcsi on DSB repair marker 53BP1. 53BP1 foci formation was investigated in 3 HNSCC cell lines. Cells were treated for 1 h with 1 μ M DNA-PKcsi or 10 μ M DMSO, exposed to 4 Gy proton irradiation and fixed and stained for 53BP1 4 h and 8 h post irradiation. NI: non irradiated. Values were the means of 2 biologically independent experiments, were normalised against the non irradiated DMSO treated cells, which was set to 1, and are presented with their standard error.

5.3.3.3 Impact of DNA-PKcsi on Rad51

The number of Rad51 foci did not differ in DMSO treated cells and DNA-PKcsi treated cells in the absence of protons as seen in Figure 5.19 and Figure 5.10. After exposure to proton irradiation, Rad51 foci in DMSO treated cells peaked at 16 h (3- to 4.3- fold above baseline) in all cell lines, and were considerably reduced by 24 h post irradiation in UMSCC6 and UMSCC7A. However, foci appeared to persist for longer in UMSCC47 cells indicating increased HR dependence at the 24 h time point, which was not observed post x – rays. Combination of DNA-PKcsi and protons considerably reduced Rad51 foci formation at 16 h post proton irradiation in the HPV-negative cells, by a factor of \sim 1.5 in

UMSCC6 cells, and ~ 2 in UMSCC74A cells. Less of an effect was produced by DNA-PKcsi and protons in the HPV-positive UMSCC47 cells, which exhibited a reduction in Rad51 foci by ~ 1.2 fold compared to DMSO treated cells. At 24 h post irradiation the difference between DMSO and DNA-PKcsi treated cells was diminished. This suggested that DNA-PKcsi suppressed Rad51 recruitment post proton irradiation at 16 h, although the difference was negligible at the later time point.

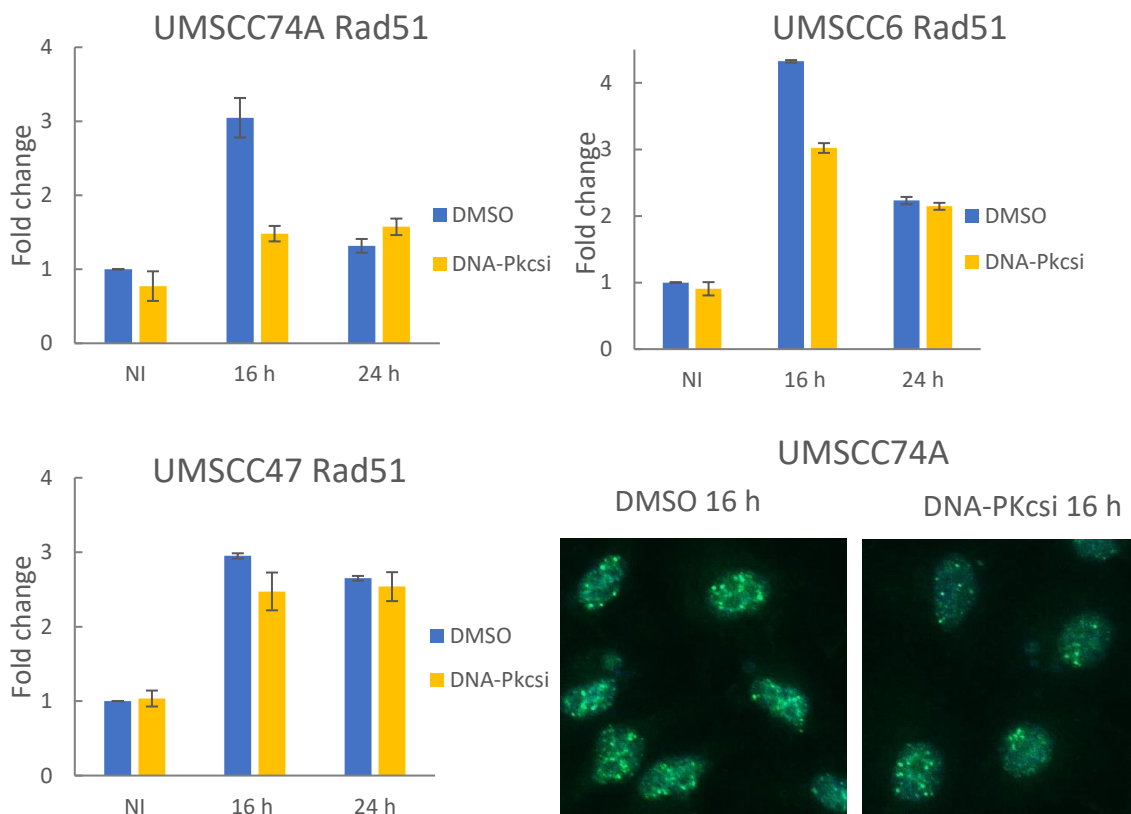


Figure 5. 19. Impact of DNA-PKcsi on DSB repair marker Rad51. Rad51 foci formation was investigated in 3 HNSCC cell lines. Cells were treated for 1 h with 1 μ M DNA-PKcsi or 10 μ M DMSO, exposed to 4 Gy proton irradiation and fixed and stained for Rad51 16 h and 24 h post irradiation. NI: non irradiated. Values were the means of 2 biologically independent experiments, were normalised against the non irradiated DMSO treated cells, which was set to 1, are presented with their standard error.

5.4 Conclusions

The DNA repair inhibitors that effectively reduced phosphorylation in crucial sites of their target proteins, as observed by Immunoblotting (see Chapter 4), were then utilised to investigate the outcome of this inhibition in the signalling of the DNA damage response and DSB repair. Particularly, the impact of ATMi, ATRi and DNA-PKcsi on DNA repair focus formation was examined in HNSCC cell lines, as a monotherapy but also in combination with either x – ray or proton irradiation. In order of appearance, γ H2AX foci are one of the first to be formed, as a marker of DSB recognition. In response to IR alone, they are reported to pick within 30 – 60 minutes post irradiation and then gradually drop, although DSB are shown to pick shortly after exposure to IR and then gradually drop depending on the repair proficiency of the cells. 53BP1 foci are formed almost simultaneously and have very similar kinetics to γ H2AX and were studied as a marker of DSB repair via the NHEJ pathway (207, 235). Lastly, Rad51 foci were assessed as a marker of DSB repair via the HR pathway and they are reported to pick later approximately 12 h post exposure to IR and then gradually to be resolved (236).

In the absence of IR, HNSCC cells were incubated with either of the drug for 24 h before been fixed and analysed. ATMi had generally no major impact on formation of γ H2AX and 53BP1 foci, while resulted in only a small increase in Rad51 foci, specifically in UMSCC6 cells. This constituted an indication that 24 h treatment with the inhibitor alone, in the absence of IR, did not severely affect normal DSB recognition and repair. Although the small increase in Rad51 foci in the radioresistant UMSCC6 cells, could indicate a respective increase in the amounts of DSBs accumulating later in the cell cycle. ATRi, as a monotherapy, had no major effect on the formation of 53BP1 foci, yet had a small upregulating effect on γ H2AX and Rad51 foci accumulation in HPV-negative UMSCC6 cells, as shown in both data sets, and UMSCC74A cells as shown in the proton data set. Increased levels of γ H2AX could indicate that the drug alone promoted DSB recognition or DSB induction something that was also supported by the upregulated levels of Rad51 showing increased amounts of DSBs undergoing HR repair. However, the apparent lack of impact on 53BP1 recruitment (NHEJ repair marker) was an indicator that these endogenous DSBs accumulated later in the cell cycle and were resolved mainly by Rad51 recruitment via the HR pathway. In contrast, treatment with DNA-PKcsi

alone, resulted in no difference in γ H2AX and Rad51 foci formation, but downregulated 53BP1 foci in all cell lines. This suggested no impact on DSB induction or recognition by DNA-PKcs alone, but only a reduction in repair of endogenous DSB via NHEJ pathway.

Combination therapy of ATMi and IR generally resulted in a delay in γ H2AX foci formation in all cell lines examined (summarised in Table 5.1). The same trend was observed in both x – ray irradiated and proton irradiated cells demonstrating that the drug was equally effective following both radiation modalities. The delayed DSB recognition should therefore predictably lead to delayed DSB repair, which was investigated via the 53BP1 and Rad51 foci formation. Indeed, reduced numbers of 53BP1 foci following x – ray irradiation in all cell lines, suggested reduced NHEJ repair in the early time points. Interestingly, however, this was not observed following proton irradiation. In fact, NHEJ repair as shown by 53BP1 foci, was not delayed but instead exhibited increased foci numbers in the later time points in all cell lines, indicating persistent DSB. Therefore, the drug appeared to have an impact on the progression rather than the initiation of NHEJ repair, in combination with protons. Next, Rad51 foci was examined and found to be downregulated by ATMi, at 16 h post irradiation in all cell lines, either exposed to x – rays or protons, demonstrating reduced HR activity.

Table 5. 1. Impact of ATMi treatment on γ H2AX, 53BP1, and Rad51 foci formation and persistence alone (NI), or in combination with x – rays or protons. NI: non irradiated; 24 h: time of drug treatment alone, 1 h, 8 h, and 16 h: time post irradiation; \uparrow : upregulated, \downarrow : downregulated, -: no impact.

| Cell line \ Foci | γ H2AX | | | 53BP1 | | | | | Rad51 | | |
|------------------|---------------|--------------|--------------|--------------|--------------|----|---------|------------|------------|--------------|--------------|
| | NI | x – rays | protons | NI | x – rays | | protons | | NI | x – rays | protons |
| | 24h | 1h | 1h | 24h | 1h | 8h | 1h | 8h | 24h | 16h | 16h |
| UMSCC6 | \uparrow | \downarrow | \downarrow | - | \downarrow | - | - | \uparrow | \uparrow | \downarrow | \downarrow |
| UMSCC74 | \uparrow | \downarrow | \downarrow | \downarrow | \downarrow | - | - | \uparrow | - | \downarrow | \downarrow |
| UMSCC47 | - | \downarrow | \downarrow | - | \downarrow | - | - | \uparrow | - | \downarrow | \downarrow |

The impact of ATRi in combination with IR, was altogether not important on impacting on γ H2AX foci formation and therefore in DSB induction or recognition (summarised in Table 5.2). However, a small downregulation observed in the early time points post IR,

in most cell lines, could constitute evidence of ATR involvement in the initiation of the DDR. Equally, 53BP1 foci formation was not majorly affected in the presence of ATRi and x – rays or protons, confirming that ATR is not associated or affecting NHEJ repair. In contrast, ATR is directly involved in HR repair, and indeed treatment with ATRi and IR had a detrimental effect on Rad51 foci formation, and therefore HR activity in all cell lines, particularly at the later time points post irradiation. Overall, inhibition of either ATM or ATR was found sufficient to almost completely block Rad51 foci formation suggesting that one cannot be adequately substituted by the other and that they work synergistically rather than competitively. Generally, no difference was exhibited in all foci measured between x – ray and proton induced DNA damage, indicating that the drug affected the DNA repair factors in a similar manner in response to the two radiation modalities.

Table 5. 2. Impact of ATRi treatment on γ H2AX, 53BP1, and Rad51 foci formation and persistence alone (NI), or in combination with x – rays or protons. NI: non irradiated; 24 h: time of drug treatment alone, 1 h, 8 h, and 16 h: time post irradiation; \uparrow : upregulated \downarrow : downregulated, -: no impact.

| Foci Cell line | γ H2AX | | | 53BP1 | | | Rad51 | | |
|-------------------|---------------|--------------|--------------|--------------|--------------|------------|------------|--------------|--------------|
| | NI | x – rays | protons | NI | x – rays | protons | NI | x – rays | protons |
| | 24h | 1h | 1h | 24h | 1h | 1h | 24h | 16h | 16h |
| UMSCC6 | \uparrow | \downarrow | - | \downarrow | - | - | \uparrow | \downarrow | \downarrow |
| UMSCC74 | \uparrow | - | - | - | - | - | \uparrow | \downarrow | \downarrow |
| UMSCC47 | - | \downarrow | \downarrow | - | \downarrow | \uparrow | - | \downarrow | \downarrow |

Treatment with DNA-PKcsi in combination with either x – rays or proton irradiation, was not found to regulate γ H2AX foci in the early time points, yet the increased persistency in the later time points indicated persistent unrepaired DSB damage, most likely due to inefficient NHEJ repair (summarised in Table 5.3). This was supported by the 53BP1 foci formation, which were increased at 4 h and particularly at 8 h post x – ray irradiation, highlighting persistent DSBs and ongoing NHEJ. However, the increased persistency of 53BP1 foci was more important at 4 h post proton irradiation and DNA-PKcsi treatment but was almost reduced to baseline at 8 h. This could be further evidence that protons lead to increased accumulation of unrepaired DSB than x – rays. Subsequently this

suggested that possibly more cells are led to apoptosis in response to DNA-PKcsi and protons, as also suggested by the increased apoptosis observed by immunoblotting (see Chapter 4). Therefore, less cells are actively being repaired, hence the drop in 53BP1 foci at almost baseline levels. Lastly, the increase in Rad51 foci after DNA-PKcsi and x – ray treatment suggested that inhibition of NHEJ repair could potentially be substituted by increased HR repair of DSBs. Interestingly though, this was not observed following proton irradiation, where Rad51 foci were considerably reduced in the later time points following protons. This contradicting outcome between x – rays and protons could also be correlated to increased apoptosis following protons.

Table 5. 3. Impact of DNA-PKcsi treatment on γ H2AX, 53BP1, and Rad51 foci formation and persistence alone (NI), or in combination with x – rays or protons. NI: non irradiated; 24 h: time of drug treatment alone, 1 h, 8 h, and 16 h: time post irradiation; \uparrow : upregulated, \downarrow : downregulated, -: no impact.

| Foci Cell line | γ H2AX | | | 53BP1 | | | | | Rad51 | | | | |
|-------------------|---------------|------------|------------|--------------|----------|------------|------------|----|--------------|------------|------------|--------------|-----|
| | NI | x – rays | protons | NI | x – rays | | protons | | NI | x – rays | | protons | |
| | 24h | 4h/8h | 4h/8h | 24h | 4h | 8h | 4h | 8h | 24h | 16h | 24h | 16h | 24h |
| UMSCC6 | - | \uparrow | \uparrow | \downarrow | - | \uparrow | \uparrow | - | - | \uparrow | \uparrow | \downarrow | - |
| UMSCC74 | - | \uparrow | \uparrow | \downarrow | - | \uparrow | \uparrow | - | \downarrow | \uparrow | \uparrow | \downarrow | - |
| UMSCC47 | - | \uparrow | \uparrow | - | - | \uparrow | \uparrow | - | \downarrow | - | \uparrow | \downarrow | - |

In conclusion, the three inhibitors were shown to impact the DNA damage response to DSB in HNSCC cells, in combination with x – rays as well as protons, constituting evidence that the inhibitors are functional and should therefore impact on cell survival. It is worth noting that despite some small cell line dependence on the inhibitor effectiveness, there was no evidence that this differed based on HPV status. Nevertheless, some scoring issues should be noted as this affected the reproducibility of the independent experiments. One of the main issues was resolving of overlapping foci that were scored as a single focus particularly due to the high IR dose received by the cells, chosen mainly for consistency with previous work in the Parsons group. More detailed analysis was necessary to estimate the overall impact of the protein kinase inhibitors and to investigate their potential in radiosensitising of HNSCC cells.

Chapter 6: Results III

Impact of the DNA repair inhibitors on cell survival

6.1 Introduction

In the previous Chapters 4 and 5, I demonstrated that inhibition of the three protein kinases directly involved in DDR, ATM, ATR and DNA-PKcs, was found to suppress their phosphorylation on critical sites that regulate DNA repair progression. Moreover, this was shown to delay or even restrain DSB repair via NHEJ and HR repair pathways, as demonstrated using immunofluorescence staining. In this chapter, the impact on cell proliferation and survival of the three potent and well established inhibitors was examined in HNSCC cell lines, as a monotherapy as well as a combination therapy with x – ray or proton irradiation.

First, colony formation assays were utilised to investigate the ability of single cells treated with the inhibitor alone or in combination with IR, to grow into colonies of at least 50 cells *in vitro*. Clonogenic assays are the gold standard for measuring cell sensitivity to DNA damaging agents, particularly IR. Therefore, this is an essential tool to examine cell proliferation and subsequently cell death in 2D monolayer cultures. A defined number of cells was seeded, treated and allowed to grow in order to calculate their surviving fractions (SF), a variable that described the percentage of cell survival (237), and thus indicated the efficacy of the treatment when compared against untreated cells.

Second, 3D spheroid growth assays were utilised, which more accurately reflect the complex and heterogenous structure as well as the environment of the original tumour, including physiological tissue-like morphology and close cell – cell contacts. Spheroids constituted of layers of cells with different nutrient and oxygen supplies, that resulted in uneven drug penetration and therefore diverse response and resistance to the given treatment that better mimic the tumour behaviour, compared to 2D cultures where exponential proliferation is dominant (238). In this technique cells were left to form microscopic spheres approximately 200 µm in diameter, that grew in suspension and not attached in culture plastic, before treatment with the inhibitor alone or in combination with IR. Spheroid volume increase in response to a given treatment

compared against the volume increase in the untreated spheroids was determined using microscopy and image analysis, to investigate the inhibitors impact on cell growth but also on radiosensitisation of HNSCC 3D spheroids.

6.2 Impact of the DNA repair inhibitors as a monotherapy in 2D

Given the inhibitors affected the DDR in HNSCC cells in the absence of IR, as illustrated by some differences in the number of DNA repair foci observed in Chapter 5, the impact of the drug alone on cell survival was firstly assessed via colony formation assays. Comparison of cell survival was performed in 4 HNSCC cell lines, the HPV-negative UMSCC6 and UMSCC74A, and the HPV-positive UMSCC47 and UPCI-SCC090 in the presence of DSB repair inhibitors. Single cells were treated for 24 h with either of the drug or DMSO and left to grow colonies before been fixed and counted. It should be noted that due to cell dependent growth rate, different variables were introduced for each cell lines, including the number of cells seeded, the growing period, and the colony size. However, colony counting settings (using the GelCount colony counter) were optimised for each cell line and the same settings used across the various treatments for consistency. Plating efficiencies (PE), the ratio of the number of colonies over the number of cells seeded, were ~10 % for UMSCC6, UMSCC74A and UMSCC47 and ~2 % for UPCI-SCC090.

Analysis of cell survival, as illustrated in Figure 6.1, showed that ATMi (10 μ M) significantly reduced survival in 3 HNSCC cell lines, UMSCC6, UMSCC74A and UMSCC47, between 25 % to 45 % Interestingly, no difference was observed in the 4th cell line examined, UPCI-SCC090. Next, ATRi had the most detrimental effect on cell survival among the three drugs. Indeed, ATRi considerably reduced colony formation in all cell lines by 40% to 65 %. Finally, DNA-PKcsi significantly downregulated cell survival in only one cell line, the HPV-positive UMSCC47 by 60 %, while also reduced survival in the HPV-negative UMSCC6 by 23 %, although this result was not statistically significant ($p > 0.05$ as analysed by one sample t-test). Therefore, DNA-PKcsi as a monotherapy appears to be the least toxic inhibitor to HNSCC cell lines.

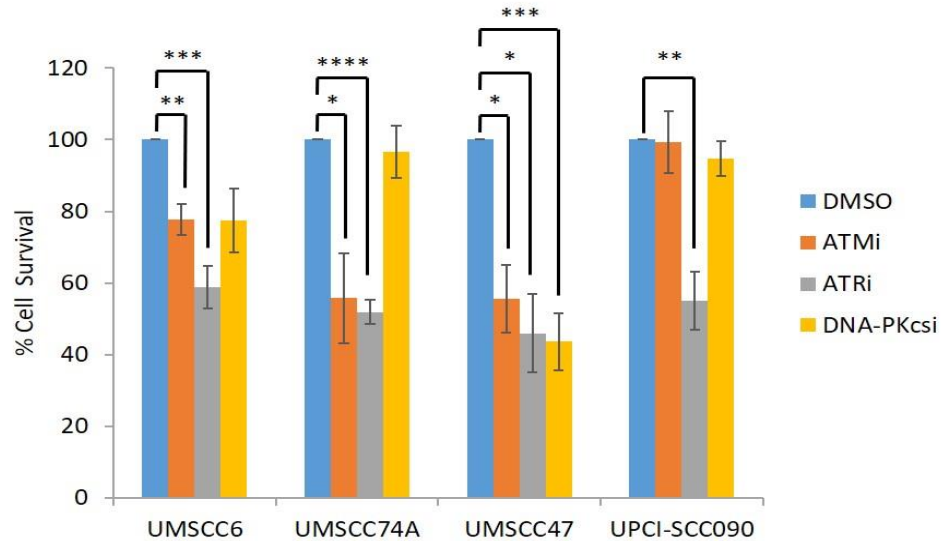


Figure 6. 1. Impact of DNA repair inhibitors on cell survival as a monotherapy. Clonogenic survival assays were utilised in 4 HNSCC cell lines. Cells were treated for 24 h with 10 μ M ATMi, 1 μ M ATRi, 1 μ M DNA-PKcsi or 10 μ M DMSO as controls. Survival was analysed from six biologically independent experiments and values were normalised against the DMSO treated control (blue bar) which was set to 100 %. * $p < 0.02$, ** $p < 0.01$, *** $p < 0.005$, **** $p < 0.0001$ as analysed by a one sample t-test.

6.3 Impact of IR on cell survival in 2D

It has been previously demonstrated that there is increased radiosensitivity of cells derived from HPV-positive HNSCC in comparison to HPV-negative HNSCC, which reproduces the effects observed following radiotherapy treatment of the respective tumours (168, 206, 207). Therefore, the comparative radiosensitivity between 4 HNSCC cell lines, HPV-negative UMSSC6 and UMSSC74A, and HPV-positive UMSSC47 and UPCI-SCC090, was investigated in response to increasing dose of x – ray and proton irradiation. Single cells were exposed to IR and left to grow in colonies before been fixed and counted.

6.3.1 Comparative radiosensitivity in response to x – rays.

Cells were exposed to 0 – 3 Gy x – rays, and survival was observed to be exponentially decreasing with increasing radiation dose. However, the intrinsic radiosensitivity of each cell line, related to their ability to efficiently repair their DNA damage and survive, resulted in varying surviving fractions (SF) (Figure 6.2). Indeed, the by clonogenic assays data reproduced the difference in radiosensitivity expected between the two HPV-positive and the two HPV-negative HNSCC cell lines, in response to x – ray irradiation.

Therefore, the HPV-positive UPCI-SCC090 cells were the most radiosensitive, exhibiting the lowest survival from 1 Gy x – rays, followed by the second HPV-positive cell line, UMSCC47, that exhibited reduced survival from 2 Gy compared to the two HPV-negative cell lines. Next in terms of radiosensitivity was the UMSCC74A cells, closely followed by UMSCC6.

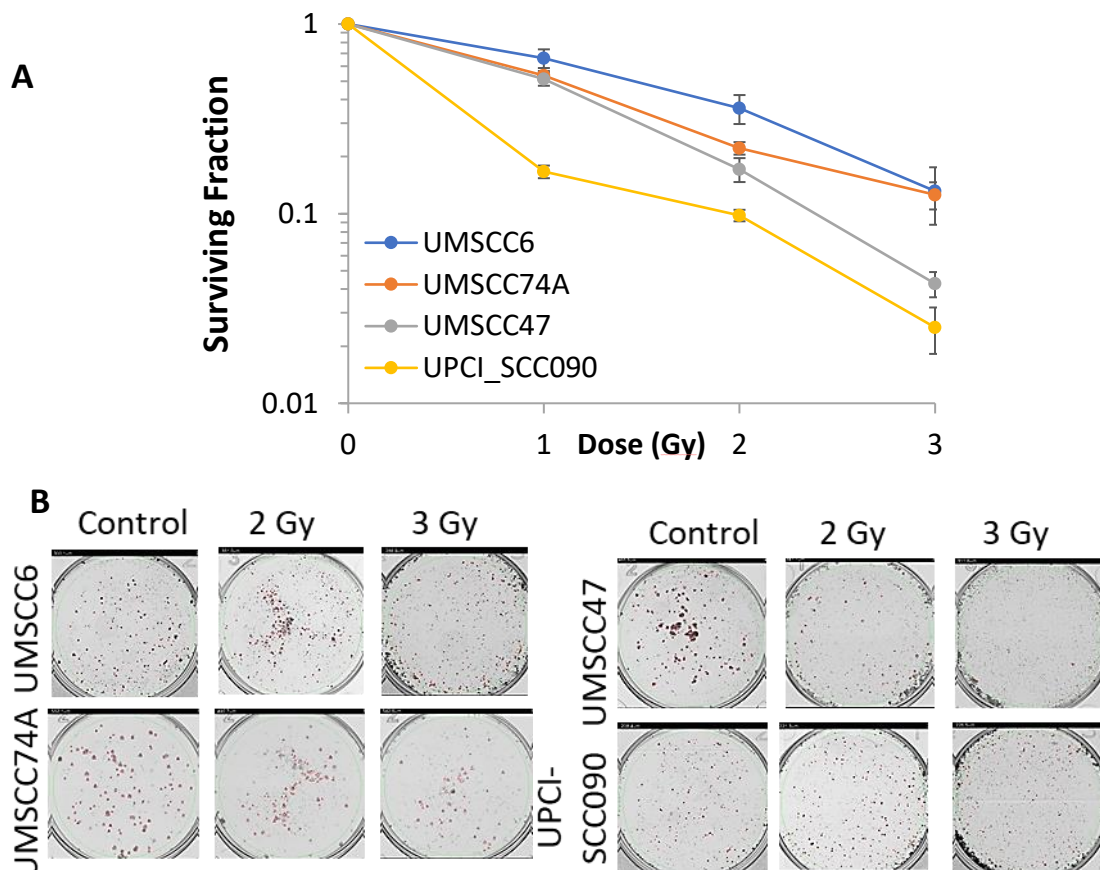


Figure 6.2. Impact of x – ray irradiation on cell survival. A. Clonogenic survival assays in response to increasing dose of x – ray irradiation in 4 HNSCC cell lines. Values were analysed from three biologically independent experiments and normalised against the 0 Gy of each cell line, which was set to 1. Statistical analysis using one sample t-test of SF rays reveals significant differences of: UMSCC6 vs UPCI-SCC090 $p < 0.002$ at 1 Gy, $p < 0.03$ at 2 Gy and $p < 0.004$ at 3 Gy x-rays. UMSCC74A vs UPCI-SCC090 $p < 0.00003$ at 1 Gy, $p < 0.005$ at 2 Gy and $p < 0.02$ at 3 Gy x-rays. UMSCC6 vs UMSCC47 $p < 0.01$ at 3 Gy x-rays. UMSCC74A vs UMSCC47 $p < 0.03$ at 3 Gy x-rays. B. Representative images of colony formation in cells treated with 0 Gy (control), 2 Gy and 3 Gy x – rays. The irradiated dishes contained 4x and 8x more cells, for 2 Gy and 3 Gy, to account for plating efficiencies.

6.3.2 Comparative radiosensitivity in response to protons.

Cells were exposed to 0 – 6 Gy protons, and in fact these exhibited a very similar trend to x – rays irradiations. Survival was exponentially decreasing with increasing radiation

dose, confirming that intrinsic radiosensitivity related to ability to repair proton induced DNA damage was proportional with radiation dose. This resulted in varying surviving fractions, shown in Figure 6.3, highlighting their individual radiosensitivity in response to protons.

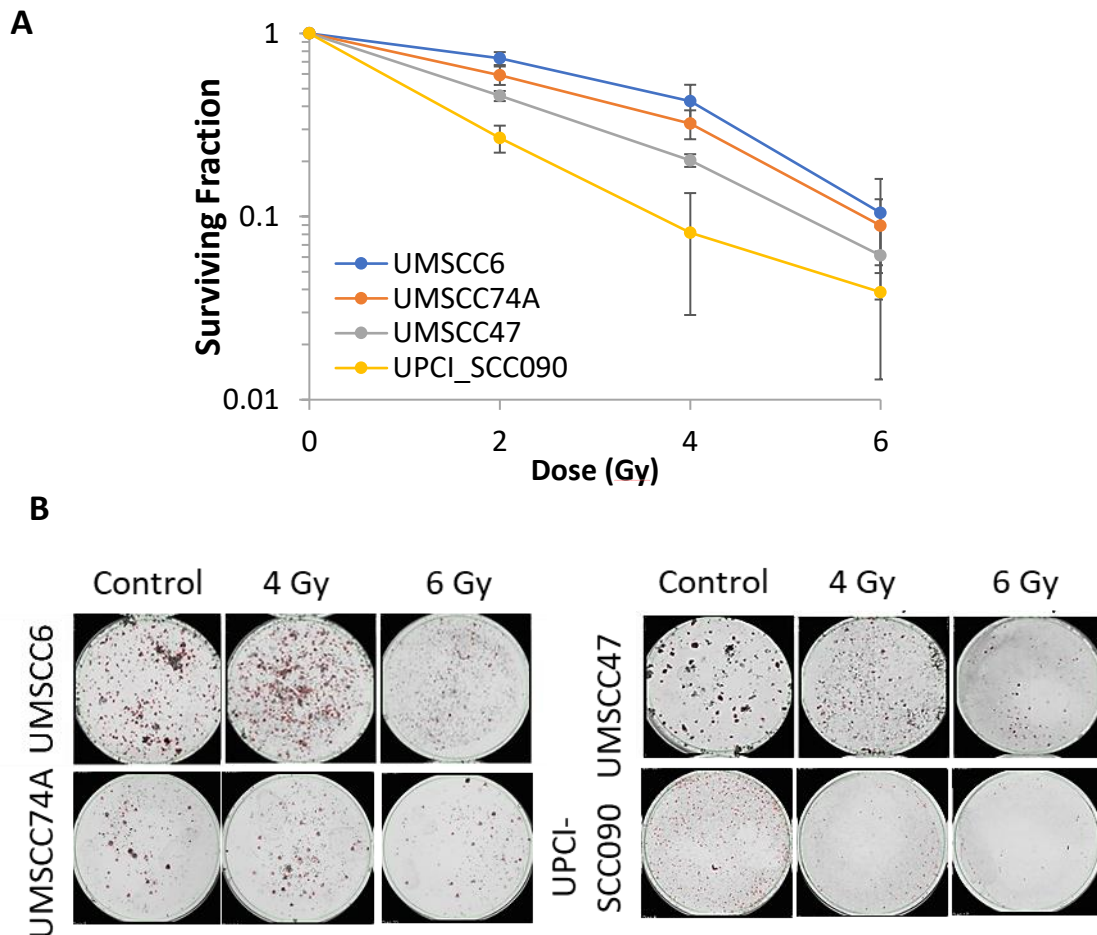


Figure 6.3. Impact of proton irradiation on cell survival. A. Clonogenic survival assays in response to increasing dose of proton irradiation in 4 HNSCC cell lines. Values were analysed from four biologically independent experiments and were normalised against the 0 Gy of each cell line, which was set to 1. Statistical analysis using one sample t-test of SF reveals significant differences of: UMSCC6 vs UPCI-SCC090 $p < 0.002$ at 2 Gy and $p < 0.04$ at 4 Gy protons. UMSCC6 vs UMSCC47 $p < 0.01$ at 2 Gy. UMSCC74A vs UPCI-SCC090 $p < 0.01$ at 2 Gy and $p < 0.04$ at 4 Gy protons. B. Representative images of colony formation in cells treated with 0 Gy (control), 2 Gy and 3 Gy x-rays. The irradiated dishes contained 4x and 8x more cells, for 4 Gy and 6 Gy respectively, to account for plating efficiencies.

The data reproduced the difference in radiosensitivity expected between the two HPV-positive and the two HPV-negative HNSCC cell lines, in response to proton irradiation by clonogenic assays. The HPV-positive UPCI-SCC090 cells were the most sensitive to

proton irradiation, exhibiting the lowest survival from 2 Gy protons, followed by the second HPV-positive cell line, UMSCC47, that exhibited reduced survival from 4 Gy, compared to the two HPV-negative cell lines. Next in radiosensitivity was the UMSCC74A cells, closely followed by UMSCC6. No major differences were observed in the relative response of cells the various inhibitors with protons compared to the response to x – rays. It is worth noting that cells were positioned in the entrance of the pristine beam of high energy – low LET protons where dosimetry was performed.

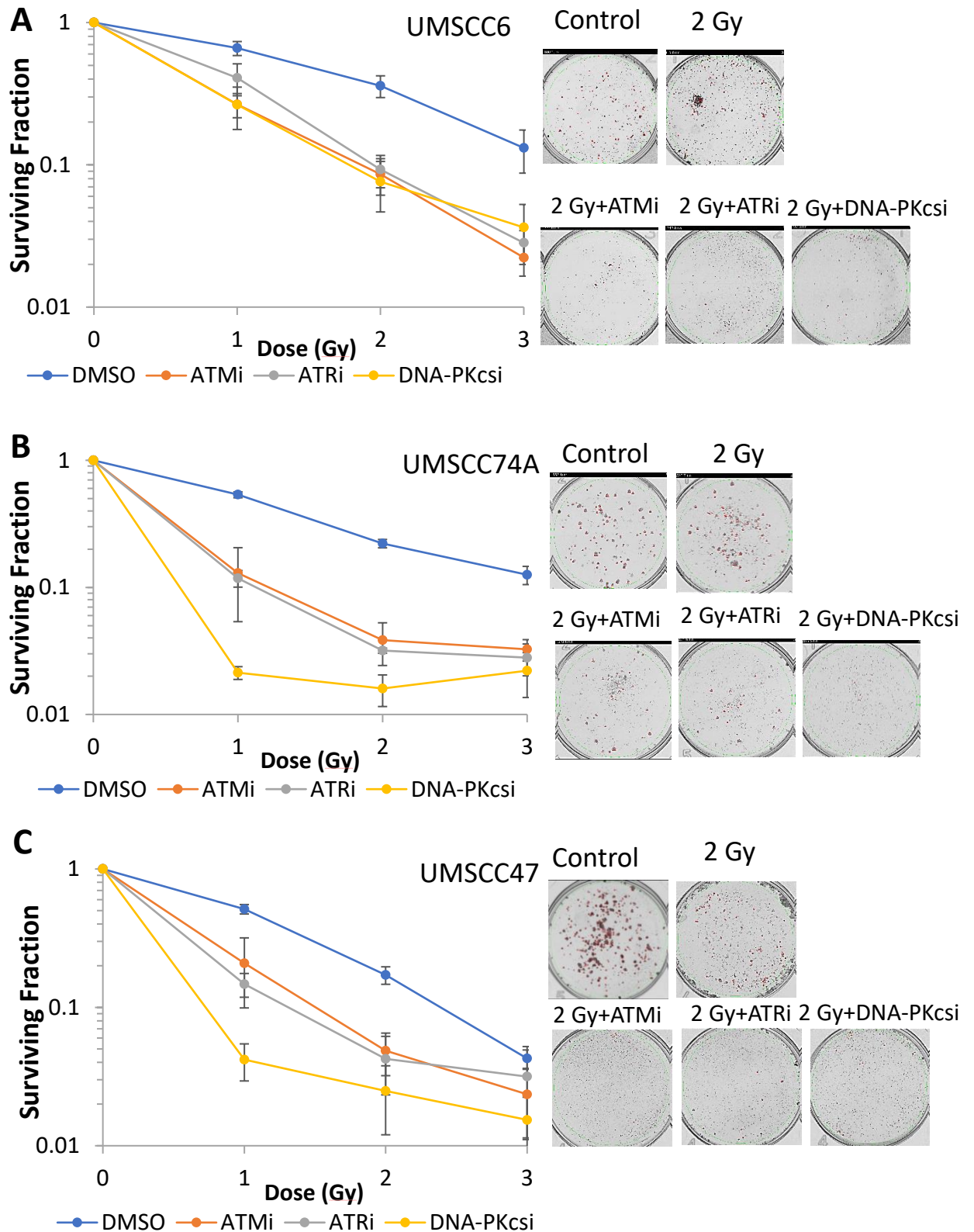
6.4 Impact of DNA repair inhibitors on 2D cell survival in combination with IR.

Cell survival was then studied via colony formation assays in 4 HNSCC cell lines, UMSCC6, UMSSC74A, UMSCC47 and UPCI-SCC090, following combination treatment of DNA repair inhibitors and IR. Their variable endogenous radiosensitivity, provided the opportunity to study the impact of the drugs in cells with different DDR capabilities, that were more representative of the HNSCC group. Cells were pre-treated with 10 μ M ATMi, 1 μ M ATRi, 1 μ M DNA-PKcsi or 10 μ M DMSO for 1 h before and for 24 h after exposure to increasing doses of x – ray or proton irradiation. Cell were then left to grow in colonies, fixed and counted.

6.4.1 X- rays

Firstly, survival and proliferation were examined in HNSCC cells treated with ATMi, ATRi, or DNA-PKcsi following exposure to x – rays. As seen in Figure 6.4, the three DSB repair inhibitors had a dramatic impact on reducing cell survival in UMSCC6, UMSCC74A and UMSCC47, even from the lowest radiation dose of 1 Gy, compared to the survival observed in DMSO treated cells. Survival was further reduced following 2 Gy of radiation in all cell lines, where p values of two sample t-test were from <0.04 to <0.001 (Table 6.1). The difference was limited following 3 Gy irradiation particularly in the radio sensitive UMSCC47 cell line, due to the effect of radiation alone (Figure 6.4 C), but also a tailing was observed in UMSCC74A and UMSCC47 in the inhibitor treated cells as colony formation was already extremely low. In the most radiosensitive cell line, UPCI-SCC090, two of the drugs, ATMi and DNA-PKcsi, significantly reduced survival, particularly following 2 Gy x – rays (Figure 6.4 D). However, ATRi was not suppressing

colony formation in these cells compared to DMSO. Interestingly, whilst ATRi was the most effective drug as a monotherapy, in all cell lines, but these findings indicated that it did not further radiosensitise this, already sensitive, HPV-positive cell line.



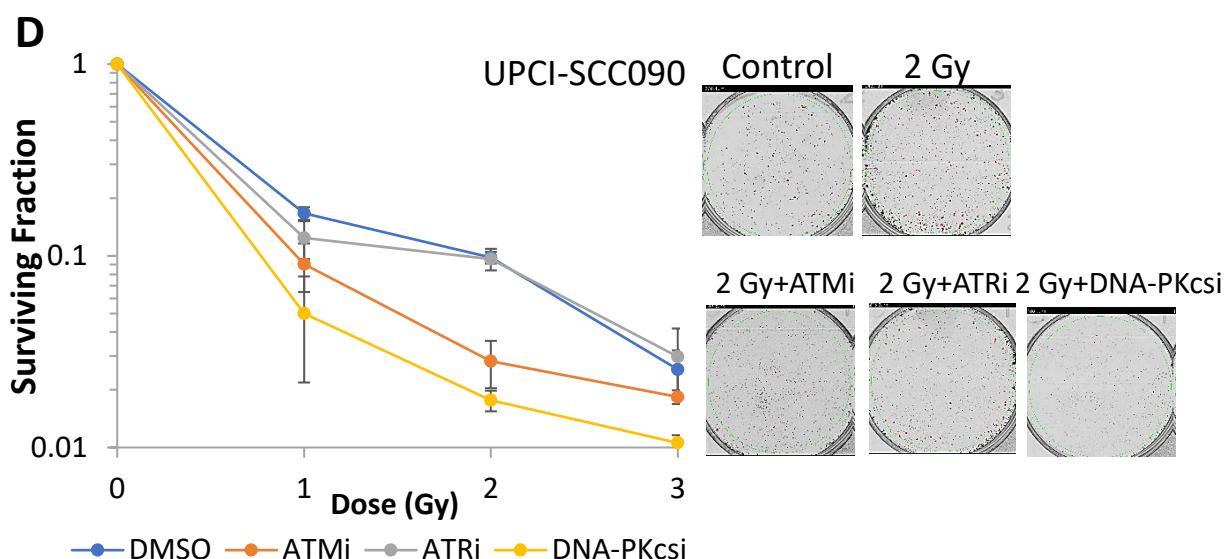


Figure 6. 4. Impact of DSB inhibitors in combination with x – rays on cell survival. Comparative surviving fraction were analysed following treatment with increasing dose of x – rays in 4 HNSCC cell lines, from three biologically independent experiments and are presented along with representative images A. UMSCC6; B. UMSCC74A; C. UMSCC47; D. UPCI-SCC090. Cells were treated with 10 μ M ATMi, 1 μ M ATRi, 1 μ M DNA-PKcsi or 10 μ M DMSO for 1 h before and for 24 h after irradiation with 0 – 3 Gy x – rays. The irradiated dishes contained 2x 4x and 8x times more cells, to account for PE with increasing radiation dose. Values were normalised against the 0 Gy of each treatment, which was set to 1. Statistical analysis using a two sample t-test of surviving fractions at a 2 Gy dose of x – rays revealed significant differences between DMSO and each drug summarised in Table 6.1.

Table 6. 1. Inhibition of ATM, ATR and DNA-PKcs decreases HNSCC cell survival in response to x - rays irradiation

| Inhibitor | UMSCC6 | UMSCC74A | UMSCC47 | UPCI-SCC090 |
|-----------|--------|----------|---------|-------------|
| ATM | p<0.03 | p<0.003 | p<0.03 | p<0.02 |
| ATR | p<0.04 | p<0.001 | p<0.03 | p=0.06 |
| DNA-Pkcs | p<0.03 | p<0.001 | p<0.02 | p<0.003 |

Statistical analysis performed using a two sample t-test of surviving fractions at 2 Gy dose of x-rays

Dose enhancement ratios (DER) were calculated, to describe the comparative radiation dose required to achieve a certain biological damage in DMSO treated cells, versus drug treated cells. The values summarised in Table 6.2, were calculated at D₅₀, the dose required for 50 % reduction in survival. Higher values were exhibited in HPV-negative HNSCC cell lines, UMSCC6 and UMSCC74A, with DER varying between 1.91 and 2.39, in comparison with the HPV-positive HNSCC cell lines, UMSCC47 (1.38 – 1.69) and UPCI-

SCC090 (1.02 – 1.36). This indicates that radiosensitisation was more effective in the HPV-negative HNSCC cell lines, which are relatively radioresistant compared to their HPV-positive counterparts.

Among the three inhibitors, DNA-PKcsi appeared to be the most prominent in cell killing in response to x – rays, reducing the radiation dose required by 2.39- fold in UMSCC74A, 1.93- fold in UMSCC6, 1.69- fold in UMSCC47 and 1.36- fold to UPCI-SCC090. Given the role of DNA-PKcsi in NHEJ repair, these findings demonstrated the predominant role of NHEJ repair in response to DSBs induced by x – ray irradiation, irrespective of the HPV status. ATMi and ATRi resulted in comparable DERs, reducing the radiation dose required for 50 % survival in DMSO treated cells by approximately 2- fold, in the HPV-negative cells, by 1.37 fold in UMSCC47, but had minimal impact in UPCI-SCC090. This suggested that ATM and ATR might already have a relatively reduced role in regulating DSB repair in HPV-positive cell lines resulting in their increased radiosensitivity, and thus the drug could not further enhance this response.

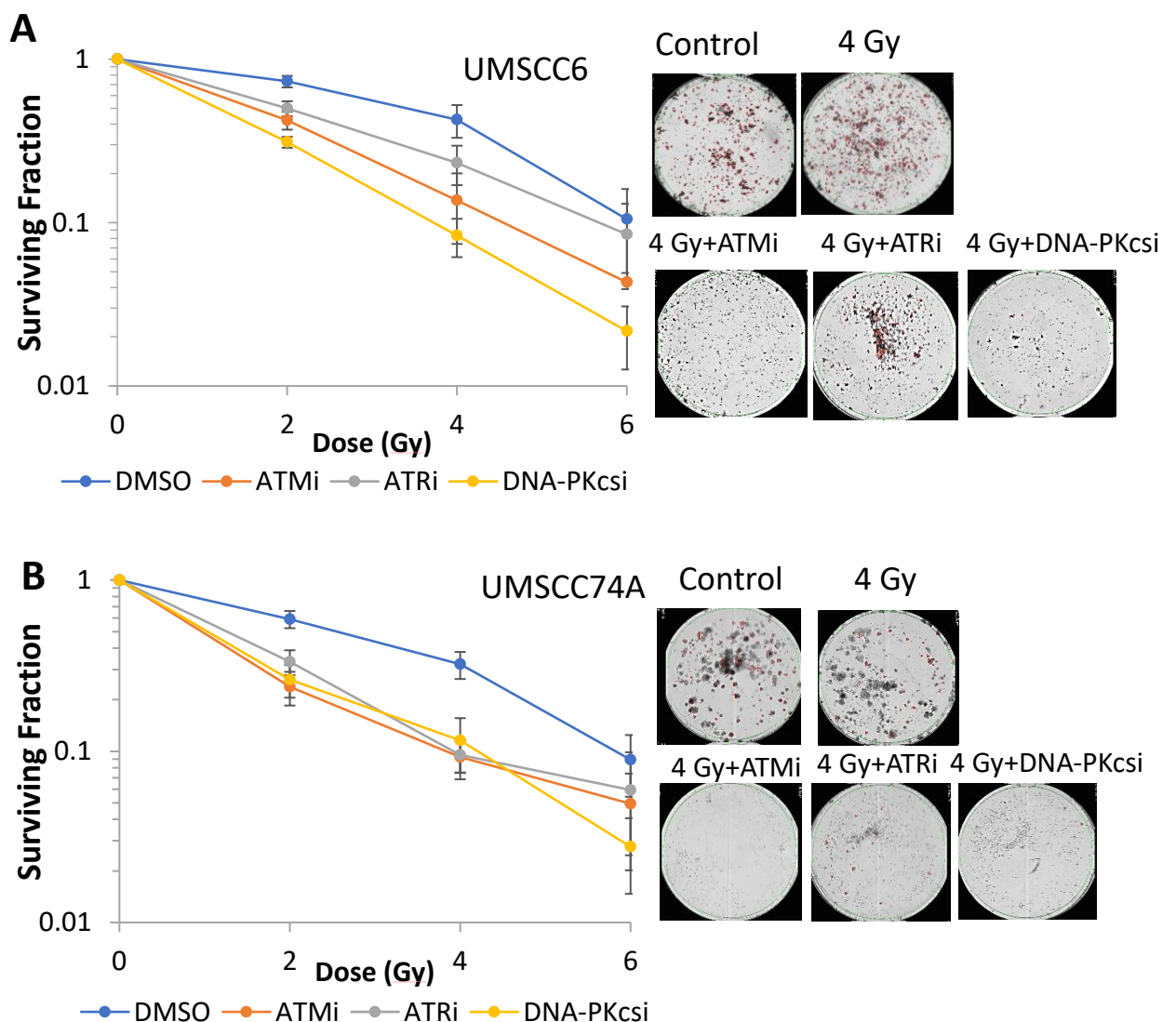
Table 6. 2. Dose enhancement ratios calculated at 50 % cell survival (DER) following ATM, ATR and DNA-PKcs inhibition versus DMSO controls in HNSCC cells in response to x- rays.

| Inhibitor | UMSCC6 | UMSCC74A | UMSCC47 | UPCI-SCC090 |
|------------------|---------------|-----------------|----------------|--------------------|
| ATMi | 2.06 | 1.91 | 1.38 | 1.15 |
| ATRi | 1.91 | 2.01 | 1.36 | 1.02 |
| DNA-PKcsi | 1.93 | 2.39 | 1.69 | 1.36 |

6.4.2 Protons

Similarly, survival and proliferation of HNSCC cells in response to proton irradiation, was examined in ATMi, ATRi, or DNA-PKcsi treated cells, and compared against DMSO treated cells. Irradiation of up to 6 Gy low LET protons (at entrance dose) was utilised, in order to obtain equivalent response to x – rays induced DNA damage. The DSB repair inhibitors considerably reduced cell survival in response to protons, but radiosensitised each of the four HNSCC cell lines to a different extent, as illustrated in Figure 6.5. The drugs, particularly ATMi and DNA-PKcsi, reduced cell survival from 2 Gy of radiation in all cell lines. Then the survival was further reduced at 4 Gy, where two sample t-test p values indicated significance in three of the four cell lines, UMSCC6, UMSCC74A and

UMSCC47, varying between <0.05 and <0.0004 , summarised in Table 6.3, except for ATRi in UMSCC6 cells which was not significant ($p = 0.2$). However, the difference in survival between DMSO and inhibitor treated cells did not change much at 6 Gy, due to significant cell killing by proton irradiation alone, which was observed in all cell lines. In UPCI-SCC090 cells, although all inhibitors appeared to radiosensitise the cells compared to DMSO, the results were not statistically significant with p values ≥ 0.4 (Table 6.3). This showed, again, that these cells are the most radiosensitive of all those tested. Again, some tailing was observed at the higher proton doses, particularly in UMSCC74A and UPCI-SCC090 cells possibly due to the very low number of the remaining viable colonies.



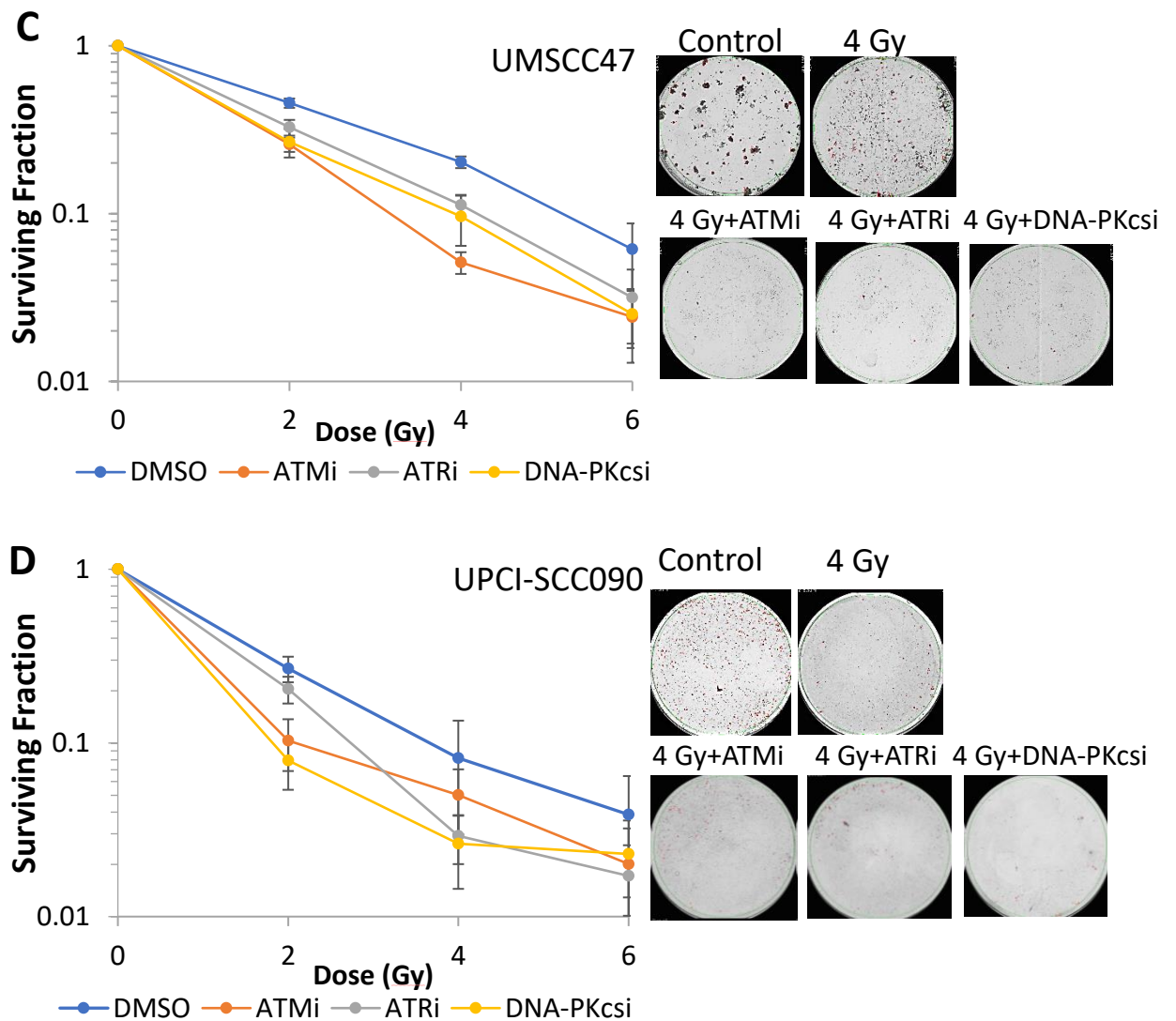


Figure 6.5. Impact of DSB inhibitors in combination with protons on cell survival. Comparative surviving fraction were analysed following treatment with increasing dose of protons in 4 HNSCC cell lines, from four biologically independent experiments and are presented along with representative images A. UMSCC6; B. UMSCC74A; C. UMSCC47; D. UPCI-SCC090. Cells were treated with 10 μ M ATMi, 1 μ M ATRi, 1 μ M DNA-PKcsi or 10 μ M DMSO for 1 h before and for 24 h after irradiation with 0 – 6 Gy protons. The irradiated dishes contained 2x 4x and 8x times more cells, to account for PE with increasing radiation dose. Values were normalised against the 0 Gy of each treatment, which was set to 1. Statistical analysis using a two-sample t-test of surviving fractions at a 4 Gy dose of protons revealed significant differences between DMSO and each drug summarised in Table 6.3.

Table 6. 3. Inhibition of ATM, ATR and DNA-PKcs decreases HNSCC cell survival in response to proton irradiation.

| Inhibitor | UMSCC6 | UMSCC74A | UMSCC47 | UPCI-SCC090 |
|------------------|---------------|-----------------|----------------|--------------------|
| ATM | p<0.05 | p<0.02 | p<0.0004 | p=0.6 |
| ATR | p=0.2 | p<0.02 | p<0.02 | p=0.4 |
| DNA-PKcs | p<0.03 | p<0.05 | p<0.05 | p=0.4 |

Statistical analysis performed using a two sample t-test of surviving fractions at 4 Gy dose of protons.

Dose enhancement ratios were calculated in response to protons at the D_{50} , the dose required for 50 % reduction in survival in DMSO versus inhibitor treated cells, and are summarised in Table 6.4. Cumulatively, DER values were reduced in response to protons, demonstrating relatively lower impact of the drug in combination with protons in comparison to photons possibly due to the smaller difference between the numerator and denominator of the ratio following protons. Similarly to x – rays, HPV-negative HNSCC cell lines, UMSCC6 and UMSCC74A, exhibited higher DERs than HPV-positive cells, UMSCC47 and UPCI-SCC090, yet the difference was not as dramatic following protons. This was due to increased cell killing by proton irradiation alone compared to x – rays.

Comparing the three inhibitors, DNA-PKcsi was the most effective in downregulating cell survival in response to protons, in all cell lines expect UMSCC47, where it was similar to the impact of ATMi. The DERs that expressed the radiation dose required for 50 % survival in DNA-PKcsi treated cell was lower than that required in DMSO treated cells by 2.01- fold in UMSCC6, 1.64- fold in UMSCC74, 1.38- fold in UMSCC47 and 1.32- fold in UPCI-SCC090. Next in effectiveness of increasing radiosensitivity was ATMi, where DERs were between 1.62 to 1.25. Interestingly, ATRi was the least effective of the three inhibitors, with DERs revealing radiation dose reduction by 1.42- to 1.25- fold in ATRi compared to DMSO treated cells. These findings, nevertheless, demonstrated that DNA-PKcsi was the most prominent inhibitor in combination with protons, as was in combination with x – rays, indicating that NHEJ repair is the predominant mechanism for the repair of x – ray as well as low LET proton induced DNA damage.

Table 6. 4. Dose enhancement ratios calculated at 50 % cell survival (DER) following ATM, ATR and DNA-Pkcs inhibition versus DMSO controls in HNSCC cells in response to protons.

| Inhibitor | UMSCC6 | UMSCC74A | UMSCC47 | UPCI-SCC090 |
|------------------|---------------|-----------------|----------------|--------------------|
| ATM | 1.62 | 1.52 | 1.49 | 1.24 |
| ATR | 1.25 | 1.42 | 1.28 | 1.30 |
| DNA-Pkcs | 2.01 | 1.64 | 1.38 | 1.32 |

6.5 3D spheroid growth in HNSCC cell lines

Growth of 3D spheroids, which better mimic the conditions and environment of the original tumour growth, were then analysed in HNSCC cell lines. Two HPV-negative, UMSCC6 and UMSCC74A, and two HPV-positive, UMSCC47 and UPCI-SCC090, HNSCC cell lines, originating from the oropharynx area, were utilised. Cells were left two days post seeding to form spheroids of ~200 µm in diameter and their growth was monitored for 15 days. At first, normal spheroid growth was monitored in response to IR without any inhibitor treatment, and representative images are shown in Figure 6.6. Unfortunately, the HPV-positive UMSCC47 cells, although forming nice symmetrical spheroids, these did not grow over the two-week monitoring period. There was also no impact in response to x – ray or proton irradiation. Therefore, an additional HPV-positive HNSCC cell line, also originating from the oropharynx area, was introduced, UPCI-SCC154, although spheroids derived from these cells also did not grow majorly over the monitoring period neither the controls nor the irradiated spheroids (Figures 6.7 D and 6.8 D).

In the other 3 HNSCC lines, spheroid growth was inversely proportional to radiation dose, as seen in Figures 6.7 (x – rays) and 6.8 (protons). Specifically, UMSCC74A control spheroids exhibited a 7- fold increase in growth that peaked between Day 8 – 10, before been reduced by Day 15. X – ray irradiation mildly suppressed spheroid growth at 1 Gy, although this was more important following higher dose, 2-3 Gy (Figure 6.7 A). Following

proton irradiation, spheroid growth was also suppressed from 2 Gy but higher doses of 4-6 Gy almost diminished spheroid development (Figure 6.8 A). UMSCC6 control spheroids grew into nice symmetric spheres, their volume increased by 5- to 6- fold, between Day 8 – 12 and then dropped. However, exposure to IR, x – rays or protons, reduced the spheroid growth as well as impacted on their shape, resulting in fuzzy edges and loss of integrity (Figure 6.6), particularly later in the monitoring period, indicating increased cell death. Spheroid growth was inversely proportional to the x – ray radiation dose (Figure 6.7 B) yet was severely decreased following proton doses of 4 – 6 Gy (Figure 6.8 B). A comparative delay in growth was observed in UPCI-SCC090 control spheroids, that gradually increased from Day 5 – 12 and peaked at Day 15, exhibiting an 8- fold volume increase in the absence of IR. Exposure to IR had a detrimental effect on spheroid growth from the lowest radiation dose of 1 Gy x – rays (Figure 6.7 C) or 2 Gy protons (Figure 6.8 C), highlighting the enhanced radiosensitivity of this cell line. Overall, in HPV-negative cell lines, a higher radiation dose (2 Gy x – rays, 4 Gy protons) was required to achieve growth suppression similar to that observed in the HPV-positive cell line in response to 1 Gy x – rays or 2 Gy protons, highlighting their increased endogenous radioresistance. Further increase in radiation dose, up to 3 Gy x – rays or 6 Gy protons, did not further reduce spheroid growth in all cell lines irrespective of the HPV status.

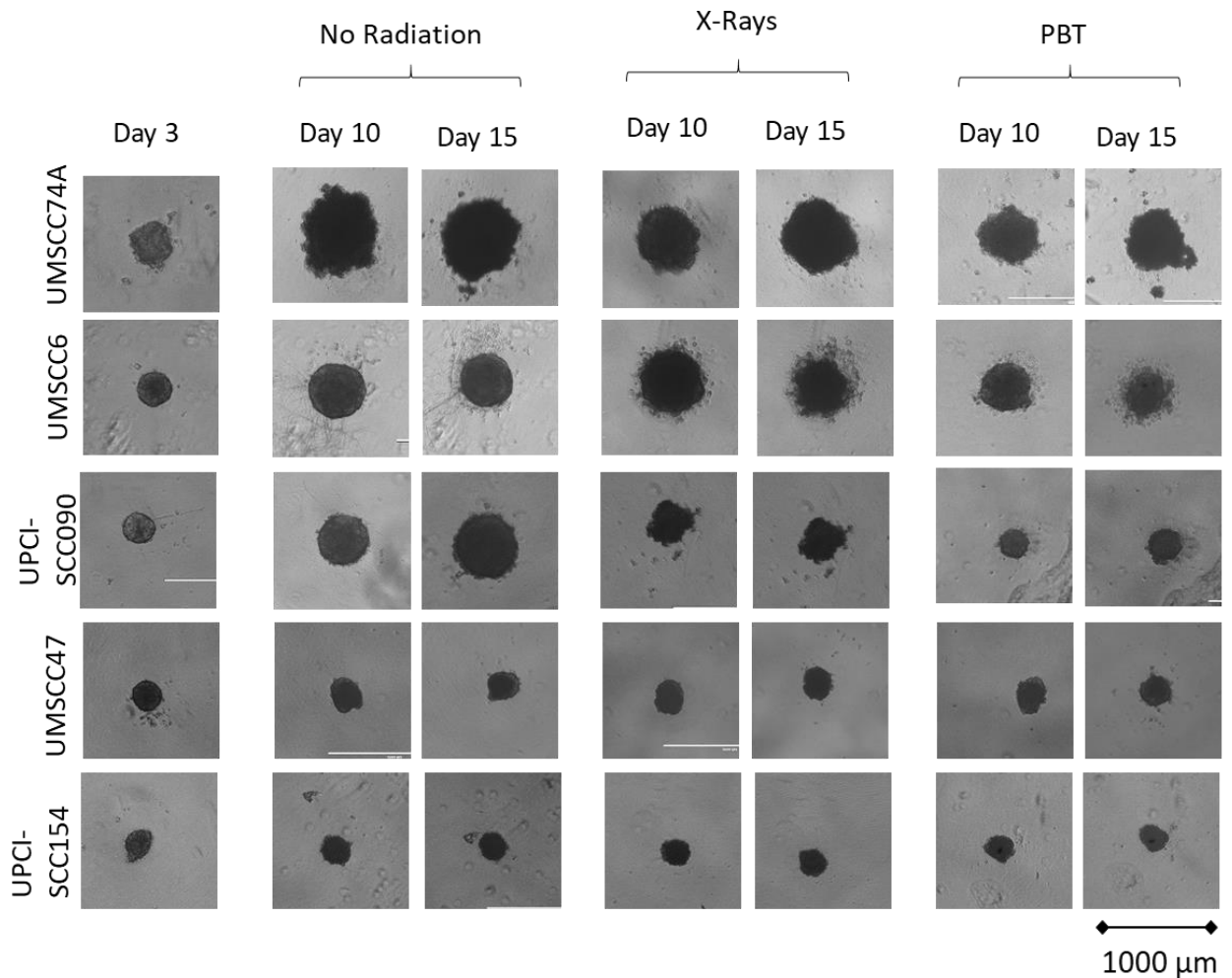


Figure 6. 6. 3D spheroid formation and growth in HNSCC cell lines. Spheroid growth was monitored for 15 days post seeding in 5 HNSCC cell lines, 2 HPV-negative, UMSCC74A and UMSCC6, and 3 HPV-positive, UPCI-SCC090, UMSCC47, and UPCI-SCC154. On Day 3, spheroids were exposed to 1 - 3 Gy x – rays, 2 - 6 Gy protons while controls were not irradiated. Here are displayed representative images of non irradiated, 1 Gy x – ray and 2 Gy proton irradiated spheroids on Day 3, 10 and 15 post seeding.

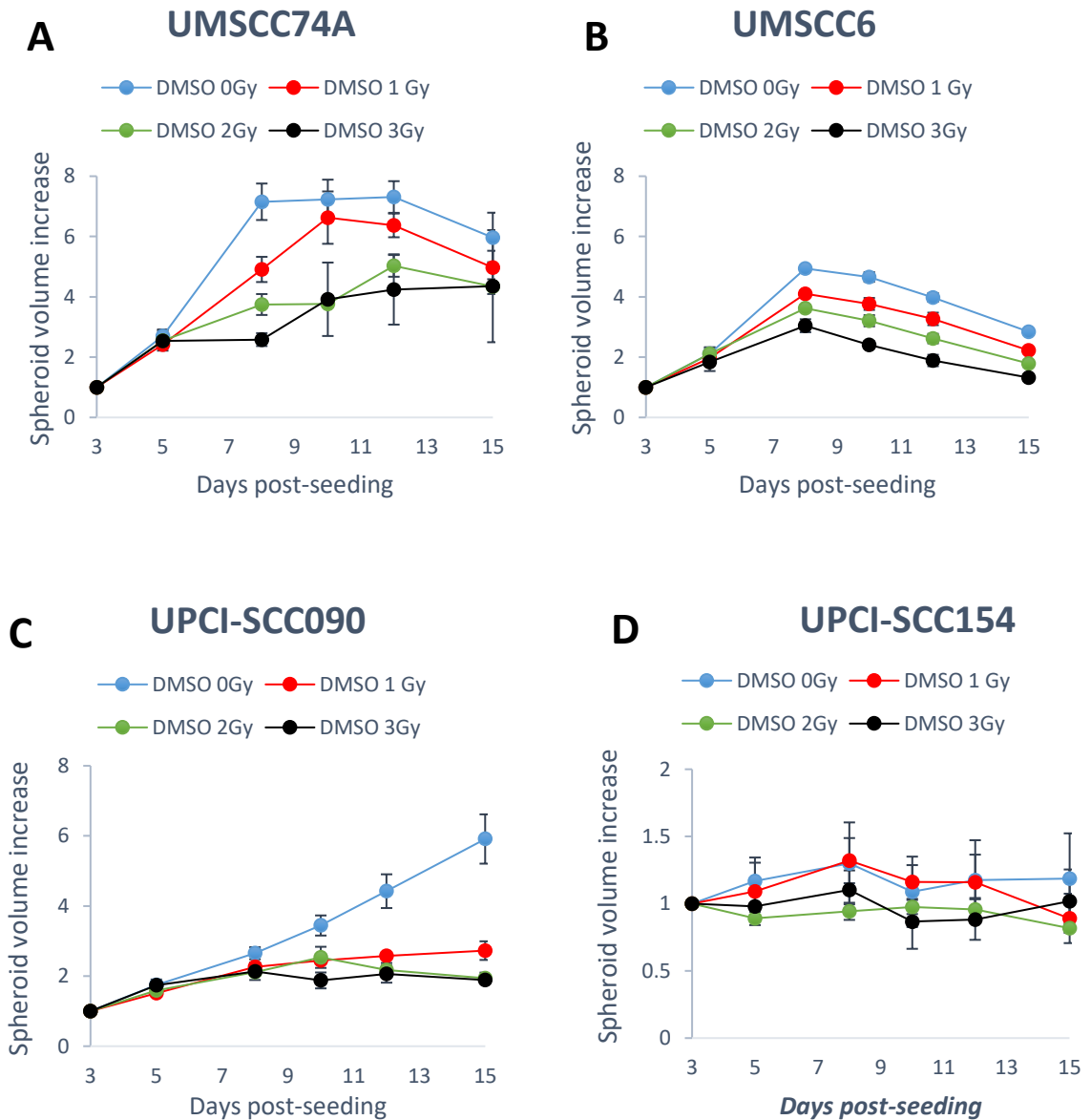


Figure 6.7. 3D spheroid growth following x – ray irradiation in HNSCC cell lines. Spheroid growth was monitored for 15 days post seeding in HPV-negative UMSCC74A (A) and UMSCC6 (B) and HPV-positive UPCI-SCC090 (C), and UPCI-SCC154 (D) HNSCC spheroids. On Day 3, spheroids were exposed to 0 - 3 Gy x – rays. Values were analysed from three biologically independent experiments and normalised to Day 3 post seeding for each condition that was set to 1, and are presented with their standard errors.

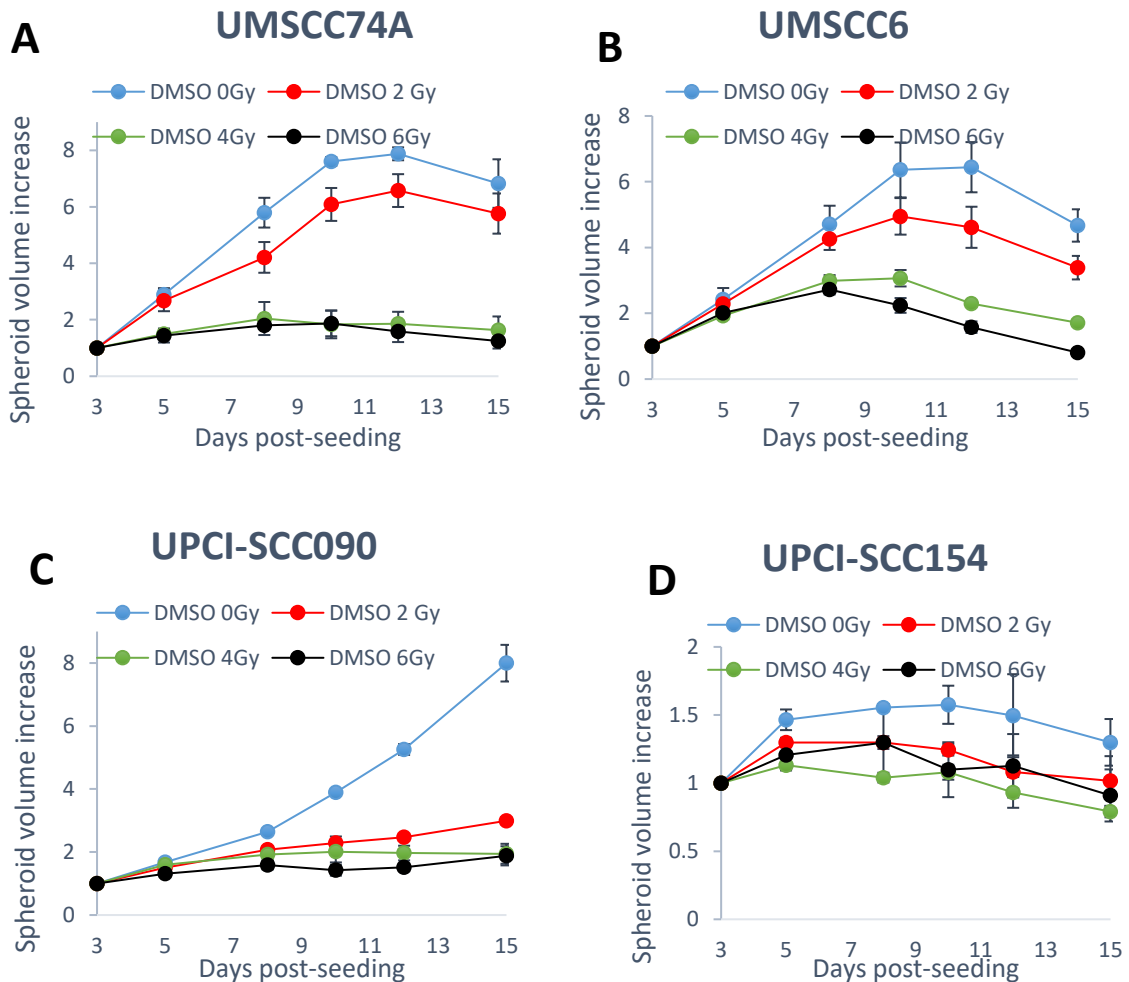


Figure 6. 8. 3D spheroid growth following proton irradiation in HNSCC cell lines. Spheroid growth was monitored for 15 days post seeding in HPV-negative, UMSCC74A (A) and UMSCC6 (B), and HPV-positive UPCI-SCC090 (C) and UPCI-SCC154 (D) HNSCC spheroids. On Day 3, spheroids were exposed to 0 - 6 Gy protons. Values were analysed from three biologically independent experiments, were normalised to Day 3 post seeding for each condition that was set to 1, and are presented with their standard errors.

Two additional HPV-negative HNSCC cell lines, FaDu and A253 originating from the hypopharynx and oral cavity respectively, were introduced, to broaden the radioresistant model. These radioresistant cells grew into spheroids, that were 50- fold (FaDu) and 20- fold (A253) bigger 15 days post seeding in the absence of IR or inhibitor treatment, and representative images are shown in Figure 6.9. Exposure to 1 Gy x – ray irradiation only partly suppressed growth in A253 spheroids, yet higher radiation dose, 2 – 3 Gy sufficiently suppressed growth, Figure 6.10 A. Similarly, low dose of protons (2 Gy) reduced A253 spheroid growth but it was only after 4 – 6 Gy that this was diminished (Figure 6.10 C). In contrast, FaDu spheroids, even though suppressed by IR, they grew

even after exposure to 3 Gy x – rays, and 4 Gy protons, Figure 6.10 B, D. The growth was only sufficiently suppressed following 6 Gy protons (Figure 6.10 D), highlighting the extreme tolerance of this cell line to IR, and particularly x – rays.

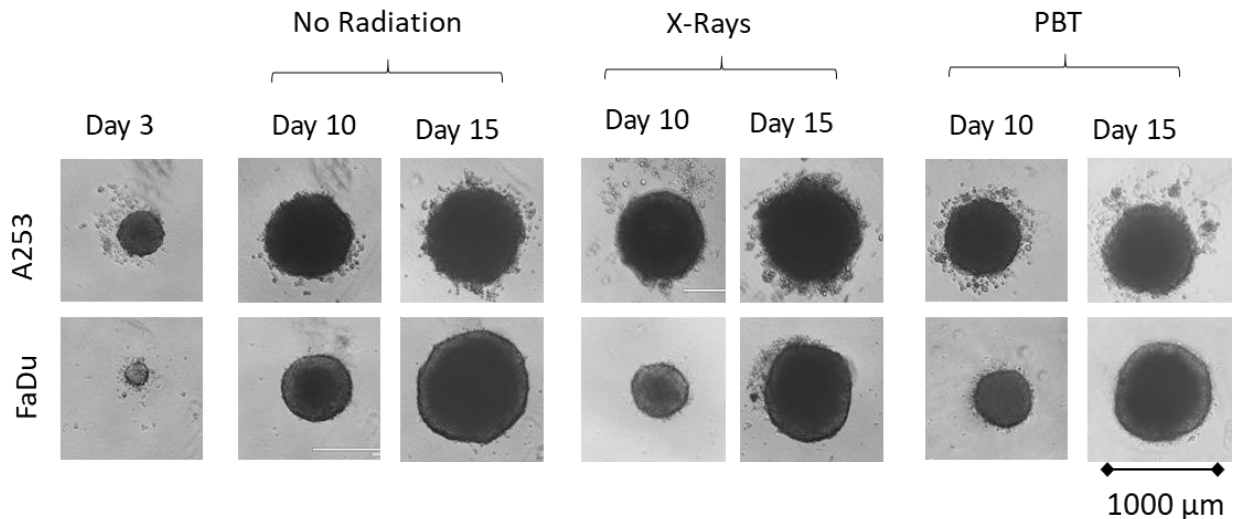
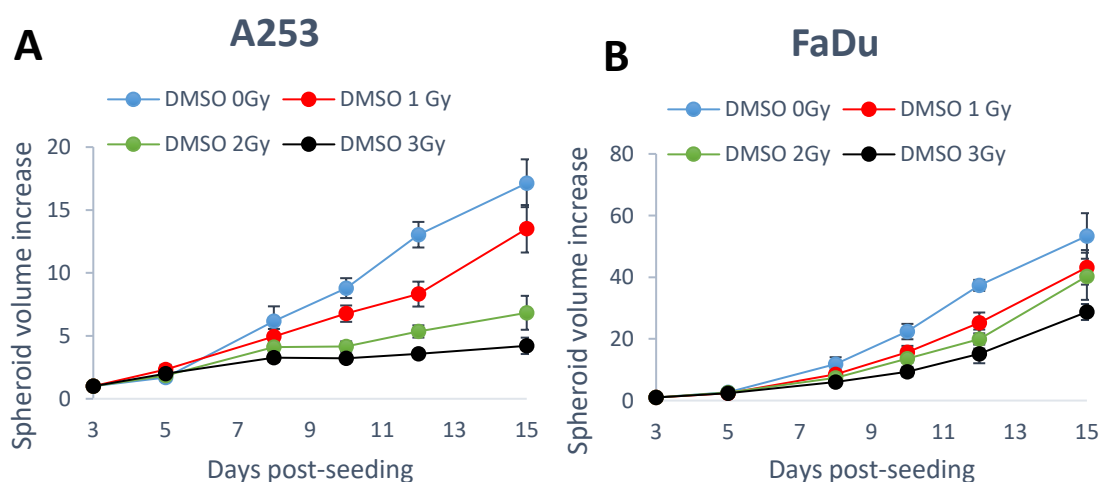


Figure 6. 9. 3D spheroid formation and growth in HNSCC cell lines. Spheroid growth was monitored for 15 days post seeding in 2 HPV-negative HNSCC cell lines, FaDu and A253. On Day 3, spheroids were exposed to 1 - 3 Gy x – ray irradiation or 1 - 6 Gy proton irradiation while controls were left unirradiated. Here are displayed representative images of non irradiated, 1 Gy x – ray and 2 Gy proton irradiated spheroids on Day 3, 10 and 15 post seeding.



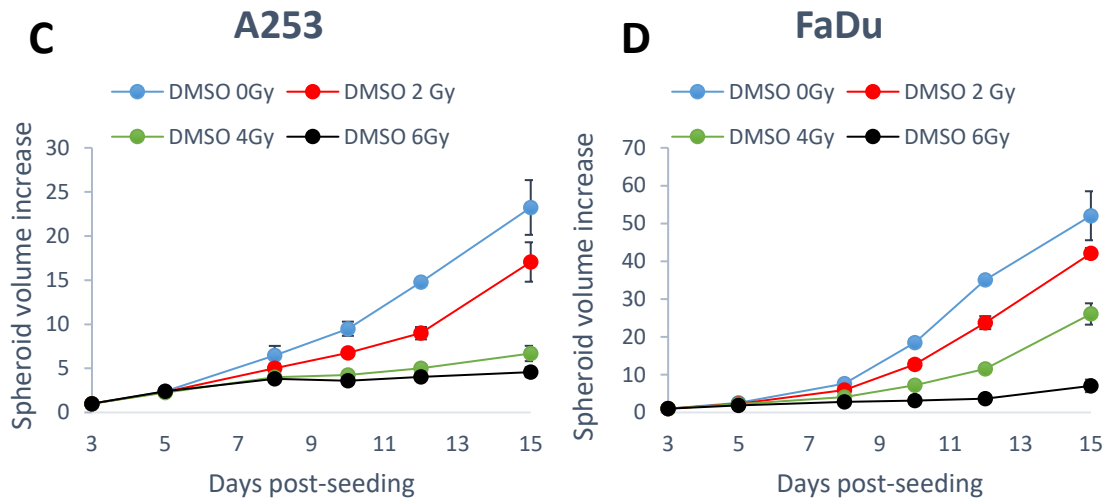


Figure 6. 10. 3D spheroid growth following x - rays or protons irradiation in HNSCC cells. Spheroid growth was monitored for 15 days post seeding in 2 HPV-negative HNSCC cell lines, FaDu and A253. On Day 3, spheroids were exposed to A - B) 0 - 3 Gy x- rays and C - D) 0 - 6 Gy protons. Values were analysed from three biologically independent experiments and normalised to Day 3 post seeding for each condition that was set to 1, and are presented with their standard errors.

6.6 Impact of DNA repair inhibition on non irradiated 3D spheroid growth in HNSCC.

The impact of three DSB repair inhibitors ATMi, ATRi and DNA-PKcsi on spheroid growth in HNSCC in the absence of IR, either x – rays or protons, was investigated both in HPV-negative and HPV-positive cell lines, as a model that better represented in vivo tumour growth. Cells were left to form spheroids and on Day 3 post seeding these were treated with 10µM ATMi, 1 µM ATRi, 1 µM DNA-PKcsi or 10 µM DMSO for 24 h. Spheroid growth was then monitored for an extra 12-day period, equalling a 15-day growth period overall. Growth suppression ratio (GSR), a ratio that describes the volume of DMSO treated over the volume of drug treated spheroids across the 15- day monitoring period were utilised to compare the relative growth suppression by the inhibitors alone. Six HNSCC cell lines were utilised, the HPV-negative UMSCC74A, UMSCC6, A253 and FaDu cell lines, and the HPV-positive UPCI-SCC090 and UPCI-SCC154 cell lines (Figure 6.11). Unfortunately, UPCI-SCC154 spheroids did not grow sufficiently over the two-week monitoring period and therefore no significant difference could be observed between inhibitor treated versus DMSO treated spheroids (Figure 6.11 F).

In the majority of the HNSCC cell lines examined, treatment with ATMi alone did not significantly affect spheroid growth, which were similar in size to the DMSO treated spheroids, (Figure 6.11 and Tables 6.5, 6.6). Yet, growth suppression was exhibited in two HPV-negative non-irradiated spheroids treated with ATMi. UMSCC74A spheroids exhibited an GSR of 1.58, meaning a 1.58- fold growth suppression introduced by the drug alone (Figure 6.11 A) and this was statistically significant with a p value < 0.0002. This suppression by ATMi alone was equivalent to 2 Gy of x – ray irradiation. In A253, a similar 1.63- fold suppression in spheroid growth was induced by ATMi (however this was not statistically significant, p=0.49). This was an indication of increased dependence on ATM driven repair of endogenous DSBs on these particular cell lines.

The impact of ATRi as a monotherapy was found to be the most important among the three DSB repair inhibitors where it was found to reduce spheroid growth in the 4 out of 6 cell lines examined in the absence of IR, Figure 6.11 and Tables 6.5 and 6.6, although this was statistically significant in 3 of them. ATRi suppressed growth on UMSCC74A and UMSCC6 spheroids, that exhibited GSRs 1.40 (p<0.003) and 1.50 (p<0.002) respectively (Figure 6.11 A, B). Moreover, ATRi inhibited the HPV-positive UPCI-SCC090 by 1.45 (p<0.006), Figure 6.11 E, and the HPV-negative A253 spheroid growth by 1.73- fold, although this was not statistically significant (Figure 6.11 D). The suppression by the drug alone was found to be equivalent or even greater than that induced by 1 Gy x – ray radiation. In contrast, growth of the radioresistant FaDu spheroids was not impaired by ATRi alone.

DNA-PKcsi was then examined as a monotherapy, in HNSCC spheroids. This was found to be the least effective in reducing spheroid growth in the absence of IR, compared to ATM and ATR inhibition. As illustrated in Figure 6.11, DNA-PKcsi alone did not impact growth on UMSCC74A, UMSCC6, FaDu and UPCI-SCC090 spheroids, in fact these HNSCC cell lines exhibited GSR values around 1 which indicates equivalent volume between DMSO versus DNA-PKcsi treated spheroids throughout the two week monitoring period. Nevertheless, DNA-PKcsi moderately reduced spheroid volume on A253 with a GSR of 1.35 yet this suppression was not statistically significant (Figure 6.11D and Tables 6.5, 6.6).

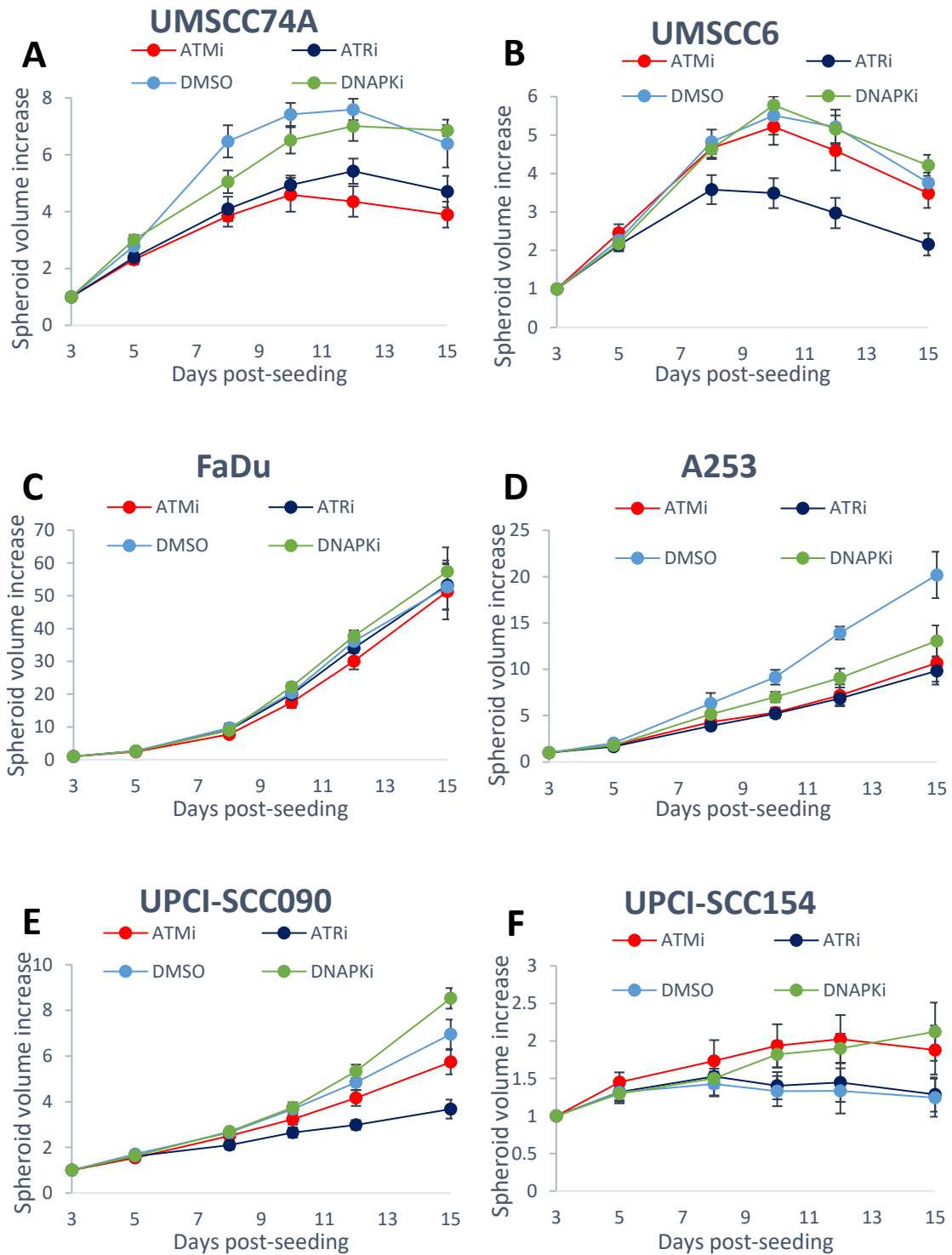


Figure 6. 11. 3D spheroid growth following DSB repair inhibition in HNSCC cells. Spheroid growth was monitored for 15 days post seeding in 4 HPV-negative HNSCC cell lines, UMSCC74A (A), UMSCC6 (B), FaDu (C) and A253 (D), and 2 HPV-positive cell lines UPCI-SCC090 (E) and UPCI-SCC154 (F). On Day 3, spheroids were treated with either of 10 μ M ATMi, 1 μ M ATRi, 1 μ M DNA-PKcsi or 10 μ M DMSO for 24 h. Values were analysed from six biologically independent experiments and normalised to Day 3 post seeding for each condition that was set to 1, and are presented with their standard errors.

Table 6. 5. Impact of targeting of DSB repair as a monotherapy on HNSCC spheroid growth.

| Cell line | ATMi | ATRi | DNA-PKcsi |
|------------------|-------------|-------------|------------------|
| UMSCC74A | p<0.0002 | p<0.003 | p=0.59 |
| UMSCC6 | p=0.60 | p<0.002 | p=0.89 |
| FaDu | p=0.69 | p=0.89 | p=0.82 |
| A253 | p=0.49 | p=0.72 | p=0.88 |
| UPCI-SCC090 | p=0.34 | p<0.006 | p=0.44 |
| UPCI-SCC154 | p=0.11 | p=0.72 | p=0.2 |

Statistical analysis was performed across the 15-day growth period using a one-way ANOVA, comparing the growth of inhibitor treated spheroids against the appropriate DMSO control.

Table 6. 6. Growth suppression ratio (GSR) calculated over the 15-day growth period following ATMi, ATRi or DNA-PKcsi alone. GSR=DMSO spheroid volume/ ATMi spheroid volume for each condition.

| Cell line | ATMi | ATRi | DNA-PKcsi |
|------------------|-------------|-------------|------------------|
| UMSCC74A | 1.58 | 1.40 | 1.07 |
| UMSCC6 | 1.04 | 1.50 | 0.99 |
| FaDu | 1.15 | 1.03 | 0.98 |
| A253 | 1.63 | 1.74 | 1.35 |
| UPCI-SCC090 | 1.14 | 1.45 | 0.95 |
| UPCI-SCC154 | 0.79 | 0.98 | 0.84 |

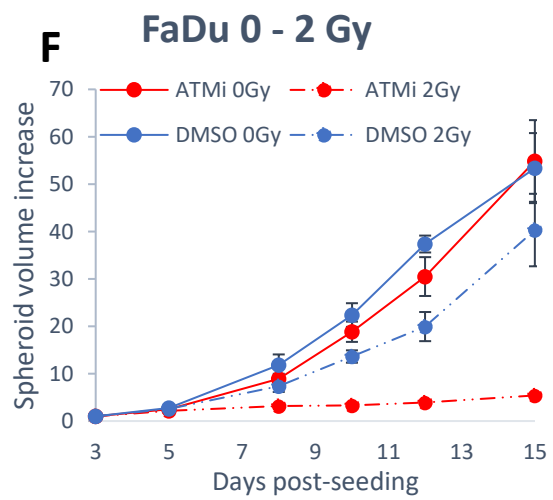
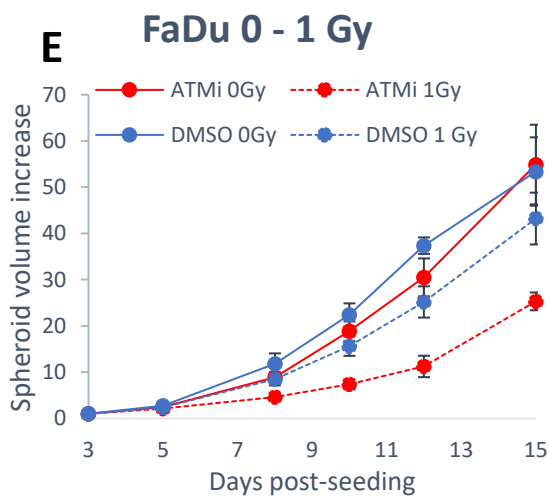
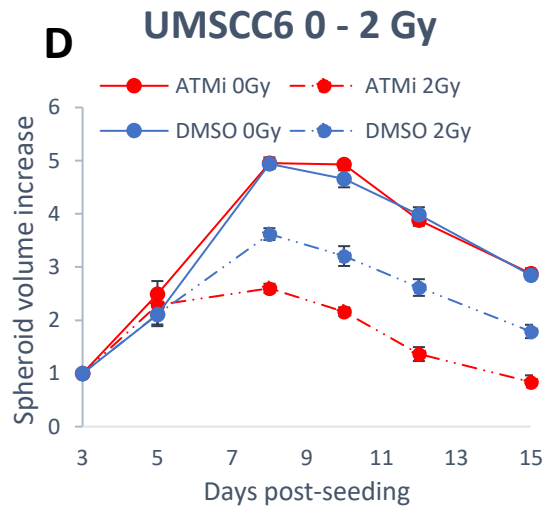
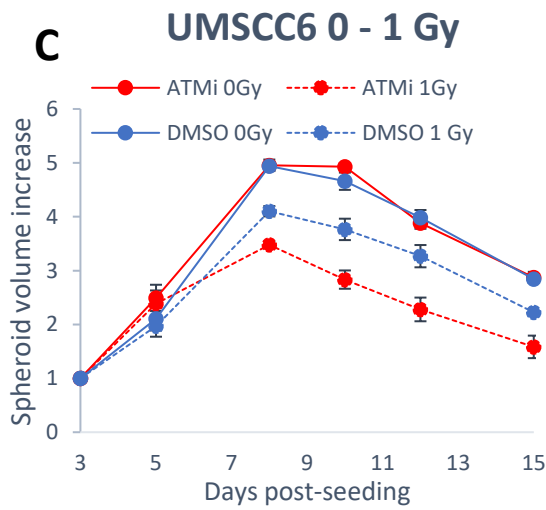
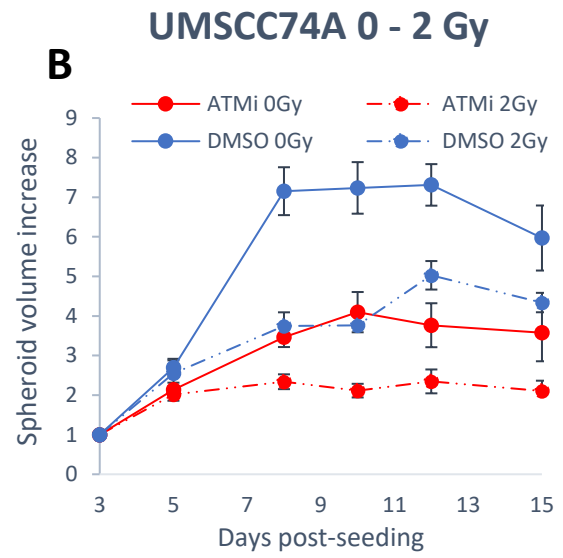
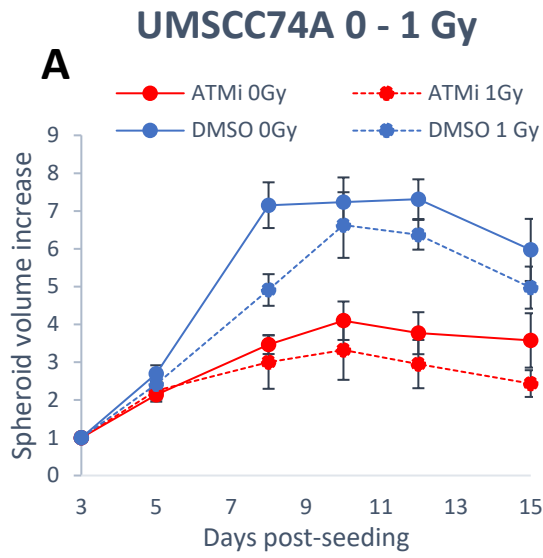
6.7 Impact of DNA repair inhibition in combination with x – rays on 3D spheroid growth in HNSCC.

The impact of the DSB repair inhibitors targeting ATM, ATR and DNA-PKcs in sensitisation of HNSCC to IR, both in radiosensitive HPV-positive cell lines and radioresistant HPV-negative cell lines, was investigated by spheroid growth, as a model that better represented *in vivo* tumour growth. Five HNSCC cell lines were utilised, UMSCC74A, UMSCC6, FaDu, A253 and UPCI-SCC090. Unfortunately, the limited UPCI-SCC154 control spheroid growth did not allow for reliable results in the distinction

between treated and untreated spheroids and therefore analysis of the treatments' impact was not achieved and is not included in this thesis. Cells were left to form spheroids and on Day 3 post seeding these were treated with 10 μ M ATMi, 1 μ M ATRi, 1 μ M DNA-PKcsi or 10 μ M DMSO for 1 h before and for 24 h after irradiation with a single dose (0 - 3 Gy) of x – rays. Spheroid growth was then monitored for a 12-day period post-irradiation, equalling a 15-day growth period overall. Growth suppression ratio (GSR), a ratio that describes the volume of DMSO treated over the volume of drug treated spheroids for a given radiation dose across the 15- day monitoring period were utilised to compare the relative growth suppression.

6.7.1 ATMi

Combination treatment of ATMi with x – rays, resulted in reduced spheroid growth in all HPV-negative cell lines, to a different extend (Figure 6.12 and Tables 6.7 and 6.8). The growth of UMSCC74A and A253 spheroids, that were already reduced by the inhibitor alone, were further suppressed in response to ATMi and 1 Gy x – rays with GSR values of 1.96 ($p < 0.004$) and 3.08 ($p < 0.001$) respectively, although there was no further decrease following a 2 Gy x – ray dose, even though the suppression was still statistically significant ($p < 0.0004$ and $p < 0.01$ respectively), (Figure 6.12 A-B, G-H). In UMSCC6 spheroids, growth was reduced by 1.34- fold in response to ATMi treatment and 1 Gy x – rays, that was further reduced, to 1.7- fold, yet this suppression was statistically significant ($p < 0.02$) only following inhibitor treatment and 2 Gy irradiation (Figure 6.12 C-D). Interestingly, ATMi treated FaDu spheroids exhibited a delay and suppression in growth in response to 1 Gy x – rays, but this was more important, with GSR 4.73, and statistically significantly ($p < 0.004$) only after 2 Gy x – rays. This demonstrates that FaDu is a very radioresistant cell line and that x – ray induced DSB repair in FaDu is only moderately ATM dependant. Regarding the HPV-positive cell line, ATMi treatment did not further reduce growth in combination with IR in UPCI-SCC090 spheroids, as due to their increased endogenous radiosensitivity, radiation alone at 1 Gy x – rays almost completely suppressed their growth. Cumulatively, these findings demonstrated the ATMi efficacy in enhancing the impact of IR, in radioresistant cell lines, even from low radiation doses and representative images are demonstrated in Figure 6.15.



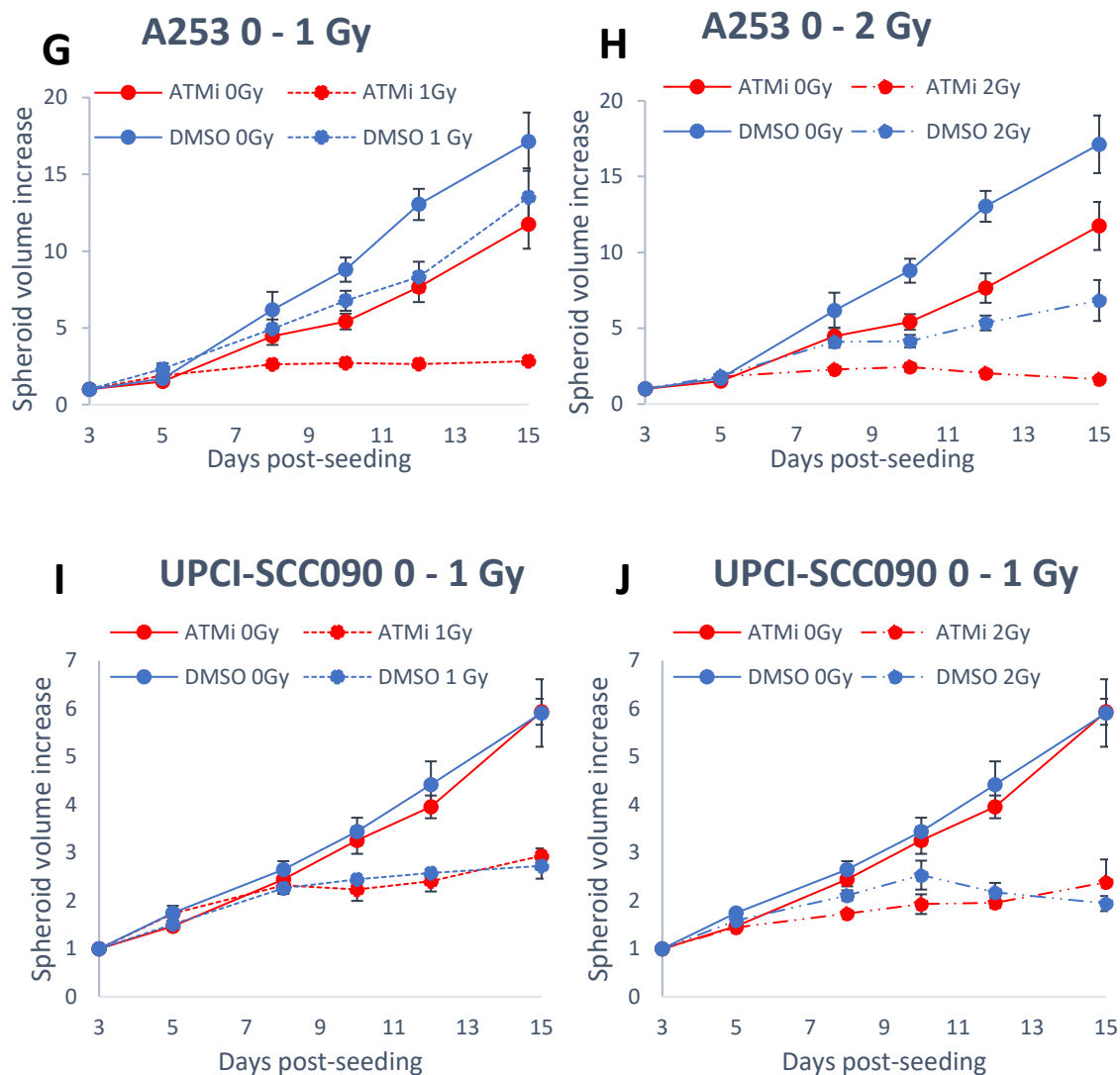


Figure 6. 12. Impact of ATMi on 3D spheroid growth following x - rays in HNSCC cells. Spheroid growth was monitored for 15 days in HPV-negative UMSCC74A (A-B), UMSCC6 (C-D), FaDu (E-F) and A253 (G-H), and HPV-positive, UPCI-SCC090 (I-J), HNSCC cell lines. On Day 3, spheroids were treated with 10 μ M ATMi or 10 μ M DMSO as control, and were exposed to 0, 1 or 2 Gy x - rays. Values were normalised to Day 3 post seeding for each condition that was set to 1, were the means of 3 biologically independent experiments and are presented with their standard errors. Statistical analysis using one way ANOVA revealed significant differences between DMSO and ATMi summarised in Table 6.5.

Table 6. 7. Targeting of ATM in combination with x – rays decreased HNSCC spheroid growth.

| Cell line | ATMi + 1 Gy | ATMi + 2 Gy |
|------------------|--------------------|--------------------|
| UMSCC74A | p<0.004 | p<0.0004 |
| UMSCC6 | p=0.18 | p<0.02 |
| FaDu | p=0.09 | p<0.004 |
| A253 | p<0.001 | p<0.001 |
| UPCI-SCC090 | p=0.76 | p=0.45 |

Statistical analysis was performed across the 15-day growth period using a one-way ANOVA, comparing the growth of inhibitor treated spheroids against the appropriate DMSO control.

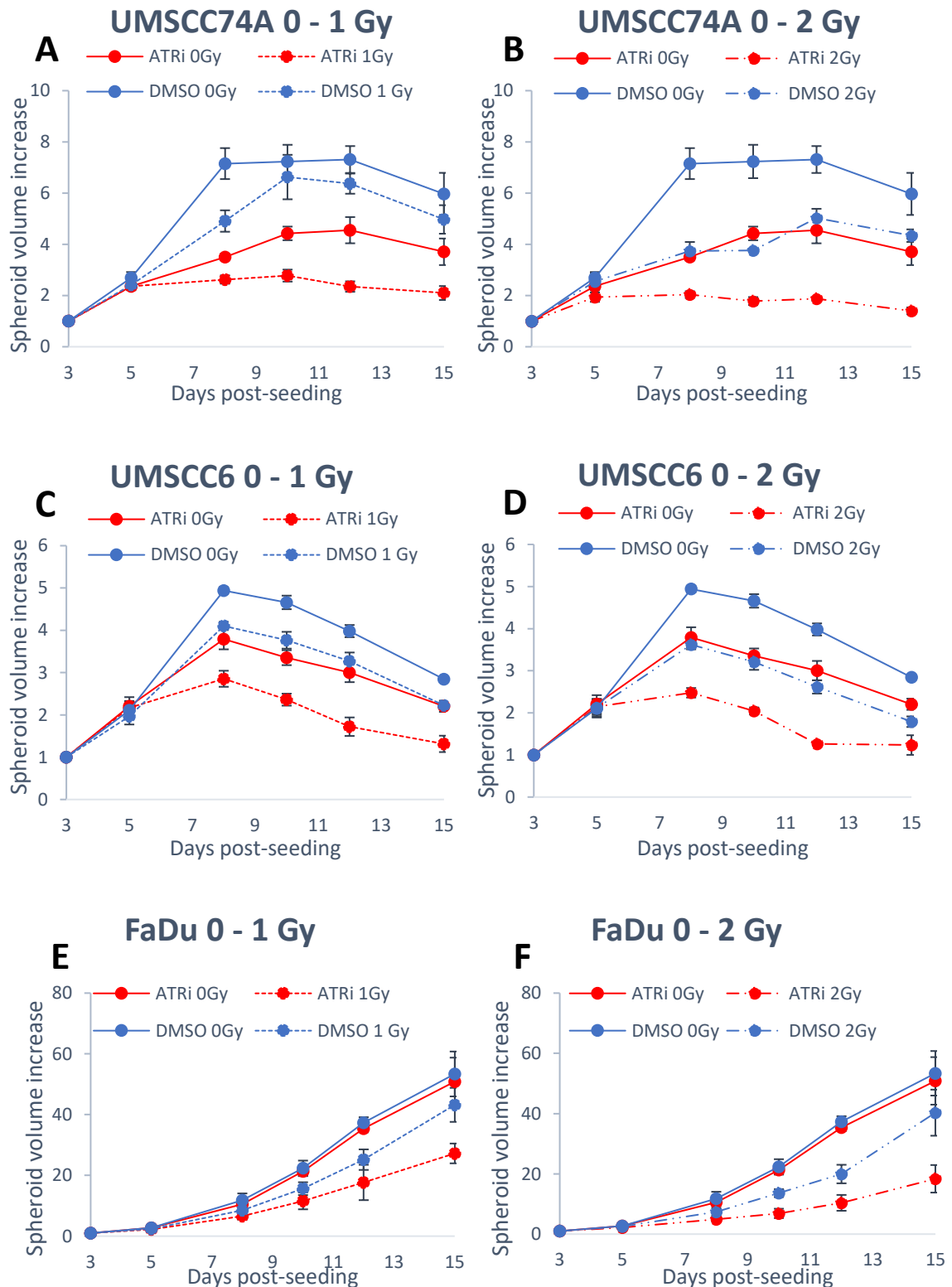
Table 6. 8. Growth suppression ratio (GSR) calculated over the 15-day growth period following ATM inhibition in combination with x – rays. GSR=DMSO spheroid volume/ ATMi spheroid volume for each condition.

| Cell line | ATMi + 1 Gy | ATMi + 2 Gy |
|------------------|--------------------|--------------------|
| UMSCC74A | 1.96 | 1.90 |
| UMSCC6 | 1.34 | 1.73 |
| FaDu | 1.98 | 4.73 |
| A253 | 3.08 | 2.57 |
| UPCI-SCC090 | 1.02 | 1.11 |

6.7.2 ATRi

Treatment with ATRi in combination with x – rays reduced volume in the majority of HNSCC spheroids examined, further than that obtained by ATRi alone, Figure 6.13 and Tables 6.9 and 6.10. In UMSCC74A, UMSCC6, A253, UPCI-SCC090 spheroids, ATRi treatment and 1 Gy x – rays sufficiently suppressed their growth by 2.33-, 1.66-, 2.79-, and 1.32- fold respectively which was also statistically significant as shown in Table 6.7 (p- values <0.03 to < 0.0004). There was still significant radiosensitisation following 2 Gy x – rays which, however, was not further enhanced as shown by the equivalent GSR values. Growth in FaDu spheroids treated with ATRi and 1 Gy x – rays was delayed but not significantly inhibited. The ATRi treated FaDu spheroids kept growing even after 2 Gy x – rays, their size was reduced by almost 2- fold, although this was not statistically

significant. This suggested that FaDu spheroids were not reliant on ATR driven repair of IR-induced DSBs. Overall, ATRi was shown to increase sensitivity to x – rays in HPV-negative as well as in one HPV-positive, although to a lesser degree, HNSCC spheroids and representative images are demonstrated in Figure 6.15.



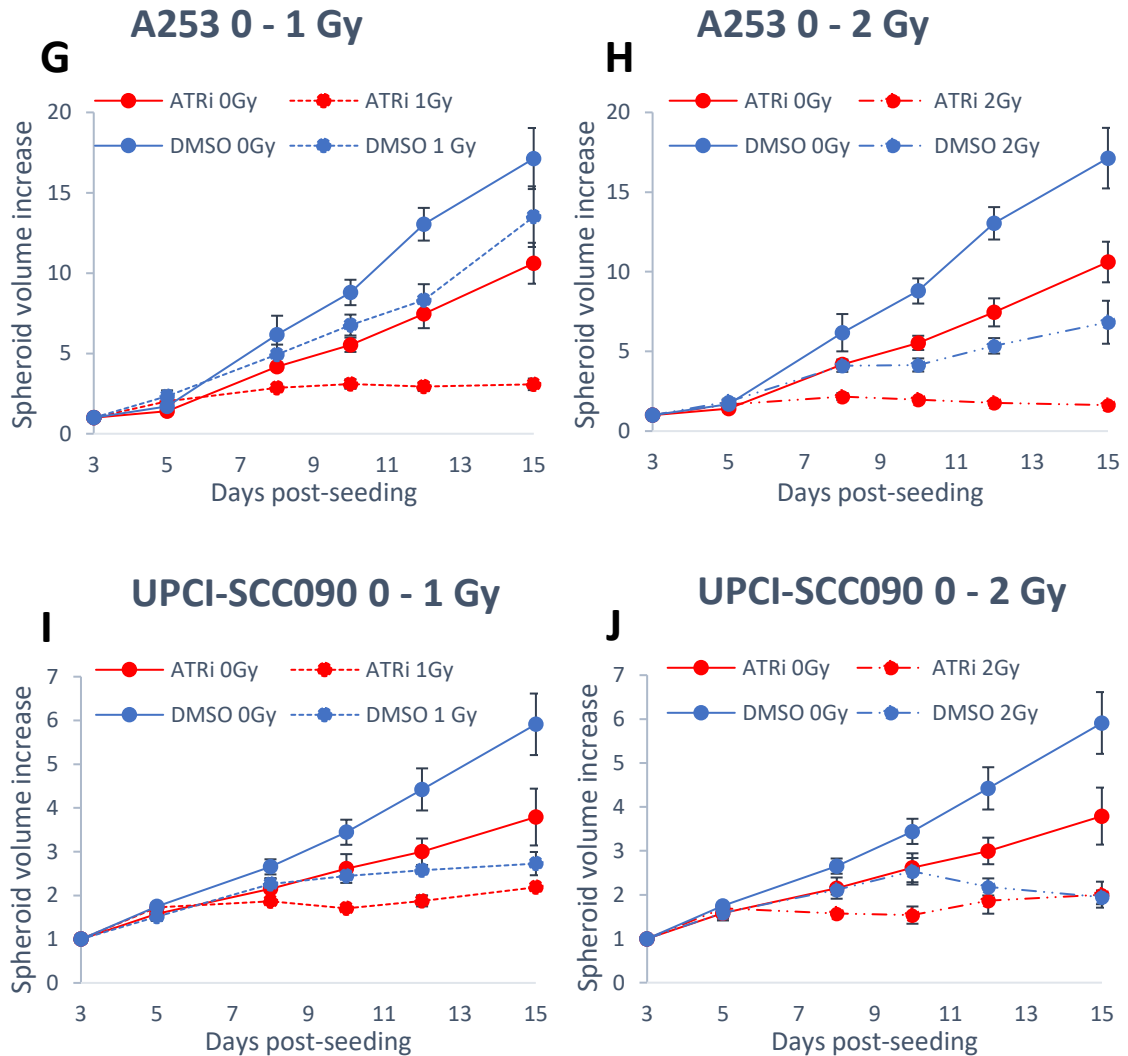


Figure 6. 13. Impact of ATRi on 3D spheroid growth following x - rays in HNSCC cells. Spheroid growth was monitored for 15 days in HPV-negative, UMSCC74A (A-B), UMSCC6 (C-D), FaDu (E-F) and A253 (G-H), and HPV-positive, UPCI-SCC090 (I-J) HNSCC cell lines. On Day 3, spheroids were treated with 1 μ M ATRi or 10 μ M DMSO as control, and were exposed to 0 - 2 Gy x - rays. Values were normalised to Day 3 post seeding for each condition that was set to 1, were the means of 3 biologically independent experiments and are presented with their standard errors. Statistical analysis using one way ANOVA revealed significant differences between DMSO and ATRi summarised in Table 6.7.

Table 6. 9. Targeting of ATR in combination with x – rays decreased HNSCC spheroid growth.

| Cell line | ATRi + 1 Gy | ATRi + 2 Gy |
|------------------|--------------------|--------------------|
| UMSCC74A | p<0.0004 | p<0.00002 |
| UMSCC6 | p<0.014 | p<0.012 |
| FaDu | p=0.28 | p=0.09 |
| A253 | p<0.002 | p<0.0004 |
| UPCI-SCC090 | p<0.03 | p=0.12 |

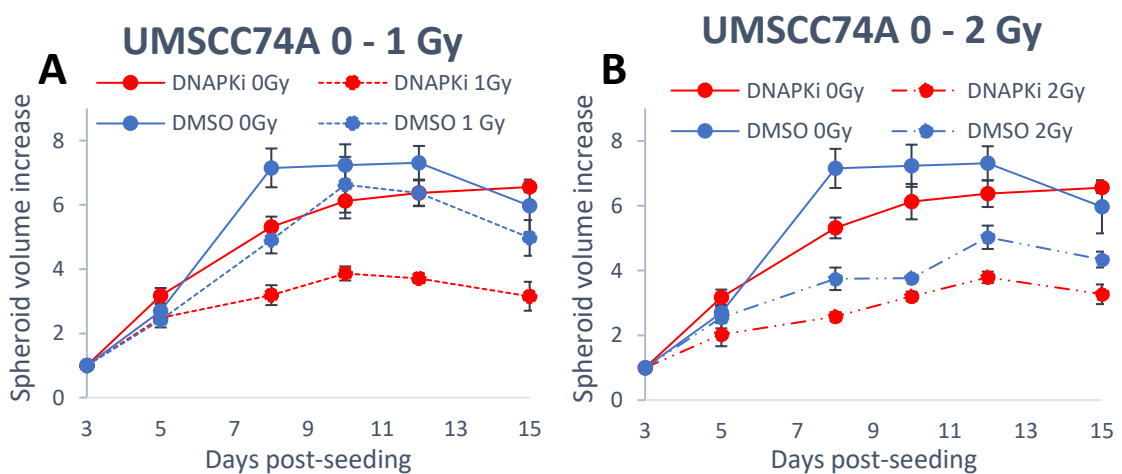
Statistical analysis was performed across the 15-day growth period using a one-way ANOVA, comparing the growth of inhibitor treated spheroids against the appropriate DMSO control.

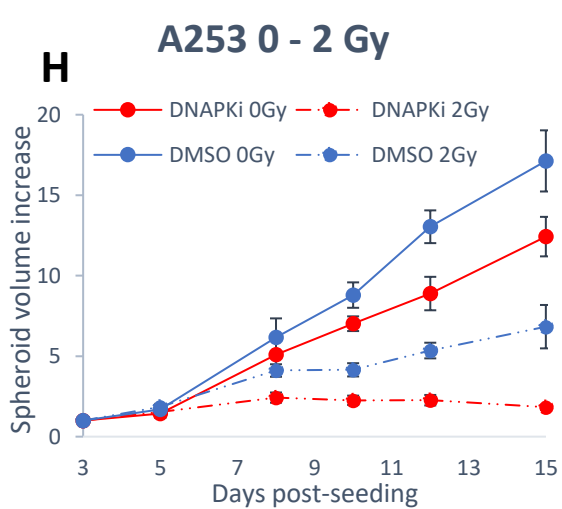
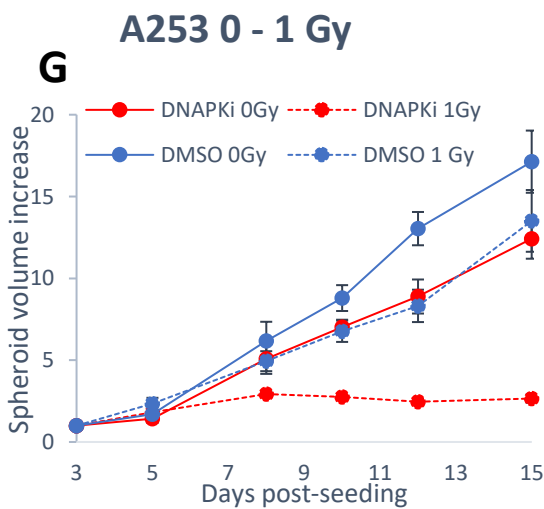
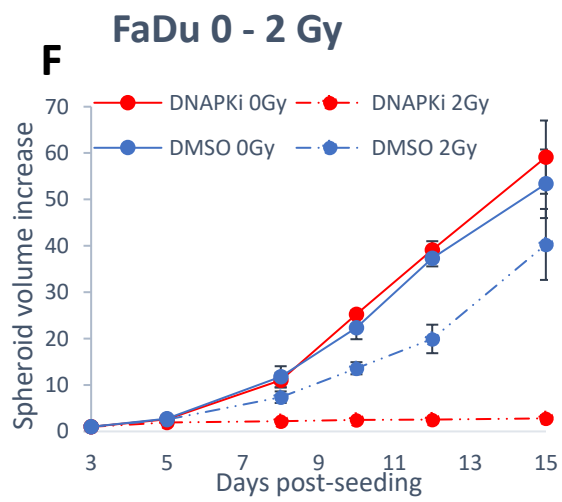
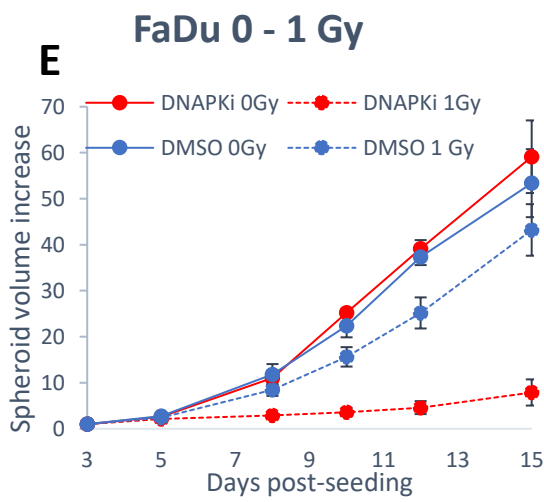
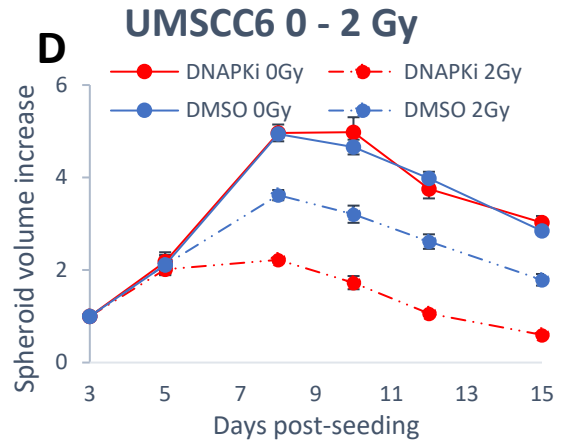
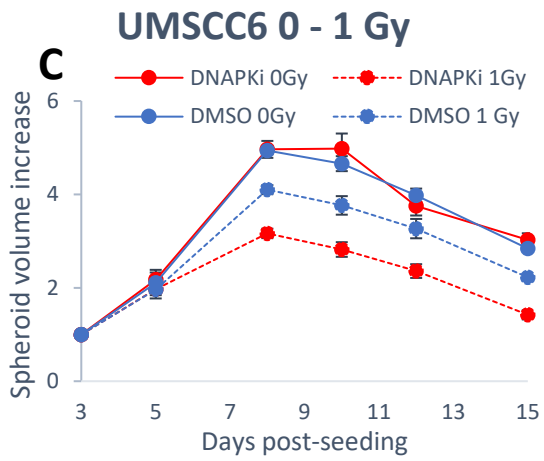
Table 6. 10. Growth suppression ratio (GSR) calculated over the 15- day growth period following ATR inhibition in combination with x – rays. GSR=DMSO spheroid volume/ ATRi spheroid volume for each condition.

| Cell line | ATRi + 1 Gy | ATRi + 2 Gy |
|------------------|--------------------|--------------------|
| UMSCC74A | 2.33 | 2.43 |
| UMSCC6 | 1.66 | 1.64 |
| FaDu | 1.41 | 1.90 |
| A253 | 2.79 | 2.8 |
| UPCI-SCC090 | 1.32 | 1.28 |

6.7.3 DNA-PKcsi

The impact of DNA-PKcsi in combination with x – rays was then examined. Following 1 Gy x – rays, DNA-PKcsi statistically significantly suppressed spheroid growth in all HPV-negative cell lines, leading to severe radiosensitisation (Figure 6.14, Tables 6.11, 6.12). In UMSCC74A and UMSCC6 the GSR values were 1.64 ($p<0.17$) and 1.40 ($p<0.047$) respectively (Figure 6.14 A, C). Increasing the x – ray dose up to 2 Gy, reduced the impact of the inhibitor in UMSCC74A spheroids, where growth was suppressed by 1.32- fold and significance was lost (Figure 6.14 B). However, increasing the dose to 2 Gy enhanced the DNA-PKcsi impact on UMSCC6 spheroids that were suppressed by 2.24- fold ($p<0.001$) (Figure 6.14 D). Moreover, 1 Gy x – ray irradiation in combination with DNA-PKcsi was enough to completely suppress growth of A253 spheroids, with GSR of 3.15 ($p<0.001$), as well as in the most radioresistant FaDu spheroids, with a GSR of 4.55 ($p<0.003$) (Figure 6.14 E, G), while increase of radiation dose further enhanced growth suppression in FaDu spheroids (GSR 7.71, $p<0.002$) (Figure 6.14 F). This highlights the increased dependence of HPV-negative cells, including FaDu, to DNA-PKcs and therefore NHEJ repair in response to x – ray induced DNA damage. Regarding the HPV-positive spheroids, UPCI-SCC090, these were not statistically significantly impacted by DNA-PKcsi in combination with x – rays due to their increased intrinsic radiosensitivity (Figure 6.14 I-J). Summing up, DNA-PKcsi was effective in sensitising all HPV-negative spheroids to x – rays, even from the lowest radiation dose of 1 Gy and representative images are demonstrated in Figure 6.15.





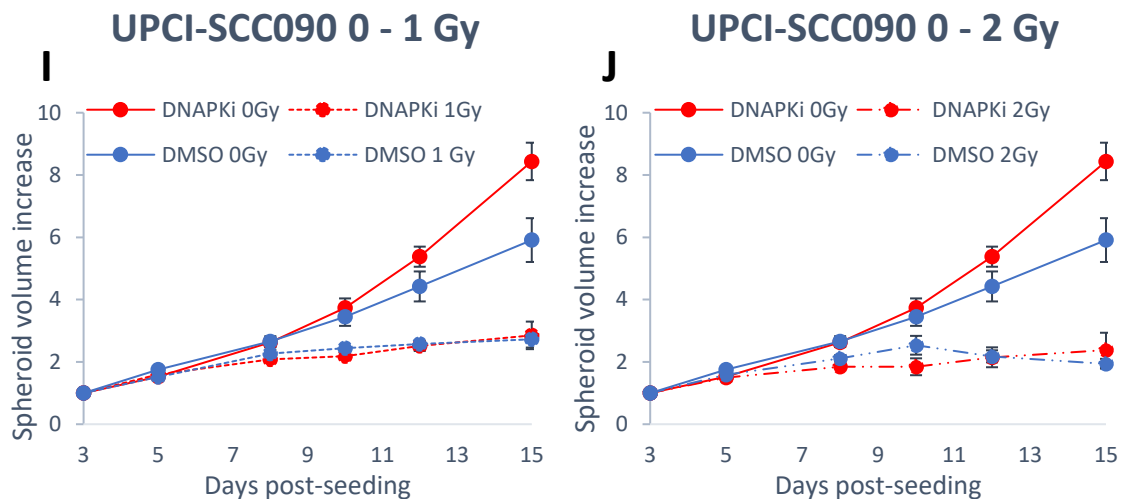


Figure 6. 14. *Impact of DNA-PKcsi on 3D spheroid growth following x - rays in HNSCC cells. Spheroid growth was monitored for 15 days in 4 HPV-negative, UMSCC74A (A-B), UMSCC6 (C-D), FaDu (E-F) and A253 (G-H), and 1 HPV-positive, UPCI-SCC090 (I-J) HNSCC cell lines. On Day 3, spheroids were treated with 1 μ M DNA-PKcsi or 10 μ M DMSO as control, and were exposed to 0 - 2 Gy x - rays. Values were normalised to Day 3 post seeding for each condition that was set to 1, were the means of 3 biologically independent experiments and are presented with their standard errors. Statistical analysis using one way ANOVA revealed significant differences between DMSO and DNA-PKcsi, summarised in Table 6.9.*

Table 6. 11. Targeting of DNA-PKcs in combination with x – rays decreased HNSCC spheroid growth.

| Cell line | DNA-PKcsi + 1 Gy | DNA-PKcsi + 2 Gy |
|-------------|------------------|------------------|
| UMSCC74A | p<0.017 | p=0.076 |
| UMSCC6 | p<0.047 | p<0.001 |
| FaDu | p<0.003 | p<0.002 |
| A253 | p<0.001 | p<0.001 |
| UPCI-SCC090 | p=0.08 | p=0.61 |

Statistical analysis was performed across the 15-day growth period using a one-way ANOVA, comparing the growth of inhibitor treated spheroids against the appropriate DMSO control.

Table 6. 12. Growth suppression ratio (GSR) calculated over the 15-day growth period following DNA-PKcsi inhibition in combination with x – rays. $GSR = \text{DMSO spheroid volume} / \text{DNA-PKcsi spheroid volume}$ for each condition.

| Cell line | DNA-PKcsi + 1 Gy | DNA-PKcsi + 2 Gy |
|-------------|------------------|------------------|
| UMSCC74A | 1.64 | 1.32 |
| UMSCC6 | 1.4 | 2.24 |
| FaDu | 4.55 | 7.71 |
| A253 | 3.15 | 2.41 |
| UPCI-SCC090 | 1.05 | 1.09 |

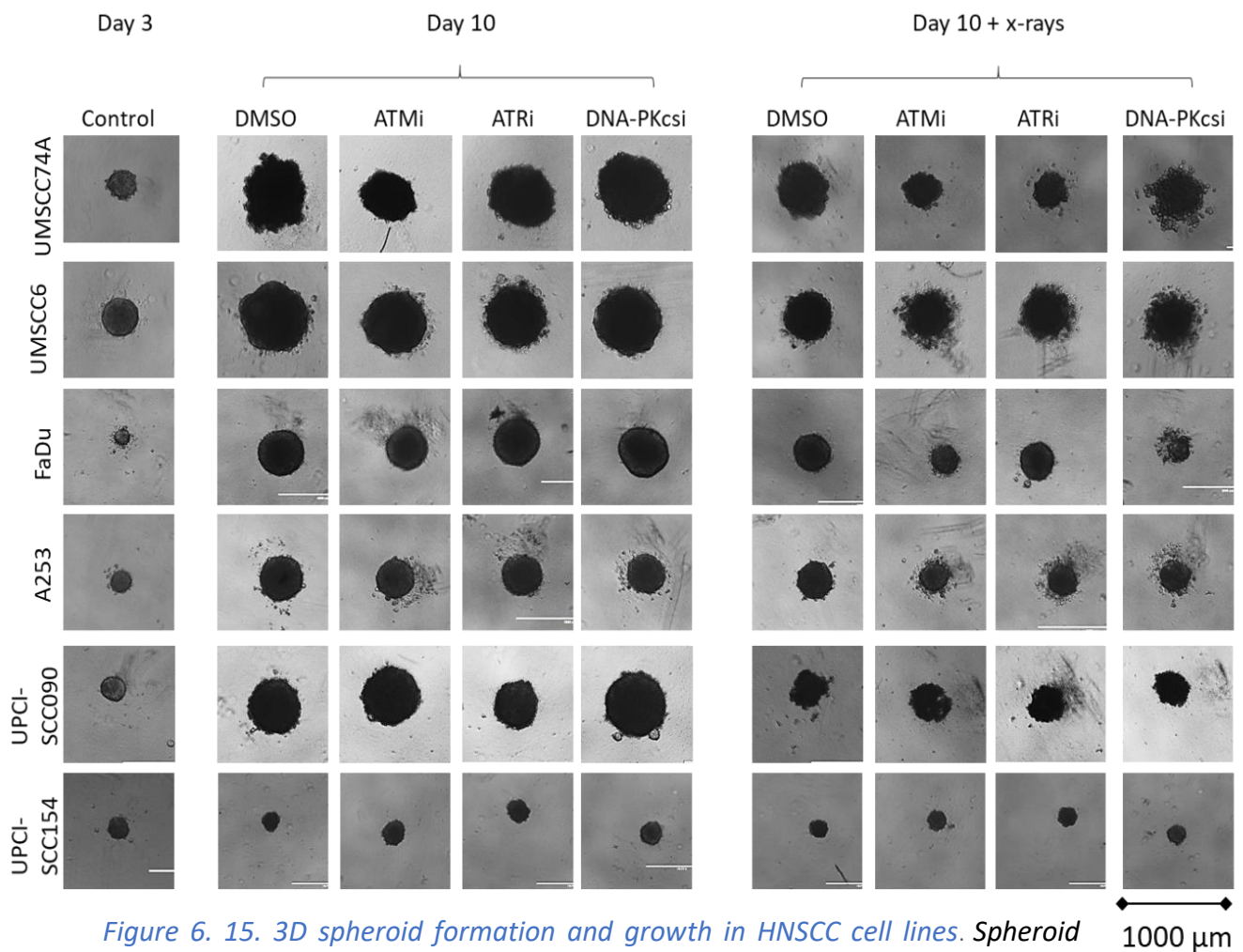


Figure 6. 15. 3D spheroid formation and growth in HNSCC cell lines. Spheroid growth was monitored post treatment with 10µM ATMi, 1µM ATRi, 1 µM DNA-PKcsi or 10 µM DMSO alone, or in combination with 1 Gy x – rays. 6 HNSCC cell line spheroids, 4 HPV-negative (UMSCC74A, UMSCC6, FaDu and A253) and 2 HPV-positive (UPCI-SCC090 and UPCI-SCC154), were imaged on Day 3 post seeding prior to any treatment and for a 2 week period. UPCI-SCC154 spheroids did not grow over the two-week monitoring period and therefore no impact of the drugs could be observed and were excluded from further analysis. Here are displayed representative images of spheroids on Day 3 and 10 post seeding-treatment.

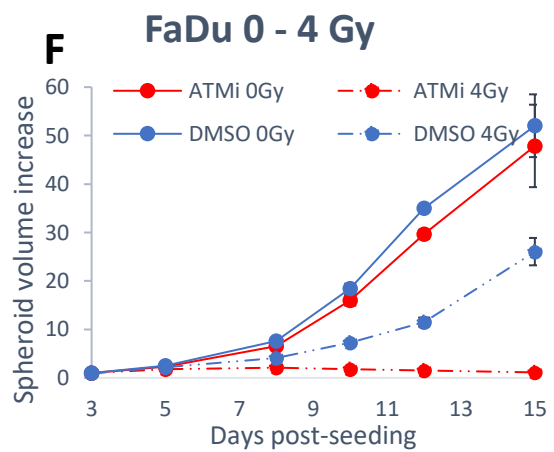
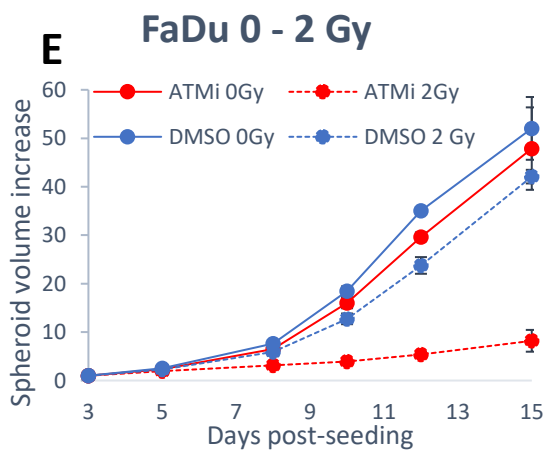
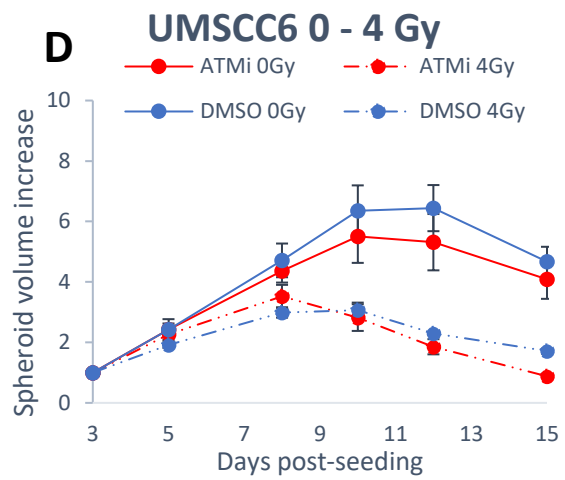
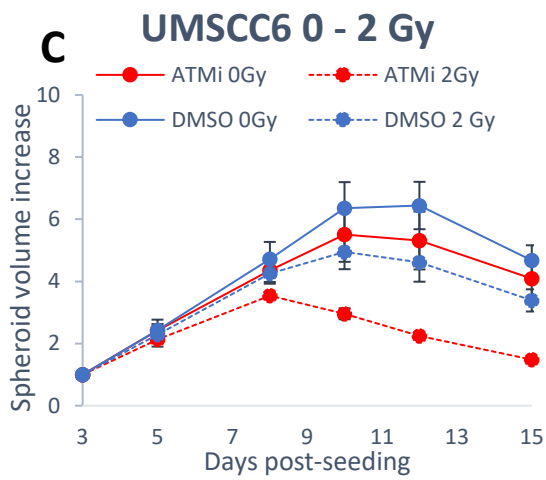
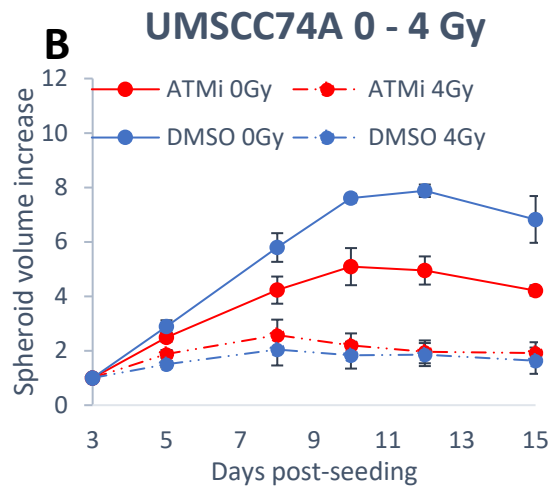
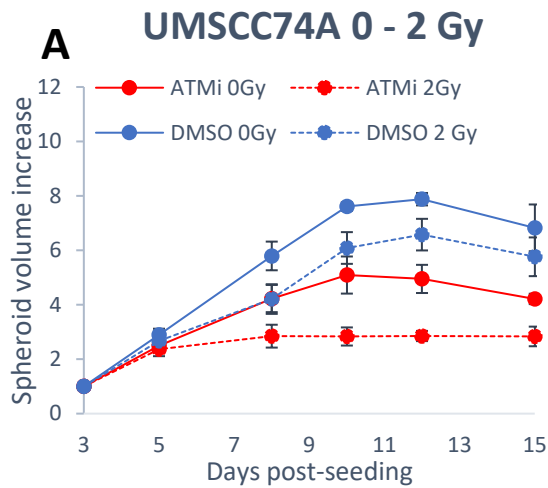
6.8 Impact of DNA repair inhibition in combination with proton irradiation on 3D spheroid growth in HNSCC.

Next, the impact of inhibiting ATM, ATR and DNA-PKcs in combination with proton irradiation on spheroid growth was investigated in HNSCC cell lines. Four (relatively radioresistant) HPV-negative cell lines, UMSCC6, UMSCC74A, FaDu and A253, and one (relatively radiosensitive) HPV-positive cell line, UPCI-SCC090, were examined. Cells were left to form spheroids and on Day 3 post seeding these were treated with 10 μ M ATMi, 1 μ M ATRi, 1 μ M DNA-PKcsi or 10 μ M DMSO for 1 h before and for 24 h after irradiation with 0 – 4 Gy protons. Spheroid growth was then monitored for a 15-day period and GSR were calculated.

6.8.1 ATMi

Treatment with 2 Gy low LET protons, in combination with ATMi resulted in statistically significant suppression of spheroid growth in all HPV-negative HNSCC cell lines, with p values varying between <0.05 to <0.005 (Figure 6.16, Tables 6.13 and 6.14). The GSR were 1.81-1.99 in UMSCC74 and UMSCC6 and 3.66-3.67 in A253 and FaDu (Table 6.14). Notably, growth suppression of the FaDu spheroids was achieved with the lowest proton dose of 2 Gy, demonstrating the enhanced impact of ATMi in combination with protons in this very radioresistant cell line. An increase in radiation dose to 4 Gy, did not further suppress growth in the inhibitor treated spheroids. GSR values were lower and significance was lost as the gap between DMSO and ATMi treated spheroids was reduced by the excess cell killing by radiation alone, in UMSCC74A and UMSCC6. A253 spheroids were suppressed to a lesser degree yet the radiosensitisation was significant even after 4 Gy protons ($p < 0.0006$). Interestingly, FaDu spheroids were further radiosensitised following 4 Gy protons and the GSR rose to 9.05 ($p < 0.002$) (Tables 6.13, 6.14).

Regarding the HPV-positive UPCI-SCC090 spheroids, their radiosensitivity was not impacted by ATMi, as growth was already diminished by proton irradiation, and thus no impact of the drug could be observed. This again highlighted the extreme radiosensitive nature of these spheroids. Representative images are demonstrated in Figure 6.19.



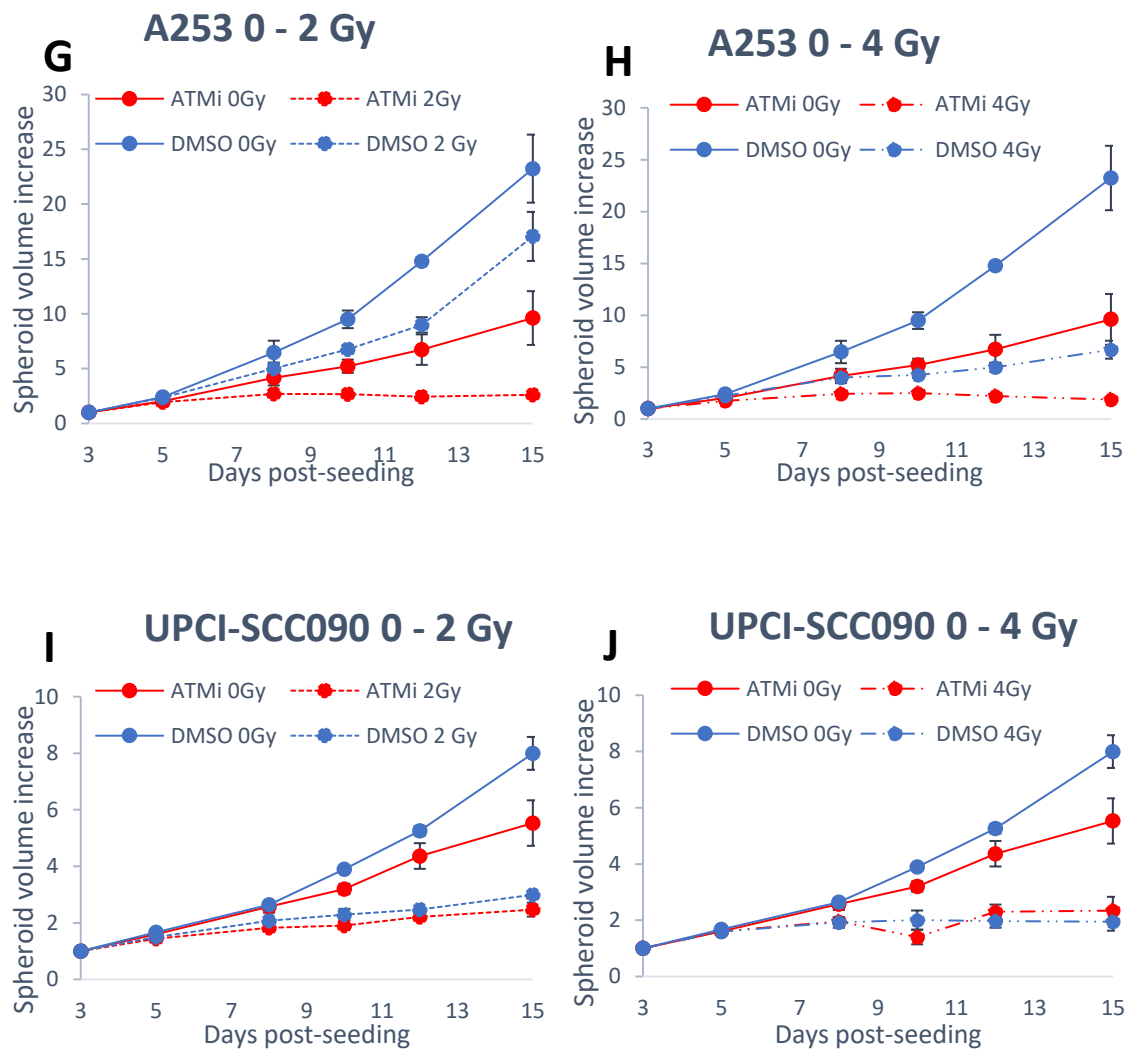


Figure 6. 16. Impact of ATMi on 3D spheroid growth post proton irradiation in HNSCC cells. Spheroid growth was monitored for 15 days post seeding in 4 HPV-negative, UMSCC74A (A-B), UMSCC6 (C-D), FaDu (E-F) and A253 (G-H), and HPV-positive, UPCI-SCC090 (I-J) HNSCC cell lines. On Day 3, spheroids were treated with 10 μ M ATMi or 10 μ M DMSO as control, and were exposed to 0-4 Gy protons. Values were normalised to Day 3 post seeding for each condition that was set to 1, were the means of 3 biologically independent experiments and are presented with their standard errors. Statistical analysis using one way ANOVA revealed significant differences between DMSO and ATMi, summarised in Table 6.11.

Table 6. 13. *Targeting of ATM in combination with protons decreased HNSCC spheroid growth.*

| Cell line | ATMi + 2 Gy | ATMi + 4 Gy |
|------------------|--------------------|--------------------|
| UMSCC74A | p<0.014 | p=0.33 |
| UMSCC6 | p<0.05 | p=0.74 |
| FaDu | p<0.024 | p<0.002 |
| A253 | p<0.005 | p<0.0006 |
| UPCI-SCC090 | p=0.24 | p=0.89 |

Statistical analysis was performed across the 15-day growth period using a one-way ANOVA, comparing the growth of inhibitor treated spheroids against the appropriate DMSO control.

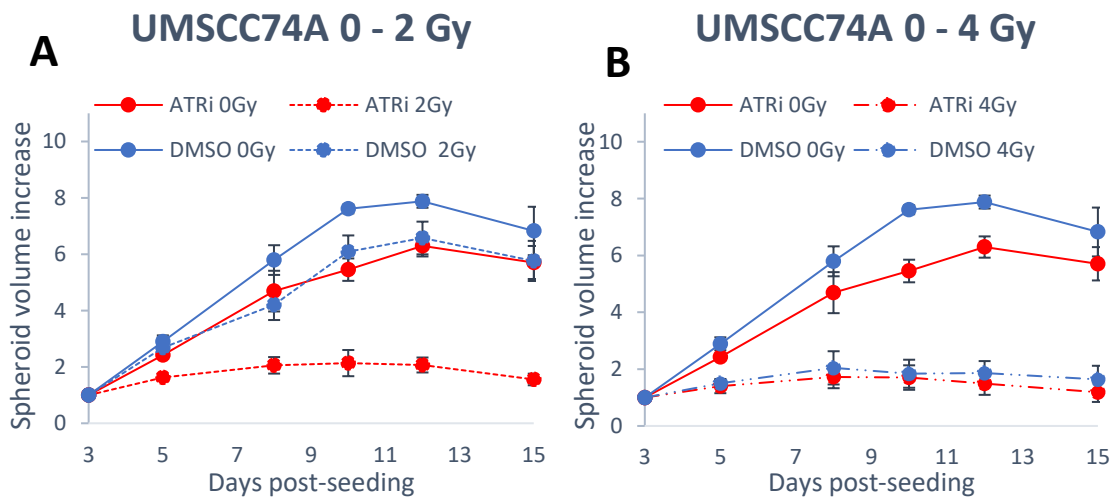
Table 6. 14. *Growth suppression ratios (GSR) calculated over the 15-day growth period following ATM inhibition in combination with protons. GSR=DMSO spheroid volume/ATMi spheroid volume for each condition.*

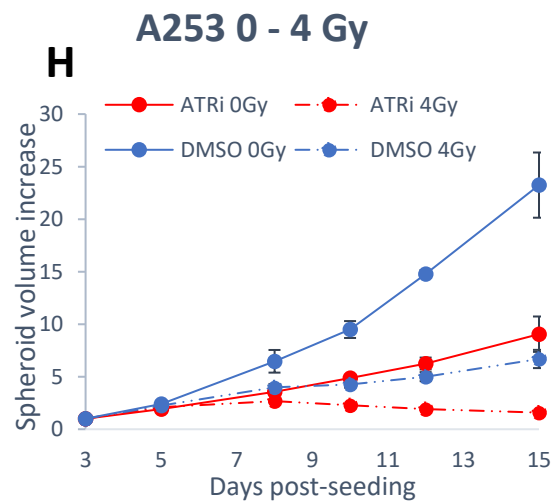
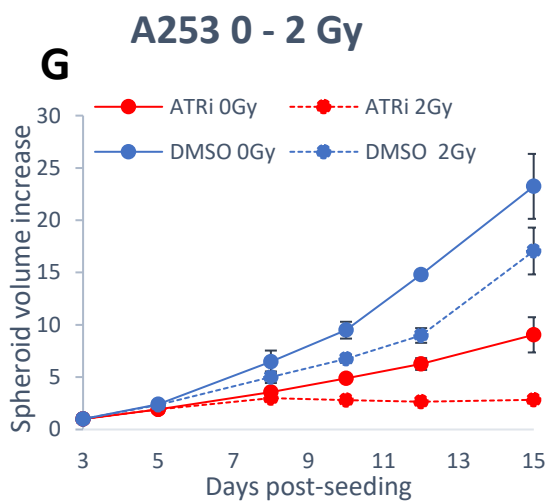
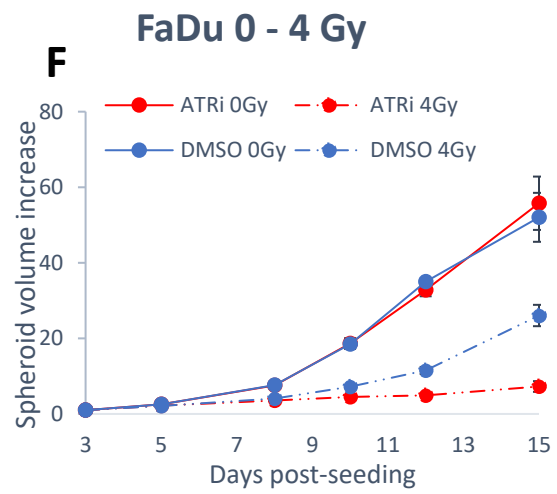
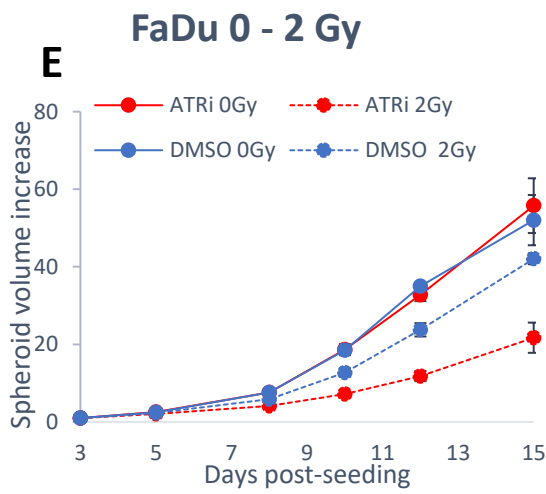
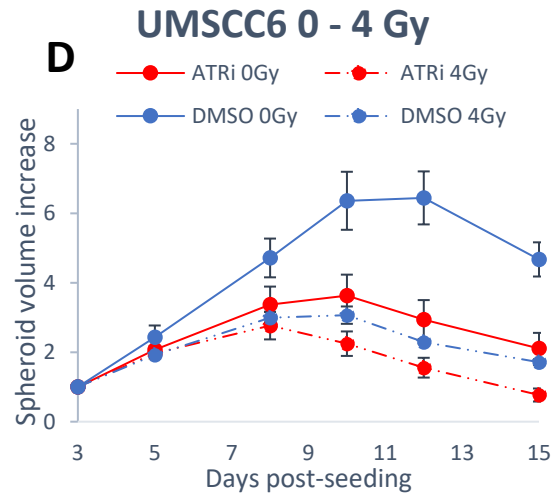
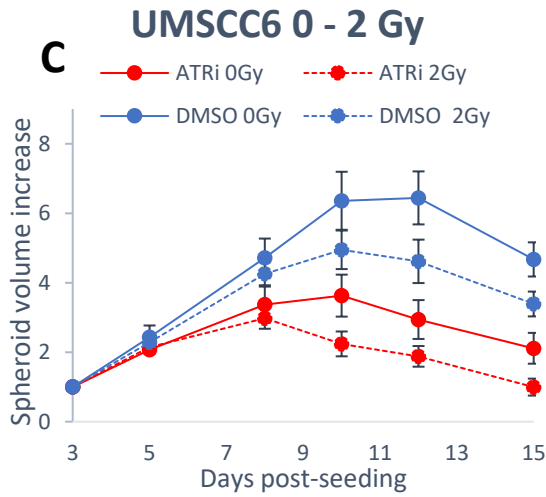
| Cell line | ATMi + 2 Gy | ATMi + 4 Gy |
|------------------|--------------------|--------------------|
| UMSCC74A | 1.99 | 0.86 |
| UMSCC6 | 1.81 | 1.28 |
| FaDu | 3.67 | 9.05 |
| A253 | 3.66 | 2.29 |
| UPCI-SCC090 | 1.17 | 1.05 |

6.8.2 ATRi

The impact of ATRi on cell survival and therefore spheroid growth was found to be the most detrimental among the three DSB repair inhibitors, upon exposure to proton irradiation. ATRi contributed to suppress spheroid growth in all HPV-negative cell lines, as well as in the HPV-positive UPCI-SCC090, as seen in Figure 6.17 and Tables 6.15, 6.16. Specifically, ATRi treated UMSCC74A, and UMSCC6 spheroids exhibited statistically significant ($p < 0.003$ – < 0.0002) growth suppression following 2 Gy proton irradiation,

with GSR values of 2.94 and 2.37 respectively. However, no further growth suppression was obtained by exposure to higher radiation dose up to 4 Gy protons, due to increased cell killing particularly by protons alone (Figure 6.17 B, D, and Tables 6.15 and 6.16). The growth of ATRi treated FaDu and A253 spheroids was delayed in response to 2 Gy protons (GSR 1.78 and 3.37), although the growth suppression was statistically significant ($p < 0.004 - < 0.0005$) only after 4 Gy protons with GSR of 2.18 and 2.55 respectively. Regarding the HPV-positive HNSCC UPCI-SCC090 spheroids, ATRi treatment in combination with 2 Gy protons almost completely suppressed spheroid growth ($p < 0.0008$, GSR 1.63), while increase in the radiation dose up to 4 Gy resulted in almost equivalent suppression ($p < 0.01$, GSR 1.44). Overall, ATRi was found to be effective in suppressing growth in HNSCC spheroids in response to protons by radiosensitising all HPV-negative and one HPV-positive spheroids and representative images are demonstrated in Figure 6.19.





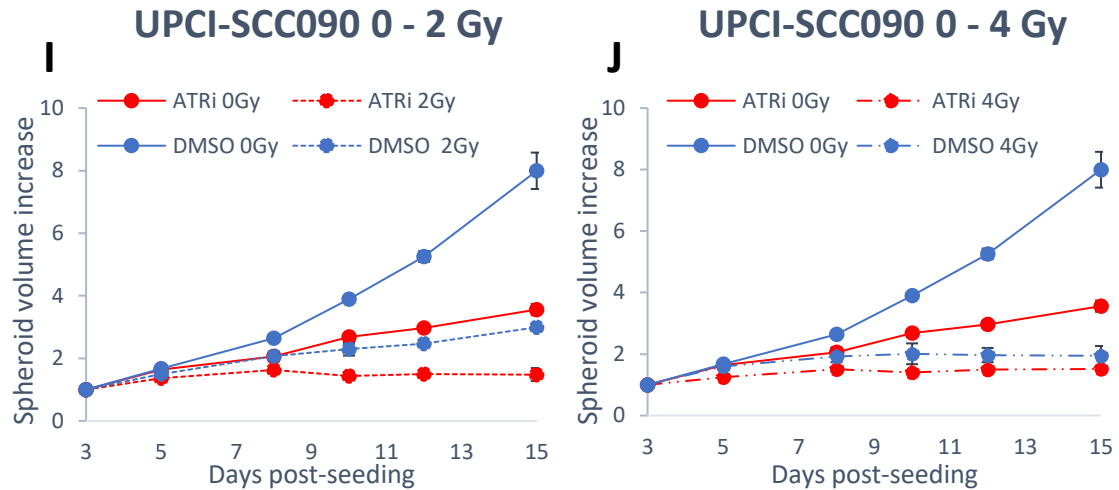


Figure 6.17. *Impact of ATRi on 3D spheroid growth post proton irradiation in HNSCC cells. Spheroid growth was monitored for 15 days in 4 HPV-negative, UMSCC6, UMSCC74A (A-B), UMSCC6 (C-D), FaDu (E-F) and A253 (G-H), and the HPV-positive UPCI-SCC090 (I-J) HNSCC cell lines. On Day 3, spheroids were treated with 1 μ M ATRi or 10 μ M DMSO as control, and were exposed to 0-4 Gy protons. Values were normalised to Day 3 post seeding for each condition that was set to 1, were the means of 3 biologically independent experiments and are presented with their standard errors. Statistical analysis using one way ANOVA revealed significant differences between DMSO and ATRi, summarised in Table 6.13.*

Table 6.15. Targeting of ATR in combination with protons decreased HNSCC spheroid growth.

| Cell line | ATRi + 2 Gy | ATRi + 4 Gy |
|-------------|-------------|-------------|
| UMSCC74A | p<0.0002 | p=0.36 |
| UMSCC6 | p<0.003 | p=0.11 |
| FaDu | p=0.23 | p<0.04 |
| A253 | p=0.106 | p<0.0005 |
| UPCI-SCC090 | p<0.0008 | p<0.01 |

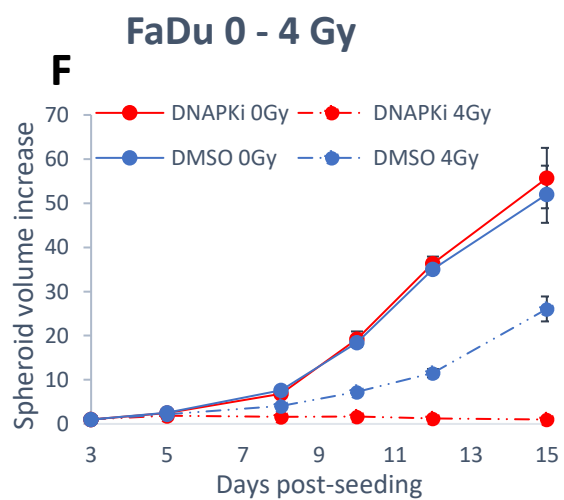
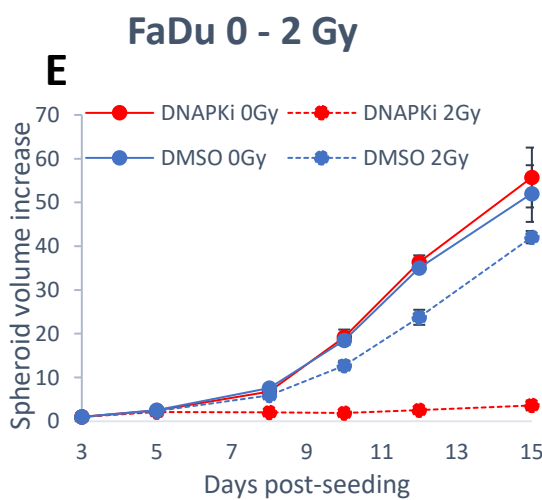
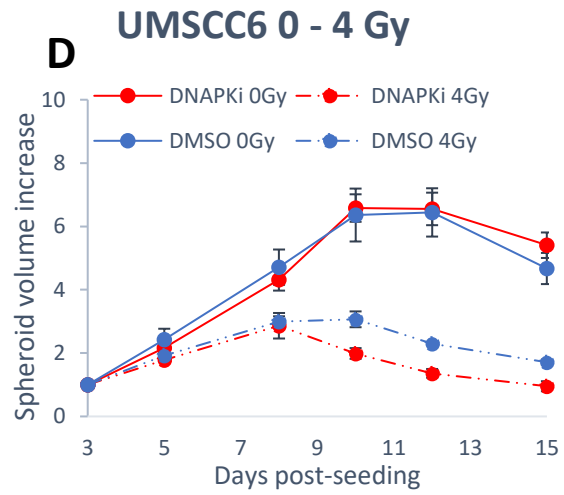
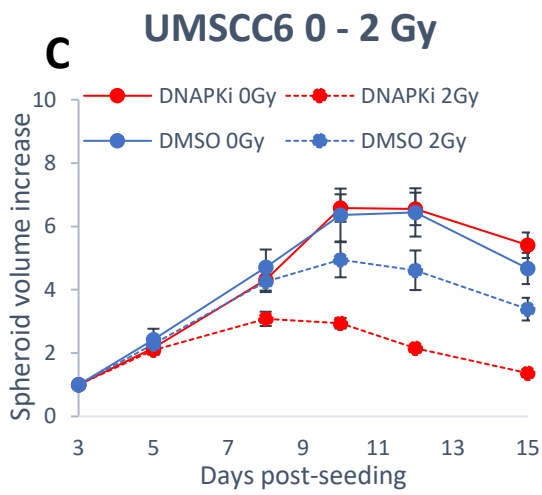
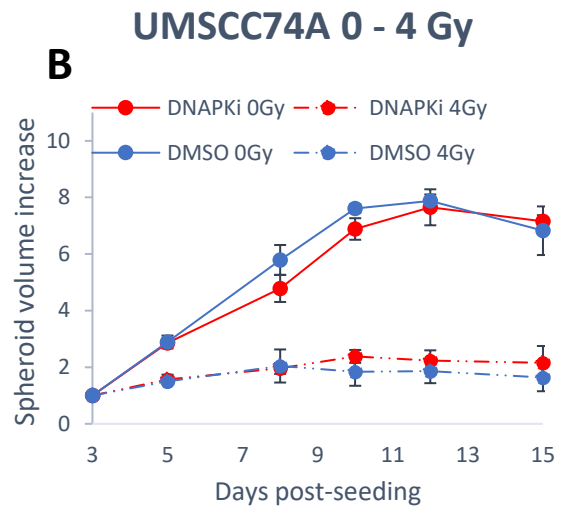
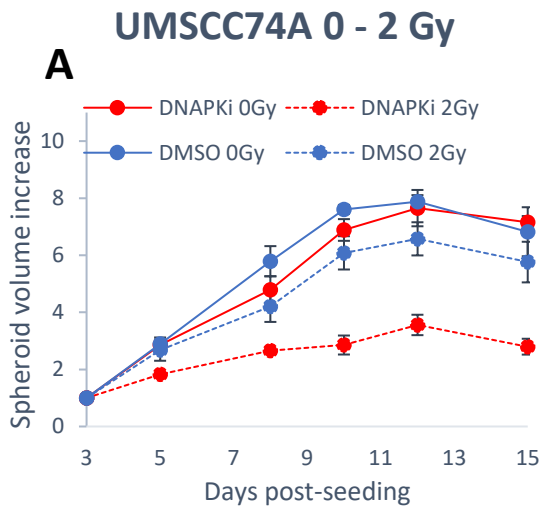
Statistical analysis was performed across the 15-day growth period using a one-way ANOVA, comparing the growth of inhibitor treated spheroids against the appropriate DMSO control.

Table 6. 16. Growth suppression ratios (GSR) calculated over the 15-day growth period following ATR inhibition in combination with protons. SGR=DMSO spheroid volume/ ATR spheroid volume for each condition.

| Cell line | ATRi + 2 Gy | ATRi + 4 Gy |
|------------------|--------------------|--------------------|
| UMSCC74A | 2.94 | 1.22 |
| UMSCC6 | 2.37 | 1.54 |
| FaDu | 1.78 | 2.18 |
| A253 | 3.37 | 2.55 |
| UPCI-SCC090 | 1.63 | 1.44 |

6.8.3 DNA-PKcsi

Treatment with DNA-PKcsi and 2 Gy protons resulted in severe radiosensitisation in all HPV-negative cell lines as illustrated in Figure 6.18 and Tables 6.17, 6.18. The growth was statistically significantly reduced by 1.91-1.92- fold in UMSCC74A ($p < 0.017$) and UMSCC6 ($p < 0.047$) spheroids, and 3.57- and 7.63- fold in A253 ($p < 0.003$) and FaDu ($p < 0.001$) spheroids respectively. Interestingly, the most radioresistant FaDu spheroids, were sufficiently suppressed by the lowest proton dose, which supports an increased dependence of FaDu to DNA-PKcs and therefore NHEJ repair in response to proton induced DNA damage. Exposure of HPV-negative spheroids to DNA-PKcsi and 4 Gy protons, further enhance GSR in FaDu spheroids (to 10.59, $p < 0.002$) but this was reduced in all the other HPV-negative cell lines, due to excess cell killing by protons alone. On the other hand, there was minimal sensitisation of the HPV-positive cell line UPCI-SCC090 to protons achieved by DNA-PKcsi, due to their high intrinsic radiosensitivity, Figure 6.18 I-J, and Tables 6.17, 6.18. Growth in inhibitor treated UPCI-SCC090 spheroids was suppressed by 1.21- fold following 2 Gy protons, which was increased to 1.31- fold post 4 Gy protons, although these were not statistically significant. Altogether, these findings suggested that DNA-PKcsi sufficiently radiosensitised HPV-negative HNSCC spheroids to proton irradiation, and that the advantage of combination treatment was more eminent in the lowest proton radiation dose. Representative images are demonstrated in Figure 6.19.



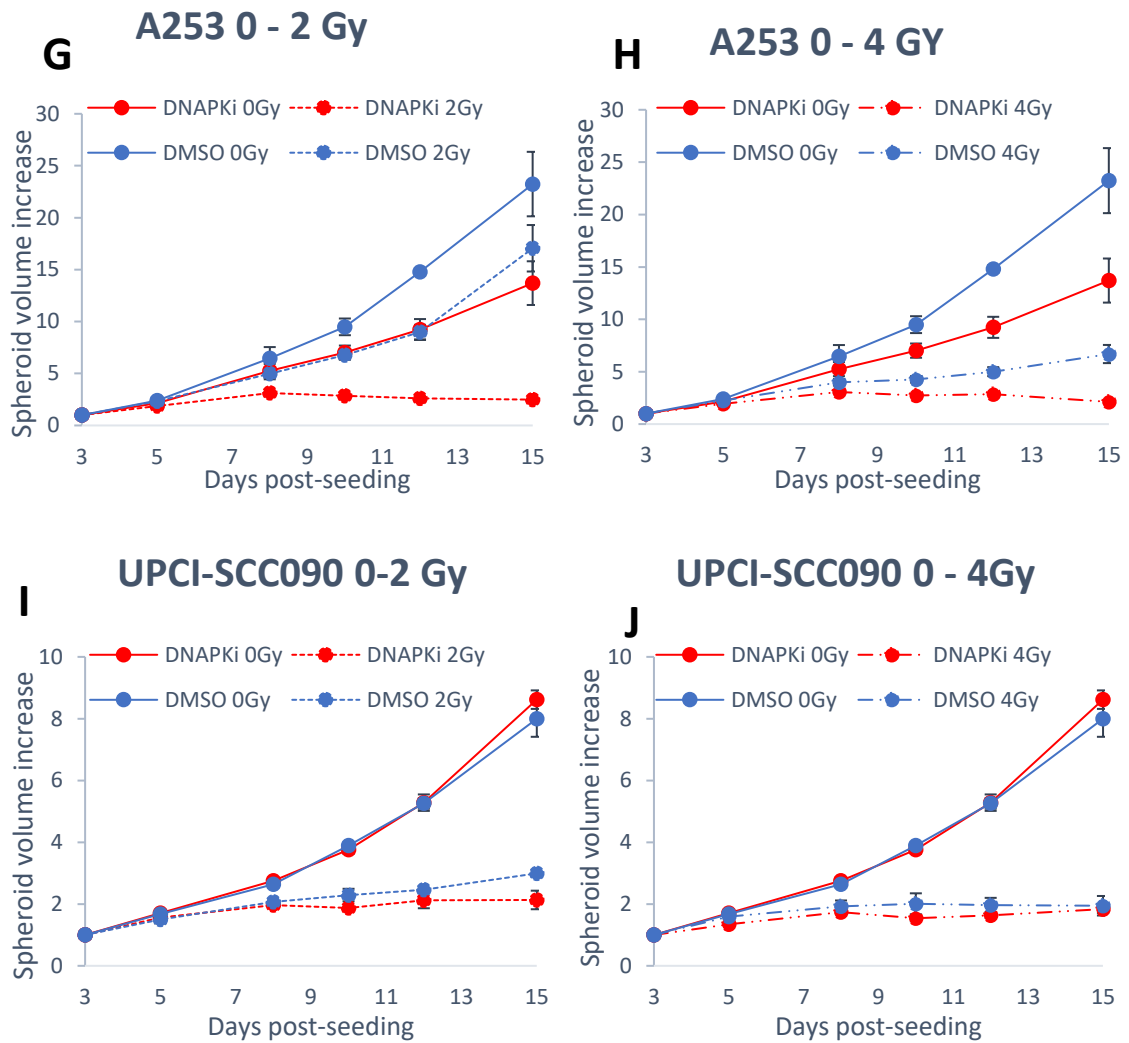


Figure 6. 18. Impact of DNA-PKcsi on 3D spheroid growth post proton irradiation in HNSCC cells. Spheroid growth was monitored for 15 days in 4 HPV-negative, UMSCC74A (A-B), UMSCC6 (C-D), FaDu(E-F) and A253 (G-H), and the HPV-positive, UPCI-SCC090 (I-J) HNSCC cell lines. On Day 3, spheroids were treated with 1 μ M DNA-PKcsi or 10 μ M DMSO as control, and were exposed to 0 - 4 Gy protons. Values were normalised to Day 3 post seeding for each condition that was set to 1, were the means of 3 biologically independent experiments and are presented with their standard errors. Statistical analysis using one way ANOVA revealed significant differences between DMSO DNA-PKcsi, summarised in Table 6.15.

Table 6. 17. Targeting of DNA-PKcs in combination with protons decreased HNSCC spheroid growth.

| Cell line | DNA-PKcsi + 2 Gy | DNA-PKcsi + 4 Gy |
|------------------|-------------------------|-------------------------|
| UMSCC74A | p<0.017 | p=0.36 |
| UMSCC6 | p<0.047 | p<0.05 |
| FaDu | p<0.003 | p<0.002 |
| A253 | p<0.001 | p<0.004 |
| UPCI-SCC090 | p=0.08 | p=0.14 |

Statistical analysis was performed across the 15-day growth period using a one-way ANOVA, comparing the growth of inhibitor treated spheroids against the appropriate DMSO control.

Table 6. 18. Growth suppression ratios (GSR) calculated over the 15-day growth period following DNA-PKcsi inhibition in combination with protons. GSR=DMSO spheroid volume/ DNA-PKcsi spheroid volume for each condition.

| Cell line | DNA-PKcsi + 2 Gy | DNA-PKcsi + 4 Gy |
|------------------|-------------------------|-------------------------|
| UMSCC74A | 1.91 | 0.85 |
| UMSCC6 | 1.92 | 1.52 |
| FaDu | 7.63 | 10.59 |
| A253 | 3.57 | 1.94 |
| UPCI-SCC090 | 1.21 | 1.31 |

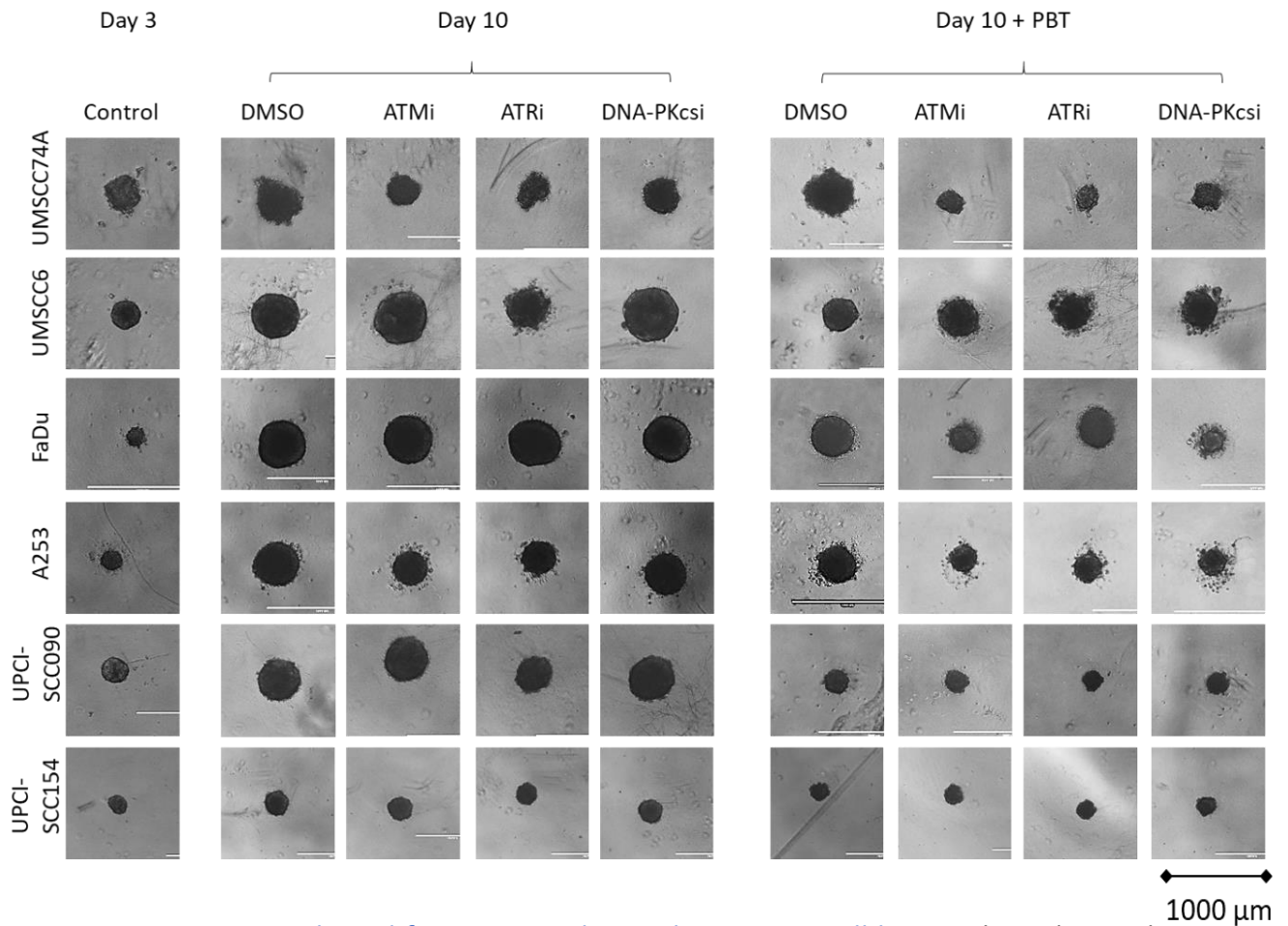


Figure 6. 19. 3D spheroid formation and growth in HNSCC cell lines. Spheroid growth was monitored post treatment with 10μM ATMi, 1μM ATRi, 1 μM DNA-PKcsi or 10 μM DMSO alone, or in combination with 2 Gy protons. 6 HNSCC cell line spheroids, 4 HPV-negative (UMSCC74A, UMSCC6, FaDu and A253) and 2 HPV- positive (UPCI-SCC090 and UPCI-SCC154), were imaged on Day 3 post seeding prior to any treatment and for a 2 week period. UPCI-SCC154 spheroids did not grow over the two-week monitoring period and therefore no impact of the drugs could be observed and were excluded from further analysis. Here are displayed representative images of spheroids on Day 3 and 10 post seeding.

6.9 Conclusions

Over Chapters 4 and 5, the three DSB repair inhibitors were shown to regulate phosphorylation of their target proteins in crucial sites that promote and mediate DNA repair in HNSCC cells. This was correlated with altered DNA damage response, in response to x – rays as well as low LET protons, constituting a promising tool for radiosensitisation. Therefore, in the last section of this research project, the impact of DSB repair inhibition on cell survival was investigated, as the ultimate end-point. This was studied both as a result of inhibitor monotherapy, as well as a combination of inhibitor with x – rays and low LET protons in HNSCC cells, via two independent techniques. First by utilising 2D via colony formation (clonogenic) assays, a gold-standard technique in cell biology for investigating potential effectiveness of specific treatments, and next by assessing 3D spheroid growth assays, a state-of-art technique which more accurately reflect the complex and heterogenous structure as well as the environment of the original tumour.

Monotherapy with the inhibitors, particularly ATRi and ATMi, resulted in a reduction in cell survival despite the apparent small impact of the inhibitors alone on DNA damage response, as discussed in the Chapters 4 and 5. Among the three drugs, ATRi had the most dramatic impact, with approximately a 2 fold and statistically significant reduction in colony formation in 2 HPV-negative (UMSCC74A, UMSCC6) and 2 HPV-positive (UMSCC47, UPCI-SCC090) HNSCC cell lines, which was also reflected in spheroid growth that was suppressed in 3 HPV-negative (UMSCC74A, UMSCC6, A253) and 1 HPV-positive (UPCI-SCC090) HNSCC spheroids (Table 6.19). Next was ATMi, that resulted in statistically significant reduced cell survival, in 2 HPV-negative (UMSCC76A, UMSCC6) and 1 HPV positive (UMSCC47) HNSCC cells, but also suppressed growth in 2 HPV-negative HNSCC spheroids (UMSCC74A, A253) (Table 6.19). Finally, DNA-PKcsi was the least impacting inhibitor as a monotherapy, that statistically significantly downregulated colony formation in only 1 HPV-positive (UMSCC47) cell line and suppressed growth in only 1 HPV-negative (A253) spheroid, although this was not statistically significant (Table 6.19). Interestingly, a small, but not significant, spheroid growth increase was observed in the HPV-positive UPCI-SCC090. This suggested that insufficient NHEJ repair of endogenous DSBs in this specific cell line could contribute to increased spheroid growth

possibly via upregulated alternative DNA repair routes. Collectively these data indicate an increased dependence on ATM and ATR, and less on DNA-PKcsi in controlling survival and proliferation of HNSCC cells in the absence of IR, through the repair of endogenous DSBs.

Table 6. 19. Impact of DSB repair inhibitor as a monotherapy on cell survival in 2D (clonogenic assay) and 3D (spheroid growth assay).

| Non irradiated | Clonogenic Assay | | | Spheroid Growth Assay | | |
|----------------|------------------|------|-----------|-----------------------|------|-----------|
| | ATMi | ATRi | DNA-PKcsi | ATMi | ATRi | DNA-PKcsi |
| UMSCC74A | ↓ | ↓ | - | ↓ | ↓ | - |
| UMSCC6 | ↓ | ↓ | ↓ | - | ↓ | - |
| FaDu | * | * | * | - | - | - |
| A253 | * | * | * | ↓ | ↓ | ↓ |
| UMSCC47 | ↓ | ↓ | ↓ | * | * | * |
| UPCI-SCC090 | - | ↓ | - | ↓ | ↓ | ↑ |

↓: downregulated cell survival, ↑: upregulated cell survival, -: no impact, *: no data

Treatment with ATMi severely radiosensitised all HNSCC cell lines examined, to x – rays and protons even from the lowest radiation dose, as seen via both clonogenic and spheroid growth assays. Indeed, a statistically significant reduction in colony formation with simultaneously reduced D₅₀ values, was observed in all cell lines in response to x – rays and in all but 1 HPV-positive (UPCI-SCC090) cell line in response to protons (Table 6.20). Similarly, spheroid growth was suppressed in all HPV-negative cell lines, in response to the lowest radiation dose, 1 Gy x – rays or 2 Gy protons. The radiosensitisation of the HPV-negative cell lines persisted following higher x – ray dose (2 Gy), however was limited to only two of them (FaDu, A253) following higher proton dose (4 Gy). This was possibly due to increase cell killing by proton radiation alone, that did not allow to distinct between the radiation and inhibitors impact. Moreover, in spheroid growth assay a potential radiosensitisation by x – rays or low LET protons was less evident in the HPV-positive cell line (UPCI-SCC090), irrespective of the radiation dose, due to increased intrinsic radiosensitivity. Even though this was achieved in 2D in response to x – ray irradiation.

Table 6. 20. Impact of ATMi in combination with x – rays or low LET protons on cell survival in 2D (clonogenic assay) D50 and 3D (spheroid growth assay) GSR.

| ATMi | Clonogenic | | Spheroid | | | |
|-------------|-----------------|-----------------|----------|------|---------|------|
| | X - rays | Protons | X - rays | | Protons | |
| | D ₅₀ | D ₅₀ | 1 Gy | 2 Gy | 2 Gy | 4 Gy |
| UMSCC74A | ↓ | ↓ | ↓ | ↓ | ↓ | - |
| UMSCC6 | ↓ | ↓ | ↓ | ↓ | ↓ | - |
| FaDu | * | * | ↓ | ↓ | ↓ | ↓ |
| A253 | * | * | ↓ | ↓ | ↓ | ↓ |
| UMSCC47 | ↓ | ↓ | * | * | * | * |
| UPCI-SCC090 | ↓ | - | - | - | - | - |

↓: downregulated cell survival, ↑: upregulated cell survival, -: no impact, *: no data

Next, inhibition of ATR was found to promote cell killing in response to x – rays or low LET protons, both in 2D colony formation and 3D spheroid growth. In fact, ATRi, which as a monotherapy already impacted cell survival, further reduced colony formation in all but 1 HPV-positive (UPCI-SCC090) HNSCC cells, in response to x – rays as well as protons. In addition, ATRi considerably suppressed growth in all HPV-negative spheroids, that was statistically significant in all except FaDu spheroids, and surprisingly in the HPV-positive UPCI-SCC090, from the lowest radiation dose, 1 Gy x – rays or 2 Gy protons. After exposure to higher radiation dose the impact of ATRi was weakened due to increased cell killing by the radiation alone, yet remained significant for UMSCC6 and UMSCC74A spheroids following (2 Gy x – rays) and FaDu A253 and UPCI-SCC090 spheroids (4 Gy protons) (Table 6.21).

Table 6. 21. Impact of ATRi in combination with x – rays or low LET protons on cell survival in 2D (clonogenic assay) D50 and 3D (spheroid growth assay) GSR.

| ATRi | Clonogenic | | Spheroid | | | |
|-------------|-----------------|-----------------|----------|------|---------|------|
| | X - rays | Protons | X - rays | | Protons | |
| | D ₅₀ | D ₅₀ | 1 Gy | 2 Gy | 2 Gy | 4 Gy |
| UMSCC74A | ↓ | ↓ | ↓ | ↓ | ↓ | - |
| UMSCC6 | ↓ | ↓ | ↓ | ↓ | ↓ | - |
| FaDu | * | * | - | - | - | ↓ |
| A253 | * | * | ↓ | - | ↓ | ↓ |
| UMSCC47 | ↓ | ↓ | * | * | * | * |
| UPCI-SCC090 | - | - | ↓ | - | ↓ | ↓ |

↓: downregulated cell survival, ↑: upregulated cell survival, -: no impact, *: no data

Lastly, DNA-PKcsi that had the least impact as a monotherapy, showed the most promising results in combination with IR, in reducing cell survival in 2D clonogenic assays and 3D spheroid growth assays. DNA-PKcsi treatment resulted in statistically significant downregulation of colony formation, and therefore D_{50} values, in all HNSCC cells examined in response to x – rays. The impact was similar in response to protons, in 3 out of four HNSCC cell lines examined, although no impact could be observed in the HPV-positive UPCI- SCC090 cells, due to excess cell killing by protons in this inherently most radiosensitive cell line. Moreover, DNA-PKcsi exhibited the strongest radiosensitisation effect among the three drugs. This was also reflected by severe growth suppression in 4 HPV-negative (UMSCC74A, UMSCC6, FaDu, A253) HNSCC spheroids in response to low (1 Gy x – rays, 2 Gy protons) radiation dose. Inhibition of DNA-PKcsi was particularly effective in the radioresistant FaDu and A253 cell lines, resulting in severe radiosensitisation following either x – rays or low LET protons, which was not as evident following ATRi, but also ATMi in combination with x – rays, indicating increased DNA-PKcs dependence. Increase in the radiation dose up to 2 Gy x – rays or 4 Gy protons, minimised the radiosensitisation in all HPV-negative spheroids apart FaDu, although this remained statistically significant for UMSCC6, A253 and FaDu spheroids. Unfortunately, similarly to ATMi, no impact of the inhibitor could be observed in the radiosensitive UPCI-SCC090.

Table 6. 22. Impact of DNA-PKcsi in combination with x – rays or low LET protons on cell survival in 2D (clonogenic assay) D_{50} and 3D (spheroid growth assay) GSR.

| DNA-PKcsi | Clonogenic | | Spheroid | | | |
|-------------|------------|----------|----------|------|---------|------|
| | X - rays | Protons | X - rays | | Protons | |
| | D_{50} | D_{50} | 1 Gy | 2 Gy | 2 Gy | 4 Gy |
| UMSCC74A | ↓ | ↓ | ↓ | - | ↓ | - |
| UMSCC6 | ↓ | ↓ | ↓ | ↓ | ↓ | ↓ |
| FaDu | * | * | ↓ | ↓ | ↓ | ↓ |
| A253 | * | * | ↓ | ↓ | ↓ | ↓ |
| UMSCC47 | ↓ | ↓ | * | * | * | * |
| UPCI-SCC090 | ↓ | - | - | - | - | - |

↓: downregulated cell survival, ↑: upregulated cell survival, -: no impact, *: no data

In conclusion, the DSB repair inhibitors ATMi, ATRi and DNA-PKcsi were found to enhance the impact of IR in HNSCC cells *in vitro*, offering the potential to reduce the IR

associated toxicity. radiosensitisation with x – rays and low LET protons was observed in both HPV-negative as well as HPV-positive HNSCC cell lines, although arguably to a lesser extent in the later precisely due to their increased endogenous radiosensitivity. Remarkably, no major differences were observed on the impact of any of the drugs in response to x – ray versus low LET proton induced DNA damage. This highlights that DNA repair inhibition is a promising tool to be used for radiosensitisation in combination with either radiation type, as well as suggesting that corresponding DNA repair pathway choice occurs in response to x – ray or low LET proton induced DNA damage, which will be discussed in detail in the following chapter.

Chapter 7:

Discussion

7.1 Overview

Every day 10^4 DNA lesions per cell (base damages, single and double strand breaks, DNA strand cross-links and other) occur naturally in humans (239). DSBs, even though less frequent, are highly toxic and they can lead to a great loss of genetic information, mutations, or cell death, with all of these contributing to the development of human diseases, including premature aging, neurodegeneration and cancer (36). In defense of their genomic stability, cells have developed a signaling network, the DDR, which detect and repair any DNA lesions with specific repair mechanisms. There are two main repair pathways resolving DSBs: NHEJ and HR. Which pathway will be chosen is partly defined by the cell cycle stage, NHEJ is the predominant mechanism during G₀/G₁ and HR is only active during late S and G₂. Nevertheless, there are contributions of other factors such as the cell and tissue type, the DNA repair efficiencies as well as the type and the cause of DNA damage, which are not yet understood (240). Three protein kinases, ATM, ATR and DNA-PKcs, members of the PIKK, family of serine/threonine protein kinases, are actively involved in HR and NHEJ DSB repair (120, 241, 242). These repair mechanisms, although important for the cell proliferation, also contribute to tumor resistance in response to IR which complicates radiotherapy.

Radiotherapy is one of the three major cancer treatments, particularly for HNSCC where it is currently used alone or in combination with surgery and/or chemotherapy. This involves using IR to induce significant DNA lesions and particularly DSBs that promote tumor cell death. Conventional radiotherapy, using x – rays, is a well-studied and established treatment applied worldwide in the last century. In addition, proton beam therapy is increasingly being utilised for HNSCC treatment, due to precise delivery of the radiation dose to the tumor, resulting in sparing of the normal tissues and organs at risk. However, the biological impact of protons versus photons is largely unknown and debated, yet this basic knowledge is critical for the optimization of protons in clinical treatment.

HNSCC are a heterogenous group of cancers in the wider area of the pharynx, larynx, lip, oral and nasal cavity. HNSCC has been associated with excessive consumption of alcohol and tobacco products, as well as infection with the type 16 high risk HPV. Interestingly, HPV-positive HNSCC patients have improved survival rates compared to HPV-negative ones irrespective of the treatment (180-187). Although how the HPV associated cellular alterations respond to known therapies is not fully understood, recent studies have demonstrated that HPV-positive HNSCC cells are more sensitive to IR, mainly because of defects in the signaling and repair DSBs (188-191). This has revealed that targeting the DNA damage response, particularly in relatively radioresistant HPV-negative HNSCC that display proficient DNA repair mechanisms, may be an effective strategy for the radiosensitisation of the tumor.

Indeed, specific and potent inhibitors of the major DNA repair regulators exist and are widely used in research, either as monotherapy or in combination with DNA damaging agents, such as chemotherapy drugs and IR. Several studies have demonstrated that inhibition of ATM, ATR or DNA-PKcs can significantly sensitise and kill tumor cells in response to x – rays in various types of cancer cells such as breast, pancreatic, prostate and colon (120, 225, 226, 243). Also, this inhibition have been demonstrated to increase radiosensitivity of HNSCC cell lines in a few studies largely conducted during the course of this research project (209, 214, 227, 244-247) in response to x – rays. However, there is an urgent need to expand our knowledge in regard to the different impact of the DNA repair inhibitors on HPV-positive versus HPV-negative HNSCC cells, in order to exploit the potential of utilising such drugs in HNSCC therapy. Moreover, currently published studies utilising DNA repair inhibitors in combination with protons, in HNSCC but also in other tumours, are extremely limited. Considering the increased demand on proton radiotherapy, the implementation of such drugs to improve the therapeutic potential whilst minimising radiation associated risks and toxicity is necessary.

Here, three potent DNA repair inhibitors KU-55933 targeting ATM (ATMi), VE-821 targeting ATR (ATRi) and NU7441 targeting DNA-PKcs (DNA-PKcsi), directly associated with the repair IR (x – rays and protons) induced DSB, were utilised in HNSCC cells *in vitro* as a monotherapy or as a combination therapy with x – rays or low LET protons. The impact of the drugs was investigated on multiple end points, from the induction of

the DSB and initiation of DDR, to regulation of DSB repair progression and more importantly to the impact on HNSCC cell survival in 2D as well as in 3D spheroid models. It is worth noting, that direct comparison between the two radiation types was not the major target of this research project. Instead, the impact of the DNA repair inhibitors alone or in combination with IR, was investigated, as well as the differences in the inhibitor's impact in combination with either x – rays or protons. This was due to the fundamental differences of x – ray and proton irradiation, but more importantly due to the difference in the delivery technique. For x – ray irradiations, cells were treated in a laboratory x – ray unit operating at 100 kV, which is significantly less than e.g. 6MV x – rays used clinically, and with no filtration. Therefore, the low energy x – rays dominate, and LET is greater than ~ 2 keV/mm (typically quoted for 200kV x – rays), making x – rays potentially more efficient at producing DSB. For proton irradiations, cells were exposed to a passive scattered horizontal proton beam line of 60 MeV maximal energy and cells were positioned at the entrance dose of a pristine unmodulated beam, with LET of ~ 1 keV/ μm . This is resulting in an RBE significantly less than 1, hence the difference in the radiation doses chosen for proliferation experiments, 2D clonogenic assays and 3D spheroid growth assays.

7.2 DNA repair inhibitors delay or downregulate DDR activation.

The first end point investigated, was the phosphorylation of the protein kinases on sites associated with DSB repair. This was achieved via immunoblot analysis of protein levels within oropharyngeal HNSCC cells treated with either of the inhibitors in the absence or presence of IR. Phosphorylation was investigated at multiple time points, allowing adequate time for the involvement of the respective protein in the DDR. Immunoblotting was chosen to visualise the protein modifications as well as quantify the relative protein expression related to the specific treatment. This is a tool majorly used for semi-quantitative analysis and the detection of multiple proteins simultaneously, although is limited by low detection sensitivity (248, 249). As a monotherapy neither of the drugs had any significant impact in phosphorylation levels of any of the sites investigated and for all HNSCC cell lines examined, irrespective of the HPV status. This could suggest that the inhibitors alone did not regulate DDR in protein level, but more likely was associated with the low sensitivity of this technique,

considering that endogenous DSBs are at a very low level, and therefore significant activation of the respective kinases is not necessary (or at least is beyond the limits of detection). It was, therefore, further investigated via alternative end points.

The impact of ATMi was investigated on phosphorylation of ATM in S1981, which is reportedly activated through an intermolecular auto-phosphorylation in response to DSBs, and regulates a number of DNA repair proteins, such as H2AX, BRCA1, as well as proteins involved in cell cycle control, including p53 and Chk2, thus indirectly promoting DSB repair (124, 250). ATMi was found to effectively suppress ATM phosphorylation on S1981, up to 4 h post irradiation, in response to x – rays and low LET proton irradiation in oropharyngeal HNSCC cells. The drug was in fact equally effective in combination with either radiation modality. Similarly, ATMi has been reported to abrogate ATM phosphorylation on S1981 in a number of tumour cell models in response x – rays, including in E2 and G7 primary glioblastoma cell lines (251), in H460 lung cancer cells (252), and in LNCaP and PC3 prostate cancer cells (120). Such inhibition by ATMi was also observed in A549 lung adenocarcinoma cells in response to low LET protons and γ – irradiation (253), as well as in human embryonic stem (ES) cells in response to γ – irradiation (254). In addition, ATMi was also shown to downregulate S1981 phosphorylation in response to high LET carbon ion radiation, in AT5BIVA and GM0639 human fibroblast cells (255). Interestingly, my results demonstrated that the same ATM residue (S1981) was phosphorylated in response to damage induced by the two different radiation types, having similar activation levels following exposure to x – rays (between 4.2- to 12- fold) and low LET protons (between 4.2- to 10- fold). This was in contrast with a study utilising A549 lung adenocarcinoma cells, which suggested that low LET protons resulted in a massive activation of ATM in S1981 when compared to that induced by γ – radiation, that is an x – rays equivalent (253). This could possibly be explained by the relatively higher LET used in this study, 4 MeV protons versus 60 MeV protons used for the experiments in my thesis. Moreover, the impact of ATMi in suppressing activation of ATM was comparable between HPV-positive and HPV-negative oropharyngeal cell lines, indicating that the drug can be effective in both HNSCC tumour cell types.

ATR is activated in response to ssDNA structures that arise from stalled DNA replication forks and resected DNA DSBs, and in turn regulates numerous factors involved in both DNA repair and cell cycle control. Mass spectrometry revealed that activation of ATR is mediated through phosphorylation of three amino acids sites, S428, S435 and T1898. (137). Here, two of these sites were investigated following treatment with ATRi and/or IR exposure. Firstly, S428 phosphorylation was investigated, however exposure to either x – rays or protons, did not induce ATR phosphorylation on S428 up to 24 h in all oropharyngeal HNSCC cell lines irrespective of the HPV status. Therefore, no impact of ATRi in combination with IR could be observed through assessment of this specific site. This result could be an indication that phosphorylation of S428 within ATR is constant in the cells and that is independent of IR treatment and of ATRi. In fact, it has been suggested that phosphorylation of ATR in S428 is not DNA damage-regulated as it was not affected by hydroxyurea (HU) treatment in yeast (256) nor by UV treatment in 293E cells (137), with both studies suggesting that T1989 is the only critical phosphorylation site for ATR activation. Nevertheless, S428 phosphorylation has been reported to be upregulated in response to DNA breakage induced by 5,7,3',4'-tetrahydroxyisoflavone, a genistein metabolite (222). Next, T1989 phosphorylation within ATR, was investigated. Among the three sites, T1989 autophosphorylation has been identified to be the only site to regulate Chk1 and TopBP1 phosphorylation, in response to endogenous, UV induced, and IR induced DSBs, making it critical for ATR activation and thus DSB repair (137). This agreed with my findings which revealed that IR, x – rays and protons, upregulated T1989 phosphorylation *in vitro*. Treatment with ATRi delayed and decreased expression of ATR in T1989 in all 4 oropharyngeal HNSCC cell lines in response to x – rays as well as protons and for up to 24 h post IR exposure, with no major differences between the two radiation modalities. The impact of ATRi in combination with x – rays or protons on T1989 phosphorylation has not been previously reported. Although, there are few studies demonstrating similar findings regarding the inhibitors' impact on T1989 in combination with other DNA damaging agents. Indeed, ATRi in combination with Camptothecin or LMP-400 (indotecan), chemotherapeutic drugs known to produce replication-associated DSBs, suppressed T1989 phosphorylation up to 18 h post treatment, and downregulated the ATR mediated Chk1 S345 activation, in HT29 and COLO 205 colon cells, and MDA-MD-231 breast carcinoma cells (257).

Moreover, Chk1 S345 activation have also been demonstrated to be inhibited by ATRi, in response to γ – radiation (^{137}Cs radiation) and Gemcitabine, a chemotherapeutic DNA damaging drug, in pancreatic tumour cells (226). These findings along with those presented in this thesis, highlight that T1989 is the main DNA damage-regulator site for ATR activation in HNSCC cells, but importantly, that this site is targeted by ATRi irrespective of the HPV status and the DNA damage inducer, including photons and low LET protons.

Finally, two phosphorylation sites, T2609 and S2056, associated with DNA-PKcs activation and regulation of the DNA repair process, has been reported to promote the DNA-PK complex dissociation from the site of DSB allowing other NHEJ repair factors to access the site and progress repair (146-148). It was shown in this research project that T2609 phosphorylation peaked 1 h post irradiation in the HPV-negative cell lines but was delayed in the HPV-positive cell lines following x – rays, without any inhibitor treatment. The early peak can be explained considering the role of T2609 phosphorylation on initiating and promoting DNA end processing (151, 152). In a study utilising flow cytometry, T2609 phosphorylation was observed to peak shortly (within 30 minutes) after exposure to γ – radiation in human fibroblasts GM5758, GM16088 and AG07217 cells and in HCT116 colon cancer cells and A431 epidermoid SCC cells, all of which are proficient in DSB repair (258). This supported my data and moreover suggested that the inherent DSB repair deficiencies of HPV-positive cell lines are probably causing the delay in T2609 initiation in response to IR alone, without inhibitor treatment. Treatment with DNA-PKcsi, delayed T2609 phosphorylation post x - rays in one HPV-negative and one HPV-positive HNSCC cell line yet upregulated the overall phosphorylation in all HNSCC cell lines examined irrespective of the HPV status. Interestingly, the inhibitor also promoted DNA-PKcs cleavage in one HPV-positive (UMSCC47) HNSCC cell line. A similar delayed phosphorylation on T2609 has also been reported in response to DNA-PKcsi and γ – radiation, in a study utilising AG07217 and HCT116 cells, in addition to delayed dephosphorylation that was reported in the later time points (258). Moreover, increased phosphorylation on T2609, supporting my results, was demonstrated in LNCaP and PC3 prostate cancer cells following IR and DNA-PKcsi treatment (120). This could be associated with persistent unrepaired DSBs that correspondingly contributed to

increased apoptosis, shown by the increased DNA-PKcs protein cleavage, in the radiosensitive UMSCC47 cells. In contrast to the x – ray data, T2609 phosphorylation was downregulated following inhibitor and proton treatment with simultaneous upregulation of DNA-PKcs cleavage, indicating increased apoptosis in one (UMSCC74A) HNSCC cell line, although no impact could be observed in the second cell HNSCC cell line examine (HPV-positive UMSCC47) and therefore it was not feasible to reach safe conclusions. In addition, there are currently no published data examining this aspect and was not further investigated in this research project.

Phosphorylation on DNA-PKcs S2056 was assessed and found to peak 8 h post IR, both x – rays and protons, in all oropharyngeal HNSCC cells. Considering that S2056 is reported to promote DSB ligation which occurs in the final steps of DSB repair (151), the later peak in phosphorylation was expected. DNA-PKcsi downregulated phosphorylation of DNA-PKcs on S2056 in all 4 HNSCC cell lines in response to x – ray as well as proton irradiation. In agreement with this, studies have reported that inhibition of DNA-PKcs resulted in reduced S2056 phosphorylation in MCF-7, MDA-MB-231, and T47D breast cancer cells (243), and in LNCaP and PC3 prostate cancer cells (120), following DNA-PKcsi and IR treatment. In addition, formation of S2056 foci has previously been shown to be inhibited by DNA-PKcsi in human epithelial cells in response to γ – radiation (^{137}Cs) (259). On the other hand, no evidence of the inhibitor's impact on S2056 in response to proton radiation has previously been reported. It is worth noting that following proton irradiation, the inhibitor severely upregulated DNA-PKcs protein cleavage in all oropharyngeal HNSCC cell lines, in comparison to x – rays, suggesting that protons were more effective than x – rays in inducing apoptosis in DNA-PKcsi treated cells, irrespective of the HPV status. This may possibly indicate that protons induce marginally more complex DNA damage that is trickier to be resolved and which contributes more to cell death. Nevertheless, these findings described here suggest that the inhibitor effectively suppressed S2056 phosphorylation in response to both x – rays and low LET protons.

In conclusion, ATMi, ATRi, and DNA-PKcsi were found to target and inhibit phosphorylation on the respective protein sites critical to DSB repair, and therefore to impede the cellular DDR. The impact of the three protein kinase inhibitors in response

to x – ray or proton irradiation was further examined in regards to their role in DDR and cell survival.

7.3 DNA repair inhibitors delay and downregulate DDR signalling

Three DDR signalling markers, γ H2AX, 53BP1 and Rad51 associated with DSB repair via NHEJ and HR, were investigated. Exposure to IR rapidly phosphorylates the H2AX variant and generates γ H2AX foci, which is mediated by ATM and DNA-PKcs. These foci surround DSBs, in a manner of one focus per DSB, attracting other DNA repair factors (120, 225, 228). Simultaneously, 53BP1 foci, markers of DSB repair processing through NHEJ, are formed and colocalise with γ H2AX foci in an ATM, and DNA-PKcs dependent manner. γ H2AX foci are not involved in the initial recruitment of 53BP1 yet are required for the stable formation and retention of 53BP1 foci (207, 228, 229). Later in the cell cycle, Rad51 foci regulated by ATM and ATR, highlight the sites where DSB repair are being processed via HR (230, 231).

In the absence of IR there was generally no effect on DNA repair foci formation in oropharyngeal HNSCC cells following inhibition of ATM, ATR and DNA-PKcs. γ H2AX foci were mildly upregulated only following ATRi, suggesting a possible increase in endogenous DSB recognition or induction by the drug alone. 53BP1 foci were only downregulated in the presence of DNA-PKcsi, demonstrating that the inhibitor reduced the endogenous recruitment of 53BP1 in the sites of DSB repair via NHEJ. Finally, Rad51 foci were marginally upregulated in the HPV-negative UMSCC6 cells only, in response to ATMi or ATRi, indicating that both drugs affected Rad51 recruitment, possibly due to accumulated DSBs later in the cell cycle. Unfortunately, the amount of foci in non irradiated cells is relatively low, implicating the comparison of DMSO versus drug treatment, resulting in reduced sensitivity in detection of the drug's impact. Nevertheless, these findings suggested that the inhibitors could regulate DSB repair even in the absence of IR.

In response to IR, formation of γ H2AX foci were not majorly impacted by ATRi in any of the oropharyngeal HNSCC cell lines examined, which was expected given that phosphorylation of H2AX has been demonstrated to be predominantly independent of

ATR (228). ATMi in combination with either x – rays or protons, delayed and decreased γ H2AX foci 1 h post IR exposure. Similarly to my findings, ATMi in combination with IR was shown to decrease γ H2AX foci in LNCaP and PC3 prostate cancer cells (120). In addition, this study suggested that ATM is the major kinase responsible for H2AX phosphorylation and that DNA-PKcs is unable to phosphorylate H2AX in the absence of ATM, although they presented increased γ H2AX foci in the later time points after treatment with DNA-PKcsi. Interestingly, this was in accordance with my results where DNA-PKcsi did not delay the foci formation, however it increased the amount of γ H2AX foci 4h and 8 h post irradiation, indicating increased persistency of DSB in the later time points following x – rays as well as protons. The same trend was exhibited in LoVo and SW620 human colon cancer cells, where increased γ H2AX persistency was reported following DNA-PKcsi and x – rays or Etoposide treatment (109). The DSB accumulation in later time points post inhibitor and IR treatment could be correlated to the downregulated S2056 phosphorylation, that led to reduced dissociation of the DNA-PK complex, prohibiting repair and therefore promoting DSB retention. My findings highlighted that the impact of the inhibitors on γ H2AX did not differ between x – rays and protons, suggesting an equivalent degree of DDR signaling in response to the two radiation types which was also not associated with HPV status.

The initial recruitment and phosphorylation of 53BP1 is dependent on the activation of ATM and DNA-PKcs, but not of ATR since this protein kinase is not directly involved in NHEJ repair (190, 228, 229). Indeed here, 53BP1 foci formation and retention was not majorly impacted by ATRi treatment in combination with x – rays or protons in HNSCC cells, confirming that ATR is not directly involved with NHEJ repair. Increase in 53BP1 foci was only observed in one HNSCC cell line, UMSCC47 which are HPV-positive 1 h post proton irradiation highlighting a possible cell line dependent on ATR involvement in 53BP1 recruitment for DSB repair. Interestingly, a similar increase was shown in pancreatic tumor cell lines, PSN-1, MiaPaCa-2 and PANC-1, following ATRi treatment and exposure to 6 Gy γ – radiation (^{137}Cs) (226). Moreover, I found that ATMi treatment, which induced a decrease in γ H2AX foci formation 1 h post x – rays or proton irradiation, also resulted in reduced 53BP1 foci formation in response to x – rays at the same time point (1 h post IR). This has been observed following ATMi treatment and exposure to γ

– radiation (^{137}Cs), in bladder cancer cells, T24 and 5637, (260) and in human fibroblast cells, GM05757, GM18366 and GM02052 (261), as well as in primary human fibroblasts, HLEC1 and WI-38, following ATMi and x - rays (262). However here, there was no apparent reduction in 53BP1 foci formation 1 h post proton irradiation in the presence of ATMi. In fact, 53BP1 foci exhibited increased persistency 8 h post protons, in all cell lines, indicating unrepaired DSB and thus ongoing NHEJ in all oropharyngeal HNSCC cell lines examined. This possibly pinpoints to increased complexity of the DNA damage induced by protons, which is more difficult to be repaired in the presence of ATMi, resulting in DSB persistence. Next, my results demonstrated that DNA-PKcsi induced increased amount of 53BP1 foci and increased persistency in the later time points, particularly 8 h post exposure to x – rays and 4 h post proton irradiation. This was in agreement with other studies that suggested that DNA-PKcsi upregulated the amount of 53BP1 foci in primary human fibroblasts, HLEC1 and WI-38, following x – ray irradiation (262), and in A549 lung adenocarcinoma cells following treatment with DNA damaging agents AMR, CPT-11 and paclitaxel (PTX) (Topoisomerase-I inhibitors) from 1 h to 24 h post irradiation (263). It is worth noting that in the results shown here, 53BP1 foci peaked 8 h post treatment with DNA-PKcsi and x – rays, following the same trend as γH2AX , and suggesting accumulated DSB levels and thus ongoing NHEJ repair that could be associated with the downregulated S2056 phosphorylation, discussed above. However, the number of 53BP1 foci peaked at 4 h post DNA-PKcsi and proton treatment, demonstrating greater amount of DSB accumulating earlier following protons compared to x – rays, possibly due to increased complexity of the DNA damage induced. Then by 8 h, the number of 53BP1 foci in DNA-PKcsi treated cells dropped to the DMSO levels. This could be linked with increased apoptosis, which was also demonstrated by the increased cleavage of DNA-PKcs following DNA-PKcsi and proton treatment observed by immunoblotting and discussed above. My findings are supported by a study indicating that the number of 53BP1 foci was greater and persisted for longer following x – rays compared to low LET protons in A549 adenocarcinoma cells treated with the DNA-PKcs inhibitor, NU7026 (118). It was also suggested that DNA-PKcs is the major protein kinase and NHEJ repair the lead repair pathway following x – rays but not following proton irradiation. However, my findings would conflict with this evidence and largely indicate

that NHEJ repair is the major DSB repair mechanism following both radiation modalities, as inhibition of either ATM or DNA-PKcs resulted in defective DSB repair.

Later on the time course, phosphorylation of Rad51 highlights the sites where DSBs are repaired through HR. Taking into account that HR is driven by ATM and ATR protein kinases while DNA-PKcs is not directly involved (120-122), no effect on Rad51 foci formation was expected following DNA-PKcs inhibition while a reduction was anticipated following ATR and ATM inhibition. Indeed, my results illustrated a relative decrease in Rad51 foci in the presence of ATMi 16 h post IR, but that this was significantly greater with ATRi at the same time point, 16 h post IR. It should be pointed out that no major difference was observed on the ATMi and ATRi impact in combination with x – rays versus protons, with the exception of ATMi treated UMSCC47 where Rad51 foci were considerably more reduced following protons than x – rays. In agreement with my findings, ATMi was shown to reduce Rad51 foci in HeLa cells exposed to the DNA damaging agent CPT (camptothecin, topoisomerase I inhibitor used in chemotherapeutic drugs) (264). Additionally, ATRi was shown to severely downregulate Rad51 foci formation 6 h post γ – radiation (^{137}Cs) in pancreatic tumor cell lines, PSN-1 and MiaPaCa-2, although this study suggested that ATMi had no significant impact on Rad51 foci formation or persistence (226). Surprisingly, my results showed that DNA-PKcsi led to an upregulation of Rad51 foci at 16 h (UMSCC6, UMSCC74A HNSCC cells) and 24 h (all 3 cell lines examined) post x – rays but not following proton irradiation. In support of that, elevated Rad51 foci (by 3- fold), were reported following DNA-PKcsi and IR or doxorubicin treatment in 6 hepatoma cell lines HepG2, Hep3B, Huh7, SNU-182, SNU475 and PLC/PRF/5 (265). This unexpected outcome could be explained by a possible increased involvement of ATM/ATR when DNA-PKcs is unable to act earlier in the cell cycle. Thus, a blocked NHEJ pathway could be substituted by HR or other alternative pathways for the resolution of DSBs. In fact, DNA-PKcs is proposed to be critical in the DSB repair pathway choice, between NHEJ and HR, and that modulation of DNA-PKcs phosphorylation sites can promote either NHEJ or HR, the latter case where accurate repair is required (153, 154). In contrast though, DNA-PKcsi treatment in combination with proton irradiation from my data resulted in decreased Rad51 foci formation, at 16 h post irradiation. One explanation for this contradicting result could

be a possible association with increased cell death, i.e. apoptosis, as observed by the increased DNA-PKcs protein cleavage specifically following protons when compared to x – rays. Therefore, less cells could survive and undergo HR, resulting in reduced Rad51 foci formation, although this requires further investigation. This highlights the important role of DNA-PKcs in DSB repair following protons, as well as a possible role for a more complex nature of the DNA damage induced by protons causing the increased apoptosis. Altogether, inhibition of ATM, ATR and DNA-PKcs was shown to lead to a defective DNA repair process through the analysis of surrogate DSB protein markers. It appears that the role of each kinase in DSB repair is overlapping but non-redundant and there must be a more complex interaction between them through co-ordination of NHEJ and HR. More detailed studies are necessary in order to fully understand the way the repair pathways are affected by the kinase's inhibition, which was not a major scope of this research project.

7.4 DNA repair inhibitors reduce cell survival.

In the final part of this study, I analysed the effect of ATMi, ATRi and DNA-PKcsi on cell growth and proliferation on both monolayer 2D cultures, and 3D spheroid models of HPV-positive and HPV-negative HNSCC in combination with x – ray and proton irradiation. Particularly in the spheroid assays, multiple HNSCC cell lines (from oropharynx, hypopharynx and oral cavity) were examined, displaying different endogenous capacities for DNA repair and thus better representing the heterogeneous HNSCC group. Whilst the major focus was an examination of the impact of the inhibitors in combination with IR, treatment with these as a monotherapy revealed reduced colony formation and spheroid growth by ATRi in particular, and by ATMi to a lesser degree. Nevertheless, DNA-PKcsi was not found to significantly inhibit cell survival and proliferation either in 2D nor in 3D.

Interestingly, I discovered that targeting either ATM, ATR or DNA-PKcs can significantly decrease clonogenic survival of oropharyngeal HNSCC cells in response to both x – rays and protons. Although a tailing was observed in the higher IR doses in clonogenic assays in the inhibitor treated cells, which seemed to be seen across cell types and for both x-

ray and protons and consistently occurred just above the 1 % survival level. This may be related to the limitation of the current assay due to low plating efficiency and the respective small colony numbers. This could be tested by scaling up the number of dishes irradiated, and therefore surviving colonies, for these data points and may be checking for potential false positives, such as small abortive colonies, in the scoring. Between the three drugs, DNA-PKcsi appeared to be particularly effective in combination with both of the radiation modalities in all HNSCC cell lines. My findings correlated with other studies, particularly in HPV-negative HNSCC cells, which reported enhanced radiosensitisation in 2D clonogenic survival assays *in vitro*, utilising DNA-PKcs siRNA in UTSCC15 and UTSCC45 cells (266), as well as the DNA-PKcs inhibitors KU0060648 in HN4 and HN5 cells (244), and IC87361 in UTSCC54, UTSCC74B and UTSCC76B cells (245). Similarly, a study examining ATM inhibition in HNSCC cells, using the ATM inhibitor GSK635416A, reported enhanced radiosensitivity in five HPV-negative HNSCC cell lines (UTSCC2, UTSCC8, UTSCC24A, UTSCC36 and UTSCC40) which was in agreement with my results (209). In addition, a number of studies have focused on ATR as a target. Increased cell killing was reported following x – ray irradiation and ATR siRNA treatment in HPV-negative HNSCC cells UPCI-SCC029B, UPCI-SCC040 and UPCI-SCC131 (210). Improved radiosensitivity and reduced colony formation was also demonstrated following ATRi treatment and exposure to IR in HPV-negative SQ20B cells (246). An alternative and more potent ATR inhibitor, AZD6738, showed equivalent radiosensitisation in Cal27, FaDu, HN4 and HN5 cells, all of which are HPV-negative (214, 244). Nevertheless, my data suggested that ATRi was the least effective of the three drugs used, in radiosensitising HNSCC cells following both x – rays and proton radiation, most likely due to increased cell killing by the drug alone that resulted in reduced overall impact when combined with IR. I also observed less of an impact on DNA DSB repair inhibition in combination with radiation in HPV-positive oropharyngeal HNSCC cells, particularly the UPCI-SCC090 cells, principally as these are the most inherently radiosensitive as shown here, and in previous study of the Parsons group (207). This also replicates the improved response and outcome of HPV-positive HNSCC patients following radiotherapy treatment (188-191). However, how protons impact on survival on HNSCC, as well as other cancer, cell lines is largely understudied. On top of that, the impact of DSB repair inhibitors in combination with proton radiation on cell survival has

not been analysed previously. This highlights the novelty of the results presented in this research project, particularly regarding the proton data, as well as the necessity for further studies on that direction, considering the increasing demand for proton radiotherapy.

Next, utilising 3D spheroid models that more accurately replicate the structure and environment of the original tumour, the effectiveness of DNA repair inhibitors was further demonstrated. In support of the clonogenic survival assays, all of the three drugs impacted spheroid growth particularly in the relatively more radioresistant HPV-negative HNSCC models. DNA-PKcsi in combination with either x – rays or protons was the most prominent in inhibiting growth of all four HPV-negative HNSCC spheroids analysed, including those from the oropharynx, hypopharynx and oral cavity. Noticeably though, inhibition of DNA-PKcs alone did not appear to have any impact on the growth of 3D spheroids of both HPV-positive and HPV-negative HNSCC, and indicates that DNA-PKcs is not essential for HNSCC cell growth and survival in the absence of IR-induced stress. Likewise, treatment with ATMi significantly suppressed growth in just one out of four HPV-negative HNSCC spheroid model in the absence of IR, yet was found to significantly suppress spheroid growth in all four HPV-negative HNSCC spheroids exposed to either x – rays (2 Gy) or proton (2 Gy) irradiation. Nevertheless, and similar to clonogenic assays results, the combination strategy of DSB repair inhibition, particularly ATMi and DNA-PKcsi, did not majorly enhance the effect of x – rays and protons on the HPV-positive HNSCC spheroids due to these cells being the most radiosensitive. Inhibition of ATR was effectiveness in preventing spheroid growth in combination with x – rays or protons. In fact, growth was significantly suppressed in three out of four HPV-negative HNSCC spheroid models following 1 Gy or 2 Gy x – rays, while growth was significantly suppressed in two out of four HPV-negative HNSCC spheroid models following 2 Gy or 4 Gy protons. Interestingly, less of an impact was observed on the relatively radioresistant HPV-negative HNSCC spheroid models, FaDu and A253, that displayed significant spheroid growth over the time period post irradiation and required higher radiation dose to be suppressed. This observation is similar to previous data utilising the ATR inhibitor AZD6738, with x – rays only, which demonstrated that this combination did not impede growth of 3D spheroids of FaDu

cells (214). It is noteworthy that inhibition of ATR as a monotherapy, in the absence of IR, was effective in preventing growth of three out of four HPV-negative as well as the one HPV-positive HNSCC spheroids, which was comparable to the impact caused by a single dose of radiation alone. Overall, relatively similar results were observed in the effectiveness of the drugs when combined with x – rays or protons. However, following x – rays the impact of each drug was enhanced when higher radiation dose was applied (from 1 Gy to 2 Gy), while following protons the impact was reduced at the higher radiation dose (from 2 Gy to 4 Gy) due to excessive cell killing by proton irradiation alone. This may further support the hypothesis that even low LET protons induce more complex DNA damage comparative to x-rays, which is contributing to enhanced cell death.

Cumulatively, my results suggest that targeting DNA DSB repair via NHEJ (ATM and DNA-Pkcs) or HR (ATR) can exacerbate the impact of IR in sensitising HNSCC cell models. This adds to the growing preclinical evidence (209, 210, 214, 227, 244-247, 266) that targeting DSB repair is an effective combination for treatment of HNSCC that should be investigated further. Moreover, I propose that DNA-PKcsi was the most effective treatment, followed by ATMi, in enhancing the therapeutic potential of IR, x – rays as well as low LET protons, in HNSCC cells and especially for HPV-negative cell lines that are relatively radioresistant. Finally, ATRi was the most effective drug utilised as monotherapy in sensitising both HPV-negative and HPV-positive HNSCC cells, although in combination with IR, ATRi was the least effective drug precisely due to suppressed cell survival by the drug alone. This finding would contradict some very limited evidence suggesting a greater dependence on the HR pathway mediated by ATR for repairing DNA DSBs induced by protons, which was conducted using RAD51 siRNA in A549 lung cancer cells (118). In fact other studies, largely conducted in Chinese hamster ovary cells, reflect that NHEJ, co-ordinated by ATM and DNA-PKcs, is the major DSB repair pathway employed following proton irradiation (105, 116), which is in agreement with my findings. Consequently, we would advocate that inhibition of NHEJ through DNA-PKcs is the most promising strategy in optimizing radiosensitisation of HNSCC cells with either x – rays or low LET protons. Nevertheless, it should be noted that since low LET protons at the entrance dose of a pristine beam were utilised, different results may be obtained

with cells irradiated at or around the Bragg peak where the LET increases. This is due to the increased amount of complex DNA damage, where multiple lesions are generated in close proximity, which the Parsons Group have demonstrated are important for contributing to the cell killing effects of protons with increasing LET (114, 267). Therefore, the potential for protons to generate complex DNA DSBs that could have a different requirement for either NHEJ or HR, requires further investigation (268).

7.5 Future perspectives

The findings of this thesis lead to the proposal that inhibition with ATMi, ATRi and DNA-PKcsi can be used to suppress the repair of x – rays and protons induced DSBs and promote cell killing. However, and specifically following DNA-PKcsi treatment, increased DNA-PKcs protein cleavage was observed in response to protons compared to x – rays in the majority of the cell lines examined. Further investigation of this difference between the two radiation modalities in relation to cell death initiating mechanisms is required, as it could bear relevance to increased apoptosis which I hypothesise is due to increased complexity of DNA damage induced by protons, even at low LET entrance dose utilised in this project. Therefore, it would be interesting to examine the importance of apoptosis in the various cell lines and whether induction is different following x-rays and protons in the presence of the DSB inhibitors, and particularly in response to DNA-PKcsi treatment. This could be achieved via several independent techniques. The first one would be via investigation of poly(ADP-ribose) polymerase-1 (PARP-1) cleavage which is commonly used as a marker of apoptosis, as the 113 kDa nuclear enzyme is cleaved in fragments of 89 and 24 kDa by caspases 3 and 7, during apoptosis (269). The second technique would be to investigate apoptosis via Fluorescence-activated cell sorting analysis. During this, cells treated with the inhibitor and/or IR, as well as control cells, are stained with Annexin V and propidium Iodide solution and then are imaged by flow cytometry. Cells are hydrophobic in nature and express phosphatidyl-serine in the inner membrane, but during apoptosis the inner membrane flips exposing phosphatidyl-serine residues, which are detected by Annexin V. Moreover, the leaky DNA content exhibited in necrotic cells is detected by propidium Iodide and can therefore differentiate between apoptotic and necrotic cells (270, 271). Considering the findings

of this thesis, I would expect increased PARP-1 cleavage, as well as increased number of Annexin V stained apoptotic cells, following DNA-PKcsi and proton irradiation compared to DNA-PKcsi treatment and x – rays.

During this research project, I was able to investigate DDR signaling alterations caused by the DSB repair inhibitors in response to IR. Some unexpected findings included increased persistency in 53BP1 foci at the later time points following ATMi and protons compared to ATMi and x – rays. It is reasonable to suggest that the ongoing 53BP1 recruitment revealed persistent DSBs that were trickier to be resolved, which I believe is an indicator of the increased complexity of proton induced DNA damage. Moreover, the impact of DNA-PKcsi on DDR signaling differed in response to x – rays and protons. Formation of γ H2AX and 53BP1 foci peaked earlier, at 4 h post protons versus 8 h post x – rays, while Rad51 foci were decreased in response to protons compared to x – rays. The reason for this difference could also be related to the increased complexity of proton induced DNA damage. Therefore, it would be necessary to examine complex DNA damage (CDD) levels. There are several techniques to achieve that. The Parsons group recently suggested using enzyme-modified comet assays, where recombinant DNA repair enzymes (APE1, OGG1, and NTH1) were used to incise residual DNA base damage and abasic sites to allow for CDD detection (114, 267). Others suggested detection of co-localisation of OGG1/APE1 with γ H2AX by immunofluorescence, as an alternative approach (48, 272). Increased CDD levels, may lead to increased apoptosis and therefore to less cells being actively repaired. This further demonstrate that it would be particularly interesting to examine apoptotic levels following inhibitor treatment and IR as described above.

Clonogenic assays and 3D spheroid growth analysis, which better represents the tumour environment, performed in this thesis have proven that all three inhibitors severely impacted on the sensitivity of HNSCC cells to both x – rays and protons, and particularly to relatively radioresistant HPV-negative cell lines. This constitutes a promising starting point for future studies on improving radiotherapeutic results. At this point, it would be particularly interesting to investigate the impact of hypoxia within the 3D spheroids during IR exposure on the oxygen enhancement ratio (OER) in HNSCC spheroids, considering that the central cells are tightly packed and have reduced access to oxygen

and other nutrients. This could be achieved by sectioning of spheroids and looking at necrosis or mitotic catastrophe levels in the central region of the spheroids. The next logical step would be the use of these inhibitors on patient-derived xenograft (PDX) or patient-derived organoids (PDO). PDX, are generated when tumour tissue is transplanted on immunodeficient mice and is considered advantageous over cancer cell lines as they better resemble the biological characteristics of the primary tumours and more efficiently predict drug responses, although they are cost ineffective and time- and resource-consuming (273). On the other hand, PDOs are 3D cell clusters, growing in 3D gel matrixes, that form an organ-like tissue which retain the physiological characteristics and function of their source tumour, including histological complexity, and genomic and transcriptomic characteristics. This results on PDOs being more consistent with the real patient response to drugs than either cancer cell lines or PDX, and they offer a great potential for disease modeling for cancer research and anticancer drug screenings (274-277). That been said, it would be interesting to examine the impact on DSB repair inhibition in response to x – rays as well as protons in PDO in particular.

Furthermore, during this research project low LET proton irradiations were performed. Cells were positioned at the entrance dose of a pristine (unmodulated) beam (~1 keV/ μ m) and were exposed to a passive scattered horizontal proton beam line of 60 MeV maximal energy and cells. As discussed above, different results may have been obtained if cells were irradiated at or around the Bragg peak where the LET rapidly increases due to the increased amount of complex DNA damage, where multiple DSBs are generated in close proximity, contributing to increased cell killing effects. Therefore, it would be particularly interesting to further examine the potential for high LET protons versus low LET protons and x – rays, performed in this research project, as monotherapy but more so in combination with DSB repair inhibitors, to radiosensitise HNSCC *in vitro*. This would also offer the opportunity to investigate whether generation of more complex DNA DSBs would have a different requirement for either NHEJ or HR which constitutes a conflict in current literature (105, 116, 118, 268)

Another area for future extension of this research project would be to investigate the impact of DSB repair inhibitors in combination with IR on other cancer cells and more importantly to explore the response on relevant normal cells, as ideally the treatment

should be more biologically effective against cancer cells compared to normal cells. Moreover, the use of newer and more potent of DSB repair inhibitors than the ones used here, which only recently became available for research purposes, could be investigated. Specifically, selective inhibitors targeting ATM (e.g. AZD1390), ATR (e.g. AZD6738) and DNA-Pkcs (e.g. AZD7648), would require examination of their potential to radiosensitise HNSCC cell models following x – rays and proton irradiation. The way this investigation could be performed is through the standard techniques utilised in this research project, including clonogenic assays and 3D spheroid growth assays, or with more advanced techniques like PDO cultures discussed above.

Finally, it is also important to note that clinical trials are currently using DSB repair inhibitors, aiming to exploit the potential of combination treatments to improve the radiotherapeutic outcome and reduce radiation associated toxicities. There is evidence of clinical trials utilising either ATM inhibitors (AZD0156) or DNA-PKcs inhibitors (NU7441-used in this thesis-, CC-115, C-122, VX-984 and MSC2490484A) in combination with conventional radiotherapy or other DNA damaging agents that are currently underway in HNSCC, as well as in other advanced solid tumors but also in healthy volunteers (208, 278, 279). In addition, ATR inhibitor VE-822 in combination with Cisplatin, a chemotherapeutic drug that induce replication fork collapse, is being tested in an ongoing phase 1 clinical trial in HPV-negative HNSCC patients. Another ATR inhibitor, AZD6738, is tested in clinical trials for multiple cancer types as monotherapy or in combination with radiotherapy, chemotherapy or Olaparib (214, 279, 280) and there are two clinical trials examining combination of AZD6738 with Olaparib in HNSCC (208).

7.6 Conclusions

In this research project, the impact of targeting the DSB repair mechanisms in response to IR was investigated via inhibition of the protein kinases ATM, ATR and DNA-PKcs that co-ordinate DSB repair. X – ray irradiation, a well-established tool in cancer radiotherapy, and proton irradiation, a rapidly utilised radiotherapy technique clinically, were examined. DSB repair inhibition impacted cell behavior on multiple levels. From regulating phosphorylation on critical sites of the targeted protein kinases and DNA

repair signaling, to reducing survival and enhancing sensitivity to IR in 2D and 3D in HNSCC cell models. Overall, the main outcomes of this project included:

- ATMi, ATRi, and particularly DNA-PKcsi, enhanced radiosensitivity of 2D monolayer and 3D spheroid models of HNSCC *in vitro* in response to both radiation modalities, x – rays and protons,
- ATMi, ATRi and DNA-PKcsi were more prominent in increasing radiosensitivity of the HPV-negative HNSCC cells, in comparison to HPV-positive HNSCC cells that are intrinsically more radiosensitive.
- NHEJ, driven by ATM and DNA-PKcs, is proposed to be the major DSB repair mechanism for responding to both x-ray and low-LET proton irradiation in HNSCC cells.
- The impact of the three drugs did not majorly differ in IR induced protein activation and DDR signaling between HPV-negative and HPV-positive HNSCC cells.
- Low LET protons may induce more complex DNA damage compared to x – rays, which is likely to trigger increased cell death.

The work described in this research project is important as it has investigated the potential of combination therapy of DSB repair inhibitors and IR in HNSCC cells. This applied not only to the well-studied x – rays, but also to proton irradiation, whose radiobiological impact has been relatively understudied. Therefore, this thesis has contributed to widening our knowledge and understanding not only on the impact of each radiation type alone, but also on their impact in combination with DSB repair inhibition *in vitro*. A long-term goal is the use of the findings presented in this study, showing the potential of DSB repair inhibition to improve the radiotherapeutic outcome in HNSCC, while reducing radiation associated toxicities, which can contribute to increased effectiveness of IR (x – rays and protons) in the effective treatment of HNSCC patients, and to significantly improve patient outcome and survival.

References

1. Allisy-Roberts P, Williams J. Chapter 1 - Radiation physics. In: Allisy-Roberts P, Williams J, editors. *Farr's Physics for Medical Imaging (Second Edition)*: W.B. Saunders; 2008. p. 1-21.
2. Sridharan K. Chapter 1 - The Electromagnetic Spectrum. In: Sridharan K, editor. *Spectral Methods in Transition Metal Complexes*: Elsevier; 2016. p. 1-12.
3. Hall EJ, Cox JD. Chapter 1 - Physical and Biologic Basis of Radiation Therapy. In: Cox JD, Ang KK, editors. *Radiation Oncology (Ninth Edition)*. Philadelphia: Content Repository Only!; 2010. p. 3-49.
4. Yu H, Chen X, Zhou Y, Chen D, Zhang L. Impact of photoelectric effect on X-ray density logging and its correction. *Applied Radiation and Isotopes*. 2020;156:108785.
5. Scannavino FA, Cruvinel PE. A graphical tool for an analytical approach of scattering photons by the Compton effect. *Nuclear Instruments and Methods in Physics Research Section A: Accelerators, Spectrometers, Detectors and Associated Equipment*. 2012;674:28-38.
6. Mozumder A. Chapter 2 - Interaction of Radiation with Matter: Energy Transfer from Fast Charged Particles. In: Mozumder A, editor. *Fundamentals of Radiation Chemistry*. San Diego: Academic Press; 1999. p. 5-39.
7. Ahlen SP. Theoretical and experimental aspects of the energy loss of relativistic heavily ionizing particles. *Reviews of Modern Physics*. 1980;52(1):121.
8. Laughlin JS. *The Physics of Radiology*. 4th ed. Radiology. 1984;152(1):194-.
9. Obodovskiy I. Chapter 5 - Passing of Charged Particles Through Matter. In: Obodovskiy I, editor. *Radiation*: Elsevier; 2019. p. 103-36.
10. Obodovskiy I. Chapter 7 - Interaction of Neutrons With Matter. In: Obodovskiy I, editor. *Radiation*: Elsevier; 2019. p. 151-60.
11. Kónya J, Nagy NM. Chapter 5 - Interaction of Radiation With Matter. In: Kónya J, Nagy NM, editors. *Nuclear and Radiochemistry (Second Edition)*: Elsevier; 2018. p. 85-131.
12. L'Annunziata MF. Chapter 4 - Alpha Radiation. In: L'Annunziata MF, editor. *Radioactivity (Second Edition)*. Boston: Elsevier; 2016. p. 123-34.
13. Baltas D, Sakelliou L, Zamboglou N. *The physics of modern brachytherapy for oncology*: CRC Press; 2006.
14. L'Annunziata MF. Chapter 6 - Beta Radiation and Beta Decay. In: L'Annunziata MF, editor. *Radioactivity (Second Edition)*. Boston: Elsevier; 2016. p. 167-201.
15. L'Annunziata MF. Chapter 8 - Electromagnetic Radiation: Photons. In: L'Annunziata MF, editor. *Radioactivity (Second Edition)*. Boston: Elsevier; 2016. p. 269-302.
16. Healy B, van der Merwe D, Christaki K, Meghzifene A. Cobalt-60 machines and medical linear accelerators: competing technologies for external beam radiotherapy. *Clinical Oncology*. 2017;29(2):110-5.
17. Jerusalem G, Hustinx R, Beguin Y, Fillet G. PET scan imaging in oncology. *European journal of cancer*. 2003;39(11):1525-34.
18. Percuoco R. Chapter 1 - Plain Radiographic Imaging. In: Marchiori DM, editor. *Clinical Imaging (Third Edition)*. Saint Louis: Mosby; 2014. p. 1-43.

19. Elliott DA, Nabavizadeh N, Seung SK, Hansen EK, Holland JM. 13 - Radiation Therapy. In: Bell RB, Fernandes RP, Andersen PE, editors. *Oral, Head and Neck Oncology and Reconstructive Surgery*; Elsevier; 2018. p. 268-90.
20. Nachbar M, Mönnich D, Boeke S, Gani C, Weidner N, Heinrich V, et al. Partial breast irradiation with the 1.5 T MR-Linac: First patient treatment and analysis of electron return and stream effects. *Radiotherapy and Oncology*. 2020;145:30-5.
21. Menten MJ, Mohajer JK, Nilawar R, Bertholet J, Dunlop A, Pathmanathan AU, et al. Automatic reconstruction of the delivered dose of the day using MR-linac treatment log files and online MR imaging. *Radiotherapy and Oncology*. 2020;145:88-94.
22. Arns A, Wertz H, Boda-Heggemann J, Schneider F, Blessing M, Abo-Madyan Y, et al. Ultrafast single breath-hold cone-beam CT lung cancer imaging with faster linac gantry rotation. *Radiotherapy and Oncology*. 2019;135:78-85.
23. Kuriyama K, Onishi H, Sano N, Komiyama T, Aikawa Y, Tateda Y, et al. A new irradiation unit constructed of self-moving gantry-CT and linac. *International Journal of Radiation Oncology*Biophysics*Physics*. 2003;55(2):428-35.
24. Tommasino F, Durante M. Proton radiobiology. *Cancers (Basel)*. 2015;7(1):353-81.
25. Obodovskiy I. Chapter 18 - Accelerators. In: Obodovskiy I, editor. *Radiation*; Elsevier; 2019. p. 275-87.
26. vane CR, Datz S. 10 - Accelerator-Based Atomic Physics. In: Dunning FB, Hulet RG, editors. *Methods in Experimental Physics*. 29: Academic Press; 1995. p. 299-320.
27. Du S, Zou C, Ding K, Liu X, Chen Y, Song Y. Design and test of superconducting magnet for 200 MeV proton cyclotron. *Cryogenics*. 2019;97:122-5.
28. Strijkmans K. The isochronous cyclotron: principles and recent developments. *Computerized Medical Imaging and Graphics*. 2001;25(2):69-78.
29. Forton E, Stichelbaut F, Cambriani A, Kleeven W, Ahlback J, Jongen Y. Overview of the IBA accelerator-based BNCT system. *Appl Radiat Isot*. 2009;67(7-8 Suppl):S262-5.
30. Zhang T, Wang C, Li M, Cui T, Yin Z, Ji B, et al. Developments for 230MeV superconducting cyclotrons for proton therapy and proton irradiation. *Nuclear Instruments and Methods in Physics Research Section B: Beam Interactions with Materials and Atoms*. 2017;406:244-9.
31. Yan S, Lu H-M, Flanz J, Adams J, Trofimov A, Bortfeld T. Reassessment of the Necessity of the Proton Gantry: Analysis of Beam Orientations From 4332 Treatments at the Massachusetts General Hospital Proton Center Over the Past 10 Years. *International Journal of Radiation Oncology*Biophysics*Physics*. 2016;95(1):224-33.
32. Vrenken H, Schuitema R, Dermois OC, Schippers JM. A design of a compact gantry for proton therapy with 2D-scanning. *Nuclear Instruments and Methods in Physics Research Section A: Accelerators, Spectrometers, Detectors and Associated Equipment*. 1999;426(2):618-24.
33. Tsutsui H, Hashimoto A, Mikami Y, Mitsubori H, Mitsumoto T, Touchi Y, et al., editors. Design study of a superconducting AVF cyclotron for proton therapy.
34. Nobakht E, Fouladi N. Feasibility study on the use of 230MeV proton cyclotron in proton therapy centers as a spallation neutron source for BNCT. *Reports of Practical Oncology & Radiotherapy*. 2019;24(6):644-53.
35. Campajola L, Braccini S, Casolaro P, de Luca D, Ereditato A, Häffner PD, et al. Measurement of the proton beam energy of a medical cyclotron based on Rutherford

Back-scattering Analysis. Nuclear Instruments and Methods in Physics Research Section B: Beam Interactions with Materials and Atoms. 2019;440:114-7.

36. Jackson SP, Bartek J. The DNA-damage response in human biology and disease. *Nature*. 2009;461(7267):1071-8.
37. Dasgupta T, Rothenstein D, Chou JF, Zhang Z, Wright JL, Saltz LB, et al. Intensity-modulated radiotherapy vs. conventional radiotherapy in the treatment of anal squamous cell carcinoma: a propensity score analysis. *Radiother Oncol*. 2013;107(2):189-94.
38. Moon SH, Shin KH, Kim TH, Yoon M, Park S, Lee DH, et al. Dosimetric comparison of four different external beam partial breast irradiation techniques: three-dimensional conformal radiotherapy, intensity-modulated radiotherapy, helical tomotherapy, and proton beam therapy. *Radiother Oncol*. 2009;90(1):66-73.
39. Levin WP, Kooy H, Loeffler JS, DeLaney TF. Proton beam therapy. *Br J Cancer*. 2005;93(8):849-54.
40. Flynn RT, Bowen SR, Bentzen SM, Rockwell Mackie T, Jeraj R. Intensity-modulated x-ray (IMXT) versus proton (IMPT) therapy for theragnostic hypoxia-based dose painting. *Phys Med Biol*. 2008;53(15):4153-67.
41. Bryant C, Smith TL, Henderson RH, Hoppe BS, Mendenhall WM, Nichols RC, et al. Five-Year Biochemical Results, Toxicity, and Patient-Reported Quality of Life After Delivery of Dose-Escalated Image Guided Proton Therapy for Prostate Cancer. *Int J Radiat Oncol Biol Phys*. 2016;95(1):422-34.
42. Watson JD, Crick FH. Molecular structure of nucleic acids; a structure for deoxyribose nucleic acid. *Nature*. 1953;171(4356):737-8.
43. Alberts B. *Molecular Biology of the Cell* in Cell 4th. Figure; 2002.
44. Yang VW. Chapter 8 - The Cell Cycle. In: Said HM, editor. *Physiology of the Gastrointestinal Tract (Sixth Edition)*: Academic Press; 2018. p. 197-219.
45. Stillwell W. Chapter 24 - Cell Death, Apoptosis. In: Stillwell W, editor. *An Introduction to Biological Membranes (Second Edition)*: Elsevier; 2016. p. 539-46.
46. Singh A, Singh H. Time-scale and nature of radiation-biological damage: Approaches to radiation protection and post-irradiation therapy. *Progress in Biophysics and Molecular Biology*. 1982;39:69-107.
47. Holum JR. The chemical composition of the cell. *Journal of Chemical Education*. 1984;61(10):877.
48. Mavragani IV, Nikitaki Z, Souli MP, Aziz A, Newsheen S, Aziz K, et al. Complex DNA damage: a route to radiation-induced genomic instability and carcinogenesis. *Cancers*. 2017;9(7):91.
49. Goodhead DT. Initial events in the cellular effects of ionizing radiations: clustered damage in DNA. *Int J Radiat Biol*. 1994;65(1):7-17.
50. Streffer C. [The effects of low radiation doses: carcinogenesis]. *Strahlenther Onkol*. 1994;170(12):681-8.
51. Vitti ET, Parsons JL. The Radiobiological Effects of Proton Beam Therapy: Impact on DNA Damage and Repair. *Cancers*. 2019;11(7):946.
52. Calugaru V, Nauraye C, Noël G, Giocanti N, Favaudon V, Méglin-Chanet F. Radiobiological characterization of two therapeutic proton beams with different initial energy spectra used at the Institut Curie Proton Therapy Center in Orsay. *International Journal of Radiation Oncology* Biology* Physics*. 2011;81(4):1136-43.

53. Girdhani S, Sachs R, Hlatky L. Biological effects of proton radiation: what we know and don't know. *Radiation research*. 2013;179(3):257-72.
54. Gerelchuluun A, Hong Z, Sun L, Suzuki K, Terunuma T, Yasuoka K, et al. Induction of in situ DNA double-strand breaks and apoptosis by 200 MeV protons and 10 MV X-rays in human tumour cell lines. *International journal of radiation biology*. 2011;87(1):57-70.
55. Leloup C, Garty G, Assaf G, Cristovao A, Breskin A, Chechik R, et al. Evaluation of lesion clustering in irradiated plasmid DNA. *International journal of radiation biology*. 2005;81(1):41-54.
56. Reisz JA, Bansal N, Qian J, Zhao W, Furdui CM. Effects of ionizing radiation on biological molecules--mechanisms of damage and emerging methods of detection. *Antioxid Redox Signal*. 2014;21(2):260-92.
57. Azzam EI, Jay-Gerin J-P, Pain D. Ionizing radiation-induced metabolic oxidative stress and prolonged cell injury. *Cancer letters*. 2012;327(1-2):48-60.
58. Chang J, Zhang X, Vassiliev O, Gillin M, Mohan R. Proton therapy targets cancer stem cells in treatment-resistant non-small cell lung cancer. *International Journal of Radiation Oncology • Biology • Physics*. 2010;78(3):S644.
59. Giedzinski E, Rola R, Fike JR, Limoli CL. Efficient production of reactive oxygen species in neural precursor cells after exposure to 250 MeV protons. *Radiation research*. 2005;164(4):540-4.
60. Lomax ME, Folkes LK, O'Neill P. Biological consequences of radiation-induced DNA damage: relevance to radiotherapy. *Clinical oncology (Royal College of Radiologists (Great Britain))*. 2013;25(10):578-85.
61. Paganetti H, van Luijk P. Biological considerations when comparing proton therapy with photon therapy. *Semin Radiat Oncol*. 2013;23(2):77-87.
62. Paganetti H, Niemierko A, Ancukiewicz M, Gerweck LE, Goitein M, Loeffler JS, et al. Relative biological effectiveness (RBE) values for proton beam therapy. *Int J Radiat Oncol Biol Phys*. 2002;53(2):407-21.
63. Carante MP, Ballarini F. Calculating Variations in Biological Effectiveness for a 62 MeV Proton Beam. *Front Oncol*. 2016;6:76.
64. Bettega D, Calzolari P, Chauvel P, Courdi A, Herault J, Iborra N, et al. Radiobiological studies on the 65 MeV therapeutic proton beam at Nice using human tumour cells. *Int J Radiat Biol*. 2000;76(10):1297-303.
65. Paganetti H. Relative biological effectiveness (RBE) values for proton beam therapy. Variations as a function of biological endpoint, dose, and linear energy transfer. *Phys Med Biol*. 2014;59(22):R419-72.
66. Matsumoto Y, Matsuura T, Wada M, Egashira Y, Nishio T, Furusawa Y. Enhanced radiobiological effects at the distal end of a clinical proton beam: in vitro study. *J Radiat Res*. 2014;55(4):816-22.
67. Wilkens JJ, Oelfke U. A phenomenological model for the relative biological effectiveness in therapeutic proton beams. *Phys Med Biol*. 2004;49(13):2811-25.
68. Cometto A, Russo G, Bourhaleb F, Milian FM, Giordanengo S, Marchetto F, et al. Direct evaluation of radiobiological parameters from clinical data in the case of ion beam therapy: an alternative approach to the relative biological effectiveness. *Phys Med Biol*. 2014;59(23):7393-417.
69. Krokan HE, Bjørås M. Base excision repair. *Cold Spring Harb Perspect Biol*. 2013;5(4):a012583-a.

70. D'Andrea AD. Chapter 4 - DNA Repair Pathways and Human Cancer. In: Mendelsohn J, Howley PM, Israel MA, Gray JW, Thompson CB, editors. *The Molecular Basis of Cancer (Third Edition)*. Philadelphia: W.B. Saunders; 2008. p. 39-55.
71. del Rivero J, Kohn EC. PARP Inhibitors: The Cornerstone of DNA Repair-Targeted Therapies. *Oncology (Williston Park, NY)*. 2017;31(4):265-73.
72. Ronson GE, Piberger AL, Higgs MR, Olsen AL, Stewart GS, McHugh PJ, et al. PARP1 and PARP2 stabilise replication forks at base excision repair intermediates through Fbh1-dependent Rad51 regulation. *Nature Communications*. 2018;9(1):746.
73. Madders EC, Parsons JL. Base Excision Repair in Chromatin and the Requirement for Chromatin Remodelling. *Mechanisms of Genome Protection and Repair*: Springer; 2020. p. 59-75.
74. Carter RJ, Parsons JL. Base excision repair, a pathway regulated by posttranslational modifications. *Molecular and cellular biology*. 2016;36(10):1426-37.
75. Reardon JT, Sancar A. Nucleotide Excision Repair. *Progress in Nucleic Acid Research and Molecular Biology*. 79: Academic Press; 2005. p. 183-235.
76. Shuck SC, Short EA, Turchi JJ. Eukaryotic nucleotide excision repair: from understanding mechanisms to influencing biology. *Cell Research*. 2008;18(1):64-72.
77. Spivak G. Nucleotide excision repair in humans. *DNA Repair*. 2015;36:13-8.
78. Kamileri I, Karakasilioti I, Garinis GA. Nucleotide excision repair: new tricks with old bricks. *Trends in Genetics*. 2012;28(11):566-73.
79. Modrich P. Mechanisms in eukaryotic mismatch repair. *J Biol Chem*. 2006;281(41):30305-9.
80. Li G-M. Mechanisms and functions of DNA mismatch repair. *Cell Research*. 2008;18(1):85-98.
81. Stojic L, Brun R, Jiricny J. Mismatch repair and DNA damage signalling. *DNA Repair*. 2004;3(8):1091-101.
82. Watson P, Lynch HT. Cancer risk in mismatch repair gene mutation carriers. *Familial Cancer*. 2001;1(1):57-60.
83. Lehmann AR. Translesion synthesis in mammalian cells. *Exp Cell Res*. 2006;312(14):2673-6.
84. Helleday T, Petermann E, Lundin C, Hodgson B, Sharma RA. DNA repair pathways as targets for cancer therapy. *Nat Rev Cancer*. 2008;8(3):193-204.
85. Vaisman A, McDonald JP, Woodgate R. Translesion DNA Synthesis. *EcoSal Plus*. 2012;5(1).
86. Masutani C, Kusumoto R, Iwai S, Hanaoka F. Mechanisms of accurate translesion synthesis by human DNA polymerase η . *EMBO J*. 2000;19(12):3100-9.
87. Sargent RG, Brenneman MA, Wilson JH. Repair of site-specific double-strand breaks in a mammalian chromosome by homologous and illegitimate recombination. *Mol Cell Biol*. 1997;17(1):267-77.
88. Yano K, Chen DJ. Live cell imaging of XLF and XRCC4 reveals a novel view of protein assembly in the non-homologous end-joining pathway. *Cell Cycle*. 2008;7(10):1321-5.
89. Davis AJ, Chen DJ. DNA double strand break repair via non-homologous end-joining. *Transl Cancer Res*. 2013;2(3):130-43.
90. Burma S, Chen BPC, Chen DJ. Role of non-homologous end joining (NHEJ) in maintaining genomic integrity. *DNA Repair*. 2006;5(9):1042-8.

91. Dobbs TA, Tainer JA, Lees-Miller SP. A structural model for regulation of NHEJ by DNA-PKcs autophosphorylation. *DNA Repair*. 2010;9(12):1307-14.
92. Richardson C, Jasin M. Coupled homologous and nonhomologous repair of a double-strand break preserves genomic integrity in mammalian cells. *Mol Cell Biol*. 2000;20(23):9068-75.
93. Haber JE. DNA recombination: the replication connection. *Trends in biochemical sciences*. 1999;24(7):271-5.
94. Arnaudeau C, Lundin C, Helleday T. DNA double-strand breaks associated with replication forks are predominantly repaired by homologous recombination involving an exchange mechanism in mammalian cells. *J Mol Biol*. 2001;307(5):1235-45.
95. Shrivastav M, De Haro LP, Nickoloff JA. Regulation of DNA double-strand break repair pathway choice. *Cell Res*. 2008;18(1):134-47.
96. Li X, Heyer WD. Homologous recombination in DNA repair and DNA damage tolerance. *Cell Res*. 2008;18(1):99-113.
97. Wright WD, Shah SS, Heyer WD. Homologous recombination and the repair of DNA double-strand breaks. *J Biol Chem*. 2018;293(27):10524-35.
98. Tian X, Patel K, Ridpath JR, Chen Y, Zhou YH, Neo D, et al. Homologous Recombination and Translesion DNA Synthesis Play Critical Roles on Tolerating DNA Damage Caused by Trace Levels of Hexavalent Chromium. *PLoS One*. 2016;11(12):e0167503.
99. Wayne DN, Rui Z. The physics of proton therapy. *Physics in Medicine & Biology*. 2015;60(8):R155.
100. Girdhani S, Sachs R, Hlatky L. Biological effects of proton radiation: what we know and don't know. *Radiation research*. 2013;179(3):257-72.
101. Gerelchuluun A, Hong Z, Sun L, Suzuki K, Terunuma T, Yasuoka K, et al. Induction of in situ DNA double-strand breaks and apoptosis by 200 MeV protons and 10 MV X-rays in human tumour cell lines. *International journal of radiation biology*. 2011;87(1):57-70.
102. Grosse N, Fontana AO, Hug EB, Lomax A, Coray A, Augsburger M, et al. Deficiency in homologous recombination renders Mammalian cells more sensitive to proton versus photon irradiation. *Int J Radiat Oncol Biol Phys*. 2014;88(1):175-81.
103. Bee L, Fabris S, Cherubini R, Mognato M, Celotti L. The efficiency of homologous recombination and non-homologous end joining systems in repairing double-strand breaks during cell cycle progression. *PloS one*. 2013;8(7):e69061.
104. Pierce AJ, Hu P, Han M, Ellis N, Jasin M. Ku DNA end-binding protein modulates homologous repair of double-strand breaks in mammalian cells. *Genes & development*. 2001;15(24):3237-42.
105. Gerelchuluun A, Manabe E, Ishikawa T, Sun L, Itoh K, Sakae T, et al. The major DNA repair pathway after both proton and carbon-ion radiation is NHEJ, but the HR pathway is more relevant in carbon ions. *Radiat Res*. 2015;183(3):345-56.
106. Mao Z, Bozzella M, Seluanov A, Gorbunova V. DNA repair by nonhomologous end joining and homologous recombination during cell cycle in human cells. *Cell cycle*. 2008;7(18):2902-6.
107. Leloup C, Garty G, Assaf G, Cristovao A, Breskin A, Chechik R, et al. Evaluation of lesion clustering in irradiated plasmid DNA. *International journal of radiation biology*. 2005;81(1):41-54.

108. Calugaru V, Nauraye C, Noel G, Giocanti N, Favaudon V, Megnin-Chanet F. Radiobiological characterization of two therapeutic proton beams with different initial energy spectra used at the Institut Curie Proton Therapy Center in Orsay. *International journal of radiation oncology, biology, physics*. 2011;81(4):1136-43.
109. Zhao Y, Thomas HD, Batey MA, Cowell IG, Richardson CJ, Griffin RJ, et al. Preclinical evaluation of a potent novel DNA-dependent protein kinase inhibitor NU7441. *Cancer Res*. 2006;66(10):5354-62.
110. Niemantsverdriet M, van Goethem M-J, Bron R, Hogewerf W, Brandenburg S, Langendijk JA, et al. High and Low LET Radiation Differentially Induce Normal Tissue Damage Signals. *International Journal of Radiation Oncology* Biology* Physics*. 2012;83(4):1291-7.
111. Costes SV, Boissiere A, Ravani S, Romano R, Parvin B, Barcellos-Hoff MH. Imaging features that discriminate between foci induced by high- and low-LET radiation in human fibroblasts. *Radiation research*. 2006;165(5):505-15.
112. Nikitaki Z, Nikolov V, Mavragani IV, Mladenov E, Mangelis A, Laskaratou DA, et al. Measurement of complex DNA damage induction and repair in human cellular systems after exposure to ionizing radiations of varying linear energy transfer (LET). *Free radical research*. 2016;50(sup1):S64-s78.
113. Francis Z, Villagrasa C, Clairand I. Simulation of DNA damage clustering after proton irradiation using an adapted DBSCAN algorithm. *Computer Methods and Programs in Biomedicine*. 2011;101(3):265-70.
114. Carter RJ, Nickson CM, Thompson JM, Kacperek A, Hill MA, Parsons JL. Complex DNA damage induced by high linear energy transfer alpha-particles and protons triggers a specific cellular DNA damage response. *International Journal of Radiation Oncology* Biology* Physics*. 2018;100(3):776-84.
115. Gerelchuluun A, Manabe E, Ishikawa T, Sun L, Itoh K, Sakae T, et al. The Major DNA Repair Pathway after Both Proton and Carbon-Ion Radiation is NHEJ, but the HR Pathway is More Relevant in Carbon Ions. *Radiation Research*. 2015;183(3):345-56, 12.
116. Bracalente C, Ibanez IL, Molinari B, Palmieri M, Kreiner A, Valda A, et al. Induction and persistence of large gammaH2AX foci by high linear energy transfer radiation in DNA-dependent protein kinase-deficient cells. *Int J Radiat Oncol Biol Phys*. 2013;87(4):785-94.
117. Liu Q, Ghosh P, Magpayo N, Testa M, Tang S, Gheorghiu L, et al. Lung cancer cell line screen links fanconi anemia/BRCA pathway defects to increased relative biological effectiveness of proton radiation. *International Journal of Radiation Oncology* Biology* Physics*. 2015;91(5):1081-9.
118. Fontana AO, Augsburg MA, Grosse N, Guckenberger M, Lomax AJ, Sartori AA, et al. Differential DNA repair pathway choice in cancer cells after proton- and photon-irradiation. *Radiother Oncol*. 2015;116(3):374-80.
119. Reindl J, Drexler GA, Girst S, Greubel C, Siebenwirth C, Drexler SE, et al. Nanoscopic exclusion between Rad51 and 53BP1 after ion irradiation in human HeLa cells. *Physical biology*. 2015;12(6):066005.
120. Shaheen FS, Znojek P, Fisher A, Webster M, Plummer R, Gaughan L, et al. Targeting the DNA double strand break repair machinery in prostate cancer. *PLoS One*. 2011;6(5):e20311.
121. Weber AM, Ryan AJ. ATM and ATR as therapeutic targets in cancer. *Pharmacology & Therapeutics*. 2015;149:124-38.

122. Davidson D, Amrein L, Panasci L, Aloyz R. Small molecules, inhibitors of DNA-PK, targeting DNA repair, and beyond. *Frontiers in pharmacology*. 2013;4:5.
123. Bernstein C, Bernstein H, Payne CM, Garewal H. DNA repair/pro-apoptotic dual-role proteins in five major DNA repair pathways: fail-safe protection against carcinogenesis. *Mutat Res*. 2002;511(2):145-78.
124. Lee J-H, Paull TT. ATM activation by DNA double-strand breaks through the Mre11-Rad50-Nbs1 complex. *Science (New York, NY)*. 2005;308(5721):551-4.
125. Stracker TH, Petrini JH. The MRE11 complex: starting from the ends. *Nature reviews Molecular cell biology*. 2011;12(2):90-103.
126. You Z, Chahwan C, Bailis J, Hunter T, Russell P. ATM activation and its recruitment to damaged DNA require binding to the C terminus of Nbs1. *Molecular and cellular biology*. 2005;25(13):5363-79.
127. Burma S, Chen BP, Murphy M, Kurimasa A, Chen DJ. ATM phosphorylates histone H2AX in response to DNA double-strand breaks. *J Biol Chem*. 2001;276(45):42462-7.
128. Li S, Ting NS, Zheng L, Chen PL, Ziv Y, Shiloh Y, et al. Functional link of BRCA1 and ataxia telangiectasia gene product in DNA damage response. *Nature*. 2000;406(6792):210-5.
129. Gatei M, Zhou BB, Hobson K, Scott S, Young D, Khanna KK. Ataxia telangiectasia mutated (ATM) kinase and ATM and Rad3 related kinase mediate phosphorylation of Brca1 at distinct and overlapping sites. In vivo assessment using phospho-specific antibodies. *J Biol Chem*. 2001;276(20):17276-80.
130. Shiloh Y. ATM and ATR: networking cellular responses to DNA damage. *Current opinion in genetics & development*. 2001;11(1):71-7.
131. Banin S, Moyal L, Shieh S, Taya Y, Anderson CW, Chessa L, et al. Enhanced phosphorylation of p53 by ATM in response to DNA damage. *Science (New York, NY)*. 1998;281(5383):1674-7.
132. Khosravi R, Maya R, Gottlieb T, Oren M, Shiloh Y, Shkedy D. Rapid ATM-dependent phosphorylation of MDM2 precedes p53 accumulation in response to DNA damage. *Proc Natl Acad Sci U S A*. 1999;96(26):14973-7.
133. Ljungman M. Dial 9-1-1 for p53: mechanisms of p53 activation by cellular stress. *Neoplasia (New York, NY)*. 2000;2(3):208-25.
134. Matsuoka S, Huang M, Elledge SJ. Linkage of ATM to cell cycle regulation by the Chk2 protein kinase. *Science (New York, NY)*. 1998;282(5395):1893-7.
135. Hirao A, Kong YY, Matsuoka S, Wakeham A, Ruland J, Yoshida H, et al. DNA damage-induced activation of p53 by the checkpoint kinase Chk2. *Science (New York, NY)*. 2000;287(5459):1824-7.
136. Falck J, Mailand N, Syljuåsen RG, Bartek J, Lukas J. The ATM-Chk2-Cdc25A checkpoint pathway guards against radioresistant DNA synthesis. *Nature*. 2001;410(6830):842-7.
137. Liu S, Shiotani B, Lahiri M, Maréchal A, Tse A, Leung CCY, et al. ATR autophosphorylation as a molecular switch for checkpoint activation. *Molecular cell*. 2011;43(2):192-202.
138. Cortez D, Guntuku S, Qin J, Elledge SJ. ATR and ATRIP: partners in checkpoint signaling. *Science (New York, NY)*. 2001;294(5547):1713-6.
139. Brown EJ, Baltimore D. ATR disruption leads to chromosomal fragmentation and early embryonic lethality. *Genes Dev*. 2000;14(4):397-402.

140. Shieh SY, Ahn J, Tamai K, Taya Y, Prives C. The human homologs of checkpoint kinases Chk1 and Cds1 (Chk2) phosphorylate p53 at multiple DNA damage-inducible sites. *Genes Dev.* 2000;14(3):289-300.
141. Bartek J, Lukas C, Lukas J. Checking on DNA damage in S phase. *Nature reviews Molecular cell biology.* 2004;5(10):792-804.
142. Xiao Z, Chen Z, Gunasekera AH, Sowin TJ, Rosenberg SH, Fesik S, et al. Chk1 mediates S and G2 arrests through Cdc25A degradation in response to DNA-damaging agents. *Journal of Biological Chemistry.* 2003;278(24):21767-73.
143. Kumagai A, Dunphy WG. Binding of 14-3-3 proteins and nuclear export control the intracellular localization of the mitotic inducer Cdc25. *Genes & development.* 1999;13(9):1067-72.
144. Graves PR, Lovly CM, Uy GL, Piwnica-Worms H. Localization of human Cdc25C is regulated both by nuclear export and 14-3-3 protein binding. *Oncogene.* 2001;20(15):1839-51.
145. Sanchez Y, Wong C, Thoma RS, Richman R, Wu Z, Piwnica-Worms H, et al. Conservation of the Chk1 checkpoint pathway in mammals: linkage of DNA damage to Cdk regulation through Cdc25. *Science (New York, NY).* 1997;277(5331):1497-501.
146. Davis AJ, So S, Chen DJ. Dynamics of the PI3K-like protein kinase members ATM and DNA-PKcs at DNA double strand breaks. *Cell Cycle.* 2010;9(13):2529-36.
147. Chan DW, Chen BP-C, Prithivirajasingh S, Kurimasa A, Story MD, Qin J, et al. Autophosphorylation of the DNA-dependent protein kinase catalytic subunit is required for rejoining of DNA double-strand breaks. *Genes & development.* 2002;16(18):2333-8.
148. Ding Q, Reddy YV, Wang W, Woods T, Douglas P, Ramsden DA, et al. Autophosphorylation of the catalytic subunit of the DNA-dependent protein kinase is required for efficient end processing during DNA double-strand break repair. *Molecular and cellular biology.* 2003;23(16):5836-48.
149. Davidson D, Amrein L, Panasci L, Aloyz R. Small Molecules, Inhibitors of DNA-PK, Targeting DNA Repair, and Beyond. *Frontiers in Pharmacology.* 2013;4(5).
150. Chen BP, Chan DW, Kobayashi J, Burma S, Asaithamby A, Morotomi-Yano K, et al. Cell cycle dependence of DNA-dependent protein kinase phosphorylation in response to DNA double strand breaks. *Journal of Biological Chemistry.* 2005;280(15):14709-15.
151. Meek K, Douglas P, Cui X, Ding Q, Lees-Miller SP. trans Autophosphorylation at DNA-dependent protein kinase's two major autophosphorylation site clusters facilitates end processing but not end joining. *Molecular and cellular biology.* 2007;27(10):3881-90.
152. Cui X, Yu Y, Gupta S, Cho Y-M, Lees-Miller SP, Meek K. Autophosphorylation of DNA-dependent protein kinase regulates DNA end processing and may also alter double-strand break repair pathway choice. *Molecular and cellular biology.* 2005;25(24):10842-52.
153. Neal JA, Dang V, Douglas P, Wold MS, Lees-Miller SP, Meek K. Inhibition of Homologous Recombination by DNA-Dependent Protein Kinase Requires Kinase Activity, Is Titratable, and Is Modulated by Autophosphorylation. *Molecular and Cellular Biology.* 2011;31(8):1719-33.
154. Neal JA, Meek K. Choosing the right path: Does DNA-PK help make the decision? *Mutation Research/Fundamental and Molecular Mechanisms of Mutagenesis.* 2011;711(1):73-86.

155. Wang S, Guo M, Ouyang H, Li X, Cordon-Cardo C, Kurimasa A, et al. The catalytic subunit of DNA-dependent protein kinase selectively regulates p53-dependent apoptosis but not cell-cycle arrest. *Proceedings of the National Academy of Sciences*. 2000;97(4):1584-8.
156. Shieh SY, Ikeda M, Taya Y, Prives C. DNA damage-induced phosphorylation of p53 alleviates inhibition by MDM2. *Cell*. 1997;91(3):325-34.
157. Mayo LD, Turchi JJ, Berberich SJ. Mdm-2 phosphorylation by DNA-dependent protein kinase prevents interaction with p53. *Cancer Res*. 1997;57(22):5013-6.
158. Mukherjee B, Kessinger C, Kobayashi J, Chen BPC, Chen DJ, Chatterjee A, et al. DNA-PK phosphorylates histone H2AX during apoptotic DNA fragmentation in mammalian cells. *DNA Repair*. 2006;5(5):575-90.
159. Han Z, Malik N, Carter T, Reeves WH, Wyche JH, Hendrickson EA. DNA-dependent protein kinase is a target for a CPP32-like apoptotic protease. *Journal of Biological Chemistry*. 1996;271(40):25035-40.
160. Itoh T, Horio T. DNA-dependent protein kinase catalytic subunit is cleaved during UV-induced apoptosis. *Journal of Dermatological Science*. 2001;25(1):72-7.
161. Economopoulou P, Bourhis J, Psyrri A. Research Progress in Head and Neck Squamous Cell Carcinoma: Best Abstracts of ICHNO 2015. *Am Soc Clin Oncol Educ Book*. 2015:e323-8.
162. NCI Dictionary of Cancer Terms [Internet].
163. Stewart B, Wild CP. World cancer report 2014: International Agency for Research on Cancer, WHO; 2014. 609-11 p.
164. U.S. Department of Health & Human Services, National Institutes of Health, National Library of Medicine "Head and Neck squamous cell carcinoma" [Internet]. 2020 [cited April 14, 2020].
165. Siegel RL, Miller KD, Jemal A. Cancer Statistics, 2017. *CA: a cancer journal for clinicians*. 2017;67(1):7-30.
166. Pignon J, Bourhis J, Domenge Co, Designé LI, Group M-NC. Chemotherapy added to locoregional treatment for head and neck squamous-cell carcinoma: three meta-analyses of updated individual data. *The Lancet*. 2000;355(9208):949-55.
167. Xu YG, Aylward JL, Swanson AM, Spiegelman VS, Vanness ER, Teng JMC, et al. 67 - Nonmelanoma Skin Cancers: Basal Cell and Squamous Cell Carcinomas. In: Niederhuber JE, Armitage JO, Kastan MB, Doroshow JH, Tepper JE, editors. *Abeloff's Clinical Oncology (Sixth Edition)*. Philadelphia: Content Repository Only!; 2020. p. 1052-73.e8.
168. Rieckmann T, Tribius S, Grob TJ, Meyer F, Busch CJ, Petersen C, et al. HNSCC cell lines positive for HPV and p16 possess higher cellular radiosensitivity due to an impaired DSB repair capacity. *Radiother Oncol*. 2013;107(2):242-6.
169. Gollin SM. Chromosomal alterations in squamous cell carcinomas of the head and neck: window to the biology of disease. *Head & neck*. 2001;23(3):238-53.
170. Virgilio L, Shuster M, Gollin SM, Veronese ML, Ohta M, Huebner K, et al. FHIT gene alterations in head and neck squamous cell carcinomas. *Proceedings of the National Academy of Sciences*. 1996;93(18):9770-5.
171. Cowan JM, Beckett MA, Ahmed-Swan S, Weichselbaum RR. Cytogenetic evidence of the multistep origin of head and neck squamous cell carcinomas. *JNCI: Journal of the National Cancer Institute*. 1992;84(10):793-7.

172. Rodrigo JP, Suárez C, González MV, Lazo PS, Ramos S, Coto E, et al. Variability of genetic alterations in different sites of head and neck cancer. *The Laryngoscope*. 2001;111(7):1297-301.
173. Meredith SD, Levine PA, Burns JA, Gaffey MJ, Boyd JC, Weiss LM, et al. Chromosome 11q13 amplification in head and neck squamous cell carcinoma: association with poor prognosis. *Archives of Otolaryngology–Head & Neck Surgery*. 1995;121(7):790-4.
174. Namazie A, Alavi S, Olopade OI, Pauletti G, Aghamohammadi N, Aghamohammadi M, et al. Cyclin D1 amplification and p16 (MTS1/CDK4I) deletion correlate with poor prognosis in head and neck tumors. *The Laryngoscope*. 2002;112(3):472-81.
175. Huang X, Gollin SM, Raja S, Godfrey TE. High-resolution mapping of the 11q13 amplicon and identification of a gene, TAOS1, that is amplified and overexpressed in oral cancer cells. *Proceedings of the National Academy of Sciences*. 2002;99(17):11369-74.
176. Muller D, Millon R, Velten M, Bronner G, Jung G, Engelmann A, et al. Amplification of 11q13 DNA markers in head and neck squamous cell carcinomas: correlation with clinical outcome. *European Journal of Cancer*. 1997;33(13):2203-10.
177. Lin CJ, Grandis JR, Carey TE, Gollin SM, Whiteside TL, Koch WM, et al. Head and neck squamous cell carcinoma cell lines: established models and rationale for selection. *Head & neck*. 2007;29(2):163-88.
178. Gupta AK, Lee JH, Wilke WW, Quon H, Smith G, Maity A, et al. Radiation response in two HPV-infected head-and-neck cancer cell lines in comparison to a non-HPV-infected cell line and relationship to signaling through AKT. *Int J Radiat Oncol Biol Phys*. 2009;74(3):928-33.
179. Yeo-Teh NSL, Ito Y, Jha S. High-Risk Human Papillomaviral Oncogenes E6 and E7 Target Key Cellular Pathways to Achieve Oncogenesis. *Int J Mol Sci*. 2018;19(6):1706.
180. Dok R, Abbasi Asbagh L, Van Limbergen EJ, Sablina A, Nuyts S. Nuclear p16INK4a expression predicts enhanced radiation response in head and neck cancers. *Oncotarget*. 2016;7(25):38785-95.
181. Leemans CR, Braakhuis BJ, Brakenhoff RH. The molecular biology of head and neck cancer. *Nat Rev Cancer*. 2011;11(1):9-22.
182. Fakhry C, Westra WH, Li S, Cmelak A, Ridge JA, Pinto H, et al. Improved Survival of Patients With Human Papillomavirus–Positive Head and Neck Squamous Cell Carcinoma in a Prospective Clinical Trial. *JNCI: Journal of the National Cancer Institute*. 2008;100(4):261-9.
183. Ang KK, Harris J, Wheeler R, Weber R, Rosenthal DI, Nguyen-Tân PF, et al. Human papillomavirus and survival of patients with oropharyngeal cancer. *New England Journal of Medicine*. 2010;363(1):24-35.
184. Lassen P, Eriksen JG, Hamilton-Dutoit S, Tramm T, Alsner J, Overgaard J. Effect of HPV-associated p16INK4A expression on response to radiotherapy and survival in squamous cell carcinoma of the head and neck. *J Clin Oncol*. 2009;27(12):1992-8.
185. Lassen P, Overgaard J, Eriksen JG. Expression of EGFR and HPV-associated p16 in oropharyngeal carcinoma: correlation and influence on prognosis after radiotherapy in the randomized DAHANCA 5 and 7 trials. *Radiotherapy and Oncology*. 2013;108(3):489-94.

186. Ang KK, Harris J, Wheeler R, Weber R, Rosenthal DI, Nguyen-Tan PF, et al. Human papillomavirus and survival of patients with oropharyngeal cancer. *N Engl J Med.* 2010;363(1):24-35.
187. Fakhry C, Westra WH, Li S, Cmelak A, Ridge JA, Pinto H, et al. Improved survival of patients with human papillomavirus-positive head and neck squamous cell carcinoma in a prospective clinical trial. *J Natl Cancer Inst.* 2008;100(4):261-9.
188. Arenz A, Ziemann F, Mayer C, Wittig A, Dreffke K, Preising S, et al. Increased radiosensitivity of HPV-positive head and neck cancer cell lines due to cell cycle dysregulation and induction of apoptosis. *Strahlenther Onkol.* 2014;190(9):839-46.
189. Mirghani H, Amen F, Tao Y, Deutsch E, Levy A. Increased radiosensitivity of HPV-positive head and neck cancers: Molecular basis and therapeutic perspectives. *Cancer Treat Rev.* 2015;41(10):844-52.
190. Nickson CM, Moori P, Carter RJ, Rubbi CP, Parsons JL. Misregulation of DNA damage repair pathways in HPV-positive head and neck squamous cell carcinoma contributes to cellular radiosensitivity. *Oncotarget.* 2017;8(18):29963.
191. Rieckmann T, Tribius S, Grob TJ, Meyer F, Busch C-J, Petersen C, et al. HNSCC cell lines positive for HPV and p16 possess higher cellular radiosensitivity due to an impaired DSB repair capacity. *Radiotherapy and oncology.* 2013;107(2):242-6.
192. The Role of HPV E6 and E7 Oncoproteins in HPV-associated Cervical Carcinogenesis. *Cancer Research and Treatment.* 2005;37(6):319-24.
193. Boulet G, Horvath C, Vanden Broeck D, Sahebali S, Bogers J. Human papillomavirus: E6 and E7 oncogenes. *The international journal of biochemistry & cell biology.* 2007;39(11):2006-11.
194. McLaughlin-Drubin ME, Münger K. The human papillomavirus E7 oncoprotein. *Virology.* 2009;384(2):335-44.
195. Wasson CW, Morgan EL, Muller M, Ross RL, Hartley M, Roberts S, et al. Human papillomavirus type 18 E5 oncogene supports cell cycle progression and impairs epithelial differentiation by modulating growth factor receptor signalling during the virus life cycle. *Oncotarget.* 2017;8(61):103581-600.
196. Ragin CCR, Reshmi SC, Gollin SM. Mapping and analysis of HPV16 integration sites in a head and neck cancer cell line. *International journal of cancer.* 2004;110(5):701-9.
197. Bjerkvig R. *Spheroid Culture in Cancer Research* (1991): CRC press; 2017.
198. Worsham M, Wolman S, Carey T, Zarbo R, Benninger M, Van Dyke D. Chromosomal aberrations identified in culture of squamous carcinomas are confirmed by fluorescence in situ hybridisation. *Molecular Pathology.* 1999;52(1):42.
199. Forslund O, Sugiyama N, Wu C, Ravi N, Jin Y, Swoboda S, et al. A novel human in vitro papillomavirus type 16 positive tonsil cancer cell line with high sensitivity to radiation and cisplatin. *BMC cancer.* 2019;19(1):265.
200. Greaney-Davies FST, Risk JM, Robinson M, Liloglou T, Shaw RJ, Schache AG. Essential characterisation of human papillomavirus positive head and neck cancer cell lines. *Oral Oncology.* 2020;103:104613.
201. <https://www.cancerresearchuk.org/health-professional/cancer-statistics/statistics-by-cancer-type/head-and-neck-cancers#heading-Zero>. Cancer Research UK. 2020.
202. Lohaus F, Linge A, Tinhofer I, Budach V, Gkika E, Stuschke M, et al. HPV16 DNA status is a strong prognosticator of loco-regional control after postoperative

- radiochemotherapy of locally advanced oropharyngeal carcinoma: Results from a multicentre explorative study of the German Cancer Consortium Radiation Oncology Group (DKTK-ROG). *Radiotherapy and Oncology*. 2014;113(3):317-23.
203. Kumar B, Cordell KG, Lee JS, Worden FP, Prince ME, Tran HH, et al. EGFR, p16, HPV Titer, Bcl-xL and p53, sex, and smoking as indicators of response to therapy and survival in oropharyngeal cancer. *J Clin Oncol*. 2008;26(19):3128-37.
204. Lassen P, Eriksen JG, Hamilton-Dutoit S, Tramm T, Alsner J, Overgaard J. Effect of HPV-associated p16INK4A expression on response to radiotherapy and survival in squamous cell carcinoma of the head and neck. *J Clin Oncol*. 2009;27(12):1992-8.
205. Gubanov E, Brown B, Ivanov SV, Helleday T, Mills GB, Yarbrough WG, et al. Downregulation of SMG-1 in HPV-positive head and neck squamous cell carcinoma due to promoter hypermethylation correlates with improved survival. *Clin Cancer Res*. 2012;18(5):1257-67.
206. Kimple RJ, Smith MA, Blitzer GC, Torres AD, Martin JA, Yang RZ, et al. Enhanced radiation sensitivity in HPV-positive head and neck cancer. *Cancer Res*. 2013;73(15):4791-800.
207. Nickson CM, Moori P, Carter RJ, Rubbi CP, Parsons JL. Misregulation of DNA damage repair pathways in HPV-positive head and neck squamous cell carcinoma contributes to cellular radiosensitivity. *Oncotarget*. 2017;8(18):29963-75.
208. Glorieux M, Dok R, Nuyts S. Novel DNA targeted therapies for head and neck cancers: clinical potential and biomarkers. *Oncotarget*. 2017;8(46):81662-78.
209. Dohmen AJC, Qiao X, Duursma A, Wijdeven RH, Lieftink C, Hageman F, et al. Identification of a novel ATM inhibitor with cancer cell specific radiosensitization activity. *Oncotarget*. 2017;8(43):73925-37.
210. Sankunni M, Parikh RA, Lewis DW, Gooding WE, Saunders WS, Gollin SM. Targeted inhibition of ATR or CHEK1 reverses radioresistance in oral squamous cell carcinoma cells with distal chromosome arm 11q loss. *Genes, chromosomes & cancer*. 2014;53(2):129-43.
211. Pires I, Olcina M, Anbalagan S, Pollard J, Reaper P, Charlton P, et al. Targeting radiation-resistant hypoxic tumour cells through ATR inhibition. *British journal of cancer*. 2012;107(2):291-9.
212. Dillon MT, Barker HE, Pedersen M, Hafsi H, Bhide SA, Newbold KL, et al. Radiosensitization by the ATR inhibitor AZD6738 through generation of acentric micronuclei. *Molecular cancer therapeutics*. 2017;16(1):25-34.
213. Hafsi H, Dillon MT, Barker HE, Kyula JN, Schick U, Paget JT, et al. Combined ATR and DNA-PK inhibition radiosensitizes tumor cells independently of their p53 status. *Frontiers in oncology*. 2018;8:245.
214. Dillon MT, Barker HE, Pedersen M, Hafsi H, Bhide SA, Newbold KL, et al. Radiosensitization by the ATR Inhibitor AZD6738 through Generation of Acentric Micronuclei. *Mol Cancer Ther*. 2017;16(1):25-34.
215. Dickreuter E, Eke I, Krause M, Borgmann K, Van Vugt M, Cordes N. Targeting of $\beta 1$ integrins impairs DNA repair for radiosensitization of head and neck cancer cells. *Oncogene*. 2016;35(11):1353-62.
216. Lee TW, Wong WW, Dickson BD, Lipert B, Cheng GJ, Hunter FW, et al. Radiosensitization of head and neck squamous cell carcinoma lines by DNA-PK inhibitors is more effective than PARP-1 inhibition and is enhanced by SLFN11 and hypoxia. *International Journal of Radiation Biology*. 2019;95(12):1597-612.

217. Dok R, Bamps M, Glorieux M, Zhao P, Sablina A, Nuyts S. Radiosensitization approaches for HPV-positive and HPV-negative head and neck squamous carcinomas. *International journal of cancer*. 2020;146(4):1075-85.
218. Holliday EB, Frank SJ. Proton radiation therapy for head and neck cancer: a review of the clinical experience to date. *Int J Radiat Oncol Biol Phys*. 2014;89(2):292-302.
219. <https://web.expasy.org/cellosaurus/>. Bioinformatics Resource Portal. Version 34, March 2020.
220. <https://www.lgcstandards-atcc.org/#>. LGCstandards, ATCC: The Global Bioresource Center. 2020.
221. Kacperek A. Protontherapy of eye tumours in the UK: a review of treatment at Clatterbridge. *Applied Radiation and Isotopes*. 2009;67(3):378-86.
222. Vauzour D, Vafeiadou K, Rice-Evans C, Cadenas E, Spencer JP. Inhibition of cellular proliferation by the genistein metabolite 5,7,3',4'-tetrahydroxyisoflavone is mediated by DNA damage and activation of the ATR signalling pathway. *Arch Biochem Biophys*. 2007;468(2):159-66.
223. Vitzthum LK, Mell LK. The role of p16 as a biomarker in nonoropharyngeal head and neck cancer. *Oncotarget*. 2018;9(70):33247-8.
224. Hickson I, Zhao Y, Richardson CJ, Green SJ, Martin NM, Orr AI, et al. Identification and characterization of a novel and specific inhibitor of the ataxia-telangiectasia mutated kinase ATM. *Cancer research*. 2004;64(24):9152-9.
225. Zhao Y, Thomas HD, Batey MA, Cowell IG, Richardson CJ, Griffin RJ, et al. Preclinical evaluation of a potent novel DNA-dependent protein kinase inhibitor NU7441. *Cancer research*. 2006;66(10):5354-62.
226. Prevo R, Fokas E, Reaper PM, Charlton PA, Pollard JR, McKenna WG, et al. The novel ATR inhibitor VE-821 increases sensitivity of pancreatic cancer cells to radiation and chemotherapy. *Cancer biology & therapy*. 2012;13(11):1072-81.
227. Zhou C, Parsons JL. The radiobiology of HPV-positive and HPV-negative head and neck squamous cell carcinoma. *Expert Reviews in Molecular Medicine*. 2020;22.
228. Stiff T, O'Driscoll M, Rief N, Iwabuchi K, Löbrich M, Jeggo PA. ATM and DNA-PK function redundantly to phosphorylate H2AX after exposure to ionizing radiation. *Cancer research*. 2004;64(7):2390-6.
229. Celeste A, Fernandez-Capetillo O, Kruhlak MJ, Pilch DR, Staudt DW, Lee A, et al. Histone H2AX phosphorylation is dispensable for the initial recognition of DNA breaks. *Nature cell biology*. 2003;5(7):675-9.
230. Tarsounas M, Davies AA, West SC. RAD51 localization and activation following DNA damage. *Philosophical Transactions of the Royal Society of London Series B: Biological Sciences*. 2004;359(1441):87-93.
231. Velic D, Couturier AM, Ferreira MT, Rodrigue A, Poirier GG, Fleury F, et al. DNA damage signalling and repair inhibitors: the long-sought-after Achilles' heel of cancer. *Biomolecules*. 2015;5(4):3204-59.
232. MacPhail S, Banath J, Yu T, Chu E, Lambur H, Olive P. Expression of phosphorylated histone H2AX in cultured cell lines following exposure to X-rays. *International journal of radiation biology*. 2003;79(5):351-9.
233. Zhou C, Li Z, Diao H, Yu Y, Zhu W, Dai Y, et al. DNA damage evaluated by gammaH2AX foci formation by a selective group of chemical/physical stressors. *Mutation research*. 2006;604(1-2):8-18.

234. Rappold I, Iwabuchi K, Date T, Chen J. Tumor suppressor p53 binding protein 1 (53BP1) is involved in DNA damage-signaling pathways. *The Journal of cell biology*. 2001;153(3):613-20.
235. Kinner A, Wu W, Staudt C, Iliakis G. γ -H2AX in recognition and signaling of DNA double-strand breaks in the context of chromatin. *Nucleic Acids Research*. 2008;36(17):5678-94.
236. Yuan S-SF, Chang H-L, Lee EYHP. Ionizing radiation-induced Rad51 nuclear focus formation is cell cycle-regulated and defective in both ATM^{-/-} and c-Abl^{-/-} cells. *Mutation Research/Fundamental and Molecular Mechanisms of Mutagenesis*. 2003;525(1):85-92.
237. Backer MV, Backer JM, Chinnaiyan P. Chapter Three - Targeting the Unfolded Protein Response in Cancer Therapy. In: Conn PM, editor. *Methods in Enzymology*. 491: Academic Press; 2011. p. 37-56.
238. Zanoni M, Piccinini F, Arienti C, Zamagni A, Santi S, Polico R, et al. 3D tumor spheroid models for in vitro therapeutic screening: a systematic approach to enhance the biological relevance of data obtained. *Scientific Reports*. 2016;6(1):19103.
239. Helleday T, Eshtad S, Nik-Zainal S. Mechanisms underlying mutational signatures in human cancers. *Nat Rev Genet*. 2014;15(9):585-98.
240. Mao Z, Bozzella M, Seluanov A, Gorbunova V. DNA repair by nonhomologous end joining and homologous recombination during cell cycle in human cells. *Cell Cycle*. 2008;7(18):2902-6.
241. Weber AM, Ryan AJ. ATM and ATR as therapeutic targets in cancer. *Pharmacology & therapeutics*. 2015;149:124-38.
242. Davidson D, Amrein L, Panasci L, Aloyz R. Small Molecules, Inhibitors of DNA-PK, Targeting DNA Repair, and Beyond. *Frontiers in pharmacology*. 2013;4:5.
243. Ciszewski WM, Tavecchio M, Dasty J, Curtin NJ. DNA-PK inhibition by NU7441 sensitizes breast cancer cells to ionizing radiation and doxorubicin. *Breast cancer research and treatment*. 2014;143(1):47-55.
244. Hafsi H, Dillon MT, Barker HE, Kyula JN, Schick U, Paget JT, et al. Combined ATR and DNA-PK Inhibition Radiosensitizes Tumor Cells Independently of Their p53 Status. *Front Oncol*. 2018;8:245.
245. Lee TW, Wong WW, Dickson BD, Lipert B, Cheng GJ, Hunter FW, et al. Radiosensitization of head and neck squamous cell carcinoma lines by DNA-PK inhibitors is more effective than PARP-1 inhibition and is enhanced by SLFN11 and hypoxia. *Int J Radiat Biol*. 2019:1-16.
246. Pires IM, Olcina MM, Anbalagan S, Pollard JR, Reaper PM, Charlton PA, et al. Targeting radiation-resistant hypoxic tumour cells through ATR inhibition. *Br J Cancer*. 2012;107(2):291-9.
247. Fabbrizi MR, Parsons JL. Radiotherapy and the cellular DNA damage response: current and future perspectives on head and neck cancer treatment. *Cancer Drug Resistance*. 2020;3.
248. Magi B, Liberatori S. Immunoblotting techniques. *Immunochemical Protocols*: Springer; 2005. p. 227-53.
249. Gingrich JC, Davis DR, Nguyen Q. Multiplex detection and quantitation of proteins on western blots using fluorescent probes. *Biotechniques*. 2000;29(3):636-42.
250. Bakkenist CJ, Kastan MB. DNA damage activates ATM through intermolecular autophosphorylation and dimer dissociation. *Nature*. 2003;421(6922):499-506.

251. Carruthers R, Ahmed SU, Strathdee K, Gomez-Roman N, Amoah-Buahin E, Watts C, et al. Abrogation of radioresistance in glioblastoma stem-like cells by inhibition of ATM kinase. *Molecular Oncology*. 2015;9(1):192-203.
252. Tian X, Lara H, Wagner KT, Saripalli S, Hyder SN, Foote M, et al. Improving DNA double-strand repair inhibitor KU55933 therapeutic index in cancer radiotherapy using nanoparticle drug delivery. *Nanoscale*. 2015;7(47):20211-9.
253. Ghosh S, Bhat NN, Santra S, Thomas R, Gupta S, Choudhury R, et al. Low energy proton beam induces efficient cell killing in A549 lung adenocarcinoma cells. *Cancer investigation*. 2010;28(6):615-22.
254. Momčilović O, Choi S, Varum S, Bakkenist C, Schatten G, Navara C. Ionizing Radiation Induces Ataxia Telangiectasia Mutated-Dependent Checkpoint Signaling and G2 But Not G1 Cell Cycle Arrest in Pluripotent Human Embryonic Stem Cells. *STEM CELLS*. 2009;27(8):1822-35.
255. Xue L, Yu D, Furusawa Y, Okayasu R, Tong J, Cao J, et al. Regulation of ATM in DNA double strand break repair accounts for the radiosensitivity in human cells exposed to high linear energy transfer ionizing radiation. *Mutation Research/Fundamental and Molecular Mechanisms of Mutagenesis*. 2009;670(1):15-23.
256. Nam EA. Phospho-regulation of the DNA Damage Response Kinase ATR: Vanderbilt University; 2011.
257. Jossé R, Martin SE, Guha R, Ormanoglu P, Pfister TD, Reaper PM, et al. ATR inhibitors VE-821 and VX-970 sensitize cancer cells to topoisomerase I inhibitors by disabling DNA replication initiation and fork elongation responses. *Cancer research*. 2014;74(23):6968-79.
258. Abramenkova A, Stenerlöv B. Measurement of DNA-Dependent Protein Kinase Phosphorylation Using Flow Cytometry Provides a Reliable Estimate of DNA Repair Capacity. *Radiation Research*. 2017;188(6):677-84.
259. Chatterjee P, Plesca D, Mazumder S, Boutros J, Yannone SM, Almasan A. Defective chromatin recruitment and retention of NHEJ core components in human tumor cells expressing a Cyclin E fragment. *Nucleic acids research*. 2013;41(22):10157-69.
260. Zhang T, Shen Y, Chen Y, Hsieh J-T, Kong Z. The ATM inhibitor KU55933 sensitizes radioresistant bladder cancer cells with DAB2IP gene defect. *International Journal of Radiation Biology*. 2015;91(4):368-78.
261. Harding SM, Bristow RG. Discordance between phosphorylation and recruitment of 53BP1 in response to DNA double-strand breaks. *Cell Cycle*. 2012;11(7):1432-44.
262. Hamada N. Ionizing radiation response of primary normal human lens epithelial cells. *PloS one*. 2017;12(7):e0181530.
263. Yanai M, Makino H, Ping B, Takeda K, Tanaka N, Sakamoto T, et al. DNA-PK Inhibition by NU7441 Enhances Chemosensitivity to Topoisomerase Inhibitor in Non-Small Cell Lung Carcinoma Cells by Blocking DNA Damage Repair. *Yonago Acta Med*. 2017;60(1):9-15.
264. Sakasai R, Teraoka H, Takagi M, Tibbetts RS. Transcription-dependent activation of ataxia telangiectasia mutated prevents DNA-dependent protein kinase-mediated cell death in response to topoisomerase I poison. *Journal of Biological Chemistry*. 2010;285(20):15201-8.

265. Cornell L, Munck J, Curtin N, Reeves H. PTU-042 DNA-PK or ATM inhibition inhibits non-homologous end joining and enhances chemo-and radio sensitivity in hepatocellular cancer cell lines. *Gut*. 2012;61(Suppl 2):A201-A.
266. Dickreuter E, Eke I, Krause M, Borgmann K, van Vugt MA, Cordes N. Targeting of beta1 integrins impairs DNA repair for radiosensitization of head and neck cancer cells. *Oncogene*. 2016;35(11):1353-62.
267. Carter RJ, Nickson CM, Thompson JM, Kacperek A, Hill MA, Parsons JL. Characterisation of deubiquitylating enzymes in the cellular response to high-LET ionizing radiation and complex DNA damage. *International Journal of Radiation Oncology* Biology* Physics*. 2019;104(3):656-65.
268. Vitti ET, Parsons JL. The Radiobiological Effects of Proton Beam Therapy: Impact on DNA Damage and Repair. *Cancers (Basel)*. 2019;11(7).
269. Gobeil S, Boucher CC, Nadeau D, Poirier GG. Characterization of the necrotic cleavage of poly(ADP-ribose) polymerase (PARP-1): implication of lysosomal proteases. *Cell Death & Differentiation*. 2001;8(6):588-94.
270. Lakshmanan I, Batra SK. Protocol for Apoptosis Assay by Flow Cytometry Using Annexin V Staining Method. *Bio Protoc*. 2013;3(6):e374.
271. Wlodkowic D, Skommer J, Darzynkiewicz Z. Flow cytometry-based apoptosis detection. *Methods Mol Biol*. 2009;559:19-32.
272. Nikitaki Z, Nikolov V, Mavragani IV, Mladenov E, Mangelis A, Laskaratou DA, et al. Measurement of complex DNA damage induction and repair in human cellular systems after exposure to ionizing radiations of varying linear energy transfer (LET). *Free radical research*. 2016;50(sup1):S64-S78.
273. Moro M, Casanova M, Roz L. Patient-derived xenografts, a multi-faceted in vivo model enlightening research on rare liver cancer biology. *Hepatobiliary surgery and nutrition*. 2017;6(5):344.
274. Yang H, Sun L, Liu M, Mao Y. Patient-derived organoids: a promising model for personalized cancer treatment. *Gastroenterol Rep (Oxf)*. 2018;6(4):243-5.
275. Nagle PW, Plukker JTM, Muijs CT, van Luijk P, Coppes RP. Patient-derived tumor organoids for prediction of cancer treatment response. *Seminars in Cancer Biology*. 2018;53:258-64.
276. Driehuis E, Kolders S, Spelier S, Löhmußaar K, Willems SM, Devriese LA, et al. Oral Mucosal Organoids as a Potential Platform for Personalized Cancer Therapy. *Cancer discovery*. 2019;9(7):852-71.
277. Tanaka N, Osman AA, Takahashi Y, Lindemann A, Patel AA, Zhao M, et al. Head and neck cancer organoids established by modification of the CTOS method can be used to predict in vivo drug sensitivity. *Oral Oncol*. 2018;87:49-57.
278. Dietlein F, Thelen L, Reinhardt HC. Cancer-specific defects in DNA repair pathways as targets for personalized therapeutic approaches. *Trends in genetics : TIG*. 2014;30(8):326-39.
279. Brown JS, O'Carrigan B, Jackson SP, Yap TA. Targeting DNA Repair in Cancer: Beyond PARP Inhibitors. *Cancer discovery*. 2017;7(1):20-37.
280. Stover EH, Konstantinopoulos PA, Matulonis UA, Swisher EM. Biomarkers of Response and Resistance to DNA Repair Targeted Therapies. *Clin Cancer Res*. 2016;22(23):5651-60.

281. Chaturvedi AK, Anderson WF, Lortet-Tieulent J, Curado MP, Ferlay J, Franceschi S, et al. Worldwide trends in incidence rates for oral cavity and oropharyngeal cancers. *J Clin Oncol*. 2013;31(36):4550-9.
282. Marur S, D'Souza G, Westra WH, Forastiere AA. HPV-associated head and neck cancer: a virus-related cancer epidemic. *Lancet Oncol*. 2010;11(8):781-9.
283. Bray F, Ferlay J, Soerjomataram I, Siegel RL, Torre LA, Jemal A. Global cancer statistics 2018: GLOBOCAN estimates of incidence and mortality worldwide for 36 cancers in 185 countries. *CA Cancer J Clin*. 2018;68(6):394-424.
284. Weaver AN, Cooper TS, Rodriguez M, Trummell HQ, Bonner JA, Rosenthal EL, et al. DNA double strand break repair defect and sensitivity to poly ADP-ribose polymerase (PARP) inhibition in human papillomavirus 16-positive head and neck squamous cell carcinoma. *Oncotarget*. 2015;6(29):26995-7007.
285. Gillison ML, Akagi K, Xiao W, Jiang B, Pickard RKL, Li J, et al. Human papillomavirus and the landscape of secondary genetic alterations in oral cancers. *Genome Res*. 2019;29(1):1-17.
286. Akagi K, Li J, Broutian TR, Padilla-Nash H, Xiao W, Jiang B, et al. Genome-wide analysis of HPV integration in human cancers reveals recurrent, focal genomic instability. *Genome Res*. 2014;24(2):185-99.
287. Rusan M, Li YY, Hammerman PS. Genomic landscape of human papillomavirus-associated cancers. *Clin Cancer Res*. 2015;21(9):2009-19.
288. Carter RJ, Nickson CM, Thompson JM, Kacperek A, Hill MA, Parsons JL. Complex DNA Damage Induced by High Linear Energy Transfer Alpha-Particles and Protons Triggers a Specific Cellular DNA Damage Response. *Int J Radiat Oncol Biol Phys*. 2018;100(3):776-84.
289. Carter RJ, Nickson CM, Thompson JM, Kacperek A, Hill MA, Parsons JL. Characterisation of Deubiquitylating Enzymes in the Cellular Response to High-LET Ionizing Radiation and Complex DNA Damage. *Int J Radiat Oncol Biol Phys*. 2019;104(3):656-65.

cancers

Review

The Radiobiological Effects of Proton Beam Therapy: Impact on DNA Damage and Repair

Eirini Terpsi Vitti and Jason L Parsons *

Cancer Research Centre, Department of Molecular and Clinical Cancer Medicine, University of Liverpool, Liverpool L3 9TA, UK

* Correspondence: j.parsons@liverpool.ac.uk; Tel.: +44-151-794-8848

Received: 6 May 2019; Accepted: 2 July 2019; Published: date

Abstract: Proton beam therapy (PBT) offers significant benefit over conventional (photon) radiotherapy for the treatment of a number of different human cancers, largely due to the physical characteristics. In particular, the low entrance dose and maximum energy deposition in depth at a well-defined region, the Bragg peak, can spare irradiation of proximal healthy tissues and organs at risk when compared to conventional radiotherapy using high-energy photons. However, there are still biological uncertainties reflected in the relative biological effectiveness that varies along the track of the proton beam as a consequence of the increases in linear energy transfer (LET). Furthermore, the spectrum of DNA damage induced by protons, particularly the generation of complex DNA damage (CDD) at high-LET regions of the distal edge of the Bragg peak, and the specific DNA repair pathways dependent on their repair are not entirely understood. This knowledge is essential in understanding the biological impact of protons on tumor cells, and ultimately in devising optimal therapeutic strategies employing PBT for greater clinical impact and patient benefit. Here, we provide an up-to-date review on the radiobiological effects of PBT versus photon radiotherapy in cells, particularly in the context of DNA damage. We also review the DNA repair pathways that are essential in the cellular response to PBT, with a specific focus on the signaling and processing of CDD induced by high-LET protons.

Keywords: DNA damage; DNA repair; proton beam therapy; radiobiology

1. Introduction

Since its first application in the 1950s, proton beam therapy (PBT) is gaining ground in radiation oncology thanks to its radiobiological and physical advantages over photon radiotherapy [1]. Proton beams are characterized by a low entrance dose, whereby the protons lose energy along the track and just before they stop, the dose peaks in depth at a narrow and well-defined range called the Bragg peak (Figure 1A). The energy deposition drops rapidly shortly after the peak at the distal fall-off. This spares the surrounding tissue and organs at risk (OARs) in close proximity to the tumor being treated. A combination of beams with different initial energies can produce a wider peak, the so-called spread-out Bragg peak (SOBP), allowing the irradiation of larger target tumor volumes [2] (Figure 1B). However, as the protons slow down and lose energy further, their linear energy transfer (LET) increases and becomes maximal in the distal fall-off of the Bragg peak.

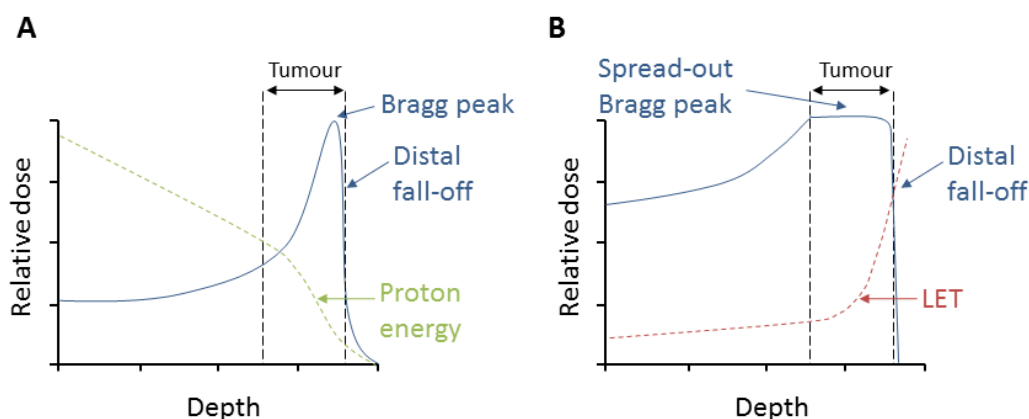


Figure 1. Depth–dose distribution of protons and relationship to energy and linear energy transfer (LET). (A) An unmodulated (pristine) Bragg peak produced by a proton beam. (B) Spread-out Bragg peak (SOBP) from several modulated proton beams.

As of now, there are 70 operative facilities worldwide for PBT and 42 under construction according to the Particle Therapy Co-Operative Group (<https://www.ptcog.ch>), with 150,000 patients receiving PBT treatment. Despite over 60 years of therapeutic use of protons, there are several uncertainties regarding the relative biological effectiveness (RBE) of the proton beam along the track, particularly throughout the SOBP where there are differences in proton energy and, therefore, LET. There is also a lack of understanding of the DNA damage induced by PBT, particularly the complexity and relative levels of clustered/complex DNA damage (CDD) induced by protons at the distal edge of the Bragg peak. Consequently, the cellular DNA damage response (DDR) and repair pathways that are required for resolving CDD generated by PBT are not fully understood. Related to this, individual human cancers will furthermore display inherent differences in radiosensitivity to PBT, of which proteins involved in the DDR play such an important role. These uncertainties limit our ability to use PBT to its full advantage, by exploiting tumor killing while reducing the exposure of healthy tissue [3].

In this review, we provide the latest knowledge of the radiobiology of PBT, particularly in the context of DNA damage and the repair pathways that are important for the cellular DDR, and discuss the areas where ongoing research is necessary, which will have a major impact on the effective clinical use of PBT for cancer treatment.

2. Relative Biological Effectiveness (RBE) and Linear Energy Transfer (LET)

RBE is used to correlate PBT to photon radiotherapy, as is it the ratio of the reference radiation (photon) dose to the dose of protons required to cause the same biological effect. In clinical practice, a constant RBE value of 1.1 is utilized throughout the Bragg curve, despite the ongoing debate about whether this is the optimal solution or not [3–5]. RBE depends on both physical factors such as the proton beam energy, the dose fractionation and dose rate, and biological factors including the type of the tissue, cell-cycle stage, the oxygenation level, and the position of irradiation along the SOBP [5–7]. Experimental evidence largely derived from *in vitro* clonogenic survival assays using PBT facilities ranging from 65–250 MeV have demonstrated that the RBE value is variable and increases with decreasing dose [3,5,8,9]. In spite of the large fluctuation derived from *in vitro* data and the biological uncertainty, a constant RBE of 1.1 is used clinically to minimize the potential for risks [3,7,10,11]. One of the parameters mainly determining RBE values is the LET, which is the energy loss and deposition along the path of the proton beam and is a measure of ionization density [3,5]. Therefore, the higher the LET is, the denser the ionization events are, resulting in more extensive damage induction. High-energy PBT is considered low-LET irradiation; however, as the proton beam energy decreases throughout the

SOBP, the LET increases particularly at the distal edge. Consequently, RBE values have been reported to rise from ~1.1 in the entrance, to ~1.2 in the center, ~1.4 at the distal edge, and ~1.7 in the distal fall-off the SOBP [11,12]. However, RBE values at the distal fall-off were shown to rise to over 3, which is supported by two other studies using clonogenic survival assays indicating RBE values of up to 2.3 [13] and 3.5 [14]. Furthermore, a dose shift around the distal edge where the biological dose extends beyond the range of the SOBP can threaten proximal healthy tissue, potentially causing unexpected side effects [15]. Interestingly a recent *in vivo* study using rat cervical spinal cords irradiated at four different positions of an SOBP demonstrated that RBE values varied from 1.1 to 1.3, dependent on LET [16]. The uncertainties and challenges with RBE are not covered at length here, and we refer the reader to the literature cited above and more recent reviews [17,18].

3. Radiobiological Effects of Protons

3.1. DNA Damage and Repair

The therapeutic effect of PBT, similar to conventional radiotherapy techniques, relies on significant DNA damage within tumorous cells leading to cell death. A variety of DNA lesions are induced along the radiation track (Figure 2), which include DNA base damage, sites of base loss (abasic sites), and DNA single-strand breaks (SSBs) that are most abundantly generated. On the other hand, the formation of DNA double-strand breaks (DSBs) and complex DNA damage (CDD) containing two or more DNA lesions in close proximity (within 1–2 helical turns of the DNA [19]) are less frequent, although these are considered the most lethal [20–22]. However, human cells have developed a sophisticated signaling network, the cellular DDR, which detects and repairs these DNA lesions [23]. DSBs are mainly resolved via two repair pathways, non-homologous end-joining (NHEJ) and homologous recombination (HR) (reviewed in [24,25]). Pathway choice is partly dependent on cell-cycle stage, with NHEJ mostly active in G₀/G₁, whereas HR is active in S/G₂ phases [26]. NHEJ can be further divided into classical NHEJ, which involves the Ku70/80 heterodimer that binds to the DSB ends and recruits the DNA-dependent protein kinase catalytic subunit (DNA-Pkcs), and X-ray repair cross-complementing protein 4 (XRCC4)–DNA ligase IV that promotes the end-joining reaction (Figure 2B). Whereas alternative NHEJ involves DNA end resection by the MRE11–RAD50–NBS1 (MRN) complex, poly(ADP-ribose) polymerase-1 (PARP-1) that binds to the DNA ends, and X-ray repair cross-complementing protein 1–DNA ligase III α (XRCC1–Lig III α) or DNA ligase I (Lig I) that seals the DSB (Figure 2C). During HR, the DNA undergoes end resection by the MRN complex and the 3′-single stranded DNA is coated by replication protein A (RPA) and RAD51 that promotes invasion into the sister chromatid. DNA synthesis is followed by resolution of Holliday junctions before completing repair (Figure 2D). CDD, given that this contains localized damage over short distances within the DNA, can include a mixture of DNA base damage, abasic sites, SSBs, and DSBs [27]. This, therefore, represents a major barrier to the cellular DDR for efficient repair; however, considering the nature of the damage, it is assumed that these CDD sites will require the relevant proteins involved in base excision repair (BER), as well as DSB repair. BER is generally coordinated through the action of damage-specific DNA glycosylases that excise the damaged DNA bases, AP-endonuclease 1 (APE1) that incises the resulting abasic sites and generates an SSB for PARP-1 binding, DNA polymerase β (Pol β) that removes the 5′-deoxyribosephosphate moiety and inserts the correct undamaged nucleotide, and a complex of XRCC1–Lig III α that seals the SSB [28,29] (Figure 2A).

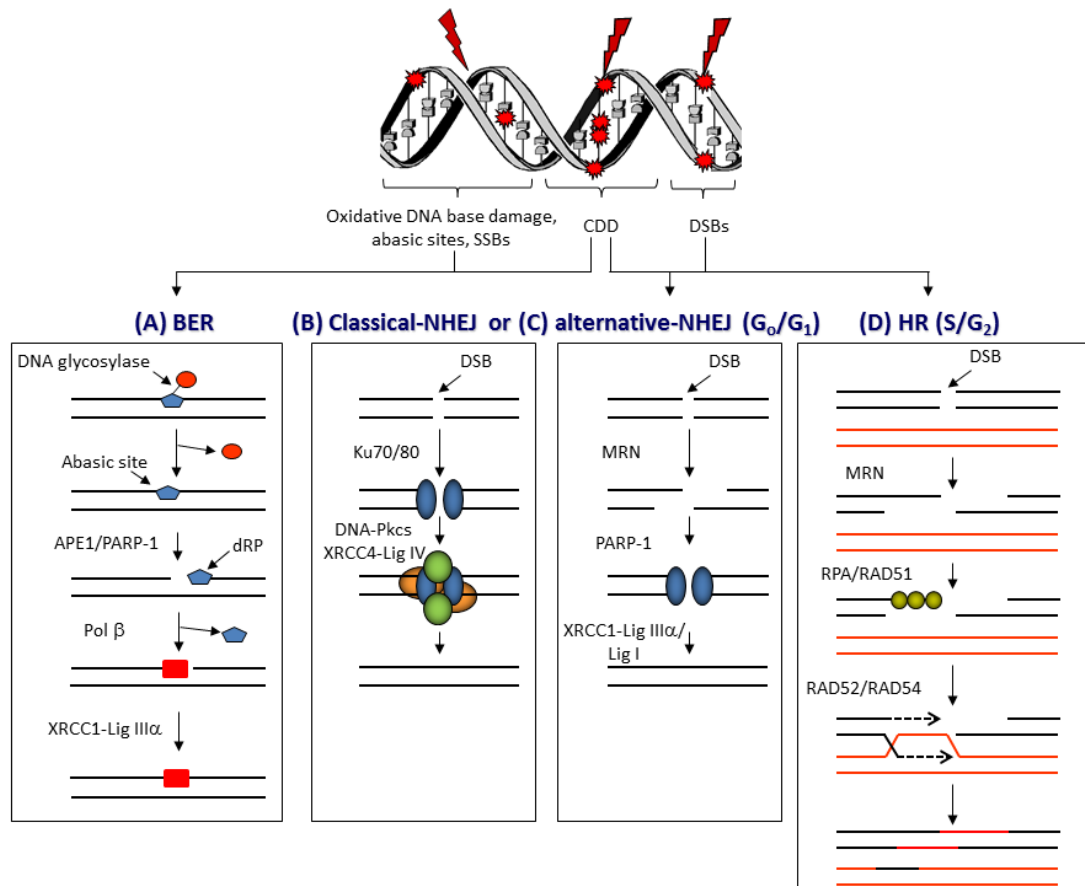


Figure 2. The response to ionising radiation (IR)-induced DNA damage. Proton beam therapy (PBT), similar to other radiotherapy techniques, targets DNA and can generate an abundance of DNA lesions, where oxidative DNA base damage, abasic sites, and single-strand breaks (SSBs) predominate, and which are repaired via (A) the base excision repair (BER) pathway. This involves recognition of the damaged base by a damage specific DNA glycosylase, incision of the abasic site by AP-endonuclease 1 (APE1) and SSB binding by poly(ADP-ribose) polymerase-1 (PARP-1), 5'-deoxyribosephosphate (dRP) removal and gap filling by DNA polymerase β (Pol β), and finally ligation by X-ray repair cross-complementing protein 1-DNA ligase III α (XRCC1-Lig III α) complex. Double-strand breaks (DSBs) are repaired by different pathways dependent on cell-cycle phase. In the G_0/G_1 phases, DSBs are repaired by either (B) classical non-homologous end-joining (NHEJ) involving Ku70/80 that binds to the DNA ends, followed by DNA-dependent protein kinase catalytic subunit (DNA-Pkcs) and XRCC4-Lig IV that promote DNA ligation, or via (C) alternative NHEJ which involves DSB end resection by the MRE11-RAD50-NBS1 (MRN) complex, PARP-1 binding to the DSB ends, and subsequent repair by Lig I or XRCC1-Lig III α . In the S/G_2 phases of the cell cycle, DSB repair is achieved by (D) homologous recombination (HR) which uses a sister chromatid for repair. Therefore, following DNA end resection by the MRN complex, replication protein A (RPA) and RAD51 bind to the single-stranded DNA overhangs that promote strand invasion and subsequent DNA synthesis in the presence of RAD52/RAD54, as well as formation and resolving of Holliday junctions. The induction of complex DNA damage (CDD), consisting of several DNA lesions in close proximity, particularly by high-LET protons at the distal edge of the SOBP, likely require multiple pathways for repair.

3.2. DNA Damage Induction and Repair Following PBT

Protons, as particles with mass and positive charge, interact with tissue completely differently from photons which have neither mass nor charge, although the specific physical aspects (e.g., beam intensity, LET, and secondary particle spectra) depend very much on the proton beam delivery system [30]. Consequently, DNA damage induction and the mechanisms

of DNA repair employed are reportedly different between PBT and conventional radiotherapy [31]. Most of the focus of current studies is on examining the induction of DSBs, given that they are one of the major contributors, along with CDD, to cell lethality post-irradiation (Table 1). Firstly, a significantly higher level (~1.2–1.6-fold) of DSBs, particularly at 30 min post-irradiation, via analysis of phosphorylated histone variant H2AX (γ H2AX) foci, was shown for a 200 MeV PBT source compared to 10 MV photons in two human tumor cell lines, ONS76 medulloblastoma cells and MOLT4 leukemia cells [32]. The disparities in foci number diminished after 6 h post-irradiation, although it was reported that the PBT-induced γ H2AX foci in the ONS76 cells appeared to be ~1.2–1.5-fold larger in size, indicating a possible CDD phenotype. The fact that these foci were resolved with similar kinetics would, however, argue that these DSBs are possibly not complex in nature, given that CDD sites usually take a longer time to resolve. Similarly, the number of DSBs in SQ23B head and neck squamous cell carcinoma (HNSCC) cells measured by pulse-field gel electrophoresis was found to be ~1.2-fold higher for both 76 MeV and 201 MeV PBT sources than with photons induced by γ -irradiation [9]. Yet interestingly, DSB numbers were not significantly different between the two PBT energies or at different positions (entrance, mid, and distal) relative to the SOBP, and any potential differences in kinetics of DSB repair were not reported. Numbers of both DSBs and SSBs were also shown to be significantly higher (~1.2–1.6-fold increases in comet percentage tail DNA) in glioblastoma stem-like cells treated with protons in comparison to 320 kV X-rays, particularly at 20–48 h post-irradiation, which was associated with a higher level of apoptosis [33]. In contrast to the above studies, the numbers of γ H2AX and 53BP1 foci (as DSB markers) induced in TrC1 prostate cancer cells and murine embryonic fibroblasts irradiated at the entrance dose of a 187 MeV PBT beam compared to 320 kV photons were observed to be the same 30 min post-irradiation [34]. The kinetics of DSB repair, specifically the resolving of γ H2AX and 53BP1 foci, were also shown to be similar in response to the two irradiation conditions. This is supported by equal numbers of 53BP1 foci induced in AG01522 skin fibroblasts 30 min post-irradiation at the entrance dose, and their repair up to 24 h post-irradiation, of a 60 MeV proton beam compared to 225 kV X-rays [35]. Additionally, it was demonstrated that the initial level of induction of DSBs (γ H2AX foci) was the same in wild-type, HR-deficient, and NHEJ-deficient Chinese hamster ovary cell lines following 1 Gy irradiation with low-LET 138 MeV PBT and 200 kV X-rays [36]. However PBT resulted in further reduced clonogenic survival in wild-type cell lines versus X-ray irradiation, suggesting that the quality of DNA damage (e.g., formation of CDD) is what differs between PBT and X-rays and their effectiveness in cell killing, although differences in levels of CDD was not proven directly.

Our recent study, using the neutral comet assay, demonstrated that the kinetics of repair of DSBs induced by the entrance dose of a proton beam (58 MeV) versus 100 kV X-rays in HeLa and HNSCC cells are not significantly different [37]. This would indicate that the nature and complexity of the DSBs following the two irradiation conditions are similar. Likewise, the kinetics of SSB/abasic site repair using the alkaline comet assay were comparatively the same. Furthermore, we observed that low-energy protons generated at the distal edge of a SOBP (11 MeV mean energy incident on the cells) had no impact on the repair of DSBs in both HeLa and HNSCC cells in comparison to 58 MeV protons and 100 kV X-rays, even though there was a significant difference in clonogenic survival between the proton irradiation conditions. However, we observed a significant delay in the repair of SSB/abasic sites only following low-energy proton irradiation. In fact, levels of SSBs were ~4–7-fold higher 2 h post-irradiation under these conditions, in comparison to cells irradiated with 58 MeV protons. This suggested that low-energy protons can generate CDD that is largely SSB-associated, which persists for several hours (>2 h) post-irradiation and contributes to decreased cell survival, although the specific nature and composition of the CDD under these conditions requires further research (see also Section 3.5).

Table 1. Comparisons of double-strand breaks (DSBs) induced by proton beam therapy (PBT) versus photon irradiation.

| Cell Line | Method(s) | Proton Energy | Photon Energy | Observation (Proton vs Photon) | Ref |
|---------------------------------------------------------------------|------------------------------------------------------------|------------------------------------------|------------------------------------------|-------------------------------------------------------------------------------------------------|------|
| ONS76 medulloblastoma; MOLT4 leukemia cells | γ H2AX foci by immunofluorescence | 200 MeV | 10 MV X-rays | ~1.2–1.6-fold increase in DSB foci and ~1.2–1.5-fold larger in size 30–180 min post-irradiation | [32] |
| HeLa; SQ20B HNSCC cells | Pulse-field gel electrophoresis | 76 MeV, 201 MeV | 622 keV ^{137}Cs γ -rays | ~1.2-fold increase in DSBs. No differences between PBT energies, nor along the SOBP | [9] |
| IN528 and T4213 glioblastoma stem-like cells | Alkaline and neutral comet assay | N.S. | 320 kV X-rays | ~1.2–1.6-fold higher numbers of DSBs at 20–48 h post-irradiation | [33] |
| TrC1 prostate cancer cells; murine embryonic fibroblasts | Histone γ H2AX and 53BP1 foci by immunofluorescence | 187 MeV entrance dose | 320 kV X-rays | Similar numbers of DSBs at 0.5–24 h post-irradiation | [34] |
| AG01522 skin fibroblasts | 53BP1 foci by immunofluorescence | 60 MeV entrance dose | 225 kV X-rays | Similar numbers of DSBs at 0.5–24 h post-irradiation | [35] |
| Wild-type, HR-, and NHEJ-deficient Chinese hamster ovary cell lines | Histone γ H2AX foci by immunofluorescence | 138 MeV | 200 kV X-rays | Similar initial induction of DSBs | [36] |
| HeLa; UMSCC74A and UMSCC6 HNSCC cells | Neutral comet assay | 58 MeV entrance dose; 11 MeV distal edge | 100 kV X-rays | No difference in DSB repair kinetics | [37] |

N.S. refers to not specified. HR—homologous recombination; NHEJ—non-homologous end-joining; SOBP—spread-out Bragg peak.

3.3. Generation of Reactive Oxygen Species and Cell-Cycle Progression Following PBT

Related to DNA damage induction is the generation of reactive oxygen species (ROS). Interestingly, a more rapid and prominent increase in ROS following PBT was reported in neural precursor cells from rat hippocampus exposed to either 250 MeV protons near the Bragg peak, versus 250 kV X-rays [38]. Proton-induced ROS peaked 6 h post-irradiation and was ~1.5-fold above the control levels, while photon-induced ROS peaked 12 h post-irradiation and was ~1.3-fold above the control levels at a 5 Gy dose equivalent. However, less prominent increases and time-dependent differences in ROS levels were observed at a 1 Gy dose. Furthermore, it was shown that protons were more effective in killing cancer stem-like cells derived from non-small-cell lung cancer cell lines, and that compared to photons, protons induced higher levels (~1.1–1.7-fold) of ROS after treating these cells with equivalent doses of radiation [39]. ROS were also demonstrated to play an important role in inducing cytotoxicity of glioblastoma stem-like cells treated with protons, and ROS levels were ~1.8-fold higher following protons versus 320 kV X-rays at 20 h post-irradiation, which led to increased cellular apoptosis [33]. Levels of ROS were continually and dramatically higher (~6–7-fold) three days following protons in comparison to photons.

Cell-cycle progression is another important factor related to proton-induced DNA damage, as DNA damage checkpoints will be activated to allow cells to undergo extensive DNA repair

prior to DNA synthesis or replication. This is also important for understanding the repair pathway choice (see Section 3.4), given that DSBs can be repaired by either NHEJ or HR in different cell-cycle phases. One study conducted using human lung cancer cells suggested that, following 62 MeV protons, CRL5876 cells appeared to accumulate (~2-fold increase) in the G₁ phase at 24 h post-irradiation, but that both CRL5876 and HTB177 cells accumulate (~1.5–2-fold increase) in G₂/M at 48 h post-irradiation, versus unirradiated controls [40]. However, no comparisons against photon irradiation were performed. We also recently noted an accumulation (~1.5-fold increase) of HeLa cells in G₂/M, particularly at 8–24 h post-irradiation with 58 MeV PBT, which was not LET-dependent as the same observation was seen with cells irradiated with low-energy protons generated at the distal edge of a SOBP (11 MeV mean energy incident on the cells) at higher LET [37,41]. This, however, suggests that CDD induced by high-LET protons, at least under the conditions analyzed, is not a major contributory factor to the observed cell-cycle checkpoint activation. An early study observed G₂ arrest of glioblastoma cells at 24–72 h post-irradiation following 5.7 MeV protons at relatively high-LET, which was more pronounced (~1.5–2.5-fold) than irradiation of cells using 120 kV X-rays [42], suggesting potential proton-specific effects. In contrast, there was no dramatic difference in cell-cycle distribution of Chinese hamster ovary cells when comparing the response to low-LET 138 MeV PBT and 200 keV X-rays, where a degree of G₂/M accumulation (~1.2–2-fold increase) of cells irradiated at 5 Gy dose equivalent, particularly at 6–12 h following both irradiation types, was observed [36]. Furthermore, it was shown that proton irradiation of glioblastoma stem-like cells actually led to a shortened G₂/M arrest compared to 320 kV X-ray irradiation, as demonstrated by a ~2-fold accumulation of cells in this cell-cycle phase at six days post-irradiation following photon irradiation only [33]. However, the baseline levels of cells in G₂/M in this study were noticeably different (~10 and 20 %) in the experiments comparing proton and photon irradiation. Given the variability in the observations, more studies to directly compare progression of cells through the cell cycle in response to protons versus photons in specific cell models, and the impact of LET need to be performed.

3.4. DSB Repair Pathway Choice Following PBT

NHEJ is considered the primary mechanism for DSB repair, particularly in response to photon irradiation, but there are a few conflicting reports to date suggesting that the DNA repair pathway choice specifically following PBT may in fact be different (Table 2). Firstly, by studying DNA repair kinetics in wild-type, NHEJ-deficient (XRCC4 and DNA-Pkcs) and HR-deficient (XRCC2 and XRCC3) Chinese hamster cell lines exposed to photon (γ -irradiation) versus low-LET 200 MeV protons, the same biological effect was observed in each cell line comparing the two radiation types [43]. Therefore, a delayed decrease in γ H2AX foci at 3–12 h post-irradiation, as well as significantly reduced clonogenic survival, was observed in DNA-Pkcs-deficient cells in comparison to wild-type cells. However, HR-deficient cells also displayed increased sensitivity to protons and photons, and significantly higher chromosomal aberrations (~2–4-fold increases) were found in both NHEJ- and HR-deficient cells compared to the wild-type cells following both radiation types. From this study, it was suggested that NHEJ is the major pathway, and DNA-Pkcs is the main protein involved in resolving DSBs induced not only by photons but also by low-LET protons. This is supported by another study demonstrating that there were no significant differences in γ H2AX foci formation and their repair in wild-type and DNA-Pkcs-deficient Chinese hamster ovary cell lines in response to γ -irradiation versus low-LET protons [44]. Persistent γ H2AX foci was observed in the DNA-Pkcs-deficient cells 6 h post-irradiation with higher doses (2–3 Gy) of photons or protons, correlating with increased radiosensitivity versus wild type cells. In contrast using a similar experimental set-up of Chinese hamster ovary cell lines deficient in HR (XRCC3) or treated with small interfering RNA (siRNA) targeting RAD51 and comparing low-LET 138 MeV proton and 200 kV photons, it was suggested that PBT induced more lethal chromosomal aberrations [36]. Moreover, this study reported that PBT was more

effective in killing HR-deficient cell lines than NHEJ-deficient cells and, therefore, there was an enhanced dependence on HR for repair of proton-induced DSBs. The same conclusion was found following an examination of low-LET PBT (138 MeV) versus 200 kV photon irradiation in human tumor cells that were treated with siRNA or inhibitors targeting key proteins involved in HR and NHEJ [45]. It was found that DNA-Pkcs inhibition significantly radiosensitized A549 lung cancer and glioblastoma cells to photon-irradiated cells, but that this was to a lesser degree following low-LET PBT. Photon-irradiated cells in the presence of the inhibitor also showed delayed resolving of γ H2AX foci at 6–24 h post-irradiation which were ~1.5–3-fold higher than the corresponding cells following proton irradiation. In addition, it was found that HR-deficient cell lines (RAD51 siRNA) were more sensitive to proton irradiation and similarly had difficulty resolving γ H2AX foci, again suggesting a dependence of the cells to utilize HR for repairing proton-induced lesions. Evidence examining the response of HeLa cells to 21 MeV protons by immunostaining and high-resolution microscopy demonstrated an association of RAD51 with almost every 53BP1 foci 1 h post-irradiation, also indicating that the proportion of cells undergoing HR following PBT may be higher [46]. Interestingly, when examining the comparative RBE of 17 non-small-cell lung cancer cell lines in response to 235 MeV protons and 250 kV X-rays, only five of these displayed increased sensitivity to protons and two had confirmed defects in *BRCA1* indicative of a deficiency in HR [47]. The unexpected differences in RBE between protons and photons was again predicted to be due to differences in the formation of CDD. Given these opposing findings, more definitive evidence of the DNA repair pathway choice following proton irradiation is necessary.

Table 2. DNA double strand break (DSB) repair pathway choice following proton beam therapy (PBT) versus photon irradiation.

| Cell line | Irradiations | Outcome | Ref |
|---------------------------------------------------------------------|-----------------------------------------------------------------------|----------------------------------------------------------------|------|
| Wild-type, HR- and NHEJ-deficient Chinese hamster ovary cell lines | 200 MeV protons and ^{137}Cs γ -rays | NHEJ is the major pathway for both photons and low-LET protons | [43] |
| Wild-type and NHEJ-deficient Chinese hamster ovary cell lines | 14.4 MeV plateau protons and 667 keV ^{137}Cs γ -rays | NHEJ is the major pathway for both photons and low-LET protons | [44] |
| Wild-type, HR-, and NHEJ-deficient Chinese hamster ovary cell lines | 138 MeV protons and 200-kV X-rays | Dependence on HR following protons | [36] |
| A549 lung cancer; glioblastoma cells | 138 MeV protons and 200 kV X-rays | Dependence on HR following protons | [45] |
| HeLa | 21 MeV protons | Higher proportion of cells undergoing HR following protons | [46] |
| Non-small-cell lung cancer cells | 235 MeV protons and 250 kV X-rays | HR only partly required following protons | [47] |

LET—linear energy transfer; HR—homologous recombination; NHEJ—non-homologous end-joining.

3.5. CDD Formation Following PBT

Given the increase in LET toward the distal edge of the SOBP, this is considered to be particularly effective in increasing the amount of CDD, which is similar in nature to that observed following heavy-ion irradiation [31]. CDD is considered equally as effective as DSBs in cell killing due to the difficult nature of its repair leading to its persistence in cells and tissues [27]; therefore, it should be considered as a crucial factor in the cellular response to PBT. However, to date, most of the evidence relating to CDD formation specifically following proton irradiation is indirect. Indeed, through Monte Carlo simulations, and by examining DNA damage clustering with increasing PBT energies (500 keV–50 MeV) and, thus, decreasing LET, the amount and size of both complex SSBs and complex DSBs were found to decrease [48]. Similarly, the relative

frequencies of complex SSBs and DSBs were also shown to increase proportionally with increasing LET, which is dependent on proton energy [49,50]. A biophysical model of radiation-induced cell death and chromosomal aberrations based on the critical role of CDD, and compared to experimental data in AG01522 and V79 cells following irradiation with 62 MeV protons predicted that these end-points increased along the SOBP and were highest at the distal fall-off due to low-energy protons [6]. Cell death at a 2 Gy dose was calculated to increase ~1.5-fold and chromosome aberrations (dicentrics per cell) increased ~4-fold at the distal fall-off compared to the entrance dose. Additionally, more recently, Monte Carlo simulations were utilized to examine unrepaired DSBs 24 h after proton irradiation, which were observed to increase ~1.5-fold (2 Gy) and 1.7-fold (5 Gy) toward the distal fall-off of the SOBP at higher LET, predictably through increased DSB complexity [51].

In relation to experimental evidence, apart from observations of changes in RBE via clonogenic survival assays, which are suggestive of CDD formation, direct evidence is lacking, as CDD is notoriously difficult to measure and specifically define in terms of the nature of DNA damage complexity *in vivo* [21,52]. However in SQ23B HNSCC cells CDD, specifically complex DSBs measured by utilizing the *Escherichia coli* enzymes Fpg and Nth for excision of residual oxidative DNA base damage prior to pulse-field gel electrophoresis, was found to be ~1.2-fold higher for PBT at 76 MeV, but not 201 MeV, in comparison to γ -irradiation [9]. Interestingly, CDD formation did not depend on the position of irradiation in the SOBP, which conflicts with other reported data. In particular, it was demonstrated in AG01522 skin fibroblasts that persistent 53BP1 foci, as a marker of DSBs, was evident when cells were irradiated at the distal end of the SOBP of a 60 MeV proton beam in comparison to cells irradiated at the entrance dose or at the Bragg peak itself [35]. These persistent foci were evident at 24 h post-irradiation with Bragg peak protons and were elevated ~2-fold in comparison to the entrance dose and to 225 kV X-ray irradiation. This is supported by observations of a delay in resolving γ H2AX and 53BP1 foci in TrC1 prostate cancer cells and murine embryonic fibroblasts irradiated at the Bragg peak (31 MeV) compared to those irradiated at the entrance dose (187 MeV) [34]. Whilst the initial numbers of γ H2AX and 53BP1 foci under the comparative conditions were observed to be the same, there were significantly (~1.1–1.3-fold) higher levels of foci particularly at 1–4 h post-irradiation in cells irradiated at the Bragg peak, and these foci were also shown to be on average ~1.3-fold larger in size at 0.5 h and 6 h post-irradiation. However, all foci, indicative of DSB levels, were shown to be resolved by 24 h irrespective of the irradiation set-up. These two studies are suggestive of the formation of complex DSBs, particularly at higher LET, which have a longer lifetime to resolve, although direct evidence for this was not presented. More recently, we described utilization of different versions of the comet assay to directly demonstrate that CDD is generated in HeLa and HNSCC cells by low-energy protons (11 MeV mean energy incident on the cells; relatively high-LET) at the distal edge of an SOBP, in comparison to the cells irradiated at the entrance of a proton beam (58 MeV mean energy; low LET) that do not [37]. In particular, using an alkaline version of the comet assay, we showed that low-energy protons caused a reduced rate of repair of cellular SSBs and alkali-labile sites, suggesting that CDD was largely SSB/abasic site in nature. Under these conditions, we observed that SSB levels in cells were ~4–7-fold higher 2 h post-irradiation in comparison to cells irradiated with 58 MeV protons. Interestingly, there was no defect in the repair of DSBs visualized using the neutral comet assay. Furthermore, an enzyme-modified neutral comet assay employing recombinant DNA repair enzymes to excise any residual oxidative DNA base damage and abasic sites in association with DSBs confirmed direct evidence that CDD is formed by low-energy protons generated at the distal end of the SOBP. We demonstrated that CDD formation in HeLa cells was increased by ~1.3-fold immediately post-irradiation with low-energy protons versus 58 MeV protons, and that this damage persisted for at least 4 h post-irradiation. These findings altogether highlight the ability of PBT to induce potentially more lethal CDD at and around the Bragg peak where the highest LET occurs.

3.6. Cellular Response to CDD Generated by PBT

CDD sites are considered lethal, although this very much depends on the degree of complexity and the nature of the damage. Indeed, given that, broadly speaking, these are likely to consist of either complex SSBs or complex DSBs, the cellular response to these may require multiple DNA repair pathways and proteins, including, as indicated above (Figure 2), a combination of BER and NHEJ/HR [22,27]. However, despite an appreciation that CDD is a critical factor in the radiobiology of PBT, the cellular response to CDD induced by PBT, particularly with increasing LET along the SOBP, is surprisingly understudied. Predictably, there should be a signaling (DDR) mechanism within cells, similar to γ H2AX for DSBs, which is responsible for promoting the repair of CDD sites. We recently reported for the first time that monoubiquitylation of lysine 120 on histone H2B is promoted in HeLa and HNSCC cells in response to CDD induced by low-energy (11 MeV mean energy incident on the cells) protons at the distal edge of an SOBP, catalyzed by the E3 ubiquitin ligases ring finger 20/40 complex (RNF20/40) and male-specific lethal 2 homolog (MSL2) [37]. In fact, levels of histone H2B ubiquitylation increased by ~1.3–1.6-fold in HeLa cells and ~1.6–2.2-fold in HNSCC cells at 3–6 h post-irradiation. We demonstrated that this mechanism is important for the efficient repair of CDD sites, as revealed by delayed repair and significant persistence of CDD induced by low-energy protons in RNF20/40 and MSL2 siRNA-depleted cells using the enzyme-modified neutral comet assay, where CDD levels were ~2.3-fold higher compared to the non-targeting control siRNA treated cells at 4 h post-irradiation. Furthermore, RNF20/40 and MSL2 were shown to be required for promoting cell survival under these conditions, as revealed by clonogenic assays. We, therefore, believe that this is a mechanism for signaling recruitment of DNA repair proteins and/or for chromatin remodeling necessary for CDD repair (Figure 3). We also described possible evidence that other chromatin changes, particularly through histone trimethylation, are evident following irradiation of cells with low-energy protons; however, whether this is directly related to CDD repair is currently unknown. As a development of these findings, we also recently performed siRNA screening of deubiquitylation enzymes (DUBs) to further identify the specific enzymes controlling protein ubiquitylation that are involved in modulating cell survival in response to CDD induced by low energy (11 MeV; relatively high LET) protons at the distal edge of an SOBP, versus more simple DNA damage generated by both low-LET (58 MeV) protons and 100 kV X-ray irradiation [41]. This study revealed that ubiquitin-specific protease 6 (USP6) is required to promote survival in HeLa and HNSCC cells specifically in response to low-energy protons, and that this effect is mediated through stabilization of the SSB repair protein PARP-1 required for efficient CDD repair. In fact, levels of CDD were ~1.8-fold higher in USP6 siRNA-depleted cells compared to the non-targeting control siRNA treated cells at 4 h post-irradiation. This evidence was strengthened and mimicked using the PARP inhibitor olaparib, or through depletion of PARP-1 using siRNA, which was demonstrated to increase the radiosensitivity of cells to low-energy protons as a consequence of a significant deficiency in CDD repair. This correlates with our previous evidence suggesting that CDD generated under these conditions is largely SSB in nature [37], and that PARP-1 plays a critical role in its repair. However, our study revealed significant synergy between PARP inhibition and CDD induced by low-energy protons in enhancing cancer cell killing. Predictably, there is also dependence on other proteins in the BER pathway (such as APE1, Pol β , and XRCC1–Lig III α ; Figure 2A) required to promote CDD repair.

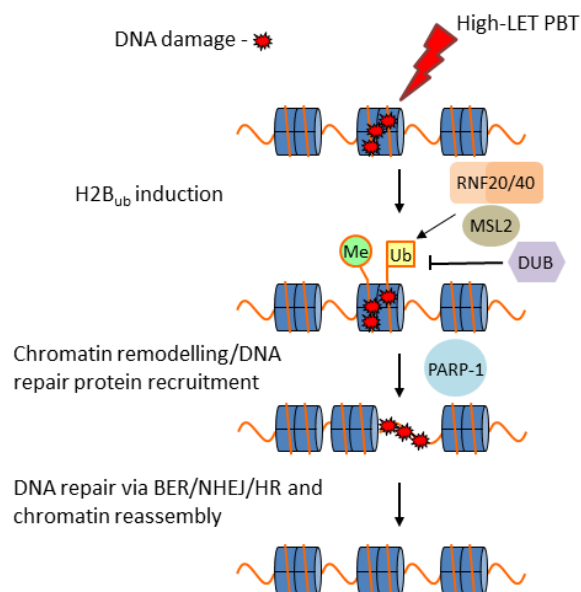


Figure 3. Proposed model for the cellular response to complex DNA damage (CDD) induced by proton beam therapy (PBT) in chromatin. On induction of CDD, this triggers monoubiquitylation of histone H2B on lysine 120 (Ub) by the E3 ubiquitin ligases ring finger 20/40 complex (RNF20/40) and male-specific lethal 2 homolog (MSL2). This stimulates recruitment of the necessary DNA repair proteins and/or chromatin remodeling factors that promote CDD accessibility. Poly(ADP-ribose) polymerase-1 (PARP-1) in particular is essential for efficient CDD repair. Our evidence also suggests the involvement of histone trimethylation (Me) and predictably a deubiquitylation enzyme (DUB) that is able to regulate access to CDD. Repair then proceeds through the respective DNA repair pathway dependent on the nature of the damage, although we suggest a particular dependence on the base excision repair (BER) pathway in the cellular response to high-LET protons, prior to subsequent chromatin assembly.

Previous studies of CDD have largely focused on high-LET heavy-ion irradiations. Here, these have demonstrated that in irradiated cells, CDD increases with increasing LET, but that these are predominantly unrepairable CDD that generate either chromosome aberrations through the lack of cell-cycle checkpoint activation or drive cells into senescence [53,54]. Therefore, it is important not to draw direct parallels between the unrepairable, highly complex CDD generated by heavy ions, and CDD sites generated by PBT which are likely to be less complex in nature and indeed repairable. Furthermore, it is thought that CDD may also be prone to generating increases in mutation frequency due to abortive or slow repair of CDD sites [55]. Nevertheless, due to technical limitations and lack of experimental studies in this area, we do not have a full appreciation of the cellular response to CDD specifically generated by PBT at different energies along the radiation track, and whether the nature of the damage, particularly toward the distal edge, is of sufficient complexity to drive mutagenesis and/or chromosomal aberrations. Therefore, more extensive research in this area is necessary.

4. Conclusions and Outlook

The utilization of PBT for cancer treatment is increasing worldwide and is appreciated to be advantageous over conventional radiotherapy as the maximum energy deposition occurs in a well-defined region (the Bragg peak) that can be specifically targeted to the tumor, which minimizes unnecessary irradiation of the surrounding normal tissues and OAR. However, there are still uncertainties with the radiobiology of PBT along the track of the proton beam and particularly the generation of high-LET protons at the distal edge that can have a greater impact on the molecular and cellular effects. Therefore, there is an urgent need to further understand the

biological effects of PBT, and particularly to understand the impact on DNA and how this varies with LET. Indeed, whilst it is widely accepted that CDD is induced at the distal edge of the SOBP, there is little information on the nature of the damage (e.g., DSB- or SSB-associated) related to proton energy/LET, and how cells are able to process this through cellular DDR pathways. This is challenging given that CDD is difficult to measure *in vivo*; thus, new strategies need to be devised to tackle this problem. There is also conflicting evidence that simple DSBs induced by PBT are largely repaired by HR, in contrast to NHEJ which is employed in response to photon irradiation, and whether this is cell-type-dependent. Furthermore, there are potential differences in the levels of ROS and impact of cell-cycle progression between protons and photons, although again more experimental data are required to substantiate these findings. These essential studies have to be carefully designed, particularly as cancer cell lines frequently have defects in DNA repair and in the cellular DDR; furthermore, irradiation of cells in specific cell-cycle phases must be taken into account given the dependence of cells to largely utilize HR in S/G₂ phases.

Another consideration is that additional experimental models and techniques need to be utilized in PBT research, rather than the conventional *in vitro* experiments using cultured monolayer cell lines mostly used to assess clonogenic survival post-irradiation. Increasingly, three-dimensional (3D) models are being employed in translational research, which more accurately reflect the structure and environment of the original tumor. Therefore, either 3D spheroid models of cancer cell lines, or multicellular spheroids encapsulating the tumor cells within the correct cellular microenvironment should be used to examine spheroid growth in response to PBT. These models will also allow a further examination of PBT radiobiology in terms of the types of DNA damage (e.g., DSBs and CDD) induced throughout the SOBP, the DNA repair pathways essential for their repair, and the impact of combinations of targeted drugs or inhibitors (e.g., those targeting the DDR [56]) with PBT in effective suppression of 3D spheroid growth. The next level would be to employ patient-derived organoids for examining how these respond to PBT *in vitro*, and possibly in the future to use these as predictive models for determining tumor response and ultimately patient outcome to PBT. Finally, more *in vivo* experiments employing xenograft models to assess growth of specific tumors following PBT, such as those conducted using HNSCC [57], should be conducted. These additional models and experiments bring their challenges, such as the availability and use of clinical facilities for performing animal irradiations, and technical challenges including the precise positioning and delivery of PBT to animals. In addition, a large proportion of PBT facilities worldwide are not usually equipped with on-site laboratories to effectively perform biological experiments *in vitro* and *in vivo*.

There is also an added level of complexity in terms of considering biological factors that may have a significant impact on the cellular DDR to PBT, particularly on overall efficacy of the treatment. For example, tumor hypoxia is well known to represent a barrier to the effectiveness of photon radiotherapy, although there is evidence that particle therapy with higher LET, particularly carbon ions, has a lower oxygen enhancement ratio and can, therefore, overcome radioresistance of the tumors. However, whether PBT, particularly at the Bragg peak and the associated distal edge with higher LET, is able to have the same impact on experimental models is unclear. Also, the tumor microenvironment is of particular importance given the recent success of immune checkpoint inhibitors (e.g., targeting PD-1/PD-L1) and their effective combination with radiotherapy for cancer treatment. However, again, there is little evidence available to understand the added benefit of immunotherapy strategies in combination with PBT. Nevertheless, there should be a drive from the clinical and scientific community to collaborate and engage in driving this preclinical and translational research which will ultimately be utilized for the optimization and personalization of PBT for patient benefit.

In summary, future PBT research should focus on the following:

- Further understanding of the biological effect of PBT at different energy/LET on the cellular DDR;

- Employing additional *in vitro* models (e.g., 3D spheroids/organoids) in radiobiology experiments;
- Increased utilization of *in vivo* experiments employing specific tumor models;
- Consideration of other biological factors (e.g., hypoxia, tumor microenvironment).

Author Contributions: Conceptualization, J.L.P.; writing—original draft preparation, E.T.V.; writing—review and editing, E.T.V. and J.L.P.; supervision, J.L.P.; funding acquisition, J.L.P.

Funding: This research was funded by North West Cancer Research, CR CC7, to J.L.P.

Conflicts of Interest: The authors declare no conflicts of interest.

References

1. Durante, M.; Loeffler, J.S. Charged particles in radiation oncology. *Nat. Rev. Clin. Oncol.* **2010**, *7*, 37–43, doi:10.1038/nrclinonc.2009.183.
2. Tommasino, F.; Durante, M. Proton radiobiology. *Cancers* **2015**, *7*, 353–381, doi:10.3390/cancers7010353.
3. Paganetti, H.; van Luijk, P. Biological considerations when comparing proton therapy with photon therapy. *Semin. Radiat. Oncol.* **2013**, *23*, 77–87, doi:10.1016/j.semradonc.2012.11.002.
4. Cometto, A.; Russo, G.; Bourhaleb, F.; Milian, F.M.; Giordanengo, S.; Marchetto, F.; Cirio, R.; Attili, A. Direct evaluation of radiobiological parameters from clinical data in the case of ion beam therapy: An alternative approach to the relative biological effectiveness. *Phys. Med. Biol.* **2014**, *59*, 7393–7417, doi:10.1088/0031-9155/59/23/7393.
5. Paganetti, H.; Niemierko, A.; Ancukiewicz, M.; Gerweck, L.E.; Goitein, M.; Loeffler, J.S.; Suit, H.D. Relative biological effectiveness (RBE) values for proton beam therapy. *Int. J. Radiat. Oncol. Biol. Phys.* **2002**, *53*, 407–421.
6. Carante, M.P.; Ballarini, F. Calculating variations in biological effectiveness for a 62 MeV proton beam. *Front. Oncol.* **2016**, *6*, 76, doi:10.3389/fonc.2016.00076.
7. Bettega, D.; Calzolari, P.; Chauvel, P.; Courdi, A.; Herault, J.; Iborra, N.; Marchesini, R.; Massariello, P.; Poli, G.L.; Tallone, L. Radiobiological studies on the 65 MeV therapeutic proton beam at Nice using human tumour cells. *Int. J. Radiat. Biol.* **2000**, *76*, 1297–1303.
8. Vassiliev, O.N. Uncertainties in the relative biological effectiveness of therapeutic proton beams associated with bias towards high doses per fraction in radiobiological experiments. *Int. J. Cancer Ther. Oncol.* **2017**, *4*, 446, doi:10.14319/ijcto.44.6.
9. Calugaru, V.; Nauraye, C.; Noel, G.; Giocanti, N.; Favaudon, V.; Megnin-Chanet, F. Radiobiological characterization of two therapeutic proton beams with different initial energy spectra used at the Institut Curie Proton Therapy Center in Orsay. *Int. J. Radiat. Oncol. Biol. Phys.* **2011**, *81*, 1136–1143, doi:10.1016/j.ijrobp.2010.09.003.
10. Loeffler, J.S.; Durante, M. Charged particle therapy—optimization, challenges and future directions. *Nat. Rev. Clin. Oncol.* **2013**, *10*, 411–424, doi:10.1038/nrclinonc.2013.79.
11. Paganetti, H. Relative biological effectiveness (RBE) values for proton beam therapy. Variations as a function of biological endpoint, dose, and linear energy transfer. *Phys. Med. Biol.* **2014**, *59*, R419–R472, doi:10.1088/0031-9155/59/22/R419.
12. Wilkens, J.J.; Oelfke, U. A phenomenological model for the relative biological effectiveness in therapeutic proton beams. *Phys. Med. Biol.* **2004**, *49*, 2811–2825.
13. Britten, R.A.; Nazaryan, V.; Davis, L.K.; Klein, S.B.; Nichiporov, D.; Mendonca, M.S.; Wolanski, M.; Nie, X.; George, J.; Keppel, C. Variations in the RBE for cell killing along the depth-dose profile of a modulated proton therapy beam. *Radiat. Res.* **2013**, *179*, 21–28, doi:10.1667/RR2737.1.
14. Chaudhary, P.; Marshall, T.I.; Perozziello, F.M.; Manti, L.; Currell, F.J.; Hanton, F.; McMahon, S.J.; Kavanagh, J.N.; Cirrone, G.A.; Romano, F.; et al. Relative biological effectiveness variation along monoenergetic and modulated Bragg peaks of a 62-MeV therapeutic proton beam: A preclinical assessment. *Int. J. Radiat. Oncol. Biol. Phys.* **2014**, *90*, 27–35, doi:10.1016/j.ijrobp.2014.05.010.
15. Matsumoto, Y.; Matsuura, T.; Wada, M.; Egashira, Y.; Nishio, T.; Furusawa, Y. Enhanced radiobiological effects at the distal end of a clinical proton beam: In vitro study. *J. Radiat. Res.* **2014**, *55*, 816–822, doi:10.1093/jrr/rrt230.

16. Saager, M.; Peschke, P.; Brons, S.; Debus, J.; Karger, C.P. Determination of the proton RBE in the rat spinal cord: Is there an increase towards the end of the spread-out Bragg peak? *Radiother. Oncol.* **2018**, *128*, 115–120, doi:10.1016/j.radonc.2018.03.002.
17. Willers, H.; Allen, A.; Grosshans, D.; McMahon, S.J.; von Neubeck, C.; Wiese, C.; Vikram, B. Toward A variable RBE for proton beam therapy. *Radiother. Oncol.* **2018**, *128*, 68–75, doi:10.1016/j.radonc.2018.05.019.
18. Mohan, R.; Peeler, C.R.; Guan, F.; Bronk, L.; Cao, W.; Grosshans, D.R. Radiobiological issues in proton therapy. *Acta Oncol.* **2017**, *56*, 1367–1373, doi:10.1080/0284186X.2017.1348621.
19. Goodhead, D.T. Energy deposition stochastics and track structure: What about the target? *Radiat. Prot. Dosim.* **2006**, *122*, 3–15, doi:10.1093/rpd/ncl498.
20. Sage, E.; Harrison, L. Clustered DNA lesion repair in eukaryotes: Relevance to mutagenesis and cell survival. *Mutat. Res.* **2011**, *711*, 123–133, doi:10.1016/j.mrfmmm.2010.12.010.
21. Eccles, L.J.; O'Neill, P.; Lomax, M.E. Delayed repair of radiation induced clustered DNA damage: Friend or foe? *Mutat. Res.* **2011**, *711*, 134–141, doi:10.1016/j.mrfmmm.2010.11.003.
22. Lomax, M.E.; Folkes, L.K.; O'Neill, P. Biological consequences of radiation-induced DNA damage: Relevance to radiotherapy. *Clin. Oncol. R. Coll. Radiol.* **2013**, *25*, 578–585, doi:10.1016/j.clon.2013.06.007.
23. Jackson, S.P.; Bartek, J. The DNA-damage response in human biology and disease. *Nature* **2009**, *461*, 1071–1078, doi:10.1038/nature08467.
24. Ranjha, L.; Howard, S.M.; Cejka, P. Main steps in DNA double-strand break repair: An introduction to homologous recombination and related processes. *Chromosoma* **2018**, *127*, 187–214, doi:10.1007/s00412-017-0658-1.
25. Pannunzio, N.R.; Watanabe, G.; Lieber, M.R. Nonhomologous DNA end-joining for repair of DNA double-strand breaks. *J. Biol. Chem.* **2018**, *293*, 10512–10523, doi:10.1074/jbc.TM117.000374.
26. Mao, Z.; Bozzella, M.; Seluanov, A.; Gorbunova, V. DNA repair by nonhomologous end joining and homologous recombination during cell cycle in human cells. *Cell Cycle* **2008**, *7*, 2902–2906, doi:10.4161/cc.7.18.6679.
27. Georgakilas, A.G.; O'Neill, P.; Stewart, R.D. Induction and repair of clustered DNA lesions: What do we know so far? *Radiat. Res.* **2013**, *180*, 100–109, doi:10.1667/RR3041.1.
28. Carter, R.J.; Parsons, J.L. Base Excision Repair, a Pathway Regulated by Posttranslational Modifications. *Mol. Cell. Biol.* **2016**, *36*, 1426–1437, doi:10.1128/MCB.00030-16.
29. Dianov, G.L.; Parsons, J.L. Co-ordination of DNA single strand break repair. *DNA Repair* **2007**, *6*, 454–460, doi:10.1016/j.dnarep.2006.10.009.
30. Newhauser, W.D.; Zhang, R. The physics of proton therapy. *Phys. Med. Biol.* **2015**, *60*, R155–R209, doi:10.1088/0031-9155/60/8/R155.
31. Girdhani, S.; Sachs, R.; Hlatky, L. Biological effects of proton radiation: What we know and don't know. *Radiat. Res.* **2013**, *179*, 257–272, doi:10.1667/RR2839.1.
32. Gerelchuluun, A.; Hong, Z.; Sun, L.; Suzuki, K.; Terunuma, T.; Yasuoka, K.; Sakae, T.; Moritake, T.; Tsuboi, K. Induction of in situ DNA double-strand breaks and apoptosis by 200 MeV protons and 10 MV X-rays in human tumour cell lines. *Int. J. Radiat. Biol.* **2011**, *87*, 57–70, doi:10.3109/09553002.2010.518201.
33. Alan Mitteer, R.; Wang, Y.; Shah, J.; Gordon, S.; Fager, M.; Butter, P.P.; Jun Kim, H.; Guardiola-Salmeron, C.; Carabe-Fernandez, A.; Fan, Y. Proton beam radiation induces DNA damage and cell apoptosis in glioma stem cells through reactive oxygen species. *Sci. Rep.* **2015**, *5*, 13961, doi:10.1038/srep13961.
34. Oeck, S.; Szymonowicz, K.; Wiel, G.; Krysztofiak, A.; Lambert, J.; Koska, B.; Iliakis, G.; Timmermann, B.; Jendrossek, V. Relating linear energy transfer to the formation and resolution of DNA repair foci after irradiation with equal doses of X-ray photons, plateau, or Bragg-peak protons. *Int. J. Mol. Sci.* **2018**, *19*, doi:10.3390/ijms19123779.
35. Chaudhary, P.; Marshall, T.I.; Currell, F.J.; Kacperek, A.; Schettino, G.; Prise, K.M. Variations in the processing of DNA double-strand breaks along 60-MeV therapeutic proton beams. *Int. J. Radiat. Oncol. Biol. Phys.* **2016**, *95*, 86–94, doi:10.1016/j.ijrobp.2015.07.2279.
36. Grosse, N.; Fontana, A.O.; Hug, E.B.; Lomax, A.; Coray, A.; Augsburger, M.; Paganetti, H.; Sartori, A.A.; Pruschy, M. Deficiency in homologous recombination renders mammalian cells more sensitive

- to proton versus photon irradiation. *Int. J. Radiat. Oncol. Biol. Phys.* **2014**, *88*, 175–181, doi:10.1016/j.ijrobp.2013.09.041.
37. Carter, R.J.; Nickson, C.M.; Thompson, J.M.; Kacperek, A.; Hill, M.A.; Parsons, J.L. Complex DNA damage induced by high linear energy transfer alpha-particles and protons triggers a specific cellular DNA damage response. *Int. J. Radiat. Oncol. Biol. Phys.* **2018**, *100*, 776–784, doi:10.1016/j.ijrobp.2017.11.012.
 38. Giedzinski, E.; Rola, R.; Fike, J.R.; Limoli, C.L. Efficient production of reactive oxygen species in neural precursor cells after exposure to 250 MeV protons. *Radiat. Res.* **2005**, *164*, 540–544.
 39. Zhang, X.; Lin, S.H.; Fang, B.; Gillin, M.; Mohan, R.; Chang, J.Y. Therapy-resistant cancer stem cells have differing sensitivity to photon versus proton beam radiation. *J. Thorac. Oncol.* **2013**, *8*, 1484–1491, doi:10.1097/JTO.0b013e3182a5fdcb.
 40. Keta, O.D.; Todorovic, D.V.; Bulat, T.M.; Cirrone, P.G.; Romano, F.; Cuttone, G.; Petrovic, I.M.; Ristic Fira, A.M. Comparison of human lung cancer cell radiosensitivity after irradiations with therapeutic protons and carbon ions. *Exp. Biol. Med.* **2017**, *242*, 1015–1024, doi:10.1177/1535370216669611.
 41. Carter, R.J.; Nickson, C.M.; Thompson, J.M.; Kacperek, A.; Hill, M.A.; Parsons, J.L. Characterisation of deubiquitylating enzymes in the cellular response to high-LET ionising radiation and complex DNA damage. *Int. J. Radiat. Oncol. Biol. Phys.* **2019**, *104*, 656–665, doi:10.1016/j.ijrobp.2019.02.053.
 42. Moertel, H.; Georgi, J.C.; Distel, L.; Eyrich, W.; Fritsch, M.; Grabenbauer, G.; Sauer, R. Effects of low energy protons on clonogenic survival, DSB repair and cell cycle in human glioblastoma cells and B14 fibroblasts. *Radiother. Oncol.* **2004**, *73* (Suppl. 2), S115–S118.
 43. Gerelchuluun, A.; Manabe, E.; Ishikawa, T.; Sun, L.; Itoh, K.; Sakae, T.; Suzuki, K.; Hirayama, R.; Asaithamby, A.; Chen, D.J.; et al. The major DNA repair pathway after both proton and carbon-ion radiation is NHEJ, but the HR pathway is more relevant in carbon ions. *Radiat. Res.* **2015**, *183*, 345–356, doi:10.1667/RR13904.1.
 44. Bracalente, C.; Ibanez, I.L.; Molinari, B.; Palmieri, M.; Kreiner, A.; Valda, A.; Davidson, J.; Duran, H. Induction and persistence of large gammaH2AX foci by high linear energy transfer radiation in DNA-dependent protein kinase-deficient cells. *Int. J. Radiat. Oncol. Biol. Phys.* **2013**, *87*, 785–794, doi:10.1016/j.ijrobp.2013.07.014.
 45. Fontana, A.O.; Augsburger, M.A.; Grosse, N.; Guckenberger, M.; Lomax, A.J.; Sartori, A.A.; Pruschy, M.N. Differential DNA repair pathway choice in cancer cells after proton- and photon-irradiation. *Radiother. Oncol.* **2015**, *116*, 374–380, doi:10.1016/j.radonc.2015.08.014.
 46. Reindl, J.; Drexler, G.A.; Girst, S.; Greubel, C.; Siebenwirth, C.; Drexler, S.E.; Dollinger, G.; Friedl, A.A. Nanoscopic exclusion between Rad51 and 53BP1 after ion irradiation in human HeLa cells. *Phys. Biol.* **2015**, *12*, 066005, doi:10.1088/1478-3975/12/6/066005.
 47. Liu, Q.; Ghosh, P.; Magpayo, N.; Testa, M.; Tang, S.; Gheorghiu, L.; Biggs, P.; Paganetti, H.; Efstathiou, J.A.; Lu, H.M.; et al. Lung cancer cell line screen links fanconi anemia/BRCA pathway defects to increased relative biological effectiveness of proton radiation. *Int. J. Radiat. Oncol. Biol. Phys.* **2015**, *91*, 1081–1089, doi:10.1016/j.ijrobp.2014.12.046.
 48. Francis, Z.; Villagrasa, C.; Clairand, I. Simulation of DNA damage clustering after proton irradiation using an adapted DBSCAN algorithm. *Comput. Methods Programs Biomed.* **2011**, *101*, 265–270, doi:10.1016/j.cmpb.2010.12.012.
 49. Nikjoo, H.; O'Neill, P.; Wilson, W.E.; Goodhead, D.T. Computational approach for determining the spectrum of DNA damage induced by ionizing radiation. *Radiat. Res.* **2001**, *156*, 577–583.
 50. Watanabe, R.; Rahmanian, S.; Nikjoo, H. Spectrum of radiation-induced clustered non-DSB damage—A Monte Carlo track structure modeling and calculations. *Radiat. Res.* **2015**, *183*, 525–540, doi:10.1667/RR13902.1.
 51. Henthorn, N.T.; Warmenhoven, J.W.; Sotiropoulos, M.; Mackay, R.I.; Kirkby, N.F.; Kirkby, K.J.; Merchant, M.J. In silico non-homologous end joining following ion induced DNA double strand breaks predicts that repair fidelity depends on break density. *Sci. Rep.* **2018**, *8*, 2654, doi:10.1038/s41598-018-21111-8.
 52. Mavragani, I.V.; Nikitaki, Z.; Souli, M.P.; Aziz, A.; Nowsheen, S.; Aziz, K.; Rogakou, E.; Georgakilas, A.G. Complex DNA Damage: A route to radiation-induced genomic instability and carcinogenesis. *Cancers* **2017**, *9*, doi:10.3390/cancers9070091.

53. Zhang, X.; Ye, C.; Sun, F.; Wei, W.; Hu, B.; Wang, J. Both complexity and location of DNA damage contribute to cellular senescence induced by ionizing radiation. *PLoS ONE* **2016**, *11*, e0155725, doi:10.1371/journal.pone.0155725.
54. Asaithamby, A.; Hu, B.; Chen, D.J. Unrepaired clustered DNA lesions induce chromosome breakage in human cells. *Proc. Natl. Acad. Sci. USA* **2011**, *108*, 8293–8298, doi:10.1073/pnas.1016045108.
55. Sage, E.; Shikazono, N. Radiation-induced clustered DNA lesions: Repair and mutagenesis. *Free Radic. Biol. Med.* **2016**, *107*, 125–135, doi:10.1016/j.freeradbiomed.2016.12.008.
56. Brown, J.S.; O’Carrigan, B.; Jackson, S.P.; Yap, T.A. Targeting DNA repair in cancer: Beyond PARP inhibitors. *Cancer Discov.* **2017**, *7*, 20–37, doi:10.1158/2159-8290.CD-16-0860.
57. Zlobinskaya, O.; Siebenwirth, C.; Greubel, C.; Hable, V.; Hertenberger, R.; Humble, N.; Reinhardt, S.; Michalski, D.; Roper, B.; Multhoff, G.; et al. The effects of ultra-high dose rate proton irradiation on growth delay in the treatment of human tumor xenografts in nude mice. *Radiat. Res.* **2014**, *181*, 177–183, doi:10.1667/RR13464.1.



© 2019 by the authors. Submitted for possible open access publication under the terms and conditions of the Creative Commons Attribution (CC BY) license

(<http://creativecommons.org/licenses/by/4.0/>).

Targeting DNA Double-Strand Break Repair Enhances Radiosensitivity of HPV-Positive and HPV-Negative Head and Neck Squamous Cell Carcinoma to Photons and Protons

Eirini Terpsi Vitti ¹, Andrzej Kacperek ² and Jason L. Parsons ^{1,2,*}

¹ Cancer Research Centre, Department of Molecular and Clinical Cancer Medicine, University of Liverpool, 200 London Road, Liverpool L3 9TA, UK; E.Vitti@liverpool.ac.uk

² Clatterbridge Cancer Centre NHS Foundation Trust, Clatterbridge Road, Bebington CH63 4JY, UK; andrzej.kacperek@nhs.net

* Correspondence: j.parsons@liverpool.ac.uk; Tel.: +44-151-794-8848

Received: 16 April 2020; Accepted: 3 June 2020; Published: date

Abstract: The response of head and neck squamous cell carcinoma (HNSCC) to radiotherapy depends on human papillomavirus type 16 (HPV) status, and where improved outcome and survival is observed in HPV-positive disease. However, strategies to further radiosensitise the tumours, particularly relatively radioresistant HPV-negative HNSCC, are actively being sought. The impact of targeting the major protein kinases involved in the signaling of DNA double-strand break (DSB) repair, namely ataxia telangiectasia-mutated (ATM), ataxia telangiectasia and Rad3-related (ATR), and the catalytic subunit of DNA-dependent protein kinase (DNA-Pkcs), on the radiosensitisation of HNSCC cells was examined. The response to both conventional photon radiotherapy, but also proton beam therapy, was analysed by clonogenic assays and 3D spheroid growth. We observed that inhibition of ATM, ATR, and particularly DNA-Pkcs, caused a significant reduction in HNSCC cell survival post-irradiation with both photons and protons, with less of an impact on the most radiosensitive HPV-positive cell line. The inhibition of DNA-Pkcs and, to a lesser extent ATM, in combination with radiation was also more effective at inhibiting the growth of 3D spheroids derived from relatively radioresistant HPV-negative HNSCC. Similar effects of the inhibitors were observed comparing photon and proton irradiation, demonstrating the potential for targeting DSB repair as an effective combination treatment for HNSCC.

Keywords: ATM; ATR; DNA-PKcs; DNA repair; ionising radiation; proton beam therapy

1. Introduction

The incidence of head and neck squamous cell carcinoma (HNSCC) has been reported to be ~800,000 cases per year, and linked with this is the increased rise in oropharyngeal tumours associated with human papillomavirus type 16 (HPV) infection (281-283). It has been clearly demonstrated that patients with HPV-positive squamous cell carcinoma of the oropharynx display improved outcomes and survival rates in comparison to patients with HPV-negative disease (186, 187, 203, 204), which is largely due to the increased responsiveness of HPV-positive tumours to radiotherapy and chemotherapy. Indeed, this difference in radiotherapy response between HPV-positive and HPV-negative HNSCC has been observed in cultured cells derived from patients (168, 178, 206). Several studies have indicated that this is caused by defects in the signaling and repair of DNA double-strand breaks (DSBs) in HPV-positive HNSCC cells, largely

through the measurement of the DNA damage by neutral comet assays, but also through analysis of surrogate markers, including γ H2AX, 53BP1 and RAD51 foci (168, 207, 284). However, there are some discrepancies in relation to the specific DSB repair defect, as the reduced expression of proteins involved in both non-homologous end joining (NHEJ; 53BP1 and DNA-Pkcs) and homologous recombination (HR; BRCA2 and RAD51) have been observed. We also recently reported that HPV-positive HNSCC cells have upregulated levels of enzymes involved in the base excision repair (BER) pathway, including XRCC1 and PARP-1 (207). Furthermore, studies conducted at the genomic level have identified significant genome instability in HPV-positive HNSCC cells and tissues, including alterations in DNA repair genes (285-287).

Given that HPV-positive HNSCC cells display an altered capacity for DNA repair, this has revealed that targeting the DNA damage response, particularly in relatively radioresistant HPV-negative HNSCC that display proficient DNA repair mechanisms, may be an effective strategy for the radiosensitisation of the tumour (208). Specifically, the major protein kinases that coordinate the repair of DNA DSBs through NHEJ and HR, namely ataxia telangiectasia-mutated (ATM), ataxia telangiectasia and Rad3-related (ATR), and the catalytic subunit of DNA-dependent protein kinase (DNA-Pkcs), are increasingly being investigated as targets for inhibitors to increase cellular radiosensitisation, principally in response to conventional (photon) radiotherapy. For example, the DNA-Pkcs inhibitors KU0060648 (244) and IC87361 (245), and the ATM inhibitor GSK635416A (209) have been demonstrated to increase radiosensitivity of HNSCC cell lines. A number of studies have also focused on ATR as a target to radiosensitise HNSCC cells, through the inhibitors VE821 (246) and AZD6738 (214, 244). Whilst the majority of these studies have focused on utilising clonogenic assays as an end-point, the ATR inhibitor AZD6738 was shown to impede the growth of 3D spheroids of hypopharyngeal (FaDu) cells in combination with radiation, which are more representative of the original tumour *in vivo* (214). Cumulatively, these data would suggest that targeting the DSB repair pathway can be an effective approach for increasing the (photon) radiosensitivity of HNSCC cells.

In addition to conventional (photon) radiotherapy, proton beam therapy is increasingly being utilised for HNSCC treatment (218). This is due to precise delivery of the radiation dose to the tumour via this radiotherapy technique, resulting in sparing of the normal tissues and organs at risk. However, there is still significant uncertainty regarding the biological impact of protons versus photons, which is important in defining potential combinatorial strategies using targeted drugs to optimise tumour cell radiosensitivity (reviewed in (268)). Specifically, and given that DNA DSBs are the major lesion contributing to ionising radiation-induced cell killing, there are contrasting studies suggesting a dependence on either NHEJ or HR for DNA DSB repair in response to protons. For example, it has been suggested that HR is the major pathway for the repair of DNA DSBs induced in response to protons in A549 lung cancer and glioblastoma cell lines, which would indicate that targeting ATR may be a successful radiosensitisation strategy (118). However, studies analysing the comparative response of HPV-positive and HPV-negative HNSCC cells to photons versus protons, and the impact of targeting the major kinases involved in DSB repair has not been reported previously. Additionally, utilising HNSCC cells grown as monolayers, but also as 3D spheroids that more accurately reflect the structure and environment of the original tumour, is necessary.

Herein, we have characterised the impact of ATM, ATR and DNA-Pkcs inhibition on the response of HPV-positive and HPV-negative HNSCC cells from the oropharynx to both photons and protons, through the utilisation of clonogenic survival assays and 3D spheroid growth assays. Given that the HPV-negative HNSCC cells are relatively radioresistant compared to their HPV-positive counterparts, we also expanded the results using cells derived from the hypopharynx and oral cavity focusing on 3D spheroid growth, which is more representative of the original tumour and its treatment *in vivo*. We report that the clonogenic survival and growth of 3D spheroids of cells derived from HPV-positive and HPV-negative HNSCC can be significantly reduced using inhibitors targeting ATM, ATR, and particularly DNA-Pkcs, in

combination with both photon and proton irradiation. This suggests that these potential therapeutic strategies could be exploited for the effective treatment of HNSCC, and particularly for relatively radioresistant HPV-negative tumours.

2. Results

2.1. HPV-Positive HNSCC Cells Are More Radiosensitive than HPV-Negative HNSCC Cells to Photons and Protons

We, and others, have previously demonstrated that there is increased radiosensitivity of cells derived from HPV-positive HNSCC in comparison to HPV-negative HNSCC, which reproduces the effects observed following irradiation of the respective tumours (168, 206, 207). To expand on these observations, we used two cell lines derived from each tumour type, where the expression of E6 and E7 oncogenes was confirmed by p16 expression (Figures 1A and S1). Similar to previous data, we were indeed able to reproduce the difference in radiosensitivity of two HPV-positive HNSCC cell lines (UMSCC47 and UPCI-SCC090) in comparison to two HPV-negative HNSCC cell lines (UMSCC6 and UMSCC74A; Figure 1B,C) in response to photon irradiation by clonogenic assays. It should be noted that the colony size was variable between the cell lines, but that colony counting settings were optimised for each cell line and the same settings used across the various treatments for consistency. We also analysed the survival of the same cells following proton irradiation and demonstrated that, similar to results observed following photons, the two most radiosensitive were from HPV-positive HNSCC (Figure 1D,E). The radiosensitivity of the cell lines was generally in the order UMSCC6 > UMSCC74A > UMSCC47 > UPCI-SCC090, and statistical analysis reveals the significantly increased radiosensitivity of UPCI-SCC090 in comparison to UMSCC6 and UMSCC74A (see also Figure S2A,B for linear scale graphs and data fitting).

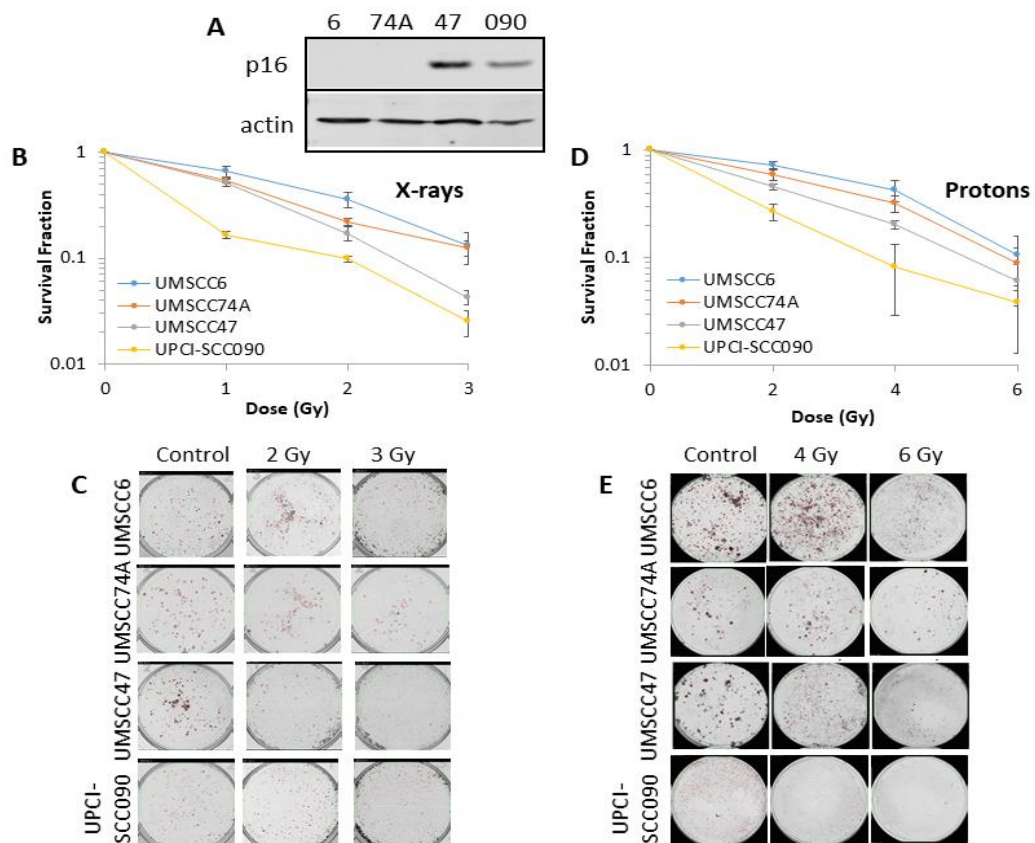


Figure 1. Comparative radiosensitivity of human papillomavirus type 16 (HPV)-negative and HPV-positive head and neck squamous cell carcinoma (HNSCC) cells in response to photons and protons. (A) Whole cell extracts from HNSCC cells were prepared and analysed by immunoblotting with the indicated antibodies. Clonogenic survival of HNSCC cells following treatment with increasing doses of (B,C) x-rays or (D,E) protons was analysed from three to four biologically independent experiments. (B and D) Shown is the surviving fraction \pm S.E. (C and E) Representative images of colonies in non-irradiated and irradiated plates (the latter were seeded with four times and eight times the number of cells, accordingly). Statistical analysis using a one sample *t*-test of surviving fractions at a 2 Gy dose of x-rays reveals significant differences of $p < 0.03$ (UMSCC6 vs. UPCI-SCC090), $p < 0.005$ (UMSCC74A vs. UPCI-SCC090); and at a 4 Gy dose of protons of $p < 0.04$ (UMSCC6 vs. UPCI-SCC090), $p < 0.04$ (UMSCC74A vs. UPCI-SCC090). The uncropped blots and molecular weight markers of Figure 1 are shown in Figure S1.

2.2. Survival of HNSCC Cells Following by Photon and Proton Irradiation Can Be Reduced by Targeting ATM, ATR and DNA-Pkcs

Using clonogenic assays, we first analysed the impact of targeting the major protein kinases involved in DNA DSB repair using specific and characterised inhibitors (ATMi, KU-55933; ATRi, VE-821; DNA-Pkcsi, KU-57788) on the survival of HPV-positive and HPV-negative HNSCC incubated with the inhibitors for 24 h in the absence of radiation, versus a vehicle-only control (DMSO). This demonstrated a varied response dependent on the cell line utilised (Figure S3), although ATRi significantly decreased cell survival by 41–54% in all HNSCC cell lines, ATMi by 22–44% in three cell lines (UMSCC6, UMSCC74A and UMSCC47), and DNA-Pkcsi had a significant impact on survival of only one of the four cell lines (UMSCC47) by ~56%. We then analysed the impact of the inhibitors on HNSCC cell survival post-irradiation. As a starting point, we demonstrated that the respective inhibitors, following a 1 h pre-incubation of the cells prior to irradiation, were functional in suppressing ATM, ATR and DNA-Pk phosphorylation, and therefore DSB signaling, in response to photons (Figure S4) and protons (Figure S5). In combination with photon irradiation, we demonstrate that there was a significant impact in reducing cell survival of HPV-negative HNSCC cells in the presence of either ATMi, ATRi or DNA-Pkcsi (1 h pre-incubation, followed by a further treatment for 24 h post-irradiation) versus the DMSO control (Figure 2A–D; see also Figure S6A–D for linear scale graphs and data fitting), with dose enhancement ratios (DER) of 1.91–2.39 (Table 1). The significantly enhanced radiosensitivity of only one HPV-positive HNSCC cell line (UMSCC47) was also seen (Figure 2E–H), although the DER values of 1.36–1.69 were notably lower than those observed in the HPV-negative cells (Table 1). The cell survival of the most inherently radiosensitive HPV-positive cell line (UPI-SCC090) only appeared to be dramatically decreased in the presence of DNA-Pkcsi (DER of 1.36). These data are supported by statistical analysis (Table S1) and, in general, DNA-Pkcsi appeared the most potent radiosensitiser of all the HNSCC cell lines.

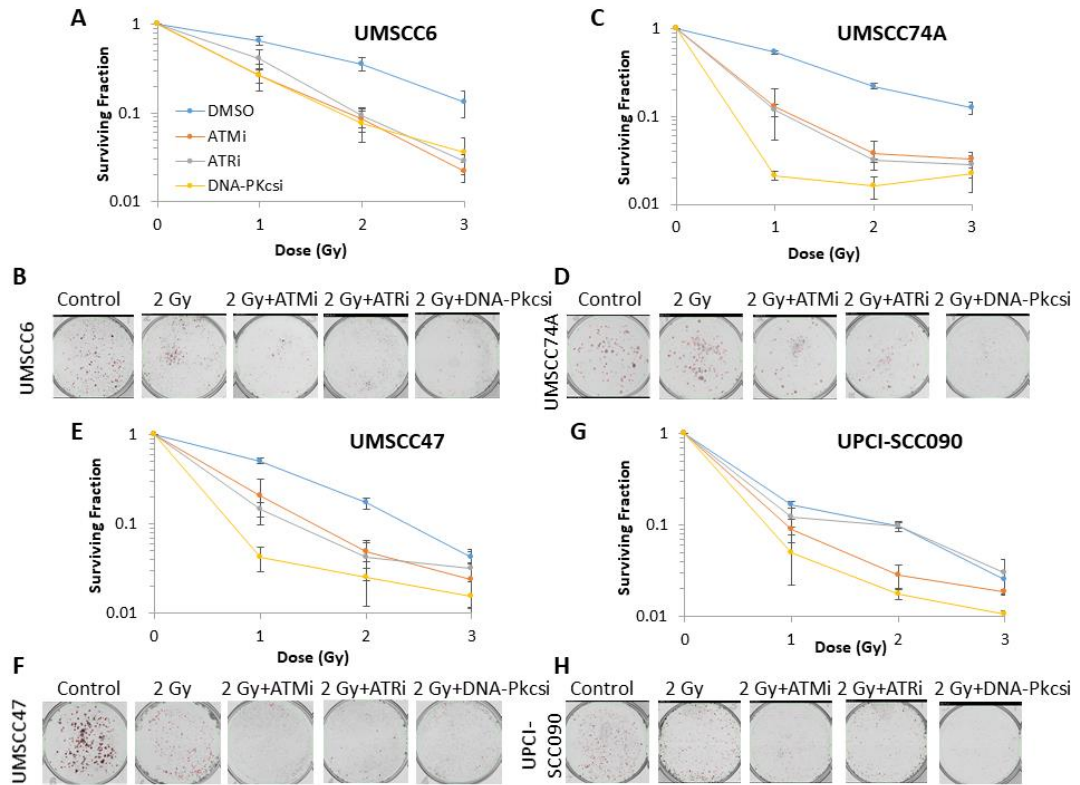


Figure 2. Inhibition of ataxia telangiectasia-mutated (ATM), ataxia telangiectasia and Rad3-related (ATR) and DNA-dependent protein kinase (DNA-Pkcs) can enhance sensitivity of HNSCC cells to photon irradiation. Clonogenic survival of HNSCC cells following treatment with increasing doses of x-rays in the presence of DMSO (Control), ATMi (10 μ M), ATRi (1 μ M) and DNA-Pkcsi (1 μ M) was analysed from three biologically independent experiments. (A, C, E and G) Shown is the surviving fraction \pm S.E. (B, D, F and H) representative images of colonies in non-irradiated and irradiated plates (the latter of which were seeded with four times the number of cells).

Table 1. Dose enhancement ratios calculated at 50% cell survival (DER) following ATM, ATR and DNA-Pkcs inhibition versus DMSO controls in HNSCC cells in response to photons.

| Inhibitor | UMSSC6 | UMSSC74A | UMSSC47 | UPCI-SCC090 |
|-----------|--------|----------|---------|-------------|
| ATM | 2.06 | 1.91 | 1.38 | 1.15 |
| ATR | 1.91 | 2.01 | 1.36 | 1.02 |
| DNA-Pkcs | 1.93 | 2.39 | 1.69 | 1.36 |

Following proton irradiation, and similar to photons, we again observed that ATMi and DNA-Pkcsi significantly enhanced the radiosensitisation of both HPV-negative HNSCC cell lines (Figure 3A–D and Table S2; see also Figure S7A–D for linear scale graphs and data fitting) with DER values of 1.52–2.01 (Table 2). HPV-positive HNSCC cell lines were also radiosensitised, with DER values of 1.24–1.49 (Table 2), following proton irradiation in combination with inhibition of ATM and DNA-Pkcs (Figure 3E–H). However, radiosensitisation was only significantly enhanced in UMSSC47, and not UPCI-SCC090 cell lines (Table S2). ATRi appeared in general less effective at radiosensitising the HNSCC cells in response to protons (DER values of 1.25–1.48; Table 2).

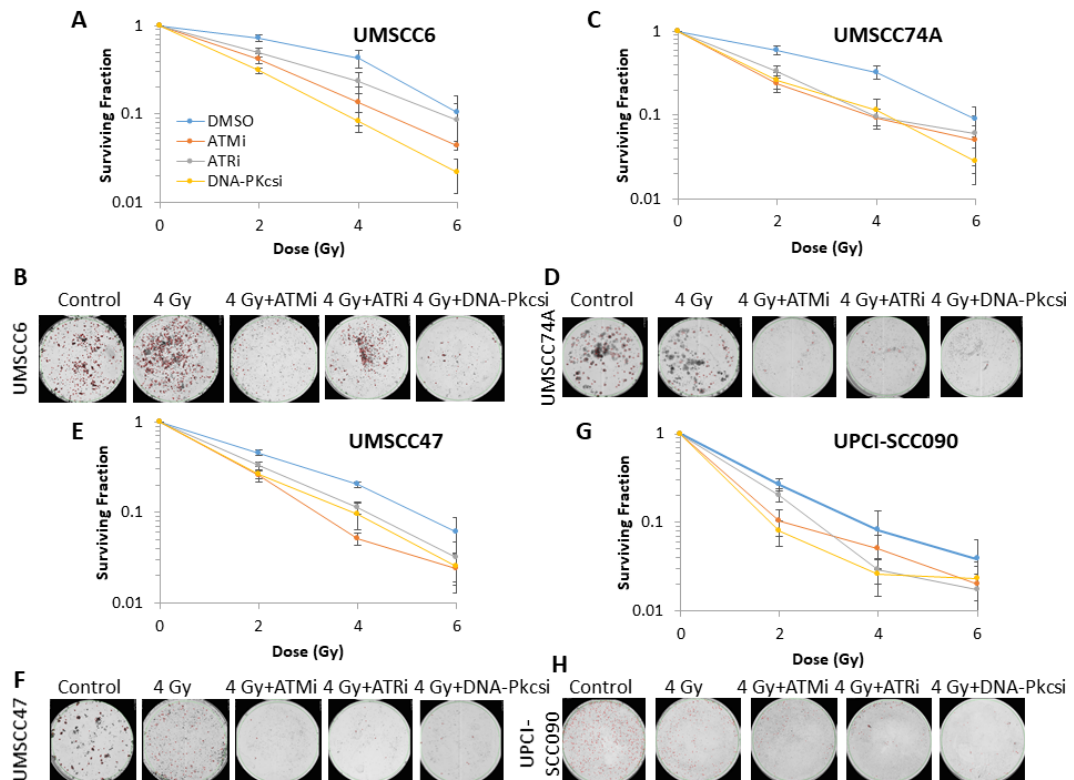


Figure 3. Inhibition of ATM, ATR and DNA-Pkcs can enhance sensitivity of HNSCC cells to proton irradiation. Clonogenic survival of HNSCC cells following treatment with increasing doses of protons in the presence of DMSO (Control), ATMi (10 μM), ATRi (1 μM) and DNA-Pkcsi (1 μM) was analysed from four biologically independent experiments. (A, C, E and G) Shown is the surviving fraction ± S.E. (B, D, F and H) representative images of colonies in non-irradiated and irradiated plates (the latter of which were seeded with four times the number of cells).

Table 2. Dose enhancement ratios calculated at 50% cell survival (DER) following ATM, ATR and DNA-Pkcs inhibition versus DMSO controls in HNSCC cells in response to protons.

| Inhibitor | UMSCC6 | UMSCC74A | UMSCC47 | UPCI-SCC090 |
|-----------|--------|----------|---------|-------------|
| ATM | 1.62 | 1.52 | 1.49 | 1.24 |
| ATR | 1.25 | 1.42 | 1.28 | 1.30 |
| DNA-Pkcs | 2.01 | 1.64 | 1.38 | 1.32 |

2.3. 3D Spheroid Growth of HNSCC Cells Following by Photon and Proton Irradiation Can Be Inhibited by Targeting ATM, ATR and DNA-Pkcs

We subsequently analysed the impact of DNA DSB repair inhibitors on the radiosensitivity of HNSCC cells utilising 3D spheroids, which more accurately reflect the structure and environment of the original tumour. Of the cells used, unfortunately one HPV-positive cell line (UMSCC47) did not form 3D spheroids that grew during the 15-day analysis period. It was also noted that spheroids from both HPV-negative HNSCC grew significantly faster (peaking at days 8–10 post-seeding) than the one remaining HPV-positive HNSCC (the increase in growth largely occurred at days 7–15 post-seeding). All spheroids grew ~5–8-fold in volume in the absence of any treatments over the analysis period (Figures 4A–I and S8). We demonstrate that ATMi alone caused a significant ~1.7-fold delay in the growth of only HPV-negative HNSCC (UMSCC74A)

spheroids, and that the combination of ATMi plus photon irradiation was effective in suppressing the growth of these spheroids by ~2.0-fold compared to radiation alone, but not of the other two spheroid models (Figure 4A–C and Table 3). In contrast, ATRi alone caused a statistically significant ~1.5–1.6-fold growth delay in all spheroid models. The inhibitor significantly exacerbated the effects of photon irradiation, by ~1.3-fold (UPCI-SCC090) to 2.3-fold (UMSCC74A) (Figure 4D–F and Table 3). DNA-Pkcs alone was, interestingly, ineffective in inhibiting spheroid growth, although the combination of DNA-Pkcs with photons was effective in suppressing the growth of HPV-negative HNSCC spheroids ~1.4-fold (UMSCC6) and ~1.6-fold (UMSCC74A) compared to the radiation alone (Figure 4G–I).

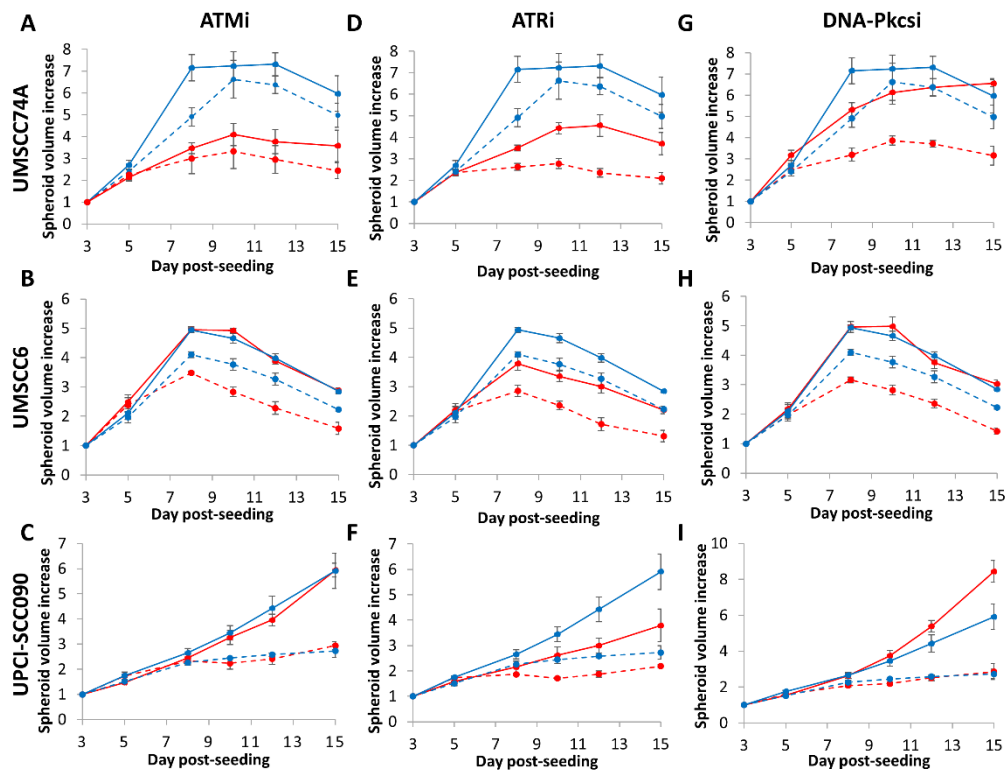


Figure 4. Inhibition of ATM, ATR and DNA-Pkcs in combination with photons can decrease growth of HNSCC 3D spheroids. Spheroids were allowed to develop for 48 h, pretreated with DMSO (Control), ATMi (10 μ M), ATRi (1 μ M) and DNA-Pkcs (1 μ M), and irradiated with a single dose (1 Gy) of x-rays. Spheroid growth of (A, D and G) UMSCC74A, (B, E and H) UMSCC6 and (C, F, and I) UPCI-SCC090 was measured by microscopy and analysed from three biologically independent experiments. Solid blue line is DMSO only, dashed blue lines are DMSO plus 1 Gy x-rays, solid red line is inhibitor only, dashed red lines are inhibitors plus 1 Gy x-rays. Shown is the spheroid volume \pm S.E.

Table 3. Targeting of ATM, ATR and DNA-Pkcs alone and in combination with photons and protons to decrease 3D HPV-positive and HPV-negative HNSCC spheroid growth.

| Inhibitor | UMSCC74A | UMSCC6 | UPCI-SCC090 |
|--------------------|--------------|-------------|-------------|
| ATM | $p < 0.0002$ | $p = 0.60$ | $p = 0.34$ |
| ATR | $p < 0.003$ | $p < 0.002$ | $p < 0.006$ |
| DNA-Pkcs | $p = 0.59$ | $p = 0.89$ | $p = 0.54$ |
| ATM + photons | $p < 0.004$ | $p = 0.18$ | $p = 0.76$ |
| ATR + photons | $p < 0.0005$ | $p < 0.02$ | $p < 0.03$ |
| DNA-Pkcs + photons | $p < 0.02$ | $p < 0.05$ | $p = 0.08$ |

| | | | |
|--------------------|--------------|-------------|--------------|
| ATM + protons | $p < 0.02$ | $p = 0.06$ | $p = 0.24$ |
| ATR + protons | $p < 0.0002$ | $p < 0.003$ | $p < 0.0008$ |
| DNA-Pkcs + protons | $p < 0.03$ | $p < 0.02$ | $p = 0.18$ |

Statistical analysis was performed on all the dataset across the 15-day growth period using a one-way ANOVA, comparing the growth of inhibitor treated spheroids against the appropriate DMSO control (\pm radiation).

We observed very similar results in HPV-negative HNSCC spheroids following proton irradiation (Table 3). Here, the combination of protons with ATMi (Figure 5A–C) was significantly effective in only one spheroid model (UMSCC74A) as observed by the ~2-fold growth inhibition versus the radiation alone, whereas ATRi (Figure 5D–F) and DNA-Pkcsi (Figure 5G–I) had a significant impact on delaying the growth of both spheroid models by ~2.5-fold and ~1.9-fold, respectively (see also Figure S9). HPV-positive HNSCC (UPCI-SCC090) spheroids were only significantly radiosensitised, by ~1.6-fold, with protons in the presence of ATRi (Figure 5F). Notably, following both photon and proton irradiation of the HPV-positive UPCI-SCC090 spheroids, there was a reduced impact of the inhibitors compared to the radiation alone, which is consistent with this being the most radiosensitive cell line, as observed by clonogenic assays (Figure 1B,D).

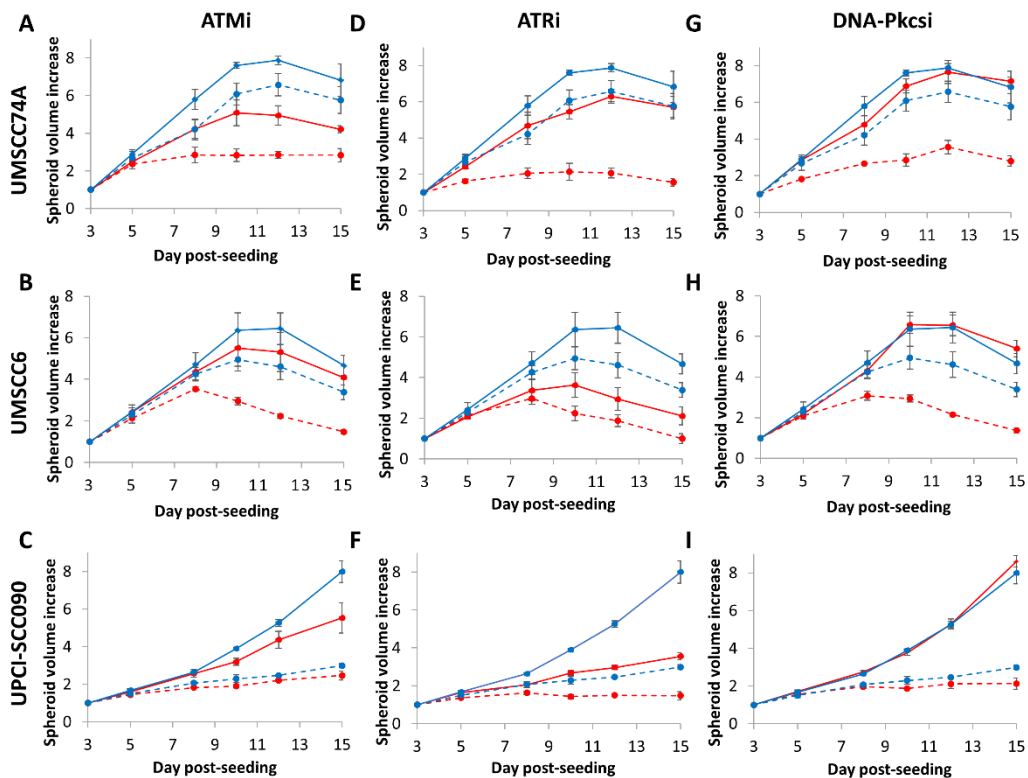


Figure 5. Inhibition of ATM, ATR and DNA-Pkcs in combination with protons can decrease growth of HNSCC 3D spheroids. Spheroids were allowed to develop for 48 h, pretreated with DMSO (Control), ATMi (10 μ M), ATRi (1 μ M) and DNA-Pkcsi (1 μ M), and irradiated with a single dose (2 Gy) of protons. Spheroid growth of (A, D and G) UMSCC74A, (B, E and H) UMSCC6 and (C, F, and I) UPCI-SCC090 was measured by microscopy and analysed from three biologically independent experiments. Solid blue line is DMSO only, dashed blue lines are DMSO plus 2 Gy protons, solid red line is inhibitor only, dashed red lines are inhibitors plus 2 Gy protons. Shown is the spheroid volume \pm S.E.

We extended our observations of the effectiveness of inhibitors targeting ATM, ATR and DNA-Pkcs in radiosensitising oropharyngeal HNSCC cells by utilising additional spheroid

models from HPV-negative HNSCC, which are relatively more radioresistant than HPV-positive HNSCC. These were designed to gain further evidence that DNA DSB repair inhibition can enhance the impact of photons and protons in preventing spheroid growth, which are more representative of the original tumour and its treatment *in vivo*. We therefore used spheroids from FaDu and A253 cell lines that originate from the hypopharynx and oral cavity, respectively, of which we observed that these increased dramatically in volume (by ~50-fold and ~15-fold, respectively) over a period of 15 days post-seeding (Figures 6A–L and S10). FaDu spheroids were particularly resistant to ATMi, ATRi and DNA-Pkcsi alone, as observed by the lack of impact on spheroid growth. The A253 spheroids appeared to display some delayed growth in the presence of the inhibitors alone, particularly at the 12- and 15-day time points, although this was not statistically significant across the whole time course (Table 4). The combination of photons with either of the inhibitors significantly suppressed the growth of A253 spheroids, which was markedly enhanced by ~2.8–3.2-fold versus the radiation alone (Figure 6A–F and Table 4). FaDu spheroids were only significantly radiosensitised in the presence of DNA-Pkcsi following photon irradiation, through a dramatic ~4.6-fold decrease in spheroid growth. In response to proton irradiation, ATRi was not significantly effective at radiosensitising the cells, but the combination of ATMi with protons was able to suppress growth of both A253 and FaDu spheroids by ~3.7-fold. Furthermore, DNA-Pkcsi was particularly effective in combination with protons as observed by the ~3.6-fold and ~7.6-fold decrease in the spheroid growth of A253 and FaDu cells, respectively, in comparison to radiation alone (Figure 6G–L and Table 4).

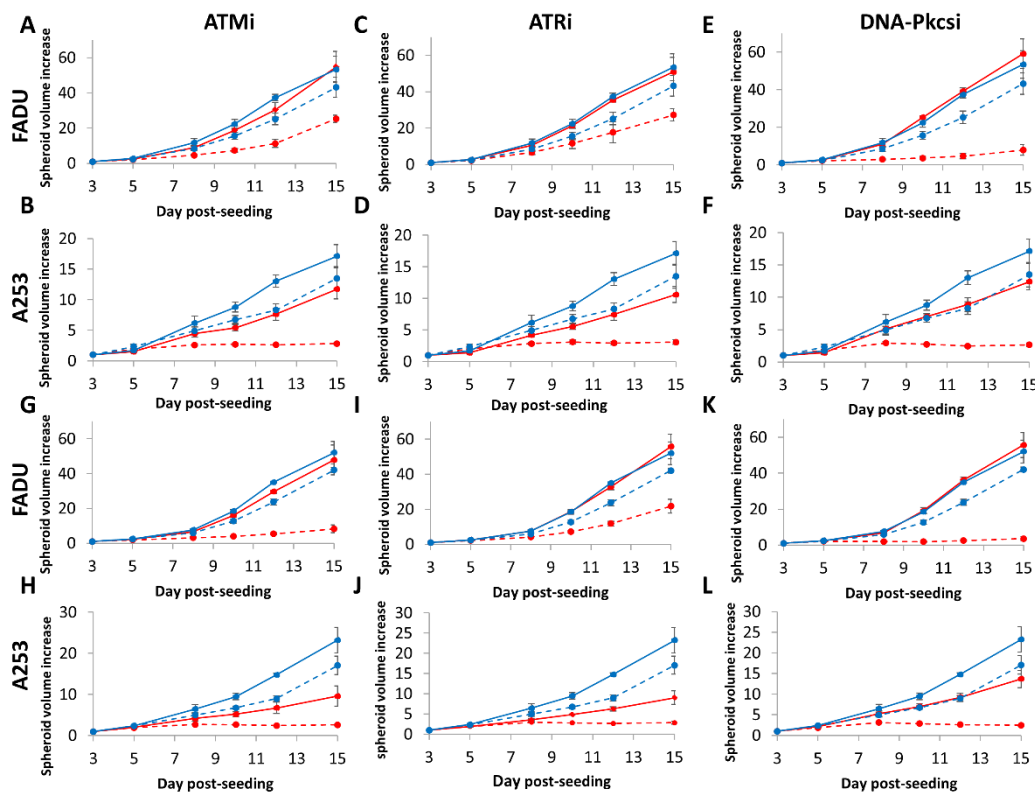


Figure 6. Inhibition of ATM, ATR and DNA-Pkcs in combination with photons and protons can decrease growth of HPV-negative HNSCC 3D spheroids. Spheroids were allowed to develop for 48 h, pretreated with DMSO (Control), ATMi (10 μ M), ATRi (1 μ M) and DNA-Pkcsi (1 μ M), and irradiated with a single dose of (A–F) x-rays at 1 Gy or (G–L) protons at 2 Gy. Spheroid growth of (A, C, E, G, I and K) hypopharynx (FaDu) and (B, D, F, H, J and L) A253 was measured by microscopy and analysed from three biologically independent experiments. Solid blue line is DMSO only, dashed blue lines (A–F) are DMSO plus 1 Gy x-rays or (G–L) 2 Gy protons, solid red lines are inhibitor only, dashed red lines are inhibitor plus (A–F) 1 Gy x-rays or (G–L) 2 Gy protons. Shown is the spheroid volume \pm S.E.

Table 4. Targeting of ATM, ATR and DNA-Pkcs alone and in combination with photons and protons to decrease 3D HPV-negative HNSCC spheroid growth.

| Inhibitor | FaDu | A253 |
|--------------------|-------------|-------------|
| ATM | $p = 0.69$ | $p = 0.49$ |
| ATR | $p = 0.89$ | $p = 0.72$ |
| DNA-Pkcs | $p = 0.82$ | $p = 0.88$ |
| ATM + photons | $p = 0.09$ | $p < 0.002$ |
| ATR + photons | $p = 0.28$ | $p < 0.003$ |
| DNA-Pkcs + photons | $p < 0.003$ | $p < 0.002$ |
| ATM + protons | $p < 0.03$ | $p < 0.006$ |
| ATR + protons | $p = 0.24$ | $p = 0.11$ |
| DNA-Pkcs + protons | $p < 0.005$ | $p < 0.002$ |

Statistical analysis was performed on the dataset across the 15-day growth period using a one-way ANOVA, comparing the growth of inhibitor treated spheroids against the appropriate DMSO control (\pm radiation).

3. Discussion

Accumulating evidence has suggested that the increased response of patients with HPV-positive versus HPV-negative HNSCC to radiotherapy, and thus the improved survival rates, is caused by defects in the repair of DNA DSBs (168, 207, 284). Therefore, targeting key enzymes involved in DNA DSB repair, particularly the protein kinases ATM, ATR and DNA-Pkcs, in relatively radioresistant HPV-negative HNSCC that are DSB repair-proficient is considered to be an approach to sensitise these tumours to radiotherapy. Indeed, there is evidence of at least one clinical trial utilising either ATRi or DNA-Pkcsi in combination with conventional radiotherapy that is currently underway (208). Additionally, while there is an increasing use of proton beam therapy for the treatment of HNSCC, there is no preclinical evidence to date examining the impact of DNA DSB repair inhibitors in combination with protons, and whether there is any substantial difference compared to that observed following photon irradiation. In this study, we have now analysed the effect of ATMi, ATRi and DNA-Pkcsi on both monolayer and 3D spheroid models of HPV-positive and HPV-negative HNSCC in combination with photons and protons.

Interestingly, we discovered that targeting either ATM, ATR or DNA-Pkcs can decrease the clonogenic survival of HNSCC cells in response to photons and protons. DNA-Pkcsi appeared particularly effective in all cell lines in combination with radiation. This would correlate with studies in HPV-negative HNSCC cells describing downregulation of DNA-Pkcs using siRNA in UTSCC15 and UTSCC45 cells (266), as well as the DNA-Pkcs inhibitors KU0060648 in HN4 and HN5 cells (244), and IC87361 in UTSCC54, UTSCC74B and UTSCC76B cells (245), which were shown to enhance radiosensitisation. Only a single study has examined ATM inhibition (GSK635416A) in HNSCC cells (209), although this demonstrated increased radiosensitivity in five HPV-negative HNSCC cell lines (UTSCC2, UTSCC8, UTSCC24A, UTSCC36 and UTSCC40), which is comparable with our data. However, there are a number of studies that have focused on ATR as a target, including using siRNA in UPCI-SCC029B, UPCI-SCC040 and UPCI-SCC131 cells (210). Additionally, the ATR inhibitor VE821 displayed improved radiosensitivity in SQ20B cells (246), and an alternative inhibitor, AZD6738, showed the same phenotype in Cal27, FaDu, HN4 and HN5 cells (214, 244). In our experiments utilising clonogenic assays, ATRi appeared to be less effective at radiosensitising cells following proton irradiation. We also observed less of an impact of DNA DSB repair inhibition in combination with radiation in HPV-positive HNSCC cells, particularly the UPCI-SCC090 cell line largely as this is the most inherently radiosensitive as shown here, and in our previous study (207).

Utilising 3D spheroid models that more accurately replicate the structure and environment of the original tumour, we further demonstrated the effectiveness of DNA-Pkcs in combination with both photons and protons in inhibiting growth of all the HPV-negative HNSCC spheroids analysed. Interestingly though, inhibition of DNA-Pkcs alone did not appear to have any impact on the growth of 3D spheroids of both HPV-positive and HPV-negative HNSCC (which was largely supported by utilising clonogenic survival assays). This suggests that DNA-Pkcs is not essential for HNSCC cell growth and survival in the absence of ionising radiation-induced stress. Nevertheless, and similar to clonogenic assay results, the combination strategy of DSB inhibition (particularly ATMi and DNA-Pkcs) did not significantly enhance the effect of radiation on the HPV-positive HNSCC spheroids (UPCI-SCC090), due to these cells being the most radiosensitive. The inhibition of ATR displayed some effectiveness in combination with photons and protons in preventing spheroid growth. However, less of an impact was observed on the relatively radioresistant HPV-negative HNSCC spheroid models, FaDu and A253, that displayed significant spheroid growth over the time period post-irradiation. This observation is similar to previous data utilising the ATR inhibitor AZD6738 with photons only, which demonstrated that this combination did not impede growth of 3D spheroids of FaDu cells (214). Noteworthy, as a monotherapy, the inhibition of ATR alone in the absence of radiation was effective in inhibiting clonogenic survival, but also the growth of HNSCC spheroids (apart from FaDu and A253), which was comparable to the impact caused by a single dose of radiation alone.

Cumulatively, our results suggest that targeting DNA DSB repair via NHEJ (ATM and DNA-Pkcs) or HR (ATR) can exacerbate the impact of photons in radiosensitising HNSCC cell models, and that the combination of DNA-Pkcs with photons in HPV-negative HNSCC cells that are relatively radioresistant was particularly effective. This adds to the growing preclinical evidence (209, 210, 214, 244-246, 266) that this is an effective combination for the treatment of HNSCC that should be investigated further, particularly using more advanced 3D models (e.g., patient-derived organoids) and appropriate *in vivo* experiments. However, we now also demonstrate that DSB repair inhibition, particularly DNA-Pkcs and to a lesser extent ATMi, are efficient in reducing the survival and spheroid growth of HNSCC cells in response to protons. In fact in general, relatively similar results were observed comparing photons and protons, although the DER values derived from clonogenic assay results were much lower with ATRi following protons than with photons. This would contradict some very limited evidence suggesting a greater dependence on the HR pathway mediated by ATR for repairing DNA DSBs induced by protons, which was obtained using RAD51 siRNA in A549 lung cancer cells (118). In fact other studies, largely conducted in Chinese hamster ovary cells, reflect that NHEJ, coordinated by ATM and DNA-Pkcs, is the major DSB repair pathway employed following proton irradiation (105, 116). This is in agreement with our results. Consequently, we would advocate that inhibition of NHEJ through DNA-Pkcs is the most promising strategy in optimising the radiosensitisation of HNSCC cells with either photons or protons. Nevertheless, it should be noted that our study utilised low linear energy transfer (LET) protons at the entrance dose of a pristine beam, and that different results may be obtained with cells irradiated at or around the Bragg peak where the LET increases. This is due to the increased amount of complex DNA damage, where multiple lesions are generated in close proximity, and therefore the potential for the generation of complex DNA DSBs that could have a different requirement for either NHEJ or HR (268). We are also acutely aware of the availability of more potent and selective inhibitors than the ones used in the current study, specifically those targeting ATM (e.g., AZD1390), ATR (e.g., AZD6738) and DNA-Pkcs (e.g., AZD7648), which require examination of their potential to radiosensitise HNSCC cell models following photon and proton irradiation. These points are consequently the subject of our ongoing and future studies.

4. Materials and Methods

4.1. Cell Lines and Culture Conditions

Oropharyngeal squamous cell carcinoma cells (UMSCC6, UMSCC74 and UMSCC47) were kindly provided by Prof T. Carey, University of Michigan, USA. Cells from the hypopharynx (FaDu) and submaxillary gland (A253) originated from ATCC (Teddington, UK). HPV-positive oropharyngeal squamous cell carcinoma cells (UPCI-SCC090) were kindly provided by Dr S. Gollin from the University of Pittsburgh. All cells, apart from UPCI-SCC090 and FaDu (which were cultured in Minimal Essential Medium (MEM)), were routinely cultured as monolayers in Dulbecco's Modified Eagle Medium (DMEM) supplemented with 10% fetal bovine serum, 2 mM L-glutamine, 1× penicillin-streptomycin and 1× non-essential amino acids. All cells were cultured under standard conditions in 5% CO₂ at 37 °C, and were authenticated in our laboratory by short tandem repeat (STR) profiling.

4.2. Clonogenic Assays

Cells were harvested and a defined number seeded in triplicate into 6-well plates or 35 mm dishes before incubation overnight in 5% CO₂ at 37 °C to allow the cells to attach. Plating efficiencies for the cells were as followed: UMSCC6 (~10%), UMSCC74A (~10%), UMSCC47 (~10%) and UPCI-SCC090 (~2%). For inhibition experiments, cells were pretreated with DMSO (as a vehicle only control), 10 µM ATM inhibitor (ATMi; KU-55933), 1 µM ATR inhibitor (ATRi; VE-821) or 1 µM DNA-Pkcs inhibitor (DNA-Pkcsi; KU-57788; Selleck Chemicals, Munich, Germany) for 1 h prior to irradiation. Cells were then irradiated using a CellRad x-ray irradiator (Faxitron Bioptics, Tucson, AZ, USA) or with a passive scattered horizontal proton beam line of 60 MeV maximal energy, as previously described (288, 289). Higher doses of protons were comparatively used due to cells being positioned at the entrance dose of a pristine (unmodulated) beam (~1 keV/µm). Following irradiation, fresh media containing inhibitors was added to the cells for 24 h, which was then replaced with fresh media alone and colonies allowed to grow for 7–12 days, prior to fixing and staining with 6% glutaraldehyde and 0.5% crystal violet for 30 min. Dishes were washed, left to air dry overnight and colonies counted using the GelCount colony analyser (Oxford Optronics, Oxford, UK). Colony counting settings were optimised for each cell line, based on inclusion of distinct colonies of specific size and intensity, although the same settings were used across the various treatments. Relative colony formation (surviving fraction) was expressed as colonies per treatment level versus colonies that appeared in the untreated control, and data was derived from at least three individual biological replicates.

4.3. Spheroid Growth Assays

Cells (500–1000/well) were seeded in triplicate in 100 µL Advanced MEM media (Life Technologies, Paisley, UK) containing 1% B27 supplement, 0.5% N-2 supplement, 2 mM L-glutamine, 1× penicillin-streptomycin, 5 µg/mL heparin, 20 ng/µL epidermal growth factor and 10 ng/µL fibroblast growth factor into 96-well ultra-low attachment plates (Corning B.V. Life Sciences, Amsterdam, The Netherlands) and spheroids of ~200 µm in diameter allowed to form for 48 h (Day 3). DMSO, ATMi, ATRi and DNA-Pkcsi were added 1 h prior to irradiation. Post-irradiation, 50 µL media was removed and replaced with 50 µL fresh media containing DMSO or inhibitors for 24 h, and then 50 µL media removed and replaced by 100 µL with fresh media alone. Images of spheroids were captured up to 15 days post-seeding using an EVOS M5000 Imaging System (Life Technologies, Paisley, UK). The diameter of the spheroids was analysed using ImageJ, and used to calculate spheroid volume using the formula $\frac{4}{3} \times \pi \times (d/2)^3$.

4.4. Statistical Analysis

Dose enhancement ratios (DER) were used to assess the significance of the clonogenic assay results. DER values are derived from the ratio of the dose (Gy) required for a surviving fraction of 0.5 in the vehicle (DMSO) treated cells ($D50_{DMSO}$), over the dose (Gy) required for the same surviving fraction in the inhibitor treated cells ($D50_{inhibitor}$) [$DER = D50_{DMSO}/D50_{inhibitor}$]. $D50$ values were calculated using a linear quadratic fitting on each curve. Statistical analysis of spheroid growth data was performed on the dataset across the 15-day growth period using a one-way ANOVA. For this, the effect of each inhibitor on the spheroid growth was compared against the vehicle (DMSO) for a given radiation dose and radiation type. p -values of <0.05 highlight statistical significance between DMSO and inhibitor treated spheroids over the growth period.

5. Conclusions

We have demonstrated that the inhibition of DNA DSB repair can effectively act in combination with both conventional (photon) radiotherapy and proton beam therapy in radiosensitising in vitro models of HNSCC. DNA-Pkcs was shown to be particularly effective in preventing clonogenic survival and 3D spheroid growth of HNSCC, and specifically models of relatively radioresistant HPV-negative HNSCC. Our data suggest that targeting DNA-Pkcs in combination with radiotherapy can be an effective strategy for the treatment of HNSCC.

Supplementary Materials: The following are available online at <https://www.mdpi.com/2072-6694/12/6/1490/s1>, Figure S1: Expression of p16 in HPV-negative and HPV-positive HNSCC cells; Figure S2: Increased radiosensitivity of HPV-positive HNSCC cells in comparison to HPV-negative cells in response to photons and protons. Figure S3: Comparison of cell survival in HNSCC cell lines in the presence of DNA DSB repair inhibitors; Figure S4: Inhibition of DSB repair signaling following photon irradiation; Figure S5: Inhibition of DSB repair signaling following proton irradiation; Figure S6. Inhibition of ATM, ATR and DNA-Pkcs increases radiosensitivity of HNSCC cells to photon irradiation; Figure S7. Inhibition of ATM, ATR and DNA-Pkcs increases radiosensitivity of HNSCC cells to proton irradiation. Figure S8: Inhibition of HNSCC spheroid growth using DSB repair inhibitors in the absence and presence of photon irradiation; Figure S9: Inhibition of HNSCC spheroid growth using DSB repair inhibitors in the absence and presence of proton irradiation; Figure S10: Inhibition of HPV-negative HNSCC spheroid growth using DSB repair inhibitors in the absence and presence of photon and proton irradiation; Table S1: Inhibition of ATM, ATR and DNA-Pkcs decreases cell survival in response to photon irradiation; Table S2: Inhibition of ATM, ATR and DNA-Pkcs decreases cell survival in response to proton irradiation

Author Contributions: Conceptualization, J.L.P.; methodology, J.L.P., A.K. and E.T.V.; validation, J.L.P. and E.T.V.; formal analysis, J.L.P. and E.T.V.; writing—original draft preparation, E.T.V.; writing—review & editing, J.L.P. and E.T.V.; supervision, J.L.P.; project administration, J.L.P.; funding acquisition, J.L.P.

Funding: Supported by a grant to J.L.P. from North West Cancer Research (CR CC7).

Acknowledgments: The authors thank T. Carey and S. Gollin for providing the HNSCC cells. We also thank Brian Marsland and Ian Taylor at the Clatterbridge Cancer Centre for technical assistance with proton irradiation of cells.

Conflicts of Interest: The authors declare no conflict of interest.

References

1. Chaturvedi, A.K.; Anderson, W.F.; Lortet-Tieulent, J.; Curado, M.P.; Ferlay, J.; Franceschi, S.; Rosenberg, P.S.; Bray, F.; Gillison, M.L. Worldwide trends in incidence rates for oral cavity and oropharyngeal cancers. *J. Clin. Oncol.* **2013**, *31*, 4550–4559, doi:10.1200/JCO.2013.50.3870.
2. Marur, S.; D'Souza, G.; Westra, W.H.; Forastiere, A.A. HPV-associated head and neck cancer: A virus-related cancer epidemic. *Lancet Oncol.* **2010**, *11*, 781–789, doi:10.1016/S1470-2045(10)70017-6.
3. Bray, F.; Ferlay, J.; Soerjomataram, I.; Siegel, R.L.; Torre, L.A.; Jemal, A. Global cancer statistics 2018: GLOBOCAN estimates of incidence and mortality worldwide for 36 cancers in 185 countries. *CA Cancer J. Clin.* **2018**, *68*, 394–424, doi:10.3322/caac.21492.

4. Ang, K.K.; Harris, J.; Wheeler, R.; Weber, R.; Rosenthal, D.I.; Nguyen-Tan, P.F.; Westra, W.H.; Chung, C.H.; Jordan, R.C.; Lu, C.; et al. Human papillomavirus and survival of patients with oropharyngeal cancer. *N. Engl. J. Med.* **2010**, *363*, 24–35, doi:10.1056/NEJMoa0912217.
5. Fakhry, C.; Westra, W.H.; Li, S.; Cmelak, A.; Ridge, J.A.; Pinto, H.; Forastiere, A.; Gillison, M.L. Improved survival of patients with human papillomavirus-positive head and neck squamous cell carcinoma in a prospective clinical trial. *J. Natl. Cancer Inst.* **2008**, *100*, 261–269, doi:10.1093/jnci/djn011.
6. Kumar, B.; Cordell, K.G.; Lee, J.S.; Worden, F.P.; Prince, M.E.; Tran, H.H.; Wolf, G.T.; Urba, S.G.; Chepeha, D.B.; Teknos, T.N.; et al. EGFR, p16, HPV Titer, Bcl-xL and p53, sex, and smoking as indicators of response to therapy and survival in oropharyngeal cancer. *J. Clin. Oncol.* **2008**, *26*, 3128–3137, doi:10.1200/JCO.2007.12.7662.
7. Lassen, P.; Eriksen, J.G.; Hamilton-Dutoit, S.; Tramm, T.; Alsner, J.; Overgaard, J. Effect of HPV-associated p16INK4A expression on response to radiotherapy and survival in squamous cell carcinoma of the head and neck. *J. Clin. Oncol.* **2009**, *27*, 1992–1998, doi:10.1200/JCO.2008.20.2853.
8. Gupta, A.K.; Lee, J.H.; Wilke, W.W.; Quon, H.; Smith, G.; Maity, A.; Buatti, J.M.; Spitz, D.R. Radiation response in two HPV-infected head-and-neck cancer cell lines in comparison to a non-HPV-infected cell line and relationship to signaling through AKT. *Int. J. Radiat. Oncol. Biol. Phys.* **2009**, *74*, 928–933, doi:10.1016/j.ijrobp.2009.03.004.
9. Rieckmann, T.; Tribius, S.; Grob, T.J.; Meyer, F.; Busch, C.J.; Petersen, C.; Dikomey, E.; Kriegs, M. HNSCC cell lines positive for HPV and p16 possess higher cellular radiosensitivity due to an impaired DSB repair capacity. *Radiother. Oncol.* **2013**, *107*, 242–246, doi:10.1016/j.radonc.2013.03.013.
10. Kimple, R.J.; Smith, M.A.; Blitzer, G.C.; Torres, A.D.; Martin, J.A.; Yang, R.Z.; Peet, C.R.; Lorenz, L.D.; Nickel, K.P.; Klingelhutz, A.J.; et al. Enhanced radiation sensitivity in HPV-positive head and neck cancer. *Cancer Res.* **2013**, *73*, 4791–4800, doi:10.1158/0008-5472.CAN-13-0587.
11. Weaver, A.N.; Cooper, T.S.; Rodriguez, M.; Trummell, H.Q.; Bonner, J.A.; Rosenthal, E.L.; Yang, E.S. DNA double strand break repair defect and sensitivity to poly ADP-ribose polymerase (PARP) inhibition in human papillomavirus 16-positive head and neck squamous cell carcinoma. *Oncotarget* **2015**, *6*, 26995–27007, doi:10.18632/oncotarget.4863.
12. Nickson, C.M.; Moori, P.; Carter, R.J.; Rubbi, C.P.; Parsons, J.L. Misregulation of DNA damage repair pathways in HPV-positive head and neck squamous cell carcinoma contributes to cellular radiosensitivity. *Oncotarget* **2017**, *8*, 29963–29975, doi:10.18632/oncotarget.16265.
13. Gillison, M.L.; Akagi, K.; Xiao, W.; Jiang, B.; Pickard, R.K.L.; Li, J.; Swanson, B.J.; Agrawal, A.D.; Zucker, M.; Stache-Crain, B.; et al. Human papillomavirus and the landscape of secondary genetic alterations in oral cancers. *Genome Res.* **2019**, *29*, 1–17, doi:10.1101/gr.241141.118.
14. Akagi, K.; Li, J.; Broutian, T.R.; Padilla-Nash, H.; Xiao, W.; Jiang, B.; Rocco, J.W.; Teknos, T.N.; Kumar, B.; Wangsa, D.; et al. Genome-wide analysis of HPV integration in human cancers reveals recurrent, focal genomic instability. *Genome Res.* **2014**, *24*, 185–199, doi:10.1101/gr.164806.113.
15. Rusan, M.; Li, Y.Y.; Hammerman, P.S. Genomic landscape of human papillomavirus-associated cancers. *Clin. Cancer Res.* **2015**, *21*, 2009–2019, doi:10.1158/1078-0432.CCR-14-1101.
16. Glorieux, M.; Dok, R.; Nuyts, S. Novel DNA targeted therapies for head and neck cancers: Clinical potential and biomarkers. *Oncotarget* **2017**, *8*, 81662–81678, doi:10.18632/oncotarget.20953.
17. Hafsi, H.; Dillon, M.T.; Barker, H.E.; Kyula, J.N.; Schick, U.; Paget, J.T.; Smith, H.G.; Pedersen, M.; McLaughlin, M.; Harrington, K.J. Combined ATR and DNA-PK Inhibition Radiosensitizes Tumor Cells Independently of Their p53 Status. *Front. Oncol.* **2018**, *8*, 245, doi:10.3389/fonc.2018.00245.
18. Lee, T.W.; Wong, W.W.; Dickson, B.D.; Lipert, B.; Cheng, G.J.; Hunter, F.W.; Hay, M.P.; Wilson, W.R. Radiosensitization of head and neck squamous cell carcinoma lines by DNA-PK inhibitors is more effective than PARP-1 inhibition and is enhanced by SLFN11 and hypoxia. *Int J. Radiat Biol* **2019**, 1–16, doi:10.1080/09553002.2019.1664787.
19. Dohmen, A.J.C.; Qiao, X.; Duursma, A.; Wijdeven, R.H.; Liefstink, C.; Hageman, F.; Morris, B.; Halonen, P.; Vens, C.; van den Brekel, M.W.M.; et al. Identification of a novel ATM inhibitor with cancer cell specific radiosensitization activity. *Oncotarget* **2017**, *8*, 73925–73937, doi:10.18632/oncotarget.18034.
20. Pires, I.M.; Olcina, M.M.; Anbalagan, S.; Pollard, J.R.; Reaper, P.M.; Charlton, P.A.; McKenna, W.G.; Hammond, E.M. Targeting radiation-resistant hypoxic tumour cells through ATR inhibition. *Br. J. Cancer* **2012**, *107*, 291–299, doi:10.1038/bjc.2012.265.

21. Dillon, M.T.; Barker, H.E.; Pedersen, M.; Hafsi, H.; Bhide, S.A.; Newbold, K.L.; Nutting, C.M.; McLaughlin, M.; Harrington, K.J. Radiosensitization by the ATR Inhibitor AZD6738 through Generation of Acentric Micronuclei. *Mol. Cancer Ther.* **2017**, *16*, 25–34, doi:10.1158/1535-7163.MCT-16-0239.
22. Holliday, E.B.; Frank, S.J. Proton radiation therapy for head and neck cancer: A review of the clinical experience to date. *Int. J. Radiat. Oncol. Biol. Phys.* **2014**, *89*, 292–302, doi:10.1016/j.ijrobp.2014.02.029.
23. Vitti, E.T.; Parsons, J.L. The Radiobiological Effects of Proton Beam Therapy: Impact on DNA Damage and Repair. *Cancers* **2019**, *11*, 946, doi:10.3390/cancers11070946.
24. Fontana, A.O.; Augsburger, M.A.; Grosse, N.; Guckenberger, M.; Lomax, A.J.; Sartori, A.A.; Pruschy, M.N. Differential DNA repair pathway choice in cancer cells after proton- and photon-irradiation. *Radiother. Oncol.* **2015**, *116*, 374–380, doi:10.1016/j.radonc.2015.08.014.
25. Dickreuter, E.; Eke, I.; Krause, M.; Borgmann, K.; van Vugt, M.A.; Cordes, N. Targeting of beta1 integrins impairs DNA repair for radiosensitization of head and neck cancer cells. *Oncogene* **2016**, *35*, 1353–1362, doi:10.1038/onc.2015.212.
26. Sankunny, M.; Parikh, R.A.; Lewis, D.W.; Gooding, W.E.; Saunders, W.S.; Gollin, S.M. Targeted inhibition of ATR or CHEK1 reverses radioresistance in oral squamous cell carcinoma cells with distal chromosome arm 11q loss. *Genes Chromosomes Cancer* **2014**, *53*, 129–143, doi:10.1002/gcc.22125.
27. Gerelchuluun, A.; Manabe, E.; Ishikawa, T.; Sun, L.; Itoh, K.; Sakae, T.; Suzuki, K.; Hirayama, R.; Asaithamby, A.; Chen, D.J.; et al. The major DNA repair pathway after both proton and carbon-ion radiation is NHEJ, but the HR pathway is more relevant in carbon ions. *Radiat. Res.* **2015**, *183*, 345–356, doi:10.1667/RR13904.1.
28. Bracalente, C.; Ibanez, I.L.; Molinari, B.; Palmieri, M.; Kreiner, A.; Valda, A.; Davidson, J.; Duran, H. Induction and persistence of large gammaH2AX foci by high linear energy transfer radiation in DNA-dependent protein kinase-deficient cells. *Int. J. Radiat. Oncol. Biol. Phys.* **2013**, *87*, 785–794, doi:10.1016/j.ijrobp.2013.07.014.
29. Carter, R.J.; Nickson, C.M.; Thompson, J.M.; Kacperek, A.; Hill, M.A.; Parsons, J.L. Complex DNA Damage Induced by High Linear Energy Transfer Alpha-Particles and Protons Triggers a Specific Cellular DNA Damage Response. *Int. J. Radiat. Oncol. Biol. Phys.* **2018**, *100*, 776–784, doi:10.1016/j.ijrobp.2017.11.012.
30. Carter, R.J.; Nickson, C.M.; Thompson, J.M.; Kacperek, A.; Hill, M.A.; Parsons, J.L. Characterisation of Deubiquitylating Enzymes in the Cellular Response to High-LET Ionizing Radiation and Complex DNA Damage. *Int. J. Radiat. Oncol. Biol. Phys.* **2019**, *104*, 656–665, doi:10.1016/j.ijrobp.2019.02.053.



© 2020 by the authors. Submitted for possible open access publication under the terms and conditions of the Creative Commons Attribution (CC BY) license (<http://creativecommons.org/licenses/by/4.0/>).